

EXPLORATION OF CHEMICAL AND BIOCHEMICAL MECHANISMS OF CATALYSIS

APPROVED BY SUPERVISORY COMMITTEE

---

Xuewu Zhang, Ph.D.

---

Elizabeth Goldsmith, Ph.D.

---

Uttam Tambar, Ph.D.

---

Melanie Cobb, Ph.D.

---

DEDICATION

*Ad majorem Dei gloriam.*

EXPLORATION OF CHEMICAL AND BIOCHEMICAL MECHANISMS OF CATALYSIS

by

KEVIN WILLIAM CORMIER

DISSERTATION

Presented to the Faculty of the Graduate School of Biomedical Sciences

The University of Texas Southwestern Medical Center at Dallas

In Partial Fulfillment of the Requirements

For the Degree of

DOCTOR OF PHILOSOPHY

The University of Texas Southwestern Medical Center at Dallas

Dallas, Texas

Degree Conferral August 2013

Copyright

by

Kevin William Cormier, 2013

All Rights Reserved

## EXPLORATION OF CHEMICAL AND BIOCHEMICAL MECHANISMS OF CATALYSIS

Publication No. \_\_\_\_\_

Kevin William Cormier, Ph.D

The University of Texas Southwestern Medical Center at Dallas, 2013

Supervising Professor: Melanie Cobb, Ph.D

Nature uses proteins to catalyze a wide range of chemical processes that control cellular signaling. One such enzyme is ERK2 which plays a role in the transmission of signals by catalyzing the phosphorylation of its substrates. The signaling pathway that it is a part of is important in the control of growth, cell survival and differentiation. As with other proteins, its function is intimately related to its structure, both its activity and selectivity for binding partners affected by its conformation. A mutant of ERK2, discovered in a human oral squamous cell carcinoma cell line, consists of a substitution of a lysine for a glutamic acid residue in the common docking domain (E320K). The effects of this mutation on the structure of ERK2 are examined along with the effect that the conformational change has on protein-protein interactions.

Because of the essential role catalysts play in lowering the activation barriers of otherwise inaccessible reaction pathways, chemists have long looked to nature for inspiration. The functionalization of C–H bonds is one such area of research, where the coveted exploitation of readily available hydrocarbon feedstock is impeded by the stability of the bonds. In this search for potential catalysts, chemists have looked to the metals that act as co-factors for many

enzymes. Vanadium, long thought to be at work in halogenation reactions taking place in marine environments, was found to selectively catalyze the oxidation of hydrocarbons at the benzylic position. Understanding the mechanism of a reaction can lead to insights into ways to better harness reactivity and selectivity, something that nature does quite efficiently. In studying the biosynthesis of pyrrole-imidazole alkaloids, a means to mimic nature's method for the dimerization of oroidin was achieved and the product outcome controlled.

## TABLE OF CONTENTS

CHAPTER ONE Introduction .....	1
The Mitogen-Activated Protein Kinase: ERK2 .....	1
Structural elements of ERK2 .....	1
Interactions with other proteins .....	6
MEK 1/2.....	8
Substrates of ERK2.....	10
MKP-3 .....	12
The role of dimerization.....	15
A Naturally Occuring Mutation of ERK2.....	19
The Sevenmaker gain-of-function mutation: ERK2 D319N .....	19
An oral squamous cancer cell mutation: ERK2 E322K.....	24
CHAPTER TWO Comparative Characterization of ERK2 E320K .....	28
Introduction.....	29
Experimental Procedures .....	32
Plasmid DNA constructs.....	32
Protein expression and purification .....	33
Kinase assays with ERK2 as substrate.....	35
Kinase assays with MBP as substrate .....	35
Phosphatase assays.....	36
<i>p</i> -NPP hydrolysis assays.....	36

Yeast two-hybrid experiments .....	37
SILAC .....	37
X-ray crystallography .....	38
Molecular dynamics simulations .....	39
Force field parameterization .....	39
Molecular dynamics simulations .....	40
Results .....	41
Differences in protein-protein interactions .....	41
Yeast two-hybrid.....	41
SILAC .....	48
Activity differences between ERK2 wt and ERK2 E320K .....	52
The activation of ERK2 by MEK1 R4F .....	53
The activity of ERK2 towards MBP.....	53
The deactivation of ERK2 by MKP-3 .....	54
The hydrolysis of <i>p</i> -NPP by MKP-3.....	55
Structural Differences .....	57
X-ray crystallography .....	57
Molecular dynamics simulations .....	59
Discussion.....	71
CHAPTER THREE Vanadium Catalyzed C–H Benzylic Oxidation .....	73
Abstract.....	73
Introduction.....	73

Experimental Procedures .....	78
Results .....	79
Discussion.....	88
CHAPTER FOUR Computational Study of Mn-Catalyzed Oxidative Radical Cyclization.....	90
Abstract.....	90
Introduction.....	90
Experimental Procedures .....	93
Results .....	94
Discussion.....	101
CHAPTER FIVE Conclusions and Recommendations .....	102
APPENDIX A Supplemental Information for Chapter Three .....	104
APPENDIX B Supplemental Information for Chapter Four .....	135
BIBLIOGRAPHY.....	174

## PRIOR PUBLICATIONS

Xiao Wang, Xiaolei Wang, Xianghui Tan, Jianming Lu, **Kevin W. Cormier**, Zhiqiang Ma, and Chuo Chen. A Biomimetic Route for Construction of the [4+2] and [3+2] Core Skeletons of Dimeric Pyrrole–Imidazole Alkaloids and Asymmetric Synthesis of Agelifेरins, *J. Am. Chem. Soc.* **2012**, *134*, 18834–18842.

Ji-Bao Xia, **Kevin W. Cormier**, and Chuo Chen. A Highly Selective Vanadium Catalyst for Benzylic C–H Oxidation, *Chem Sci.* **2012**, *3*, 2240–2245.

**Kevin W. Cormier**, Michelle Watt, and Michael Lewis. The Quadrupole Moment of Substituted Cyclopentadienyl Anions, *J. Phys. Chem. A* **2010**, *114*, 11708–11713.

**Kevin W. Cormier** and Michael Lewis. Lithium and Sodium Cation Binding of Cyclopentadienyl Anions: Electronic Effects of Cyclopentadienyl Substitution, *Polyhedron* **2009**, *28*, 3120-3128.

Michelle Watt, JiYoung Hwang, **Kevin W. Cormier**, and Michael Lewis. Preference for Na<sup>+</sup>-Dipole Binding in Na<sup>+</sup>-Arene Interactions, *J. Phys. Chem. A* **2009**, *113*, 6192-6196.

## LIST OF FIGURES

The primary and secondary structure of ERK2 (rat) .....	3
Yeast two-hybrid screen of ERK2 wt interactions with MEK and RSK .....	43
Yeast two-hybrid screen of ERK2 E320K interactions with MEK and RSK .....	44
Yeast two-hybrid screen of ERK2 interactions with MKP-3 .....	45
Yeast two-hybrid screen of dimer interactions .....	47
Yeast two-hybrid screen of dimer interactions with 0.5 mM 3-AT in medium .....	48
Mixing test distribution curve .....	50
Expression levels of for SILAC experiment .....	51
Autoradiograph of phosphorylation of ERK2 by MEK1 R4F .....	53
Rate of dephosphorylation of ERK2 by MKP-3 .....	55
Hydrolysis of <i>p</i> -NPP by MKP-3 in the presence of ERK2 .....	56
Comparison of L16 loop flexibility in wild type and mutant ERK2 .....	59
RMSD vs. simulation time plot for wild type unphosphorylated ERK2 .....	60
RMSD vs. simulation time plot for unphosphorylated ERK2 E320K .....	61
RMSD vs. simulation time plot for wild type phosphorylated ERK2 .....	62
RMSD vs. simulation time plot for phosphorylated ERK2 E320K .....	63
Map difference between contact maps of unphosphorylated and phosphorylated wild type .....	66
Map difference between contact maps of unphosphorylated and phosphorylated mutant .....	67
Map difference between contact maps of unphosphorylated wild type and mutant ERK2 .....	68
Map difference between contact maps of phosphorylated wild type and mutant ERK2 .....	69

Correlation matrices of unphosphorylated wild type (left) and mutant ERK2 (right).....	70
Correlation matrices of phosphorylated wild type (left) and mutant ERK2 (right).....	70
Olefin vs. C–H oxidation .....	77
Proposed mechanism of the Cp <sub>2</sub> VCl <sub>2</sub> –catalyzed benzylic oxidation .....	85
The two possible pathways for the C–H oxidation step .....	88
Structures of selected pyrrole–imidazole alkaloids .....	91
Energy diagram for the 6-endo and 5-exo cyclizations of 22, and the 1,2-shift of 23 .....	98
Energy diagram for the 6-endo versus 5-exo cyclization for 22, 25, and 26 .....	100

## LIST OF TABLES

Important residues in rat ERK2 .....	3
Examples of docking site sequences in ERK2 substrates.....	11
X-ray data collection statistics .....	58
Development of the vanadium-catalyzed benzylic oxidation.....	81
Scope of the Cp <sub>2</sub> VCl <sub>2</sub> -catalyzed benzylic oxidation.....	83

## LIST OF SCHEMES

Evidence for the intermediacy of a benzylic alcohol.....	86
A divergent biomimetic approach for the synthesis of [4+2] and [3+2] dimers .....	96
Proposed mechanism for the Mn(III)-promoted oxidative 5-exo/6-endo radical cyclization.....	97

## LIST OF APPENDICES

APPENDIX A Supplemental Information for Chapter Three .....	104
APPENDIX B Supplemental Information for Chapter Four .....	135

## LIST OF DEFINITIONS

3-AT – 3-amino-1,2,4-triazole

ATM – Ataxia telangiectasia mutated

ATP – Adenine triphosphate

ATR – Ataxia telangiectasia and Rad3-related protein; FRP1; FRAP-related protein 1

*boss* – *bride-of-sevenless* gene, the product of which is the ligand to Sev

BSA – Bovine serum albumin

CD domain – Common docking domain (of ERK2)

D domain – Docking domain (used for substrates of ERK2)

DEF – Docking site for ERK and FXFP

DTT – Dithiothreitol; Cleland's reagent

EGF – Epidermal growth factor

ERK2 – Extracellular signal-regulated kinase 2; MAPK1

*ERK2* – *MAPK1* gene; *PRKMI*; protein kinase, mitogen-activated 1; *P41MAPK*

F site – Substrate region with an FXF(P) motif; DEF domain

HEPES – 2-[4-(2-hydroxyethyl)piperazin-1-yl]ethanesulfonic acid

IPTG – Isopropyl-1-thio- $\beta$ -D-galactopyranoside

KIM – Kinase interaction motif (used for MKP-3)

LB – Luria-Bertani (broth)

MAP3K – Raf enzymes

MAPK1 – Mitogen-activated protein kinase 1; ERK2

MAPKAPK2 – 3pk; MK2

MBP – Myelin basic protein

MD – Molecular dynamics

MEK – MAP/ERK kinase; MAPKK; MAP2K

MNK – MAPK interacting kinase

MKP-1 – Mitogen kinase phosphatase 1; CL100

MKP-3 – Mitogen kinase phosphatase 3; Pyst1; rVH6

NMR – Nuclear magnetic resonance

PAC1 – Pituitary adenylate cyclase-activating polypeptide type I receptor; ADCYAP1R1;

PAC1R; PACAPR; PACAPRI

PCR – Polymerase chain reaction

PEA-15 – Phosphoprotein enriched in astrocytes 15

PKA – Protein kinase A

*p*-NPP – *para*-Nitrophenylphosphate

RMSD – Root-mean-square deviation

RSK – Ribosomal S6 kinase

rPTK – Receptor protein tyrosine kinase

*Sem* – *Sevenmaker* gain-of-function mutation allowing activation of *sev* pathway without Boss

*Sev* – Sevenless, a receptor protein tyrosine kinase in *Drosophila melanogaster*

SILAC – Stable isotope labeling by amino acids in cell culture

STK38 – Serine/threonine-protein kinase 38

TB – Terrific broth

## CHAPTER ONE

### Introduction

#### THE MITOGEN-ACTIVATED PROTEIN KINASE: ERK2

##### Structural elements of ERK2

ERK2 is one of two protein kinases that lie in the ubiquitous mitogen-activated protein kinase (MAPK) signaling pathway.<sup>1</sup> This MAPK signaling pathway is responsible for the control of many cellular processes including cell differentiation, proliferation and apoptosis, as well as cellular responses to environmental duress and many hormones.<sup>2</sup> Signaling in the MAPK pathway is achieved through a sequence of phosphorylation events. ERK2 is phosphorylated by upstream components of the cascade, MAP/ERK kinases (MEK)1/2 (also known as MAP kinase kinases – MKKs or MAP2Ks), which are phosphorylated by Raf enzymes (MAP3Ks). In order to become fully active, ERK2 must be dually phosphorylated on threonine 183<sup>3</sup> and tyrosine 185.<sup>4</sup> This dual phosphorylation is a step-wise process,<sup>5</sup> with tyrosine phosphorylated before threonine.<sup>6</sup> ERK2 can then in turn phosphorylate its many different substrates as appropriate in context. Inactivation of ERK2 requires dephosphorylation of one or both of these two

---

<sup>1</sup> Roux, P. P.; Blenis, J. *Microbiol. Mol. Biol. Rev.* **2004**, *68*, 320.

<sup>2</sup> (a) Chen, Z.; Gibson, T. B.; Robinson, F.; Silvestro, L.; Pearson, G.; Xu, B.; Wright, A.; Vanderbilt, C.; Cobb, M. H. *Chem. Rev.* **2001**, *101*, 2449. (b) Ray, L. B.; Sturgill, T. W. *Proc. Natl. Acad. Sci. U. S. A.* **1988**, *85*, 3753.

<sup>3</sup> N.B.: The residue numbering system adopted herein, unless stated otherwise, is from the rat sequence.

<sup>4</sup> Robbins, D. J.; Zhen, E.; Owaki, H.; Vanderbilt, C.; Ebert, D.; Geppert, T. D.; Cobb, M. H. *J. Biol. Chem.* **1993**, *268*, 5097.

<sup>5</sup> Ferrell, J. E. *TIBS* **1997**, *22*, 288.

<sup>6</sup> Robbins, D. J.; Cobb, M. H. *Mol. Biol. Cell* **1992**, *3*, 299.

phosphoresidues (but often just pY), a task that is achieved by either serine/threonine-specific phosphatase, a tyrosine-specific phosphatase or by a dual-specific phosphatase such as MKP-3 that can dephosphorylate both residues.

As has long been held by biochemists, the function of proteins is intimately related to their structure (see Table 1 for a list of important residues in the function of ERK2). Much can thus be gained by examining the structure of a particular protein. In the case of ERK2, the structures of both active<sup>7</sup> (phosphorylated) and inactive<sup>8</sup> (unphosphorylated) forms have been solved crystallographically. As illustrated in Figure 1, ERK2 consists of an N-terminal domain made up of 5 antiparallel  $\beta$  strands ( $\beta$ 1-  $\beta$ 5) and two helices,  $\alpha$  helix C ( $\alpha$ C-helix) and  $\alpha$  helix L16 ( $\alpha_{L16}$ -helix) that is part of a C-terminal extension to the catalytic core. Between the  $\beta$ 1- and  $\beta$ 2-strands there is a conserved glycine-rich (GXGXXG) ATP-phosphate-binding loop (or P-loop) that helps position the  $\beta$ - and  $\gamma$ -phosphates of ATP for catalysis. The  $\beta$ 1- and  $\beta$ 2-strands harbor the ATP adenine that makes a hydrophobic contact with a conserved valine V37 that follows the glycine-rich loop. The lysine K52 of the  $\beta$ 3-strand couples the  $\alpha$ - and  $\beta$ -phosphates of ATP to the  $\alpha$ C-helix. A salt-bridge, formed between the  $\beta$ 3-lysine and the conserved glutamate E69 of the  $\alpha$ C-helix, is a necessary but not sufficient requirement for kinase activity.<sup>9</sup>

---

<sup>7</sup> Canagarajah, B. J.; Khokhlatchev, A.; Cobb, M. H.; Goldsmith, E. *Cell* **1997**, *90*, 859.

<sup>8</sup> Zhang, F.; Strand, A.; Robbins, D.; Cobb, M. H.; Goldsmith, E. *Nature* **1994**, *367*, 704.

<sup>9</sup> Roskoski, R. *Pharmacol. Res.* **2012**, *66*, 105.

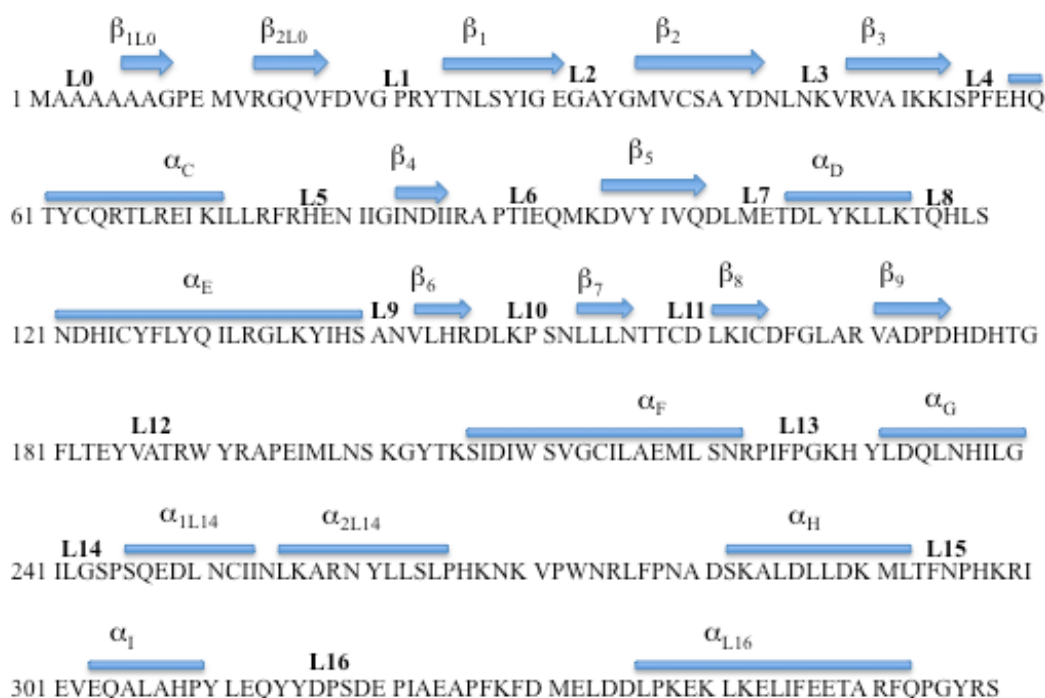


**Figure 1. The primary and secondary structure of ERK2 (rat).**  $\alpha$ -Helices are denoted by bars and  $\beta$ -strands by arrows.

**Table 1. Important residues in rat ERK2.**

	Residues for rat
Protein kinase domain	23-311
Glycine-rich loop	30-35
The K of K/D/D (the $\beta$ 3-lysine)	52
$\alpha$ C-glutamate	69
Hinge residues	104-107
Gatekeeper residue	Q103
Catalytic HRD	145-147
Catalytic loop lysine	149
DFG of the activation region	165-167
Activation loop phosphorylation sites	T183, Y185
APE end of the activation loop	193-195

The C-terminal domain of ERK2 is primarily made up of  $\alpha$  helices and four short  $\beta$  strands that contain a K/D/D signature motif that constitute the catalytic core of protein kinases.<sup>10</sup> The lysine of the  $\beta$ 3-strand, K71, forms salt-bridges with the  $\alpha$ - and  $\beta$ -phosphates of ATP. It has been suggested that D147, found in the catalytic loop, deprotonates the –OH group of the protein substrate facilitating nucleophilic attack on the  $\gamma$ -phosphorus atom of MgATP.<sup>11</sup> D165 binds  $Mg^{2+}$  ions that coordinate the  $\alpha$ -,  $\beta$ - and  $\gamma$ -phosphates of ATP. This aspartate also begins the activation loop of ERK2 that, like nearly all protein kinases, begins with DFG and ends with a conserved APE.

A flexible linker that acts as a hinge, closing the protein upon activation (though more so in other kinases based on structural data), joins the C and N termini. These two lobes rotate  $5.4^\circ$  closer in the active phosphorylated conformation than in the unphosphorylated inactive form (compared to  $20^\circ$  in PKA).<sup>12</sup> The activation loop (L12) is located at the interface of these two domains and contains the two phosphoacceptor sites, T183 and Y185. The TXY motif is conserved in the activation loop of most MAPKs and, in ERK2, it is a glutamate (E) residue that separates the two phosphoacceptors.

Phosphorylation of Y185 induces a rearrangement of L12 by binding to two basic residues on the exterior of the C-terminal domain of the kinase core. MAPKs phosphorylate serine/threonine residues that are followed by a proline. The refolding of L12 allows for Y185 to form part of the surface that binds the proline at the P + 1 residue of the protein substrate.

---

<sup>10</sup> Hanks, S. K.; Quinn, A. M.; Hunter, T. *Science* **1988**, *241*, 42.

<sup>11</sup> Zhou, J.; Adams, J. A. *Biochemistry* **1997**, *36*, 15733.

<sup>12</sup> Canagarajah, B. J.; Khokhlatchev, A.; Cobb, M. H.; Goldsmith, E. *Cell* **1997**, *90*, 859.

Meanwhile, phosphorylated T183 helps to orient active site residues in the N-terminal domain by interacting with an arginine residue (R65) in helix C.<sup>13</sup> The  $\alpha$ C-helix itself has an active (in) and inactive (out) conformation. In the active state, K52 from the  $\beta$ 3-strand forms a salt bridge with E69 from the  $\alpha$ C-helix. Also, in the active state, the aspartate side chain (D165) of the DFG activation segment faces into the ATP-binding pocket and coordinates  $Mg^{2+}$ . The ability of D165 to bind to  $Mg^{2+}$  (in the DFG-aspartate in/ $\alpha$ C-helix conformation) is key for enzyme activity, and all other combinations of conformations for the DFG aspartate side chain and  $\alpha$ C-helix represent inactive forms of the protein.<sup>14</sup>

The hydrophobic residues on the surface of ERK2 have also been used to describe it structurally.<sup>15</sup> Five non-consecutive hydrophobic residues constitute a regulatory (R-) spine and eight hydrophobic residues constitute a catalytic (C-) spine. While the C-spine governs catalysis by directing ATP binding, the R-spine controls substrate positioning. The proper alignment of both is necessary but not sufficient in an active kinase. The R-spine is formed by I84 at the beginning of the  $\beta$ 4-strand and L73 from C-terminal end of  $\alpha$ C-helix, both from the N-terminal lobe of ERK2. The remaining three residues are from the C-terminal lobe of ERK2: L168 found in the activation loop, H145 found in the catalytic loop, and D208 in the F-helix. These last two interact by a hydrogen bond. The C-spine is made up of two residues from the N-terminal lobe that bind the adenine of ATP, V37 from the  $\beta$ 2-strand and A50 from the  $\beta$ 3-strand. In the C-

---

<sup>13</sup> Knighton, D. R.; Zheng, J.; Ten Eyck, L. F.; Xuong, N.-H.; Taylor, S. S.; Sowadski, J. M. *Science* **1991**, 253, 414.

<sup>14</sup> Roskoski, R. *Pharmacol. Res.* **2012**, 66, 105.

<sup>15</sup> Kornev, A. P.; Haste, N. M.; Taylor, S. S.; Eyck, L. F. *Proc. Natl. Acad. Sci. U. S. A.* **2006**, 103, 17783.

terminal lobe, L153-155, found in the  $\beta$ 7-strand, bind to the adenine base (L154) and to M106 (L153 and L155) at the beginning of the D-helix. M106 binds to I215 and M220, both found in the F-helix.

### Interactions with other proteins

On the other side of the activation lip, and part of the L16 loop, is the common docking (CD) region that is largely responsible for substrate binding and thus substrate specificity.<sup>16</sup> The CD region is conserved in all MAPKs and is made up largely of acidic residues, DXX(D/E).<sup>17</sup> These acidic residues bind to the corresponding basic residues in the D motif of substrates consisting of two or more basic residues (lysine or arginine) usually followed by a (L/I)X(L/I) motif. Or, as in RSK1/2 and MNK1/2, a conserved LAQRR motif.<sup>18</sup> The acidic residues of ERK2 are not the only residues that contribute to MAPK specificity for substrates in the CD region.<sup>19</sup> When T157 and T158 of ERK2 were mutated to glutamic acid and aspartic acid respectively, ERK2 bound to the p38-specific substrates MK3 and MSK2. The corresponding region in p38 has been termed the ED site,<sup>20</sup> thus the corresponding T157 and T158 in ERK2 are sometimes referred to as the ED motif and is located opposite the MAPK active center.

Another important region of ERK2 that plays a role in the recognition and binding of substrates is the F-site recruitment site (FRS) that is a hydrophobic pocket between the P+1 site,

---

<sup>16</sup> Goldsmith, E. J.; Akella, R.; Min, X.; Zhou, T.; Humphreys, J. M. *Chem. Rev.* **2007**, *107*, 5065.

<sup>17</sup> Tanoue, T.; Adachi, M.; Moriguchi, T.; Nishida, E. *Nat. Cell Biol.* **2000**, *2*, 110.

<sup>18</sup> Gavin, A. C.; Nebreda, A. R. *Curr. Biol.* **1999**, *9*, 281.

<sup>19</sup> Tanoue, T.; Nishida, E. *Cell Signal.* **2003**, *15*, 455.

<sup>20</sup> Tanoue, T.; Maeda, R.; Adachi, M.; Nishida, E. *EMBO J.* **2001**, *20*, 466.

the  $\alpha$ F helix and an insert unique to the MAPKs called the MAPK insert. This region binds substrates with FXF motifs (hence F-sites or also called a DEF domain for docking site for ERK and FXFP) that are often followed by a proline residue. Because the binding site on ERK2 is only exposed upon phosphorylation, substrates favor binding to this motif when ERK2 is active.<sup>21</sup> Certain FXF sequences bind to either active or unphosphorylated ERK2. These include unstructured FG repeats present on several nuclear pore proteins.<sup>22</sup>

Hydrogen exchange mass spectrometry (HX-MS) together with site-directed mutagenesis has been used to determine the residues of ERK2 that bind to the D domain (the DRS of ERK2: D-site recruitment site) or FXF motif of substrates (the FRS of ERK2).<sup>23</sup> By incubating ERK2 with and without peptide mimics of these two substrate motifs and measuring the differences in deuterium incorporation, the residues of interaction can be deduced by the protection from the deuterated solvent granted by the peptides. These assessments are further confirmed by mutagenesis and in vitro pull-down assays. These studies showed that residues T157, T158, D316, D319, L113, L119, L155, H123, and Y126 are protected, indicating that they form the DRS. The residues corresponding to the FRS of ERK2 are Y231, L232, and L235 on one side of a hydrophobic groove along with M197, L198, and Y261.

---

<sup>21</sup> Lee, T.; Hoofnagle, A. N.; Kabuyama, Y.; Stroud, J.; Min, X.; Goldsmith, E. J.; Chen, L.; Resing, K. A.; Ahn, N. G. *Mol. Cell* **2004**, *14*, 43.

<sup>22</sup> (a) Whitehurst, A. W.; Wilsbacher, J. L.; You, Y.; Luby-Phelps, K.; Moore, M. S.; Cobb, M. H. *Proc. Natl. Acad. Sci. U. S. A.* **2002**, *99*, 7496; (b) Yacizioglu, M. N.; Goad, D. L.; Ranganathan, A.; Whitehurst, A. W.; Goldsmith, E. J.; Cobb, M. H. *J. Biol. Chem.* **2007**, *282*, 28759.

<sup>23</sup> Lee, T.; Hoofnagle, A. N.; Kabuyama, Y.; Stroud, J.; Min, X.; Goldsmith, E. J.; Chen, L.; Resing, K. A.; Ahn, N. G. *Mol. Cell* **2004**, *14*, 43.

*MEK 1/2*

MEK 1 and MEK 2 activate ERK2 by first phosphorylating Y185.<sup>24</sup> Tyrosine-phosphorylated ERK2 dissociates from MEK1/2 in order to, it is assumed, associate with another or the same active MEK1/2 that mediates the phosphorylation of T183.<sup>25</sup> MEK1/2 are themselves activated 1000-fold by phosphorylation of two serine residues<sup>26</sup> that each partially increases their activity.<sup>27</sup> In MEK1, these are S218 and S222; in MEK2 these are S222 and S226. Besides the 290 residues that make up the protein kinase domain and that includes both the ATP binding site and catalytic apparatus, the 70 residues of the N- and the 30 residues of the C-terminal domains play a role in the function of the protein. The N-terminal domain is trifunctional, having an ERK2 binding domain,<sup>28</sup> a nuclear export sequence and an inhibitory segment.<sup>29</sup> The ERK1/2 binding site, also known as a D domain, is made up of basic and hydrophobic residues that interact electrostatically with the acidic residues of the CD domain of ERK2. The only known physiological substrates of MEK1/2 are ERK1/2, though they do display some activity towards myelin basic protein. The nuclear export signal (NES), that includes amino acids 32-44 (ALQKKLEELDE),<sup>30</sup> plays an important role in the localization of ERK1/2. This active NES of MEK1 results in it being found predominantly in the cytoplasm and

---

<sup>24</sup> Haystead, T. A.; Dent, P.; Wu, J.; Haystead, C. M.; Sturgill, T. W. *FEBS Lett.* **1992**, *306*, 17.

<sup>25</sup> Ferrell, J. E.; Bhatt, R. R. *J. Biol. Chem.* **1997**, *272*, 19008.

<sup>26</sup> Zheng, C. F.; Guan, K. L. *EMBO J.* **1994**, *13*, 1123.

<sup>27</sup> Mansour, S. J.; Candia, J. M.; Matsuura, J. E.; Manning, M. C.; Ahn, N. G. *Biochemistry* **1996**, *35*, 15529.

<sup>28</sup> Xu, B.; Wilsbacher, J. L.; Collisson, T.; Cobb, M. H. *J. Biol. Chem.* **1999**, *274*, 34029.

<sup>29</sup> Roskoski, R. *Biochem. Biophys. Res. Commun.* **2012**, *417*, 5.

<sup>30</sup> Fukuda, M.; Gotoh, I.; Gotoh, Y.; Nishida, E. *J. Biol. Chem.* **1996**, *271*, 20024.

acts as a cytoplasmic anchoring protein through its interaction with ERK2.<sup>31</sup> When the nuclear export receptor CRM1 is inhibited by leptomycin, ERK2 accumulates in the nucleus.<sup>32</sup> The fusion of ERK2 and MEK1 yields a protein that is excluded from the nucleus, except when the NES is inactivated.<sup>33</sup>

The C-terminal contains a proline-rich domain that is unique in the MEK family to MEK1/2<sup>34</sup> and is required for the efficient activation of ERK2.<sup>35</sup> This domain has potential sites for interaction with SH3 domains making it a potential site of binding for linker proteins that localize components of the MAPK pathway via MEK. It also contains threonine residues T286, T292 and T386, which negatively regulate MEK1 activity upon phosphorylation.<sup>36</sup> Absent in MEK2, the phosphorylation of T292 in MEK1 by ERK2 serves to down-regulate MEK2 activity through the formation of MEK1-MEK2 heterodimers.<sup>37</sup> On the other hand, the phosphorylation of S298 of MEK1 by the p21-activated kinase-1 (PAK1) has been shown to enhance its interaction with ERK2.<sup>38</sup>

---

<sup>31</sup> Fukuda, M.; Gotoh, Y.; Nishida, E. *EMBO J.* **1997**, *16*, 1901.

<sup>32</sup> Adachi, M.; Fukuda, M.; Nishida, E. *J. Cell Biol.* **2000**, *148*, 849.

<sup>33</sup> Robinson, M. J.; Stippec, S. A.; Goldsmith, E.; White, M. A.; Cobb, M. H. *Curr. Biol.* **1998**, *8*, 1141.

<sup>34</sup> Catling, A. D.; Schaeffer, H.-J.; Reuter, C. W. M.; Reddy, G. R.; Weber, M. J. *Mol. Cell Biol.* **1995**, *15*, 5214.

<sup>35</sup> Dang, A.; Frost, J. A.; Cobb, M. H. *J. Biol. Chem.* **1998**, *273*, 19909.

<sup>36</sup> Rossomando, A. J.; Dent, P.; Sturgill, T. W.; Marshak, D. R. *Mol. Cell Biol.* **1994**, *14*, 1594.

<sup>37</sup> Catalanotti, F.; Reyes, G.; Jesenberger, V.; Galabova-Kovacs, G.; De Matos Simoes, R.; Carugo, O.; Baccarini, M. *Nat. Struct. Mol. Biol.* **2009**, *16*, 294.

<sup>38</sup> (a) Frost, J. A.; Steen, H.; Shapiro, P.; Lewis, T.; Ahn, N.; Shaw, P. E.; Cobb, M. H. *EMBO J.* **1997**, *16*, 6426. (b) Eblen, S. T.; Slack-Davis, J. K.; Tarcsafalvi, A.; Parsons, J. T.; Weber, M. J.; Catling, A. D. *Mol. Cell Biol.* **2004**, *24*, 2308.

### *Substrates of ERK2*

ERK1 and ERK2 have more than 250 documented cytoplasmic and nuclear substrates.<sup>39</sup> ERK2 phosphorylates membrane proteins; cytosolic, cytoskeletal and mitochondrial proteins; proteins of the nuclear pore complex; nuclear proteins; and downstream kinases. As with other MAPKs, ERK1/2 phosphorylate substrates at serine/threonine residues that are followed by proline. In activated ERK2, there is a surface depression where phosphotyrosine occupies what is in many other kinases a large substrate pocket for hydrophobic residues.<sup>40</sup> This makes proline, which orients its side chain away from the kinase surface, a preferred component of the primary sequence of ERK2 substrates. In fact, a primary sequence with prolines at both the -2 and +1 positions (Pro-Xxx-Ser/Thr-Pro) with respect to the phosphorylation site has been shown to be optimal, whereas proline at position -1 is unfavorable.<sup>41</sup> That said, however, glycine and even alanine follows the acceptor site instead of proline in some substrates. Not having a side chain, or only a methyl group, glycine and alanine can be accommodated at the P+1 residue.<sup>42</sup>

Besides the sequence at the phosphorylation site, various docking site sequences contribute to substrate recognition.<sup>43</sup> These can be grouped into two independent types of docking motifs. In substrates with multiple potential phosphorylation sites, these docking motifs

---

<sup>39</sup> (a) Yoon, S.; Seger, R. *Growth Factors* **2006**, *24*, 21. (b) Carlson, S. M.; Chouinard, C. R.; Labadorf, A.; Lam, C. J.; Schmelzle, K.; Fraenkel, E.; White, F. M. *Sci. Signal.* **2011**, *4*, rs11.

<sup>40</sup> Canagarajah, B. J.; Khokhlatchev, A.; Cobb, M. H.; Goldsmith, E. *Cell* **1997**, *90*, 859.

<sup>41</sup> (a) Davis, R. J. *J. Biol. Chem.* **1993**, *268*, 14553. (b) Turk, B. E. *Curr. Op. Chem. Biol.* **2008**, *12*, 4. (c) Songyang, Z.; Lu, K. P.; Kwon, Y. T.; Tsai, L.-H.; Filhol, O.; Cochet, C.; Brickey, D. A.; Soderling, T. R.; Bartleson, C.; Graves, D. J.; DeMaggio, A. J.; Hoekstra, M. F.; Blenis, J.; Hunter, T.; Cantley, L. C. *Mol. Cell. Biol.* **1996**, *16*, 6486.

<sup>42</sup> Pearson, G.; Robinson, F.; Beers Gibson, T.; Xu, B.-E.; Karandikar, M.; Berman, K.; Cobb, M. H. *Endocr. Rev.* **2001**, *22*, 153.

<sup>43</sup> Holland, P. A.; Cooper, J. A. *Curr. Biol.* **1999**, *9*, R329.

can direct phosphorylation to specific residues.<sup>44</sup> Substrates may contain both, one, or neither of these docking motifs. The first motif is called the D domain (or simply D-site), made up of both hydrophobic ( $\Phi$ ) and positively charged residues, has the canonical sequence  $(R/K)_{2-3}-X_{2-6}-\Phi_A-X-\Phi_B$ . The positively charged basic residues of the substrate D-site bind to the negatively charged component of the CD-domain of ERK2 that is made up of two aspartate residues (D316 and D319). The  $\Phi_A-X-\Phi_B$  sequence of the substrate binds to a nearby hydrophobic patch in ERK2 that is made up of L113, L119, L155, H123, and Y126.

The second type of docking motif found in substrates of ERK2 is the FXP(P) motif (or simply F-site). Mutagenesis studies have shown that the first phenylalanine in the FXP motif binds to M197 and L198 of ERK2 and that the second phenylalanine of the sequence binds to L235.<sup>45</sup> All three of these residues are buried in the unphosphorylated form of ERK2.

**Table 2. Examples of docking site sequences in ERK2 substrates.**

<b>Substrate</b>	<b>Docking site sequences</b>
MNK2, RSK	LAQRRX <sub>4</sub> L
MNK1, MSK1	LA+RR
LIN-1, ELK-1, SAP-1a, SAP-2	FXFP
ELK-1	KX <sub>2</sub> +X <sub>3</sub> LXL

<sup>44</sup> Fantz, D. A.; Jacobs, D.; Glossip, D.; Kornfeld, K. *J. Biol. Chem.* **2001**, 276, 27256.

<sup>45</sup> Sheridan, D. L.; Kong, Y.; Parker, S. A.; Dalby, K. N.; Turk, B. E. *J. Biol. Chem.* **2008**, 283, 19511.

### *MKP-3*

ERK2 activity is reduced by the dephosphorylation of the threonine and tyrosine in its activation loop. The dephosphorylation of just one of the residues leads to a great reduction in activity of the kinase. ERK2 is inactivated by all three major groups of protein phosphatases: threonine/serine specific, tyrosine specific, and the dual phosphatases that dephosphorylate both. The MAPK phosphatases (MKPs) that specifically dephosphorylate the MAPK family,<sup>46</sup> fall into the third group. The dual-specificity MKPs are grouped into three classes based on substrate specificity and localization: class I enzymes are localized within the nucleus and, with the exception of the ERK1/2 specific hVH3 (DUSP5), display a broad specificity for ERKs, p38, and JNK; class II enzymes are localized in the cytoplasm and are ERK specific; and class III enzymes are located in both the cytoplasm and the nucleus and preferentially inactivate p38 and JNK.<sup>47</sup> MKP-3 is a member of class II, and, as such, is an example of a dual-specific phosphatase located in the cytoplasm and specific for ERK. It has, however, been recently shown that MKP-3 can bind to p38 $\alpha$  and dephosphorylate its phosphotyrosine but not its phosphothreonine residue.<sup>48</sup>

All of the dual-specific phosphatases contain a MAPK binding domain (a D motif) and a phosphatase domain with a short linker of about 40 amino acid residues between them. Specificity for the MAPK family is partially achieved by dual-specificity MKPs through their N-

---

<sup>46</sup> Camps, M.; Nichols, A.; Arkininstall, S. *FASEB J.* **2000**, *14*, 6.

<sup>47</sup> Bermudez, O.; Pagès, G.; Gimond, C. *Am. J. Physiol. Cell Physiol.* **2010**, *299*, C189.

<sup>48</sup> Zhang, Y.-Y.; Wu, J.-W.; Wang, Z.-X. *J. Biol. Chem.* **2011**, *286*, 16150.

terminal MAPK binding domain,<sup>49</sup> also known as the kinase interaction motif (KIM). This domain contains a cluster of positively charged amino acids and hydrophobic residues that interact with the CD domain of ERK, p38, and JNK,<sup>50</sup> such that the canonical sequence for the KIM is  $\Phi\Phi\text{-X-RR}\Phi\text{-XX-G}$ .

The C-terminal phosphatase domain is made up of nearly 200 amino acid residues containing a HCX<sub>5</sub>R signature sequence and a conserved aspartate that acts as an acid/base for catalysis. The shallow active site cleft, with a depth of about 5.5Å, accommodates phosphotyrosine or phosphothreonine, with arginine binding to the phosphate group. The thiolate anion of the catalytic cysteine then attacks the phosphate to form a P-S bond and displaces the unphosphorylated MAPK that has been protonated by aspartate. The aspartate regains its proton from water thus forming a hydroxyl anion that releases inorganic phosphate by displacing the cysteinyl thiolate bond attaching it to the phosphatase thereby completing the catalytic cycle.<sup>51</sup>

In the case of the dual dephosphorylation of ERK2 by MKP-3, the mechanism was found to be ordered and distributive.<sup>52</sup> MKP-3 is highly specific for bisphosphorylated ERK2 with a  $k_{cat}/K_m$  of  $3.8 \times 10^6 \text{ M}^{-1} \text{ s}^{-1}$ . MKP-3 binds to ERK2/pTpY and first dephosphorylates the phosphotyrosine. It then releases ERK2/pT that can then bind to the same or another MKP-3 to dephosphorylate the phosphothreonine. Interestingly, the interaction of the KIM with the MAPK substrate increases phosphatase activity, with MKP-3 phosphatase activity stimulated 30-fold by

---

<sup>49</sup> Muda, M.; Theodosiou, A.; Gilleron, C.; Smith, A.; Chabert, C.; Camps, M.; Boschert, U.; Rodrigues, N.; Davies, K.; Ashworth, A.; Arkinstall, S. *J. Biol. Chem.* **1998**, *273*, 9323.

<sup>50</sup> Kondoh, K.; Nishida, E. *Biochim. Biophys. Acta* **2007**, *1773*, 1227.

<sup>51</sup> Farooq, A.; Zhou, M.M. *Cell. Signal.* **2004**, *16*, 769.

<sup>52</sup> Zhao, Y.; Zhang, Z. Y. *J. Biol. Chem.* **2001**, *276*, 32382.

forming a complex with ERK2.<sup>53</sup> This stimulation of phosphatase activity occurred even when a kinase-dead mutant of ERK2 was used, but did not occur with an MKP-3 mutant lacking a KIM. Unlike most other phosphatases, MKP-3 does not require ERK2 to be phosphorylated for binding. While the  $K_d$  of MKP-3 to dual phosphorylated ERK2 is about 30 nM, it is about 190 nM, only about a 6-fold change, when interacting with unphosphorylated ERK2. These are comparable to dissociation constants between ERK2 and common substrates such as Elk-1 (250 nM and > 10  $\mu$ M when ERK2 is dual phosphorylated), ribosomal S6 kinase (RSK)-1 (150 nM), and c-Fos (1  $\mu$ M).<sup>54</sup>

The deletion of the MKP-3 KIM prevents the formation of an MKP-3/ERK2 complex. X-ray crystallography of a MKP-3 KIM peptide bound to ERK2<sup>55</sup> and hydrogen/deuterium exchange mass spectrometry of full-length MKP-3 bound to ERK2,<sup>56</sup> elucidate the interaction of MKP-3 with ERK2. Basic R64 and R65 of the MKP-3 KIM interact with the highly acidic patch (E79, D160, D316, D319 in  $\alpha$ E, L<sub>5</sub>,  $\beta$ 8, and L<sub>16</sub>) of the CD-domain of ERK2 and L71, P72, V73 of the KIM interact with the ERK2 hydrophobic groove (T108, L110, L113, L119, F127, and L155 in L<sub>7</sub>,  $\alpha$ D, L<sub>8</sub>,  $\alpha$ D, and  $\beta$ 7).

The activation of MKP-3, however, does not directly involve the interaction with the CD-domain of ERK2. Instead, for activation of the phosphatase to occur, the <sup>364</sup>FTAP<sup>367</sup> sequence of MKP-3 must interact with R189, W190, E218, R223, L229, and H230 in the protein substrate

---

<sup>53</sup> Camps, M.; Nichols, A.; Gillieron, C.; Antonsson, B.; Muda, M.; Chabert, C.; Boschert, U.; Arkinstall, S. *Science* **1998**, *280*, 1262.

<sup>54</sup> Caunt, C. J.; Keyse, S. M. *FEBS J.* **2013**, *280*, 489.

<sup>55</sup> Liu, S.; Sun, J. P.; Zhou, B.; Zhang, Z. Y. *Proc. Natl. Acad. Sci. U. S. A.* **2006**, *103*, 5326.

<sup>56</sup> Zhou, B.; Zhang, J.; Liu, S.; Reddy, S.; Wang, F.; Zhang, Z. Y. *J. Biol. Chem.* **2006**, *281*, 38834.

binding site of ERK2. Activation results from conformational changes within the catalytic domain of MKP-3 that move a loop containing a conserved D into position to act as a general acid during catalysis.<sup>57</sup>

### **The role of dimerization**

The dimerization of ERK2 and its possible role is a very contested area of research.<sup>58</sup> There is both the question of whether ERK2 dimerizes in cells and, if so, what physiological role does dimerization play.

Evidence for the formation of ERK2 complexes came about from crystallographic data and studies of ERK2 localization in cells.<sup>59</sup> Unphosphorylated ERK2 was retained longer in the nucleus when co-injected into cells with thiophosphorylated kinase-deficient ERK2 K52R. That oligomers can form was then shown by gel filtration. While phosphorylated ERK2 elutes as two peaks, both phosphorylated ERK2 treated with phosphatase and unphosphorylated ERK2 elute as a single peak. Data from equilibrium sedimentation is consistent with the idea that the phosphorylated form of ERK2 forms dimers and that unphosphorylated ERK2 exists primarily as a monomer. Immunoprecipitation kinase assays of untagged phosphorylated ERK2 with tagged unphosphorylated ERK2 wild-type, the kinase dead K52R mutant, and the phosphorylation site

---

<sup>57</sup> Rigas, J. D.; Hoff, R. H.; Rice, A. E.; Hengge, A. C.; Denu, J. M. *Biochemistry* **2001**, *40*, 4398.

<sup>58</sup> Lee, S.; Bae, Y. S. *Mol. Cells* **2012**, *33*, 325.

<sup>59</sup> Khokhlatchev, A. V.; Canagarajah, B.; Wilsbacher, J.; Robinson, M.; Atkinson, M.; Goldsmith, E.; Cobb, M. H. *Cell* **1998**, *93*, 605.

deficient T183A, Y185F mutant showed that the phosphorylated ERK2 can form a dimer with unphosphorylated forms of ERK2.

A possible interface for dimerization was determined from the crystal structure of ERK2 (PDB: 2ERK) that was then assessed by gel filtration and sedimentation equilibrium analysis. In both of these experiments, the mutants – ERK2 H176E L<sub>4</sub>A (L333, 336, 341, 344) and ERK2Δ4 (deletion of P174-D177) – acted like monomers despite being phosphorylated and exhibiting normal kinase activity. Additionally, these mutants, that are incapable of homodimerizing even when thiophosphorylated, appear only transiently in the nucleus when microinjected into the cytoplasm suggesting that dimerization contributes to nuclear retention. Similarly, the Nishida group showed that the *Xenopus* ERK2 H176E L<sub>4</sub>A mutant is translocated into the nucleus of NIH 3T3 cells at a much slower rate than wild-type ERK2.<sup>60</sup>

This idea, however, that ERK2 nuclear localization is facilitated by dimerization has been contested by results from other research groups. Based on the observations<sup>61</sup> that there is a decreased amount of ERK2-associated total and phosphophorylated cytosolic phospholipase A<sub>2</sub> (cPLA<sub>2</sub>) (a known cytoplasmic substrate of ERK2)<sup>62</sup> when the ERK2 scaffold KSR1 is downregulated, and that the interaction of cPLA<sub>2</sub> and KSR1 is dependent on ERK2 activation, show that cPLA<sub>2</sub> interacts indirectly with KSR1 through ERK2. This same group showed that cPLA<sub>2</sub> binds to ERK2 at the FRS. Since ERK2 binds to KSR1 at this same site,<sup>63</sup> it is implied

---

<sup>60</sup> Adachi, M.; Fukuda, M.; Nishida, E. *EMBO J.* **1999**, *18*, 5347.

<sup>61</sup> Casar, B.; Pinto, A.; Crespo, P. *Mol. Cell*, **2008**, *31*, 708.

<sup>62</sup> Lin, L.; Wartmann, M.; Lin, A. Y.; Knopf, J. L.; Seth, A.; Davis, R. J. *Cell* **1993**, *72*, 269.

<sup>63</sup> Lee, T.; Hoofnagle, A. N.; Kabuyama, Y.; Stroud, J.; Min, X.; Goldsmith, E. J.; Chen, L.; Resing, K. A.; Ahn, N. G. *Mol. Cell* **2004**, *14*, 43.

that cPLA<sub>2</sub> binds indirectly to KSR1 through ERK2 dimers. Using the dimerization-deficient ERK2 H176E, L<sub>4</sub>A mutant, they maintain that dimerization is important for cytoplasmic substrate activation and that preventing cytosolic dimerization attenuates cellular proliferation, transformation, and tumor development. Monitoring the cytoplasmic and nuclear fractions of EGF-stimulated cells, they observed that ERK2 is mainly translocated to the nucleus as a monomer. Also, observing only the monomeric form of ERK2 when immunoprecipitated with endogenous transcription factors (Elk1, c-Fos, Fra) in EGF stimulated cells, they concluded that ERK2 dimerization is not a prerequisite either for nuclear translocation or for the activation of nuclear substrates.

Using FRET (fluorescent resonance energy transfer) measurements, Burack and Shaw showed<sup>64</sup> that the dimerization-deficient ERK2 H176E, L<sub>4</sub>A mutant fused to yellow fluorescent protein translocates normally into the nucleus of HEK 293 cells. Similarly, Lidke et al. found<sup>65</sup> by fluorescence correlation spectroscopy and energy migration Förster resonance energy transfer measurements that the dimerization-deficient the GFP-ERK1-Δ4 mutant accumulates in the nucleus to the same extent as wild-type GFP-ERK1, thus confirming that dimerization of ERK1 is not required for its translocation or retention in the nucleus. The difference in shuttling was concluded rather to be a consequence of the slower rate of phosphorylation of the mutant, the delay in cytoplasmic activation of ERK being directly translated into a delay in nuclear translocation.

---

<sup>64</sup> Burack, W. R.; Shaw, A. S. *J. Biol. Chem.* **2005**, *280*, 3832.

<sup>65</sup> Lidke, D. S.; Huang, F.; Post, J. N.; Rieger, B.; Wilsbacher, J.; Thomas, J. L.; Pouyssegur, J.; Jovin, T. M.; Lenormand, P. *J. Biol. Chem.* **2010**, *285*, 3092.

The formation of ERK2 dimers under physiological conditions by native, active ERK2 has been questioned.<sup>66</sup> Because the His<sub>6</sub>-tag of a protein can both promote self-association<sup>67,68</sup> and interact with possible trace amounts of nickel or cobalt from the purification,<sup>69</sup> the Dalby group cleaved the His<sub>6</sub>-tag for their re-evaluation study. The ability of tagless ERK2 to dimerize was measured by gel filtration followed by dynamic light scattering, and the shoulder to the main peak from gel filtration was interpreted as a different conformation of ERK2, affecting the Stokes radius but not differing significantly in molar mass from a monomer. Tagless ERK2 also behaves like a monomer in sedimentation equilibrium experiments. That phosphorylated ERK2 is monomeric in solution is further argued by measuring the translational diffusion coefficient for activated ERK2 using <sup>1</sup>H NMR. Activated tagless ERK2 diffuses faster than BSA (66 kDa) and slower than lysozyme (14.7 kDa), again supporting the idea that ERK2 is a monomer in solution. The Dalby group further put into question the idea that cytoplasmic scaffolds mediate the dimerization of ERK2. Using multiangle light scattering (MALS), a titration of ERK2 and the cytoplasmic scaffold PEA-15 was seen to support a 1:1 stoichiometry. They also suggest caution when using the dimerization-deficient mutants derived from the crystal structure of ERK2 since these exhibit impeded nuclear translocation independent of dimerization<sup>70</sup> and the similar ERK1

---

<sup>66</sup> Kaoud, T. S.; Devkota, A. K.; Harris, R.; Rana, M. S.; Abramczyk, O.; Warthaka, M.; Lee, S.; Girvin, M. E.; Riggs, A. F.; Dalby, K. N. *Biochemistry* **2011**, *50*, 4568.

<sup>67</sup> Wu, J.; Filutowicz, M. *Acta Biochim. Pol.* **1999**, *46*, 591.

<sup>68</sup> Amor-Mahjoub, M.; Suppini, J. P.; Gomez-Vrielyunck, N.; Ladjimi, M. *J. Chromatogr., B: Anal. Technol. Biomed. Life Sci.* **2006**, *844*, 328.

<sup>69</sup> Ueda, E. K.; Gout, P. W.; Morganti, L. *J. Chromatogr., A* **2003**, *988*, 1.

<sup>70</sup> Casar, B.; Arozarena, I.; Sanz-Moreno, V.; Pinto, A.; Agudo-Ibanez, L.; Marais, R.; Lewis, R. E.; Berciano, M. T.; Crespo, P. *Mol. Cell. Biol.* **2009**, *29*, 1338.

mutations are unrecognizable by a phospho-specific antibody (which however should be expected since the activation loop is mutated).<sup>71</sup>

## A NATURALLY OCCURRING MUTATION OF ERK2

The regulation of cellular processes through signaling ultimately depends on the interaction of proteins. When these interactions are disrupted, so too is the increase or decrease in regulation of a particular signal as is the case in many diseases. While there are various factors that can inhibit protein-protein interaction, from simple localization to absence of mediating scaffold proteins, a direct cause arises from conformational changes in the docking domain of one of the proteins. Much of the early analysis of signaling between cells mediated by interactions with receptor protein tyrosine kinases (rPTKs) was conducted in *Drosophila melanogaster* and *Caenorhabditis elegans* facilitated by powerful genetics. The study of these signaling pathways has led to the elucidation of mammalian pathways as well because there exists a striking homology across phyla.

### **The Sevenmaker gain-of-function mutation: ERK2 D319N**

The compound eye of *Drosophila* is made up of about 800 hexagonal units called ommatidia each consisting of eight photoreceptor cells (R1-R8). In the order of development of the photoreceptors, R8 appears first, followed by R2-R6, and then R7. R2-R6 are arranged in a

---

<sup>71</sup> Philipova, R.; Whitaker, M. J. *Cell Sci.* **2005**, *118*, 5767.

trapezoid surrounding R7 and R8, with R8 located under R7. The development of R7, which allows for the detection of UV light,<sup>72</sup> requires the product of two genes, *sevenless* (*sev*) and *bride-of-sevenless* (*boss*). The product of *sev*, a rPTK,<sup>73</sup> is required only in the R7 precursor, whereas *boss* function must be expressed in the developing R8. When R7 is being specified, the product of *boss*, a glycoprotein with a large extracellular domain and seven transmembrane segments related to the metabotropic receptors,<sup>74</sup> is only present on R8.<sup>75</sup> The binding of Boss (the ligand) to Sev (the rPTK) leads to kinase activation that determines the fate of the R7 cell, with the R7 precursor developing into a nonneuronal cone cell in the absence of a functional sevenless rPTK.<sup>76</sup> Activation of the receptor leads multiple ommatidial precursor cells developing into R7 cells.<sup>77</sup>

A simple behavioral test can be used to detect whether a fly has functional R7 cells. When given the choice between ultraviolet and a visible light, wild type flies will move towards the UV light source. Flies lacking R7 cells, however, will move towards the visible light.<sup>78</sup> This behavioral test was used to identify dominant mutations resulting in the prevention of R7 photoreceptor cell development (which led to the identification of *sev*<sup>79</sup> and *boss*<sup>80</sup>). The test was also used to screen for the activation of the *sev* signal transduction pathway in the absence of the

---

<sup>72</sup> Harris, W. A.; Stark, W. S.; Walker, J. A. *J. Physiol.* **1976**, *256*, 415.

<sup>73</sup> Hafen, E.; Basler, K.; Edstroem, J. E.; Rubin, G. M. *Science*, **1987**, *236*, 55.

<sup>74</sup> Hart, A. C.; Kramer, H.; Van Vactor, D. L.; Paidhungat, M.; Zipursky, S. L. *Genes Dev.* **1990**, *4*, 1835.

<sup>75</sup> Kramer, H.; Cagan, R. L.; Zipursky, S. L. *Nature* **1991**, *352*, 207.

<sup>76</sup> Tomlinson, S.; Ready, D. F. *Science* **1986**, *231*, 400.

<sup>77</sup> Basler, K.; Christen, B.; Hafen, E. *Cell* **1991**, *64*, 1069.

<sup>78</sup> Harris, W. A.; Stark, W. S.; Walker, J. A. *J. Physiol.* **1976**, *256*, 415.

<sup>79</sup> Harris, W. A.; Stark, W. S.; Walker, J. A. *J. Physiol.* **1976**, *256*, 415.

<sup>80</sup> Reinke, R.; Zipursky, S. L. *Cell* **1988**, *55*, 321.

*boss* protein, that is, for a gain-of-function mutation.<sup>81</sup> This gain-of-function mutation, named the *Sevenmaker* (*Sem*) mutation, was seen to induce formation of R7 cells independent of *boss* and *sev* function. The *Sevenmaker* mutation was shown to be a D334N substitution in the C-terminal end of L16 (kinase domain XI) that is conserved in the MAPK family.<sup>82</sup>

There are striking homologies that exist between this *Drosophila* signaling pathway and the ERK1/2 signaling pathway in mammals,<sup>83</sup> with the activation of Ras1 observed as an early consequence of *Sev* activity<sup>84</sup> and DmERKA identified as the ortholog of ERK1/2.<sup>85</sup> So too, for the *Sevenmaker* mutation in *Drosophila* there is an analogous mutation in mammalian ERK2, with an aspartate to asparagine substitution at amino acid residue 319.

The study of how this mutation leads to increased activity showed that it was not a constitutive form of ERK2, but rather that it had a reduced sensitivity to being dephosphorylated.<sup>86</sup> That gain-of-function was not a consequence of constitutive activation was determined by showing, by kinase assays of both immunoprecipitated protein from COS-1 cells and recombinant protein from bacteria, that basal kinase activity was no higher in ERK2 D319N than in wild type ERK2. To then determine if the gain-of-function was due to an increase in its response to signaling, and because it had previously been shown that transfection of oncogenic H-Ras or Raf leads to increased expression from the *c-fos* promoter in transient expression

---

<sup>81</sup> Brunner, D.; Oellers, N.; Szabad, J.; Biggs, W. H.; Zipursky, S. L.; Hafen, E. *Cell* **1994**, *76*, 875.

<sup>82</sup> Hanks, S. K.; Quinn, A. M.; Hunter, T. *Science* **1988**, *241*, 42.

<sup>83</sup> Gomperts, B. D.; Kramer, I. M.; Tatham, P. E. R. *Signal Transduction* **2009**, Elsevier, Burlington, MA, p. 328-331.

<sup>84</sup> Fortini, M. E.; Simon, M. A.; Rubin, G. M. *Nature* **1992**, *355*, 559.

<sup>85</sup> Biggs, W. H.; Zipurski, S. L. *Proc. Natl. Acad. Sci. U.S.A.* **1992**, *89*, 6295.

<sup>86</sup> Bott, C. M.; Thorneycroft, S. G.; Marshall, C. J. *FEBS Lett.* **1994**, *352*, 201.

systems,<sup>87</sup> they transfected NIH 3T3 cells with wild type and mutant ERK2. When no effect on c-fos driven luciferase activity was observed, they cotransfected the cells with oncogenic Raf and observed a 12-fold potentiated response with ERK2 D319N but no potentiation with wild type. Increased substrate specificity of ERK2 D319N for substrates was ruled out as an explanation for increased activity by observing decreased *in vitro* phosphorylation of Elk-1, MBP and c-jun compared to wild type. Nor was ERK2 D319N activated by lower levels of upstream kinase as shown by testing the activation of ERK2 with five different concentrations of the constitutively active<sup>88</sup> S217/221E MEK1. Finally, while both wild type and mutant were dephosphorylated in a dose-dependent manner, and ultimately to the same extent, by the phosphatase CL100 (also known as MKP-1), the mutant was significantly less susceptible to inactivation. At 0.5 µg/mL CL100, for instance, ERK2 D319N was only 53% inactivated compared with 80% for the wild type.

The ERK2 D319N mutant was also shown to be more resistant to deactivation by the dual-specific phosphatases PAC1 and MKP-2.<sup>89</sup> PAC1 is specific for ERK1/2 and p38; MKP-1 for ERK1/2, p38 and JNK; MKP-2 for ERK1/2 and JNK. ERK2 wild type and mutant were cotransfected with PAC1, MKP-1, or MKP-2 into HeLa cells, which, after 48 hours, were stimulated by EGF for 5 min and their kinase activities measured towards myelin basic protein (MBP). ERK2 D319N was resistant to inactivation in all three cases, whereas the wild type ERK2 was inactivated to near background levels.

---

<sup>87</sup> Bruder, J. T.; Heidecker, G.; Rapp, U. R. *Genes Dev.* **1992**, *6*, 545.

<sup>88</sup> Cowley, S.; Paterson, H.; Kemp, P.; Marshall, C. J. *Cell* **1994**, *77*, 1.

<sup>89</sup> Chu, Y.; Solski, P. A.; Khosravi-Far, R.; Der, C. J.; Kelly, K. *J. Biol. Chem.* **1996**, *271*, 6497.

Similar results were also shown with the ERK1/2-specific dual phosphatase, MKP-3.<sup>90</sup> In this study, binding between the phosphatase and ERK2 D319N was seen to be deficient as observed when wild type and mutant GST-tagged ERK2 immobilized on glutathione-Sepharose beads were incubated with His-tagged MKP-3. Having discovered that ERK2 is required to stimulate MKP-3 activity, they tested with *para*-nitrophenylphosphate (*p*-NPP) hydrolysis by MKP-3 and observed that D319N stimulates MKP-3 phosphatase activity only 10 to 15% as well as wild type ERK2. This was not a result of misfolding of the mutant protein since it was equally effective in phosphorylating MBP. The observations from this study led to the conclusion that mutations either in MKP-3 or ERK2 that interfere with binding would also lead to MAPK resistance to inactivation. Because the vast majority of side chain contacts in the ERK2/MKP-3 complex have been identified, from the co-crystallization of ERK2 with the MKP-3 KIM peptide, as arising from R65 of MKP-3 and D319 of ERK2, it stands to reason that mutation at this residue could lead to reduced interaction between these two proteins.<sup>91</sup>

The effect that this mutation has on binding has also been used to explain its interaction with substrates. It has been shown that the ERK2 D319N mutation increases the  $K_D$  for ELK-1, which has both a D motif and an FXF motif, by 14-fold and increases the  $K_D$  for RSK-1, which has only a D motif, by 7-fold. Mutations in the CD/ED region, however, did not affect the ability of ELK-1 to be phosphorylated on S383 that is dominated instead by interactions with the FRS. Along with inhibiting binding to ERK2, mutations in the CD/ED region were sufficient to block

---

<sup>90</sup> Camps, M.; Nichols, A.; Gillieron, C.; Antonsson, B.; Muda, M.; Chabert, C.; Boschert, U.; Arkinstall, S. *Science* **1998**, *280*, 1262.

<sup>91</sup> Liu, S.; Sun, J. P.; Zhou, B.; Zhang, Z. Y. *Proc. Natl. Acad. Sci. U. S. A.* **2006**, *103*, 5326.

phosphorylation of RSK-1 at T573, though FRS mutations (at L198 and L235) were also potent inhibitors of phosphorylation by ERK2 despite having no effect on binding.<sup>92</sup>

Interestingly, the Rolled<sup>D334N</sup> mutation in *Drosophila melanogaster* and the ERK2 D319N homolog have been observed to act synergistically with an R80S or R65S mutation respectively to accelerate autophosphorylation activity.<sup>93</sup> The arginine 65 residue of ERK2 is thought to be important for catalysis by stabilizing the active site, with R65 making contacts with T183 through a water molecule in the dually activated form. However, a serine seems to reorient the C-helix towards the phosphorylation lip even in the unphosphorylated state. The double mutant ERK2<sup>R65S + D319N</sup> is significantly more active than the single mutant ERK2 R65S and has about 43% of the activity of MEK1-activated ERK2 wild type. Mass spectrometry analysis showed that both the single and double mutant are dually phosphorylated on T183 and Y185. The mechanism for the effect of ERK2 D319N on catalysis and, more specifically, autoactivation is unknown.

### **An oral squamous cancer cell mutation: ERK2 E322K**

The catalog of somatic mutations in cancer (COSMIC) database ([www.cancer.sanger.ac.uk/cosmic](http://www.cancer.sanger.ac.uk/cosmic)) lists a tumor sample from upper aerodigestive tract tissue

---

<sup>92</sup> Burkhard, K. A.; Chen, F.; Shapiro, P. *J. Biol. Chem.* **2011**, 286, 2477.

<sup>93</sup> (a) Levin-Salomon, V.; Kogan, K.; Ahn, N. G.; Livnah, O.; Engelberg, D. *J. Biol. Chem.* **2008**, 283, 34500. (b) Emrick, M. A.; Hoofnagle, A. N.; Miller, A. S.; Eyck, L. F. T.; Ahn, N. G. *J. Biol. Chem.* **2001**, 276, 46469.

having an ERK2 D321N mutation (which is the human homolog of the ERK2 D319N).<sup>94</sup> The COSMIC database also lists two additional tumor samples having ERK2 E322K (equivalent to E320K in rat) mutations that arise from substitution missense (964G>A). Like D319N, the E320K mutation is found in the CD domain of ERK2 and could thus have similar effects on protein-protein interactions. Both of the ERK2 E322K containing tumor samples are squamous cell carcinomas, one from cervical tissue and the other from esophageal tissue.<sup>95</sup>

The ERK2 E322K mutation was originally discovered in the oral squamous cell carcinoma cell line, HSC6, by observing a faster-migrating band in denaturing gels that was then identified by PCR amplification of cDNA, cloning and sequencing.<sup>96</sup> By using comparative genetic hybridization, 22q11.2-12 had already been detected as a DNA amplification site in HSC6 and 2 other head and neck squamous cell carcinoma cell lines.<sup>97</sup> Using fluorescence in situ hybridization (FISH) analysis, 22q11.2-12 was then mapped in greater detail to define the minimum commonly amplified region in the HSC6 cell line.<sup>98</sup> The *ERK2* gene (called *MAPK1*,

---

<sup>94</sup> Agrawal, N.; Frederick, M. J.; Pickering, C. R.; Bettegowda, C.; Chang, K.; Li, R. J.; Fakhry, C.; Xie, T. X.; Zhang, J.; Wang, J.; Zhang, N.; El-Naggar, A. K.; Jasser, S. A.; Weinstein, J. N.; Treviño, L.; Drummond, J. A.; Muzny, D. M.; Wu, Y.; Wood, L. D.; Hruban, R. H.; Westra, W. H.; Koch, W. M.; Califano, J. A.; Gibbs, R. A.; Sidransky, D.; Vogelstein, B.; Velculescu, V. E.; Papadopoulos, N.; Wheeler, D. A.; Kinzler, K. W.; Myers, J. N. *Science* **2011**, *333*, 1154.

<sup>95</sup> Agrawal, N.; Jiao, Y.; Bettegowda, C.; Hutfless, S. M.; Wang, Y.; David, S.; Cheng, Y.; Twaddell, W. S.; Latt, N. L.; Shin, E. J.; Wang, L. D.; Wang, L.; Yang, W.; Velculescu, V. E.; Vogelstein, B.; Papadopoulos, N.; Kinzler, K. W.; Meltzer, S. J. *Cancer Discov.* **2012**, *10*, 899.

<sup>96</sup> Arvind, R.; Shimamoto, H.; Momose, F.; Amagasa, T.; Omura, K.; Tsuchida, N. *Int. J. Oncol.* **2005**, *27*, 1499.

<sup>97</sup> Matsumura, K. *J. Stomatol. Soc. Jpn* **1995**, *62*, 513.

<sup>98</sup> Matsumura, K.; Iritani, A.; Enomoto, S.; Torikata, C.; Matsuyama, S.; Kurita, A.; Kurahashi, H.; Tsuchida, N. *Genes Chromosomes Cancer* **2000**, *29*, 207.

*PRKMI* – protein kinase, mitogen-activated 1, or *P41MAPK*) maps within the region that was identified as the amplicon.

Besides migrating faster than wild type on a denaturing gel, the ERK2 E322K mutant was readily detected by anti-phospho ERK1/2 (pERK1/2) antibody after 48 hours of serum starvation. Wild type ERK2, on the contrary, was barely detected or detected at a low level. Pretreatment of HSC6 cells with the MEK inhibitor U0126 blocked phosphorylation of both mutant and wild type in both cells that were serum-starved or that were stimulated with EGF after the starvation. These results were interpreted as suggesting that the mutant ERK2 was phosphorylated by MEK1/2 and that the phosphorylation was relatively constitutive. Additionally, as with ERK2 D319N, the dephosphorylation of the mutant was observed to be slower. While MKP-1 binds to wild type ERK2, the phosphatase scarcely binds to the mutant. Thus, the constitutive phosphorylation of ERK2 E322K was suggested to be a result of loss of interaction with MKPs.<sup>99</sup>

A study of how nuclear import of ERK2 is affected by mutations in the CD domain showed that both ERK2 D316A/D319A and ERK2 E320K were imported equally well as the wild type in both their unphosphorylated and phosphorylated states.<sup>100</sup> In this same study, the unphosphorylated ERK2 E320K had a 15-20 fold higher ‘basal’ specific activity towards MBP than wild type ERK. The specific activity of phosphorylated ERK2 E320K, however, was similar to phosphorylated wild type ERK2.

---

<sup>99</sup> Mahalingam, M.; Arvind, R.; Ida, H.; Murugan, A. K.; Yamaguchi, M.; Tsuchida, N. *Oncol. Rep.* **2008**, *20*, 957.

<sup>100</sup> Yazicioglu, M. N.; Goad, D. L.; Ranganathan, A.; Whitehurst, A. W.; Goldsmith, E. J.; Cobb, M. H. *J. Biol. Chem.* **2007**, *282*, 28759.

The ERK2 D319N mutation has been used in most studies that have looked at protein interactions with the CD domain of ERK2, whereas the E320K mutation that was found in a human cancer cell line has been far less studied. While occurring in neighboring residues, there are two important structural observations to be made. First, the glutamate to lysine mutation involves a change in charge. This is significant in that binding of substrates to the CD domain of ERK2 is charge dependent. Secondly, the wild type glutamate residue points in towards the core of ERK2, thus the change of charge mutation could also affect protein stability or at least the stability of the docking loop. Besides the effects that the mutation has on binding, there is also the question of whether the mutation also has an effect on catalysis through increased autoactivation. These features make the ERK2 E320K an interesting subject for study.

## **CHAPTER TWO**

### **Comparative Characterization of ERK2 E320K**

#### **ABSTRACT**

The ERK1/2/MAPK signalling pathway is important in the control of growth, cell survival and differentiation. ERK2 is activated by dual phosphorylation on threonine 185 and tyrosine 187 residues, and activity is decreased by dephosphorylation at these same residues. A mutant of ERK2 that is less easily dephosphorylated than wild type, discovered in HSC6, a human oral squamous cell carcinoma cell line, consists of a substitution of a lysine for a glutamic acid residue in the common docking domain, E322K in human ERK2 or E320K in the homologous protein sequence from rat. The common docking domain is a conserved domain among members of the MAPK family used for docking to their activators, inactivators, and substrates. Due to the change in charge between the two residues involved in this substitution, there is significant disorder in the common docking domain of the mutant protein. The structural perturbations induced by this mutation are modeled using both crystal structure data and molecular dynamics simulations. The effects of this mutation on the interaction with both upstream and downstream regulators are also examined by yeast two-hybrid and SILAC experiments and the activity characterized by kinase and phosphatase assays.

## INTRODUCTION

ERK2 is a component of the MAPK signaling pathway that is responsible for the control of many cellular processes including cell differentiation, proliferation and apoptosis, as well as cellular responses to environmental stress and various hormones.<sup>101</sup> In order to become fully active, ERK2 must be dually phosphorylated on threonine 183 and tyrosine 185.<sup>102</sup> Inactivation of ERK2 requires dephosphorylation at these same two residues, a task that is achieved by either the combination of a serine/threonine-specific phosphatase together with a tyrosine-specific phosphatase or by a dual-specificity phosphatase or MAPK phosphatase (MKP) such as MKP-3 that dephosphorylates both residues.

All of the dual-specificity phosphatases contain a MAPK binding domain and a phosphatase domain with a short linker of about 40 amino acid residues between them. Specificity for the MAPK family is partially achieved by dual-specificity MKPs through their N-terminal MAPK binding domain,<sup>103</sup> also known as the kinase interaction motif (KIM). This domain contains a cluster of positively charged amino acids and hydrophobic residues that interact with the CD domain of ERKs, p38, and JNK,<sup>104</sup> such that the canonical sequence for the

---

<sup>101</sup> (a) Chen, Z.; Gibson, T. B.; Robinson, F.; Silvestro, L.; Pearson, G.; Xu, B.; Wright, A.; Vanderbilt, C.; Cobb, M. H. *Chem. Rev.* **2001**, *101*, 2449. (b) Ray, L. B.; Sturgill, T. W. *Proc. Natl. Acad. Sci. U. S. A.* **1988**, *85*, 3753.

<sup>102</sup> Robbins, D. J.; Zhen, E.; Owaki, H.; Vanderbilt, C.; Ebert, D.; Geppert, T. D.; Cobb, M. H. *J. Biol. Chem.* **1993**, *268*, 5097.

<sup>103</sup> Muda, M.; Theodosiou, A.; Gilleron, C.; Smith, A.; Chabert, C.; Camps, M.; Boschert, U.; Rodrigues, N.; Davies, K.; Ashworth, A.; Arkinstall, S. *J. Biol. Chem.* **1998**, *273*, 9323.

<sup>104</sup> Kondoh, K.; Nishida, E. *Biochim. Biophys. Acta* **2007**, *1773*, 1227.

KIM is  $\Phi\Phi$ -X-RR $\Phi$ -XX-G. The CD domain, on the other hand, is conserved in all MAPKs and is made up largely of acidic residues, DXX(D/E).<sup>105</sup>

The dual dephosphorylation of ERK2 by MKP-3 was found to be ordered and distributive.<sup>106</sup> Interestingly, the interaction of the KIM with the MAPK substrate induces phosphatase activity, with MKP-3 phosphatase activity stimulated 30-fold by forming a complex with ERK2.<sup>107</sup> This stimulation of phosphatase activity occurred even when a kinase-dead mutant of ERK2 was used, but did not occur with an MKP-3 mutant lacking a KIM. Unlike many other phosphatases, MKP-3 does not require ERK2 to be phosphorylated for binding nor to induce the conformational change in MKP-3 that renders it active.

The regulation of cellular processes through signaling ultimately depends on the interaction of proteins. When these interactions are disrupted, so too is the up- or down-regulation of a particular signal, as is the case in many diseases. While there are various factors that can inhibit protein-protein interaction, from simple localization to absence of mediating scaffold proteins, a direct cause arises from conformational changes in the docking domain of one of the proteins.

The COSMIC database lists two tumor samples having ERK2 E322K (equivalent to E320K in rat) mutations that arise from substitution missense (964G>A). This E320K mutation is found in the CD domain of ERK2 and could thus have detrimental effects on protein-protein interactions. Both of the tumor samples are squamous cell carcinomas, one from cervical tissue

---

<sup>105</sup> Tanoue, T.; Adachi, M.; Moriguchi, T.; Nishida, E. *Nat. Cell Biol.* **2000**, *2*, 110.

<sup>106</sup> Zhao, Y.; Zhang, Z. Y. *J. Biol. Chem.* **2001**, *276*, 32382.

<sup>107</sup> Camps, M.; Nichols, A.; Gillieron, C.; Antonsson, B.; Muda, M.; Chabert, C.; Boschert, U.; Arkininstall, S. *Science* **1998**, *280*, 1262.

and the other from esophageal tissue.<sup>108</sup> The mutation was originally discovered in the oral squamous cell carcinoma cell line, HSC6, by observing a faster-migrating band on denaturing gels that was then identified by PCR amplification of cDNA, cloning and sequencing.<sup>109</sup>

These results were interpreted as suggesting that the mutant ERK2 was phosphorylated by MEK and that the phosphorylation was relatively constitutive. Additionally, the dephosphorylation of the mutant was observed to be slower. While MKP-1 binds to wild type ERK2, the phosphatase scarcely binds to the mutant. Thus, the constitutive phosphorylation of ERK2 E322K was suggested to be a result of loss of interaction with MKPs.<sup>110</sup>

The ERK2 D319N mutation, that is located in the neighboring residue and referred to as the Sevenmaker mutation, has been used in most studies that have looked at protein interactions with the CD domain of ERK2. The E320K mutation, however, that was found in a human cancer cell line has been far less studied. There are two important structural observations to be made in comparing these two mutations. First, the glutamate to lysine mutation involves a change in charge. This is significant in that binding of substrates to the CD domain of ERK2 is charge dependent. Second, the wild type glutamate residue points in towards the core of ERK2, thus the change-of-charge mutation could also affect protein stability or at least the stability of the docking loop. These features make the ERK2 E320K an interesting subject for study.

---

<sup>108</sup> Agrawal, N.; Jiao, Y.; Bettegowda, C.; Hutfless, S. M.; Wang, Y.; David, S.; Cheng, Y.; Twaddell, W. S.; Latt, N. L.; Shin, E. J.; Wang, L. D.; Wang, L.; Yang, W.; Velculescu, V. E.; Vogelstein, B.; Papadopoulos, N.; Kinzler, K. W.; Meltzer, S. J. *Cancer Discov.* **2012**, *10*, 899.

<sup>109</sup> Arvind, R.; Shimamoto, H.; Momose, F.; Amagasa, T.; Omura, K.; Tsuchida, N. *Int. J. Oncol.* **2005**, *27*, 1499.

<sup>110</sup> Mahalingam, M.; Arvind, R.; Ida, H.; Murugan, A. K.; Yamaguchi, M.; Tsuchida, N. *Oncol. Rep.* **2008**, *20*, 957.

## EXPERIMENTAL PROCEDURES

### Plasmid DNA constructs

Construction of pVJL11-ERK2: The ERK2 cDNA from pGAD-ERK2<sup>111</sup> was PCR amplified using oligonucleotides (forward 5'-GATCGGATCCCATGGCGGCGGCGGCGGCGGCGGGC-3') and (reverse 5'-GATCCTGCAGTTAAGATCTGTATCCTGGCTGGAA-3') and the resulting DNA fragment was digested with *Bam*HI and *Pst*I and ligated into pVJL11<sup>112</sup> which had been cut with the same enzymes. The resulting construct encodes full-length ERK2 fused to the C terminus of the pVJL11 DNA-binding domain.

Construction of pGAD-ERK2 E320K, pET-His<sub>6</sub>-MEK1 R4F+ERK2 E320K, CMV-FLAG-ERK2 E320K, and pVJL11-ERK2 E320K: The wild type pGAD-ERK2, pET-His<sub>6</sub>-MEK1 R4F+ERK2<sup>113</sup>, CMV-FLAG-ERK2, or pVJL11-ERK2 was mutagenized by PCR using the QuikChange method from Stratagene using oligonucleotides (forward 5'-GACCCAAGTGATAAGCCCATTGCTGAAGCACC-3') and (reverse 5'-GGTGCTTCAGCAATGGGCTTATCACTTGGGTC-3').

All plasmid constructs were sequenced to confirm that spurious mutations were not introduced.

---

<sup>111</sup> Robinson, F. L.; Whitehurst, A. W.; Raman, M.; Cobb, M. H. *J. Biol. Chem.* **2002**, *277*, 14844.

<sup>112</sup> Jullien-Flores, V.; Dorseuil, O.; Romero, F.; Letourneur, F.; Saragosti, S.; Berger, R.; Tavitian, A.; Gacon, G.; Camonis, J. H. *J. Biol. Chem.* **1995**, *270*, 22473.

<sup>113</sup> Khokhlatchev, A.; Xu, S.; English, J.; Wu, P.; Shaefer, E.; Cobb, M. H. *J. Biol. Chem.* **1997**, *272*, 11057.

## Protein Expression and Purification

His<sub>6</sub>-tagged ERK2 and ERK2 E320K proteins were expressed in *E. coli* (BL21 DE3) using the NpT7-His<sub>6</sub>-ERK2 wild type and ERK2 E320K (prepared by Daryl Goad) constructs. The starter culture was made by inoculating 50 mL liquid Luria-Bertani (LB) medium containing 100 µg/mL ampicillin with a single colony. The starter culture was first incubated overnight at 37°C with shaking and then 10 mL of it was used to inoculate 1L of LB medium containing 100 µg/mL ampicillin. The 1L culture was grown with shaking at 290 rpm at 30°C until OD<sub>600</sub>=0.8 and then induced with 0.4 mM isopropyl-1-thio-β-D-galactopyranoside (IPTG). The culture was grown at 30°C in a 260 rpm shaker for 7 hours. The cells were harvested by centrifugation in Beckman J21B rotor at 3,500 rpm for 40 min at 4°C and then resuspended in 20 mL of buffer containing 20 mM Tris, pH 8.0, 0.5 M NaCl, 1 mM β-mercaptoethanol (β-ME), 5 mM imidazole. To this was added 50 µL of protease inhibitor cocktail (in 62.5 mL of DMSO: 25 mg of pepstatin A, 25 mg of leupeptin, 250 mg of N<sub>α</sub>-p-tosyl-L-arginine methyl ester, 250 mg of N<sub>α</sub>-p-tosyl-L-lysine chloromethyl ketone hydrochloride, 250 mg of N<sub>α</sub>-Benzoyl-L-arginine methyl ester, and 250 mg of soybean trypsin inhibitor). The resuspended cell pellets were frozen in liquid nitrogen and stored at -80°C until processed. The cell pellets were then thawed at 4°C and disrupted with 10 mg/mL of lysozyme and sonication. Cell debris was removed by centrifugation at 35,000 rpm for 45 min at 4°C in a Beckman centrifuge Ti45 rotor. The supernatant was passed through a 0.22 µm filter and incubated with 3 mL of Ni<sup>2+</sup> bead slurry at 4°C for 1 hour and then poured into a column. The column was washed with the binding buffer (20 mM Tris, pH 8.0, 0.5 M NaCl, 1 mM β-ME, 5 mM imidazole) until no further protein could be detected exiting the

column by Bradford assay. The column was then washed with 25 mM imidazole in binding solution until protein was no longer detected as above. The protein was then eluted with 250 mM imidazole in binding solution. Pooled fractions were dialyzed overnight in MonoQ buffer A (50 mM Tris, pH 8.0, 100 mM NaCl, 1 mM DTT, 0.1 mM PMSF). The protein was concentrated and loaded onto a MonoQ column and eluted with a NaCl gradient. The collected fractions were dialyzed overnight in ERK2 storage buffer (20 mM Tris pH 7.5, 50 mM NaCl, 1 mM DTT, 10% glycerol), frozen in liquid nitrogen and stored at -80°C.

ERK2 was activated *in vivo* by coexpressing ERK2 and MEK1 R4F,<sup>114</sup> a constitutively active MEK1 (Khokhlatchev et al., 1997).<sup>115</sup> The coexpression plasmid was used to transform competent Origami *E. coli* (EMD Millipore). An overnight culture was grown in 30 ml LB, 100 µg/ml ampicillin. Six liters of Terrific Broth (TB) medium was inoculated, and the culture grown at 30°C, and induced with 0.5 mM IPTG when OD<sub>600</sub> = 0.8 was reached. Cultures were grown for 12 to 16 hours after induction. The cells were flash frozen in liquid nitrogen and resuspended later in buffer (50 mM sodium phosphate [pH 8.0], and 300 mM NaCl). Cells were lysed in 1 mg/ml lysozyme and 0.3% NP-40 using gentle sonication. The cell lysate was clarified by centrifugation at 100,000 g for 30 min at 4°C. His60 Ni Superflow Resin (Clontech) and a 20–250 mM imidazole gradient (pH 7.0) were used to separate ERK2 and pERK2 from other cell components. ERK2 and pERK2 were further separated on MonoQ 5/50 GL column (GE

---

<sup>114</sup> (a) Mansour, S.J.; Matten, W.T.; Hermann, A.S.; Candia, J.M.; Rong, S.; Fukasawa, K.; Vande Woude, G.F.; Ahn, N.G. *Science* **1994**, *265*, 966. (b) Mansour, S.J.; Candia, J.M.; Matsuuda, J.; Manning, M.; Ahn, N.G. *Biochemistry* **1996**, *35*, 15529.

<sup>115</sup> Khokhlatchev, A.; Xu, S.; English, J.; Wu, P.; Schaefer, E.; Cobb, M.H. *J. Biol. Chem.*, **1997**, *272*, 11057.

Lifesciences) and equilibrated with MonoQ buffer A: 20 mM Tris (pH 8.0), 1 mM EDTA, 0.2 mM EGTA, 1 mM DTT, 1 mM benzamidine, and 10% glycerol. The protein was eluted using a 50 ml gradient of 0–250 mM NaCl. Activity assays using myelin basic protein (MBP) as substrate and immunoblot analysis using anti-pERK2 antibody (Sigma) verified the activity and double phosphorylation of the sample.

### **Kinase Assays with ERK2 as Substrate**

Protein concentration was determined using a NanoPhotometer (Implen). Protein kinases and substrates were incubated in 150  $\mu$ L of 10 mM Tris, pH 7.5, 10 mM  $MgCl_2$ , 50  $\mu$ M ATP, 0.01 mCi/ $\mu$ L [ $\gamma$ - $^{32}P$ ]ATP at room temperature. 20  $\mu$ L aliquots were transferred to tubes containing 5  $\mu$ L of 5x Laemmli sample buffer followed by heating for 5 min at 100°C for analysis by denaturing gels. The ERK2 bands were excised from the gels after staining and analyzed by liquid scintillation on a Beckman LS6500 with a 5 minute P32 window.

### **Kinase Assays with MBP as Substrate**

Phosphorylation reactions (20  $\mu$ L) containing 0.2-0.8  $\mu$ M (unphosphorylated) ERK2 and an excess of MEK1 R4F in kinase buffer (10 mM HEPES (pH 8.0), 10 mM  $MgCl_2$ , 1 mM benzamidine, 1 mM DTT, 50  $\mu$ M ATP) were incubated at 30°C for 1 hour and then placed on ice. Then MBP assays were initiated by the addition of 5  $\mu$ L the ERK2 phosphorylation reaction to 25  $\mu$ L of 0.67  $\mu$ g/ $\mu$ L of MBP, kinase buffer containing 216.6  $\mu$ M ATP, and 0.01 mCi/ $\mu$ L [ $\gamma$ - $^{32}P$ ]ATP. The reactions were incubated at 30°C for 1, 3, and 5 min for each of the four ERK2

concentrations. Reactions were stopped by the addition of 7.5  $\mu$ L of 5x Laemmli sample buffer followed by heating for 5 min at 100°C for analysis by denaturing gels. The MBP bands were excised from the gels after staining and analyzed by liquid scintillation on a Beckman LS6500 with a 1 minute P32 window.

### **Phosphatase Assays**

Recombinant MKP-3 (Enzo) 0.14 $\mu$ M was combined with 1  $\mu$ M recombinant pERK2 proteins (wild-type and E320K) in 10 mM HEPES (pH 8.0), 10 mM MgCl<sub>2</sub>, 1 mM benzamidine, 1 mM DTT and incubated for up to 1 h at room temperature. Aliquots were withdrawn at the indicated times and added to tubes containing 5x Laemmli sample buffer to terminate the reactions. The samples were then immunoblotted as described previously to examine the phosphorylation state of ERK2 using an pERK antibody (Sigma). Changes in the phosphorylation state of the ERK2 proteins were quantified by densitometry using a LiCor Odyssey.

### ***p*-NPP Hydrolysis Assays**

To a 96-well plate containing 1  $\mu$ L of wild type or mutant ERK2 (0.6 mg/mL) and 1  $\mu$ L of MKP-3 (0.4 mg/mL) was added by injection the assay buffer, consisting of 100 mM Tris, pH 7.5 and 40 mM NaCl and containing different concentrations of *p*-NPP. The production of *pNP* (para-nitrophenolate) was measured using a BioTek Synergy H1 multiplate reader at 405 nm.

## Yeast Two-Hybrid Experiments

Pair-wise interaction tests were carried out as follows. The yeast strain L40<sup>116</sup> was co-transformed with pGAD-ERK2 (or ERK2 E320K) and either the empty pVJL11 (LexA) vector or pVJL11-based constructs encoding LexA fusions with various sequences from rat ERK2, human MEK1, human MEK2, human MNK1, rat MKP-3, or chicken RSK using a Frozen-EZ Yeast Transformation II kit from Zymo Research. Co-transformants were selected by plating cells on complete supplemental medium (CSM) (US Biological #D9539) lacking Leu and Trp. Protein-protein interactions were tested by streaking co-transformed isolates on CSM lacking His, Leu and Trp and observing growth. All experiments were done in triplicate.

## SILAC

COS-7 cells were transfected with FLAG-tagged ERK2 wild type and E320K mutant. Transfections were performed three times over the one week culture period using a total of 9-12  $\mu$ g of plasmid. The cells were maintained in DMEM medium supplemented with 10% FBS. To generate two labeling states, the population of ERK2 wild type cells were grown in “light” SILAC medium containing L-<sup>12</sup>C<sub>6</sub><sup>14</sup>N<sub>4</sub> arginine (Arg0) and L-<sup>12</sup>C<sub>6</sub><sup>14</sup>N<sub>2</sub>-lysine (Lys0), whereas the ERK2 E320K population was grown in “heavy” SILAC medium containing L-<sup>13</sup>C<sub>6</sub><sup>15</sup>N<sub>4</sub> arginine (Arg10) and L-<sup>13</sup>C<sub>6</sub><sup>15</sup>N<sub>2</sub>-lysine (Lys8). All media were prepared at the same time, and cells to be labeled were cultured in parallel for one week and a total of six passages for a total of five 150 cm dishes of cells for each construct. Cells were lysed in 0.1% Triton X-100, 1

---

<sup>116</sup> Vojtek, A. B.; Hollenberg, S. M.; and Cooper, J. A. *Cell* **1993**, *74*, 205.

M HEPES, 300 mM NaCl. Immunoprecipitations used M2-FLAG-conjugated beads overnight at 4°C. Beads were washed with lysis buffer. Protein was stripped from beads using Laemmli sample buffer, loaded on denaturing gels, and sent for analysis.

### **X-ray crystallography**

Crystallization conditions<sup>117</sup> and the data set were obtained by Wen-Huang Ko. I obtained crystals using the same conditions she found. In hanging drops, 165  $\mu$ M ERK2 E320K in storage buffer (25 mM Tris-Cl, pH 7.5, 100 mM NaCl, 1 mM EDTA, 5 mM DTT) was mixed with an equal volume of reservoir solution containing 28% (w/v) PEG 1500, 0.1 M Tris-Cl, pH 8.0. Crystals were incubated at 20°C for 1 week. The dataset was collected at the Advanced Photon Source (APS) synchrotron x-ray facility. The data was scaled using HKL2000.<sup>118</sup> Starting phases were obtained by molecular replacement using coordinates of unphosphorylated ERK2 (PDB entry 1ERK) as the search model in the program PHENIX.<sup>119</sup> The model was built into electron density maps in COOT.<sup>120</sup> Cycles of refinement were carried out in PHENIX using 2.4Å data.

---

<sup>117</sup> Lee, S.-J.; Zhou, T.; Goldsmith, E. J. *Methods* **2006**, *40*, 224.

<sup>118</sup> Otwinowski, Z.; Minor, W. *Methods Enzymol.* **1997**, *276*, 307.

<sup>119</sup> Adams, P.D.; Afonine, P. V.; Bunkóczy, G.; Chen, V. B.; Davis, I. W.; Echols, N.; Headd, J. J.; Hung, L.-W.; Kapral, G. J.; Grosse-Kunstleve, R. W.; McCoy, A. J.; Moriarty, N. W.; Oeffner, R.; Read, R. J.; Richardson, D. C.; Richardson, J. S.; Terwilliger, T. C.; Zwart, P.H. *Acta Cryst. D.* **2010**, *66*, 213.

<sup>120</sup> Emsley, P.; Lohkamp, B.; Scott, W. G.; Cowtan, K. *Acta Cryst. D.* **2010**, *66*, 486.

## Molecular dynamics simulations

### *Force field parameterization*

For the phosphorylated residues, T183 and Y185, the alpha-helix and beta-sheet conformations of dipeptides (ACE-pTHR-NME and ACE-pTYR-NME) were constructed and submitted to run *ab initio* calculations at the HF/6-31G\* level in order to derive point charges. The *ab initio* calculations used the Gaussian 03 software package.<sup>121</sup> Then the RESP (Restrained Electrostatic Potential) charges were derived using the RESP program<sup>122</sup> in AMBER 12 taking the *ab initio* ESP as input.<sup>123</sup> The residue topologies were generated using the Antechamber module of AMBER12.<sup>124</sup>

---

<sup>121</sup> Gaussian 03, Revision E.01, M. J. Frisch, G. W. Trucks, H. B. Schlegel, G. E. Scuseria, M. A. Robb, J. R. Cheeseman, J. A. Montgomery, Jr., T. Vreven, K. N. Kudin, J. C. Burant, J. M. Millam, S. S. Iyengar, J. Tomasi, V. Barone, B. Mennucci, M. Cossi, G. Scalmani, N. Rega, G. A. Petersson, H. Nakatsuji, M. Hada, M. Ehara, K. Toyota, R. Fukuda, J. Hasegawa, M. Ishida, T. Nakajima, Y. Honda, O. Kitao, H. Nakai, M. Klene, X. Li, J. E. Knox, H. P. Hratchian, J. B. Cross, V. Bakken, C. Adamo, J. Jaramillo, R. Gomperts, R. E. Stratmann, O. Yazyev, A. J. Austin, R. Cammi, C. Pomelli, J. W. Ochterski, P. Y. Ayala, K. Morokuma, G. A. Voth, P. Salvador, J. J. Dannenberg, V. G. Zakrzewski, S. Dapprich, A. D. Daniels, M. C. Strain, O. Farkas, D. K. Malick, A. D. Rabuck, K. Raghavachari, J. B. Foresman, J. V. Ortiz, Q. Cui, A. G. Baboul, S. Clifford, J. Cioslowski, B. B. Stefanov, G. Liu, A. Liashenko, P. Piskorz, I. Komaromi, R. L. Martin, D. J. Fox, T. Keith, M. A. Al-Laham, C. Y. Peng, A. Nanayakkara, M. Challacombe, P. M. W. Gill, B. Johnson, W. Chen, M. W. Wong, C. Gonzalez, and J. A. Pople, Gaussian, Inc., Wallingford CT, 2004.

<sup>122</sup> Bayly, C. I.; Cieplak, P.; Cornell, W.; Kollman, P. A. *J. Phys. Chem.* **1993**, *97*, 10269.

<sup>123</sup> D.A. Case, T.A. Darden, T.E. Cheatham, III, C.L. Simmerling, J. Wang, R.E. Duke, R. Luo, R.C. Walker, W. Zhang, K.M. Merz, B. Roberts, S. Hayik, A. Roitberg, G. Seabra, J. Swails, A.W. Goetz, I. Kolossváry, K.F. Wong, F. Paesani, J. Vanicek, R.M. Wolf, J. Liu, X. Wu, S.R. Brozell, T. Steinbrecher, H. Gohlke, Q. Cai, X. Ye, J. Wang, M.-J. Hsieh, G. Cui, D.R. Roe, D.H. Mathews, M.G. Seetin, R. Salomon-Ferrer, C. Sagui, V. Babin, T. Luchko, S. Gusarov, A. Kovalenko, and P.A. Kollman (2012), *AMBER 12*, University of California, San Francisco.

<sup>124</sup> Wang, J.; Wang, W.; Kollman, P. A.; Case, D. A. *J. Mol. Graph. Model.* **2006**, *25*, 247.

### *Molecular Dynamics Simulations*

The Parm99SB biomolecular force field was used for all the molecular mechanics calculations.<sup>125</sup> All MD simulations were performed with the periodic boundary condition to produce isothermal-isobaric ensembles at 298.15 K using the Pmemd program in AMBER12. The Particle Mesh Ewald (PME) method was used to calculate the full electrostatic energy of a unit cell in a macroscopic lattice of repeating images.<sup>126</sup> The integration of the equations of motion was conducted at a time step of 2 femtoseconds. The covalent bonds involving hydrogen atoms were frozen with the SHAKE algorithm.<sup>127</sup> Temperature was regulated using Langevin dynamics with a collision frequency of 5 ps<sup>-1</sup>.<sup>128</sup> Pressure regulation was achieved with isotropic position scaling and the pressure relaxation time was set to 1.0 picosecond. After the systems were equilibrated for 20 ns, 4000 MD snapshots were recorded every 10 ps.

Three types of post-MD analysis were performed by Junmei Wang in order to investigate the dynamic properties of the ERK2 proteins: B-factor calculations, contact map analysis, and residue-residue correlation analysis.

---

<sup>125</sup> (a) Wang, J.; Cieplak, P.; Kollman, P. A. *J. Comp. Chem.* **2000**, *21*, 1049. (b) Hornak, V.; Abel, R.; Okur, A.; Strockbine, B.; Roitberg, A.; Simmerling, C. *Proteins* **2006**, *65*, 712.

<sup>126</sup> (a) Darden, T.; Perera, L.; Li, L.; Pedersen, L. *Structure* **1999**, *7*, R55. (b) Sagui, C.; Pedersen, L. G.; Darden, T. A. *J. Chem. Phys.* **2004**, *120*, 73.

<sup>127</sup> Miyamoto, S.; Kollman, P. A. *J. Comp. Chem.* **1992**, *13*, 952.

<sup>128</sup> Izaguirre, J. A.; Catarello, D. P.; Wozniak, J. M.; Skeel, R. D. *J. Chem. Phys.* **2001**, *114*, 2090.

## RESULTS

### Differences in Protein-Protein Interactions

Protein-protein interactions are at the basis of signaling in cells, messages that guide function being transmitted and regulated by chemical changes induced by these same interactions. I was therefore interested to know how the E320K mutation would affect the ability of ERK2 to interact and bind to other proteins.

#### *Yeast Two-Hybrid*

Because a yeast two-hybrid<sup>129</sup> screen had already been used by our lab to determine point mutations in ERK2 that disrupt binding to MEK1/2,<sup>130</sup> I used the same approach to see how the E320K mutation would alter ERK2 interactions with its binding partners. Constructs of MEK1/2, RSK, MKP-3 and their select mutations had been cloned into a pVJL11 vector that encodes the various proteins fused to the C terminus of the Lex A DNA-binding domain. I verified that all these constructs had the correct sequence and additionally subcloned MEK1 absent of the proline rich insert ( $\Delta$ PRI). By mutagenesis I also obtained ERK2 E320K cloned into the pGAD-GH<sup>131</sup> vector that encodes full-length ERK2 fused to the C terminus of the Gal4 transcription activation domain (GAD).

---

<sup>129</sup> Fields, S.; Song, O. *Nature* **1989**, *340*, 245.

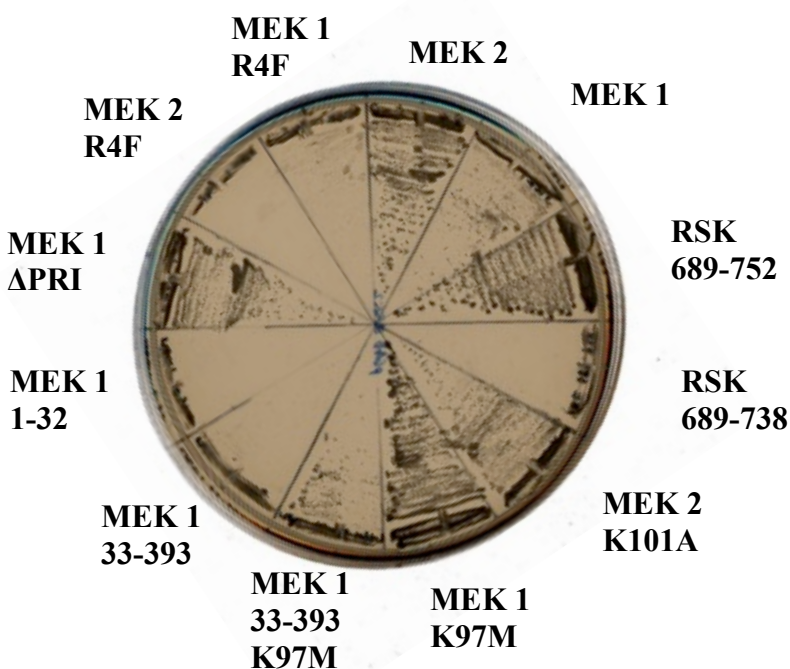
<sup>130</sup> Robinson, F. L.; Whitehurst, A. W.; Raman, M.; Cobb, M. H. *J. Biol. Chem.* **2002**, *277*, 14844.

<sup>131</sup> Van Aelst, L.; Barr, M.; Marcus, S.; Polverino, A.; Wigler, M. *Proc. Natl. Acad. Sci. U. S. A.* **1993**, *90*, 6213.

Our results for the interaction of ERK2 wild type with the various interactors replicates Fred Robinson's previously published data. Wild type MEK1 interacts only weakly with ERK2, while the catalytically inactive mutant MEK1 K97M interacts strongly. MEK2, on the other hand, interacts well with ERK2 both as wild type and as the catalytically inactive MEK2 K101A. He had also found that the D domain (residues 3-11) of MEK1 is not required for interaction with ERK2 as can be seen from the lack of growth with the N-terminal deletion MEK1 33-393 and with the D-domain containing fragment MEK1 1-32. Contrarily, the catalytically inactive form MEK1 33-393 K97M did interact despite not having a D domain. The D domain of RSK, however, was observed to be important for its association to ERK2. When the D domain is absent, as in the RSK 689-738 construct, there is no interaction with ERK2. Robinson also assessed the importance of the activation state of MEK1/2 for interaction with ERK2 by looking at the constitutively active forms, MEK1 R4F and MEK2 R4F. These did not interact with ERK2 and it was suggested that phosphorylation of ERK2 on Y185 was possibly impeding this interaction.<sup>132</sup>

---

<sup>132</sup> Adachi, M.; Fukuda, M.; Nishida, E. *EMBO J.* **1999**, *18*, 5347.

**ERK2**

**Figure 1. Yeast two-hybrid screen of ERK2 wild type interactions with MEK1/2 and RSK constructs.** The yeast strain L40 was co-transformed with pGAD-ERK2 and pLexA vector (not shown), pLexA-MEK1, or plasmids encoding LexA fusions to the indicated proteins. Interactions were tested by streaking co-transformed yeast isolates on a medium lacking His, Leu, and Trp and observing streaks for growth. A representative plate from one of three experiments is shown.

The screen I performed using these same constructs with ERK2 E320K are shown in Figure 2. There interaction with wild type MEK2 is weakened, while interaction with catalytically inactive MEK2 K101A is eliminated. Also eliminated is the interaction with RSK, both with and without its D domain. This latter result is consistent with the idea that the ERK2 E320K mutation disrupts docking interactions with D domain docking substrates. These results are also consistent with Robinson's screen of interactions with the ERK2 D316A, D319A mutant

where interactions of D domain containing interactors were eliminated. These included the RSK 689-752 fragment, MEK2, MNK1, and MKP-3. The only interaction that remained was with catalytically inactive MEK1 K97M.

### ERK2 E320K

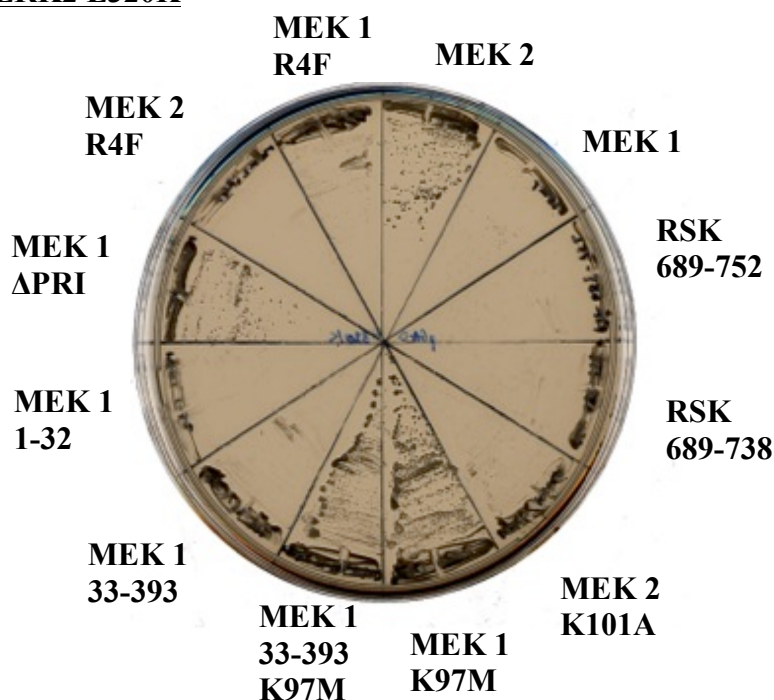


**Figure 2. Yeast two-hybrid screen of ERK2 E320K interactions with MEK and RSK constructs.** The yeast strain L40 was co-transformed with pGAD-ERK2 E320K and pLexA vector (not shown), pLexA-MEK1, or plasmids encoding LexA fusions to the indicated proteins. Interactions were tested by streaking co-transformed yeast isolates on a medium lacking His, Leu, and Trp and observing streaks for growth. A representative plate from one of three experiments is shown.

There was a striking difference between ERK2 wild type and mutant with respect to interactions with the dual phosphatase MKP-3 as illustrated in Figure 3. The ERK2 E320K mutation completely disrupted interactions with both wild type MKP-3 and the phosphate

inactive MKP-3 C293S. Important to note is that the MKP-3 C293S mutant was originally designed as a tighter binding partner of ERK2, thus making the loss of interaction that much more significant.

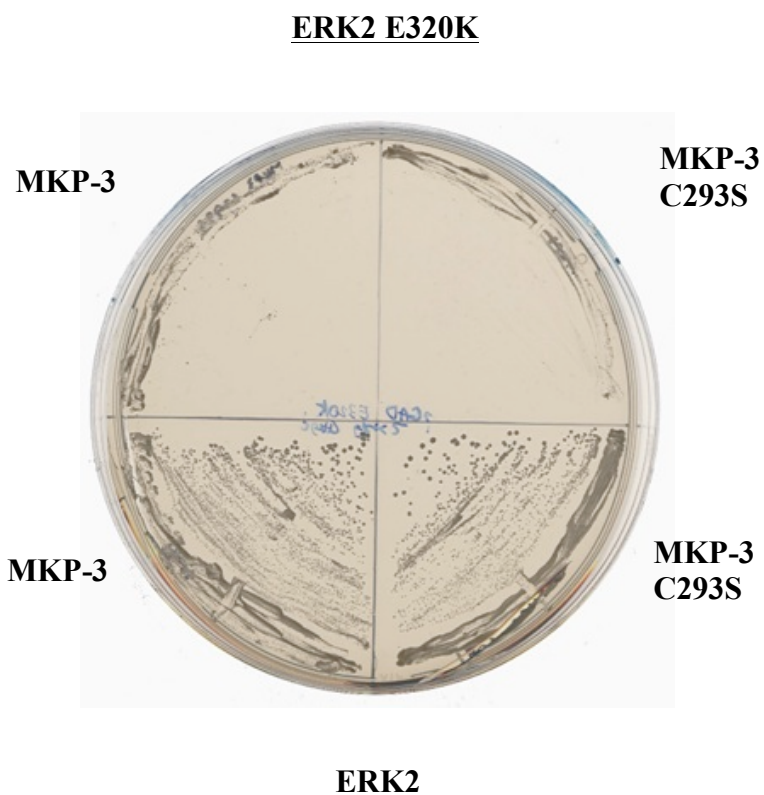


**Figure 3. The interactions of ERK2 wild type and mutant with MKP-3 wild type and phosphatase-dead C293S mutant examined using the yeast two-hybrid system.** The yeast strain L40 was co-transformed with pGAD-ERK2 (lower half of plate) or pGAD-ERK2 E320K (upper half of plate) and pLexA-MKP-3 (left half of plate) or pLexA-MKP-3 C293S (right half of plate). Interactions were tested by streaking co-transformed yeast isolates on a medium lacking His, Leu, and Trp and observing streaks for growth. A representative plate from one of three experiments is shown.

I also examined the interaction of ERK2 with itself in order to explore whether the E320K mutation possibly affects dimerization. A first attempt (Figure 4), did not show any difference in interactions between wild type and mutant. However, the pGAD vector/pVJL11 ERK2 E320K combination, which was acting as a negative control, exhibited growth on three-drop medium. This could be explained by unpublished data from our lab showing that a fusion of ERK2 to the LexA DNA-binding domain independently activated transcription of the *HIS3* auxotrophy reporter gene borne by the yeast strain L40. In order to eliminate what would essentially be background interference, added varying concentrations of 3-amino-1,2,4-triazole (3-AT) to the medium. 3-AT is a competitive inhibitor of the product of the *HIS3* gene. Of the different concentrations of 3-AT, 0.5 mM was the smallest amount required such that there would be no growth for the negative controls. The screen of ERK2 pairs grown on medium with 0.5 mM 3-AT (Figure 5) shows weakened interactions there where ERK2 E320K is one of the binding partners.

While inconclusive, the wild type/wild type ERK2 interaction is also significant as it is further evidence that ERK2 dimerizes and it is the first example of ERK2 dimerization observed under physiological conditions.

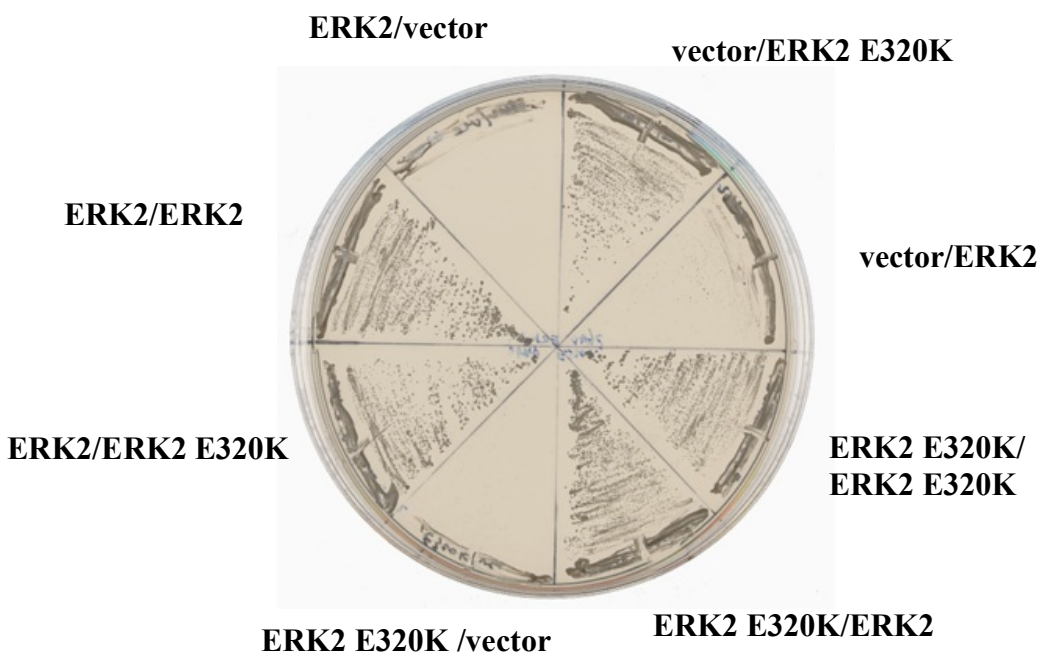


**Figure 4. Yeast two-hybrid screen of dimer interactions between ERK2 wild type and ERK2 E320K.** The yeast strain L40 was co-transformed with empty pGAD vector, pGAD-ERK2, or pGAD-ERK2 E320K and empty pLexA vector, pLexA-ERK2, or pLexA-ERK2 E320K. Interactions were tested by streaking co-transformed yeast isolates on a medium lacking His, Leu, and Trp and observing streaks for growth. A representative plate from one of three experiments is shown.

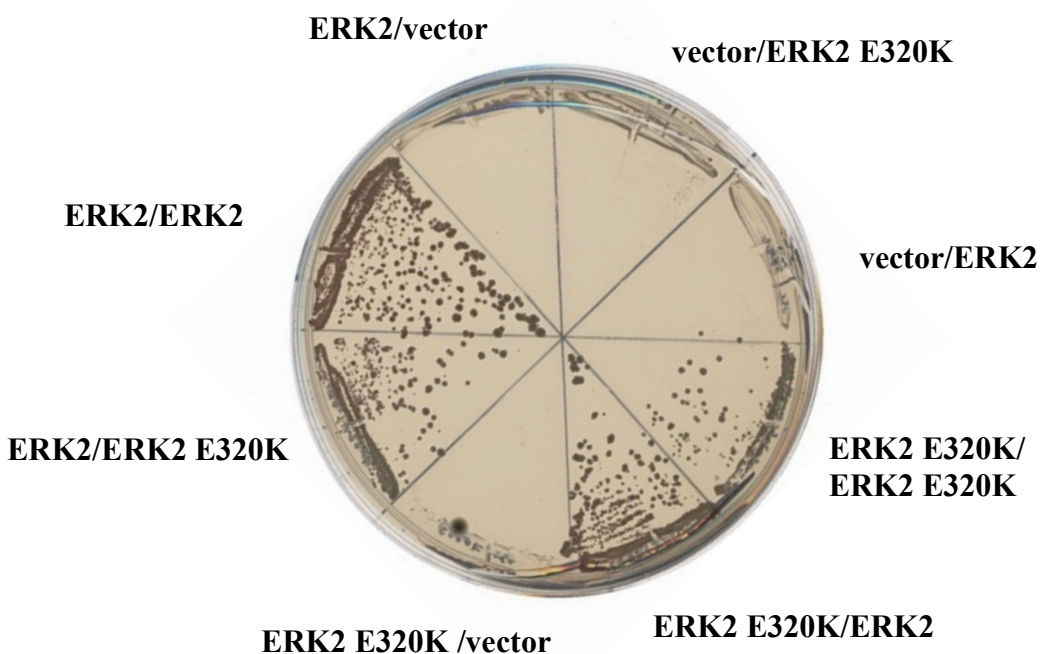


**Figure 5. Yeast two-hybrid screen of dimer interactions between ERK2 wild type and ERK2 E320K grown on medium containing 0.5 mM 3-AT.** The yeast strain L40 was co-transformed with empty pGAD vector, pGAD-ERK2, or pGAD-ERK2 E320K and empty pLexA vector, pLexA-ERK2, or pLexA-ERK2 E320K. Interactions were tested by streaking co-transformed yeast isolates on a medium containing 0.5 mM 3-AT and lacking His, Leu, and Trp and observing streaks for growth. A representative plate from one of three experiments is shown.

### *SILAC*

While the yeast two-hybrid screen offers a visual and straightforward approach for examining protein-protein interactions, it remains qualitative and limited to the binding partners chosen for the screen. In an attempt to both discover more differences in binding partners between ERK2 wild type and mutant, and to quantify these differences, I decided to try a SILAC

experiment. Stable isotope labeling by amino acids in cell culture (SILAC) is a means to distinguish using mass spectrometry between two cell populations where one has been grown in medium containing ‘heavy’ L-<sup>13</sup>C<sub>6</sub><sup>15</sup>N<sub>4</sub> arginine and L-<sup>13</sup>C<sub>6</sub><sup>15</sup>N<sub>2</sub>-lysine and the other containing only ‘light’ amino acids (L-<sup>12</sup>C<sub>6</sub><sup>14</sup>N<sub>4</sub> arginine and L-<sup>12</sup>C<sub>6</sub><sup>14</sup>N<sub>2</sub>-lysine). With the help of Jihan Osborne, a former graduate student in the Cobb lab, COS-7 cells were transfected with Flag-tagged ERK2 wild type and mutant. The ERK2 E320K transfected cells were grown in heavy medium; the wild type light. Samples were submitted to the proteomics core at UT Southwestern for analysis.

Quality controls were performed to test for incorporation of heavy atoms and for equal mixing. Unfortunately, in our first round of quality controls the incorporation was too low due to the cells being grown in heavy medium only during the last passage. Jihan thus increased the number of overall passages, using heavy medium in all passages. In our second round of testing for incorporation, out of 3366 total spectrum matches, 3282 were heavy labeled indicative of >97.5% SILAC label incorporation. The mixing test was also fine with a median ratio (H/L) of 0.98 for non-contaminant proteins with almost everything within a 2-fold distribution (Figure 6).

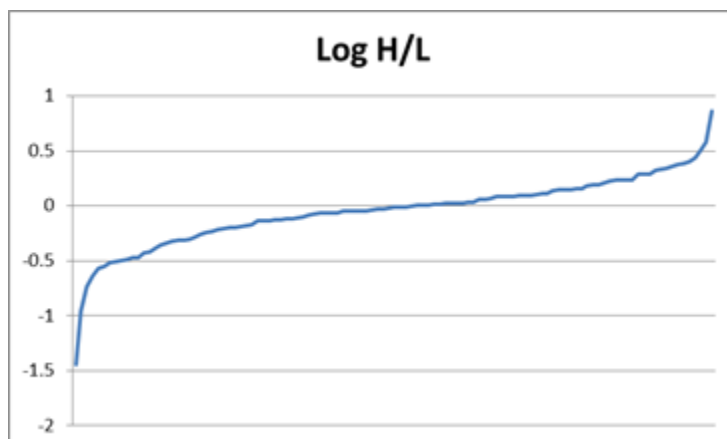


**Figure 6. Mixing test distribution curve.** The log of the ratio for heavy/light abundance of a protein as computed from the peptide ratios seen by the mass spectrometer.

Instead, what was foreseen as a possible problem was the difference in expression between wild type and mutant ERK2. As shown in Figure 7, the mutant ERK2 expressed better than wild type as assessed by blotting with a Flag antibody. While the hope was that the H/L ratio would still fall within the dynamic range of the mass spectrometer, in the actual experiment this was not the case as the H/L ratio was 4.7. With less wild type present there is also less interacting material pulled down.

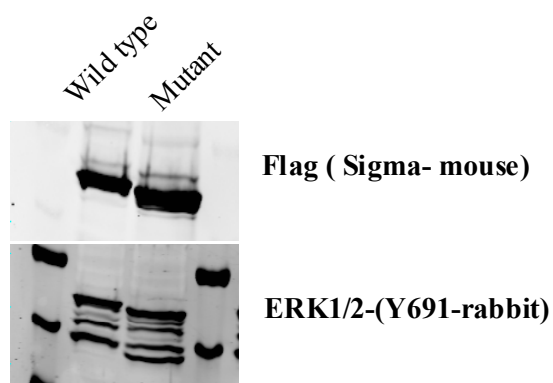


**Figure 7. Expression levels of wild type and mutant ERK2 for SILAC experiment.** Equal amounts of whole cell lysates were immunoblotted with Flag antibody and total ERK1/2 antibody to verify expression levels in COS-7 cells transfected with Flag-tagged ERK2 wild type and mutant plasmids.

Using the protein sequence database at SwissProt, with all/Human as the search, since the protein sequence database for the African green monkey (the origin of COS cells) is incomplete, 374 proteins in the experiment had H/L ratios in the computable range. 266 other proteins were identified in the sample, but in amounts below the limit of quantification. When the H/L ratio was normalized by dividing by 4.7 (the MAPK1 ratio), all of the ratios were less than 1 except for the high density lipoprotein-binding protein, Vigilin, suggesting that the mutant was binding better than wild type to the latter. That there would be fewer binding interactions with the ERK2 E320K mutant is what I had expected. This result however is still only qualitative and unreliable because the large difference in amount and the ensuing normalization is outside of the dynamic range of the instrument. Additionally, non-interacting proteins will have their ratios moved away from 1:1. The proteomics core therefore suggested only looking at the 10-20 proteins with the smallest ratios and to rely more on biochemical knowledge of the candidate interactors to

distinguish actual differences in substrate binding between ERK2 wild type and the E320K mutant.

I therefore looked at the twenty proteins with the smallest H/L ratios. This limited list of results includes both RSK-1 and RSK-2, two serine/threonine-protein kinases that act downstream of ERK2 and mediate mitogenic and stress-induced activation of transcription factors, that regulate translation, and mediate cellular proliferation, survival, and differentiation. Also included is the heat shock protein, Hsp27, which is involved in stress resistance and actin organization. It has been shown that Hsp27 indirectly regulates ERK2 nuclear translocation through the ERK2 scaffold, PEA-15.<sup>133</sup> The serine/threonine-protein kinase 38 (STK38), that is a negative regulator of MAP3K1/2 (MEKK1/2) signaling, is also in this group. Another example is the Zinc finger Ran-binding domain-containing protein 2 that mediates binding to RNA and is phosphorylated on S310 upon DNA damage (though this phosphorylation is thought to be achieved by ATM or ATR kinase).<sup>134</sup>

### **Activity Differences between ERK2 WT and ERK2 E320K**

ERK2 relies on protein-protein interactions for its activation and deactivation as well as for its phosphorylation of substrates. It is therefore of interest to look at how activity towards different components of the MAPK signaling pathway are affected by the E320K mutation.

---

<sup>133</sup> Hayashi, N.; Peacock, J. W.; Beraldi, E.; Zoubeidi, A.; Gleave, M. E.; Ong, C. J. *Cell Death Differ.* **2012**, *19*, 990.

<sup>134</sup> Matsuoka, S.; Ballif, B. A.; Smogorzewska, A.; McDonald, E. R.; Hurov, K. E.; Luo, J.; Bakalarski, C. E.; Zhao, Z.; Solimini, N.; Lerenthal, Y.; Shiloh, Y.; Gygi, S. P.; Elledge, S. J. *Science*, **2007**, *316*, 1160.

### *The activation of ERK2 by MEK1 R4F*

The activation of ERK2 by the constitutively active MEK1 R4F was measured over time. I observed both the same rate as well as final pmol/pmol activity of ERK2 in both wild type and mutant as assessed by scintillation counting. The mutation therefore does not affect the ability of ERK2 to be phosphorylated.

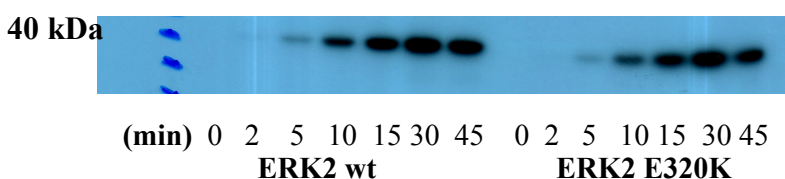


**Figure 8. Autoradiograph of the phosphorylation of ERK2 by MEK1 R4F.** Recombinant purified wild type and mutant ERK2 were incubated in the presence of MEK1 R4F and [ $\gamma$ - $^{32}$ P]ATP for the indicated amounts of time. The samples were run on denaturing gel that was then Coomassie stained, dried and exposed to film.

### *The activity of ERK2 towards MBP*

I used myelin basic protein (MBP) as a substrate to measure the specific activity of ERK2. After being initially activating ERK2 with MEK1 R4F, different concentrations of ERK2 were used to phosphorylate MBP for different lengths of time. Having plotted concentration curves, the specific activity of ERK2 towards MBP was found to be 1848 nmol/min/mg for the

wild type and 1691 nmol/min/mg for the mutant. The difference in specific activity is insignificant.

*The deactivation of ERK2 by MKP-3*

A notable difference however is observed between wild type and mutant ERK2 in the rate of dephosphorylation by MKP-3. After 5 min ERK2 wild type is nearly completely dephosphorylated as assessed by immunoblotting with pERK1/2 antibody (Figure 9), whereas it took nearly 30 min for the amount of phosphorylated ERK2 E320K to drop to a comparable level. I determined the relative amounts of phosphorylation from the immunoblot using LiCor imaging, and I then normalized values to the respective starting amounts.

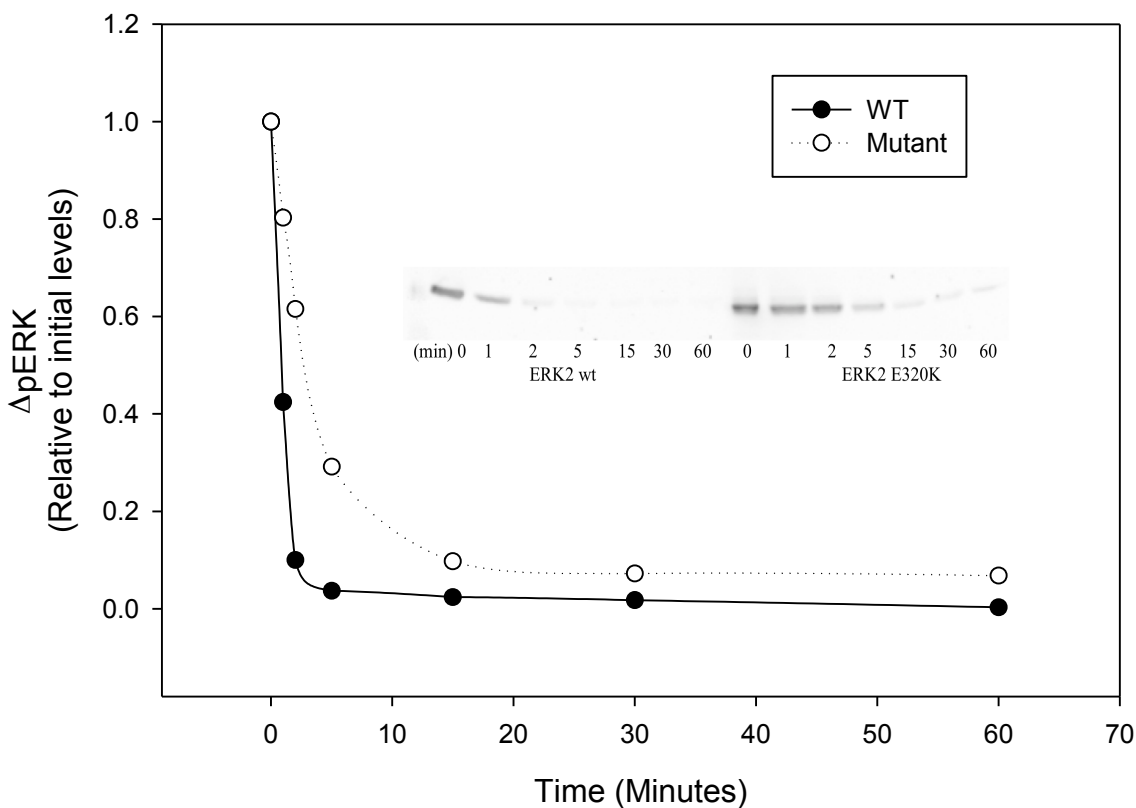


**Figure 9. Time-dependent dephosphorylation of wild type and mutant ERK2 by MKP-3.** Recombinant MKP-3 was incubated with phosphorylated wild type and mutant ERK2 at 25°C for 0-60 min. Dephosphorylation of pERK2 was determined by immunoblotting with pERK antibody (inset). The relative amounts of pERK2 present was determined by LiCor imaging and plotted against time.

#### *The hydrolysis of p-NPP by MKP-3*

Since it is known that unphosphorylated ERK2 activates MKP-3 through a conformational change in the phosphatase that occurs upon binding, I used *p*-NPP as a substrate of MKP-3 to determine its activity in the presence of both wild type and mutant ERK2. Here too, there was a striking difference between wild type ERK2 and the E320K mutant. The rate of

hydrolysis of *p*-NPP was measured by absorbance at 405 nm over the course of two hours for five different concentrations of *p*-NPP. The slope of the linear part of these different concentration curves was then plotted as the initial velocity vs. *p*-NPP concentration (Figure 10). As can be seen, there is minimal catalytic activation of MKP-3 in the presence of ERK2 E320K. This is not due to mis-folding or loss of kinase activity of the protein because ERK2 E320K exhibited similar specific activity as wild type in the MBP kinase assays described above.

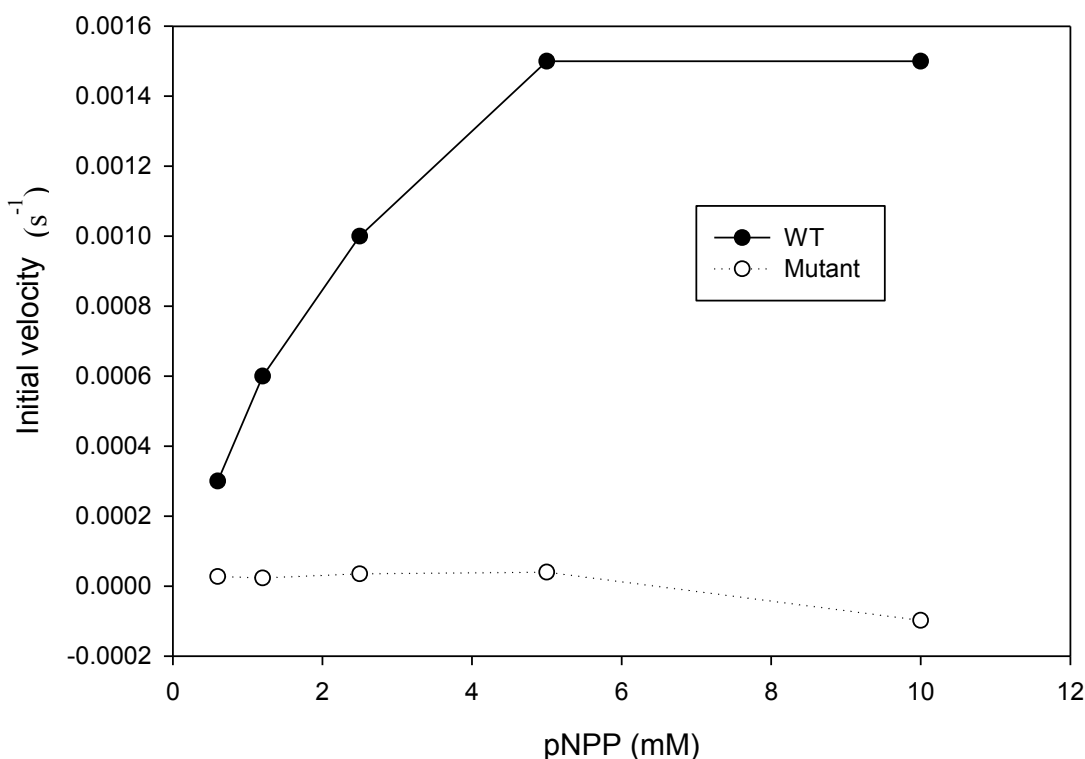


**Figure 10. Hydrolysis of *p*-NPP by MKP-3 in the presence of wild type and mutant ERK2.** The phosphatase substrate *p*-NPP, ranging in concentration from 0-10 mM, was used to examine the effect of unphosphorylated ERK2 or ERK2 E320K on the phosphatase activity of MKP-3. Reactions at each concentration of *p*-NPP were monitored for 2 hours with a multiplate reader at 405 nm. The slope of the linear range of the absorbance vs. time curves (initial velocity) for three experiments were then averaged and plotted against *p*-NPP concentrations.

This result, together with the effect on the rate of dephosphorylation by MKP-3, is consistent with what was observed in the comparison of the ERK2 D319N mutation.<sup>135</sup>

### **Structural Differences**

Function is ultimately determined by the structure of a protein, therefore to better understand the effects of the E320K mutation I needed to examine its effects on structure. This I did using both X-ray crystallographic data and molecular dynamics calculations.

#### *X-ray crystallography*

Previous to my joining the lab, data sets had been collected of ERK2 E320K by both Yu-Chi Juang and Wen-Huang Ko. I used the latter's data set, the collection statistics for which are summarized in Table 1. I performed molecular replacement using unphosphorylated ERK2 wild type (PDB: 1ERK) by dividing the search model in two between the C and N termini. This was done to lower the  $R_{\text{work}}$  by allowing for a more flexible model and because, in a first molecular replacement, most areas that did not fit the model were located in the C terminus.

By model building in COOT and refining the phases in PHENIX, I have thus far managed to reduce the R-free value to 0.32. The three major areas where the model does not yet fit the electron density map are in the area of the activation loop, the MAPK insert, and the CD domain.

---

<sup>135</sup> Kim, Y.; Rice, A. E.; Denu, J. M. *Biochemistry* **2003**, *42*, 15197.

Parameter	Value
Space Group	C 1 2 1
a,b,c (Å)	182.3, 41.9, 50.3
$\alpha=\beta=\gamma$ (degrees)	90
Resolution Range (Å)	50.0 – 2.20 (2.24 – 2.20)
$I/\sigma_1$	21.1 (2.2)
No. Reflections	17464 (568)
Redundancy	4.0 (3.6)
Completeness (%)	91.8 (60.9)
$R_{\text{merge}}$	0.060 (0.446)

**Table 1. Data collection statistics.** Statistics for the dataset collected by Wen-Huang Ko of ERK2 E320K crystals.

The L16 loop, which contains the CD domain is rendered particularly flexible by the mutation. This can be seen from the large difference in B-factors between wild type and mutant ERK2 (Figure 11). The effect on the activation loop region of ERK2 is also important, suggesting allosteric interactions across the protein.

After my initial attempts at solving the structure, I became convinced that the disorder and the resulting lack of electron density in this area caused by the flexibility of the docking loop rendered the structure unsolvable from this data set. And because this flexibility was itself the answer to my question of why protein-protein interactions were being disrupted, I abandoned the

effort of completely solving the structure. I have just recently returned to this task, which I think may offer more insights into the relationship between the docking and activation loops.

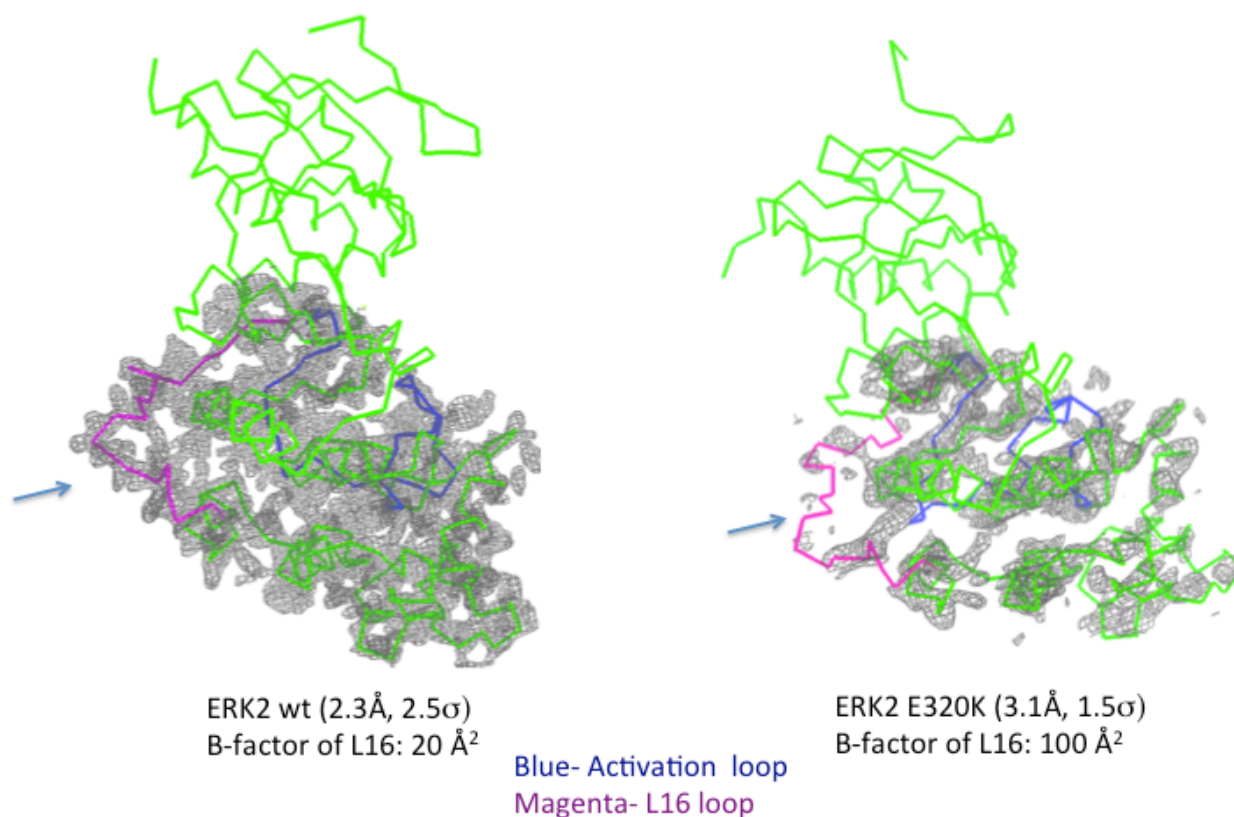


**Figure 11. Comparison of the flexibility of the L16 loop in wild type and mutant ERK2.** Residue 320 is indicated by an arrow. The ERK2 wild type structure is that of unphosphorylated ERK2 (PDB: 1ERK). The ERK2 E320K structure is the partially-solved model from Wen-Huang Ko's dataset.

### *Molecular dynamics simulations*

A different approach to the question of whether flexibility of the docking loop is induced by the E320K mutation and whether the mutation affects other parts of the protein, was to use molecular dynamics (MD) simulations. To this end I was greatly assisted by Dr. Junmei Wang. I

used the crystal structures of both unphosphorylated (PDB: 1ERK) and phosphorylated (PDB: 2ERK) wild type ERK2 as the starting models. Computational mutagenesis of both wild type structures was performed in order to generate the mutant ERK2 E320K equivalents. *Ab initio* calculations at the HF/6-31G\* level of theory were used to obtain force field charge parameters of phosphorylated residues. The MD simulations were conducted until all four protein systems were well equilibrated as suggested by the small fluctuations in RMSD between the crystal structures and the MD structures. Plots of RMSD vs. simulation time indicate that after 20 nanoseconds of MD simulations the four systems were equilibrated and that fluctuations remained small between 20-60 ns (Figures 12-15).

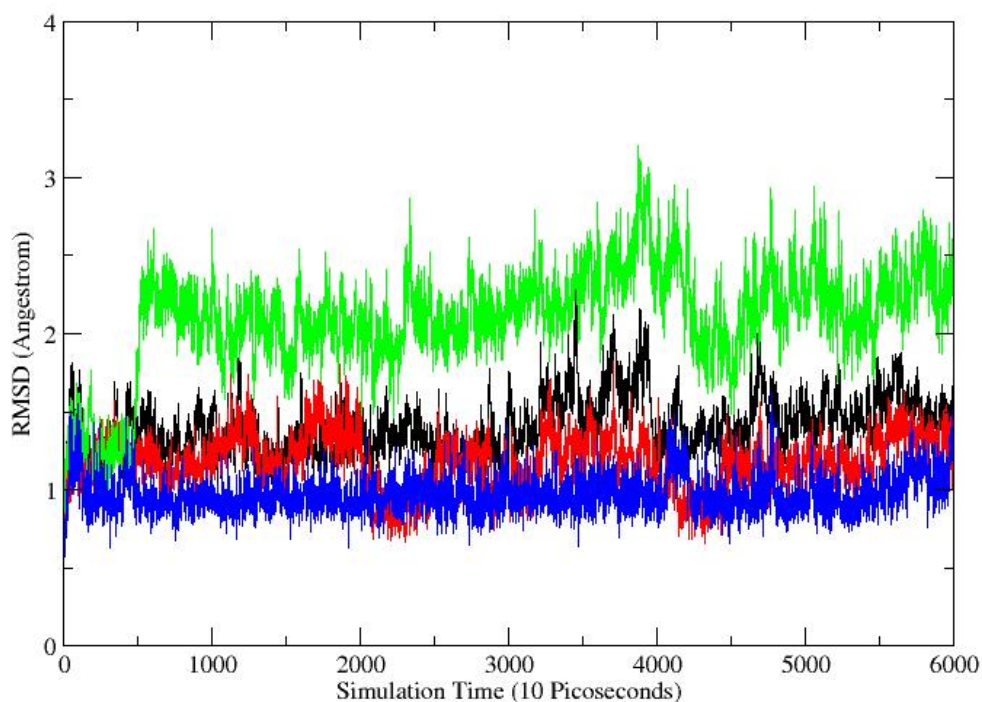


**Figure 12. RMSD vs. simulation time plot for wild type unphosphorylated ERK2.** Main chain atoms (black), the activation loop (red), the L16 loop (green), the docking domain (blue).

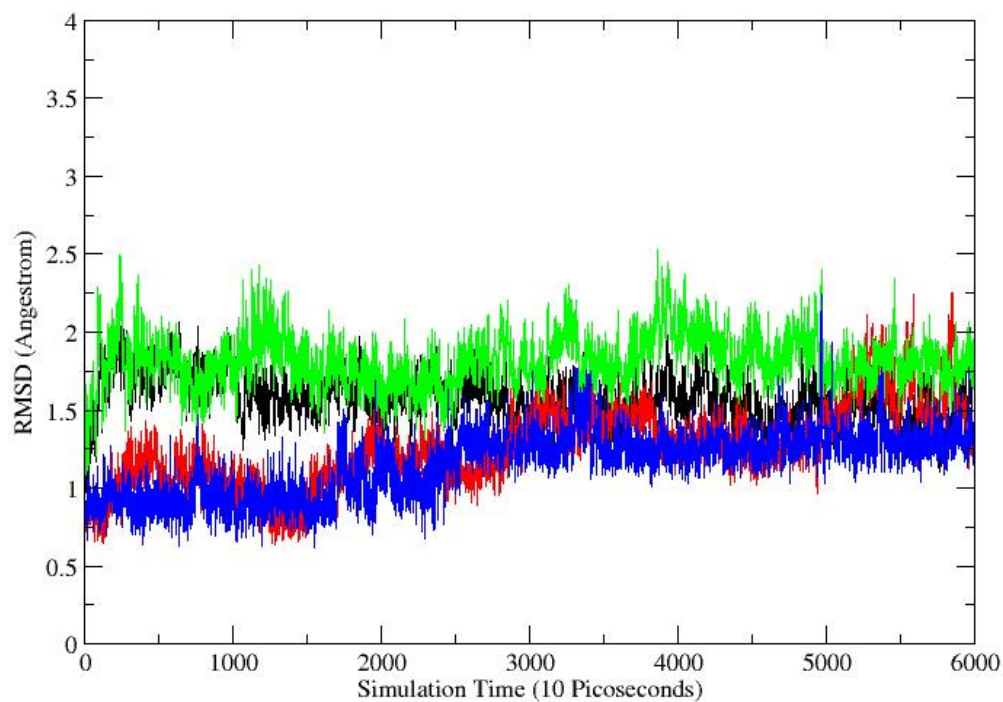


**Figure 13. RMSD vs. simulation time plot for unphosphorylated ERK2 E320K.** Main chain atoms (black), the activation loop (red), the L16 loop (green), the docking domain (blue).

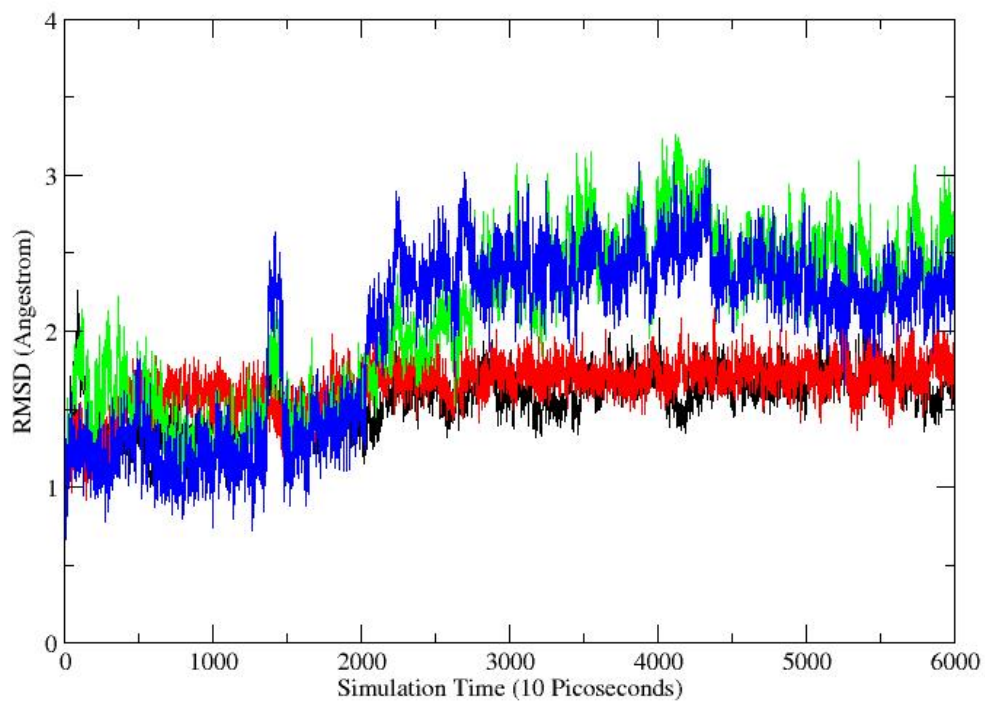


**Figure 14. RMSD vs. simulation time plot for wild type phosphorylated ERK2.** Main chain atoms (black), the activation loop (red), the L16 loop (green), the docking domain (blue).

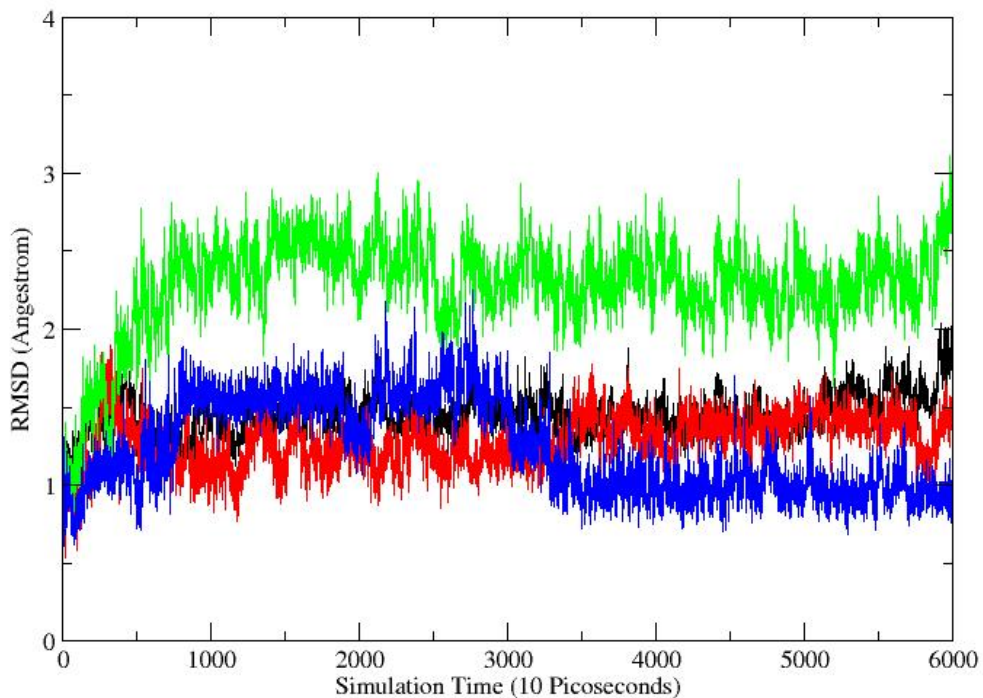


**Figure 15. RMSD vs. simulation time plot for phosphorylated ERK2 E320K.** Main chain atoms (black), the activation loop (red), the L16 loop (green), the docking domain (blue).

After MD simulations were performed, Junmei analyzed the MD trajectory to calculate the B-factors, to generate a contact map and perform correlation analysis. The B-factor calculations were validated by comparing the values from the MD trajectories to those from the crystal structure of wild type ERK2. Since Junmei completed this work, I will here only summarize the results that pertain to my dissertation.

By calculating the mean values of the B-factors of all the atoms in the CD domain (defined as residues 310-323), he demonstrated that both phosphorylation and the E320K mutation boost the

flexibility of the CD domain. The B-factor of unphosphorylated wild type ERK2 is 47.4, while for the unphosphorylated mutant it is 64.1. When phosphorylated, the B-factor for wild type ERK2 increases to 66.0, whereas it increases to 79.7 for the mutant. The individual contact maps for both mutant and wild type ERK2 in unphosphorylated and phosphorylated states appear to be essentially the same. However, when difference maps are generated (Figures 16-19), two trends become apparent. First, in both wild type and mutant, phosphorylation causes a change in contact interactions. Secondly, this difference in contacts between the unphosphorylated and phosphorylated species is enhanced in the case of mutants.

He then performed a residue-residue correlation analysis using the following equations as described by Karplus.<sup>136</sup> The residue-residue interaction energy is defined as the sum of the van der Waals (vDW), electrostatic (elec), generalized Born (GB), and non-polar interaction energies between residues  $i$  and  $j$ :

$$E_{ij} = E_{ij}^{vDW} + E_{ij}^{elec} + E_{ij}^{GB} + E_{ij}^{non-polar}$$

The mean interaction energies for the  $n$  MD snapshots is then defined as:

$$\overline{E}_{ij} = \frac{1}{n} \sum_{t=1}^n E_{ij}^t \quad |i - j| > 1$$

The correlation between two sets of residue-residue interactions,  $i,j$  and  $k,l$  is defined as:

$$C_{i,j|k,l} = \frac{\sum_{t=1}^n (E_{ij}^t - \overline{E}_{ij}^t)(E_{kl}^t - \overline{E}_{kl}^t)}{\sum_{t=1}^n \sqrt{(E_{ij}^t - \overline{E}_{ij}^t)^2 (E_{kl}^t - \overline{E}_{kl}^t)^2}}$$

---

<sup>136</sup> Kong, Y.; Karplus, M. *Proteins* **2009**, *74*, 145.

Finally, the residue correlation ( $RC$ ) matrix is calculated using the following equation with  $N$  as the number of residues:

$$RC_{mn} = \sum_{i=1}^N \sum_{j=1}^N |C_{im|jn}|$$

This analysis demonstrates that there is a strong correlation between the activation loop and the docking domain in the phosphorylated form of ERK2 and that this correlation is enhanced by the E320K mutation (Figures 20-21). The correlation analysis therefore follows the same two trends as described for the contact analysis. Furthermore, the difference is seen in fact to be an increase in correlation when the protein is either phosphorylated or contains the E320K mutation. Comparing the two methods, the contact map analysis does not capture the dynamic nature of protein systems as well as correlation analysis, thus the latter is better suited to describe the allosteric interactions across a particular protein.

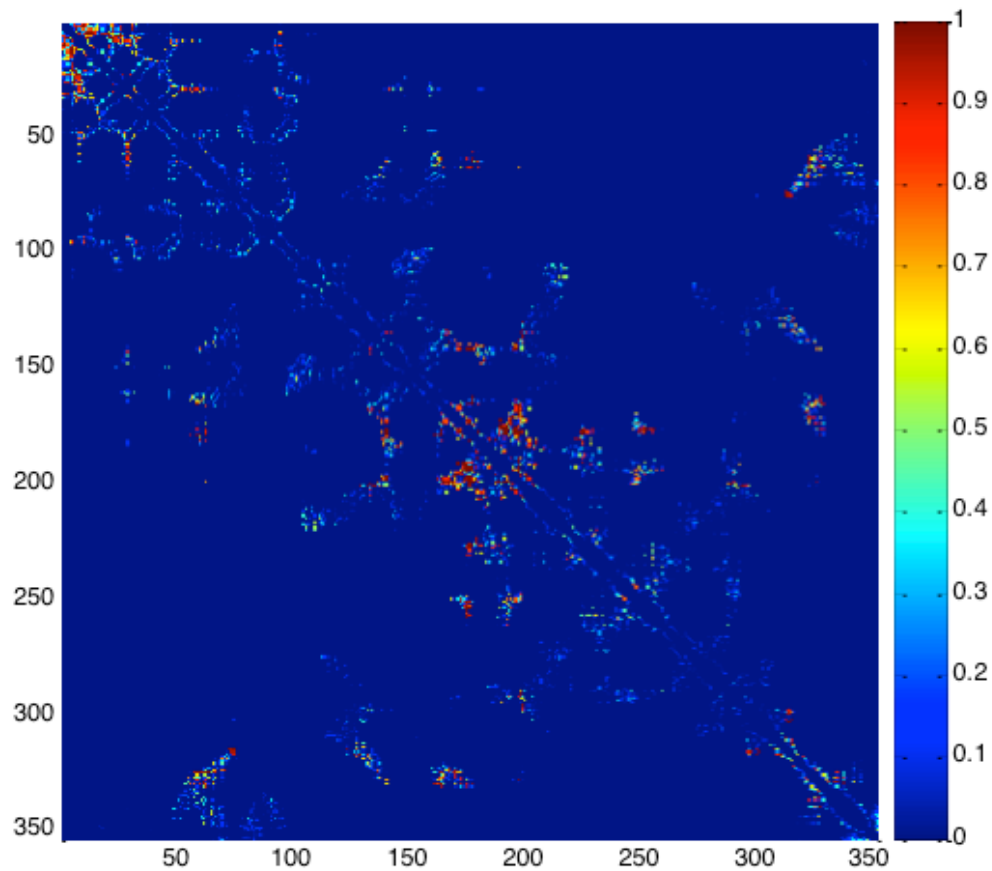


**Figure 16. Map difference between contact maps of unphosphorylated and phosphorylated wild type ERK2.** Each spot in this matrix indicates the absolute difference of the contact values from the contact maps of unphosphorylated and phosphorylated wild type ERK2. The color scale is from blue (0) to red (1), blue indicating no difference between the two contact maps.

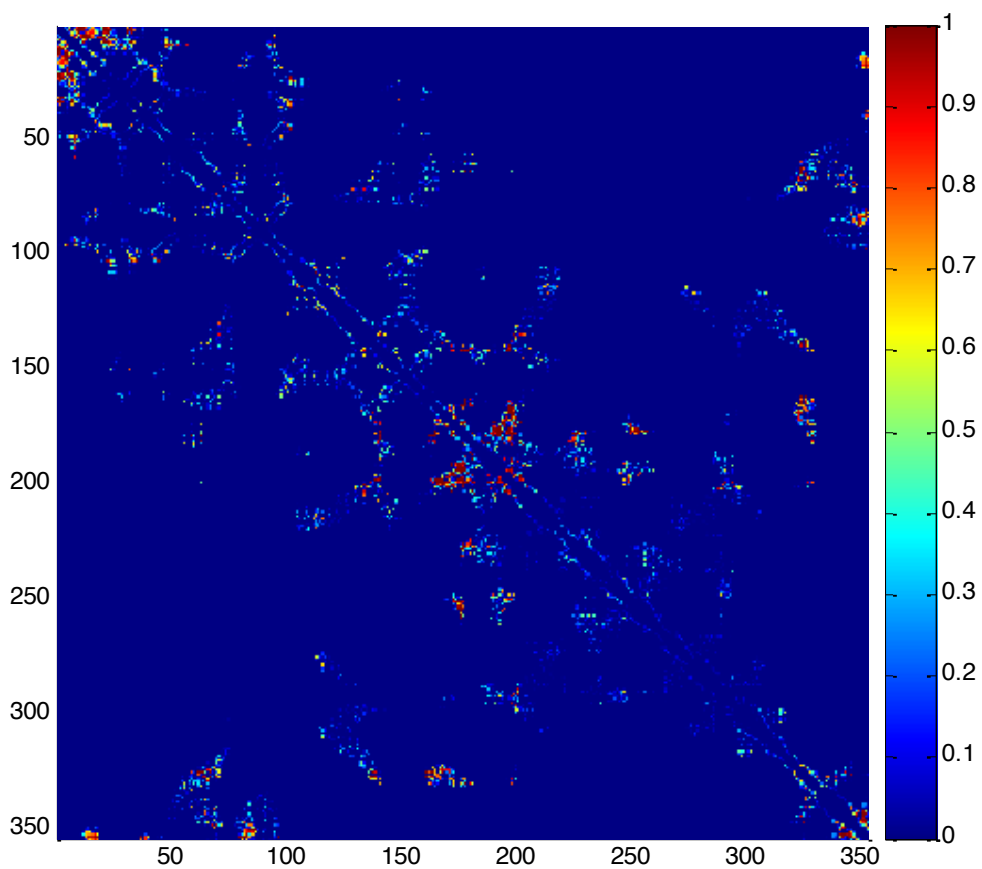


**Figure 17. Map difference between contact maps of unphosphorylated and phosphorylated ERK2 E320K.** Each spot in this matrix indicates the absolute difference of the contact values from the contact maps of unphosphorylated and phosphorylated mutant ERK2 E320K. The color scale is from blue (0) to red (1), blue indicating no difference between the two contact maps.

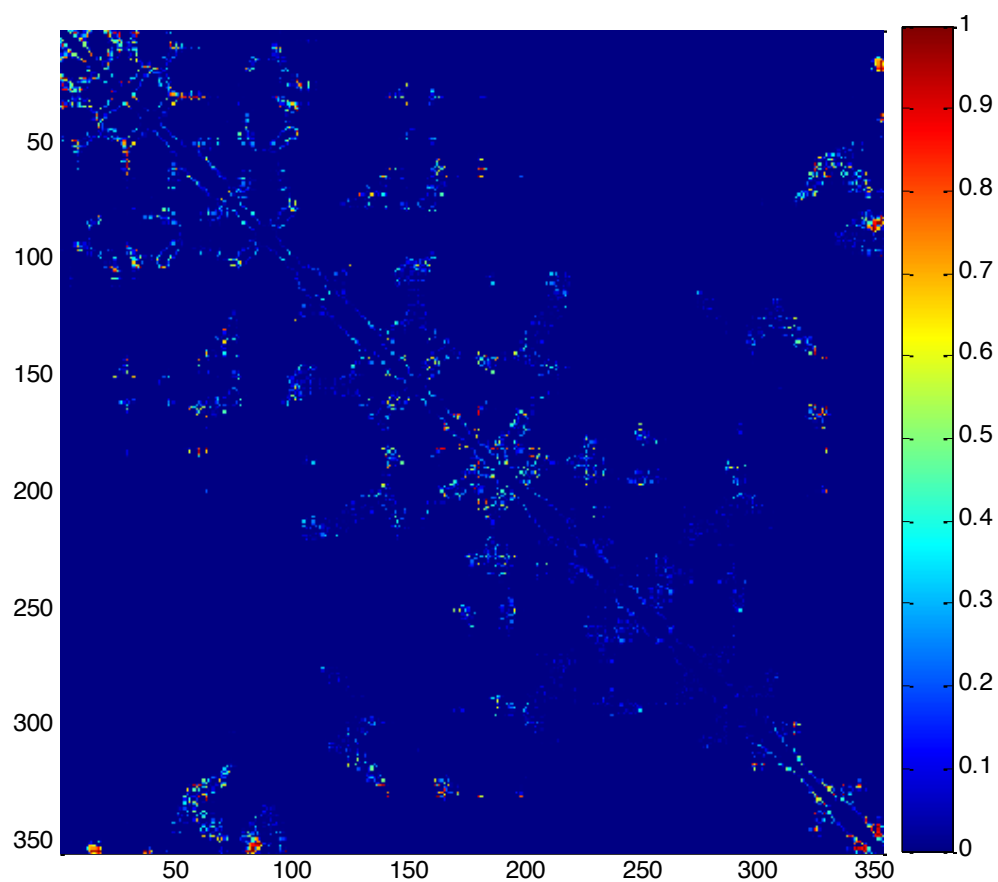


**Figure 18. Map difference between contact maps of unphosphorylated wild type and mutant ERK2.** Each spot in this matrix indicates the absolute difference of the contact values from the contact maps of unphosphorylated wild type and mutant ERK2. The color scale is from blue (0) to red (1), blue indicating no difference between the two contact maps.

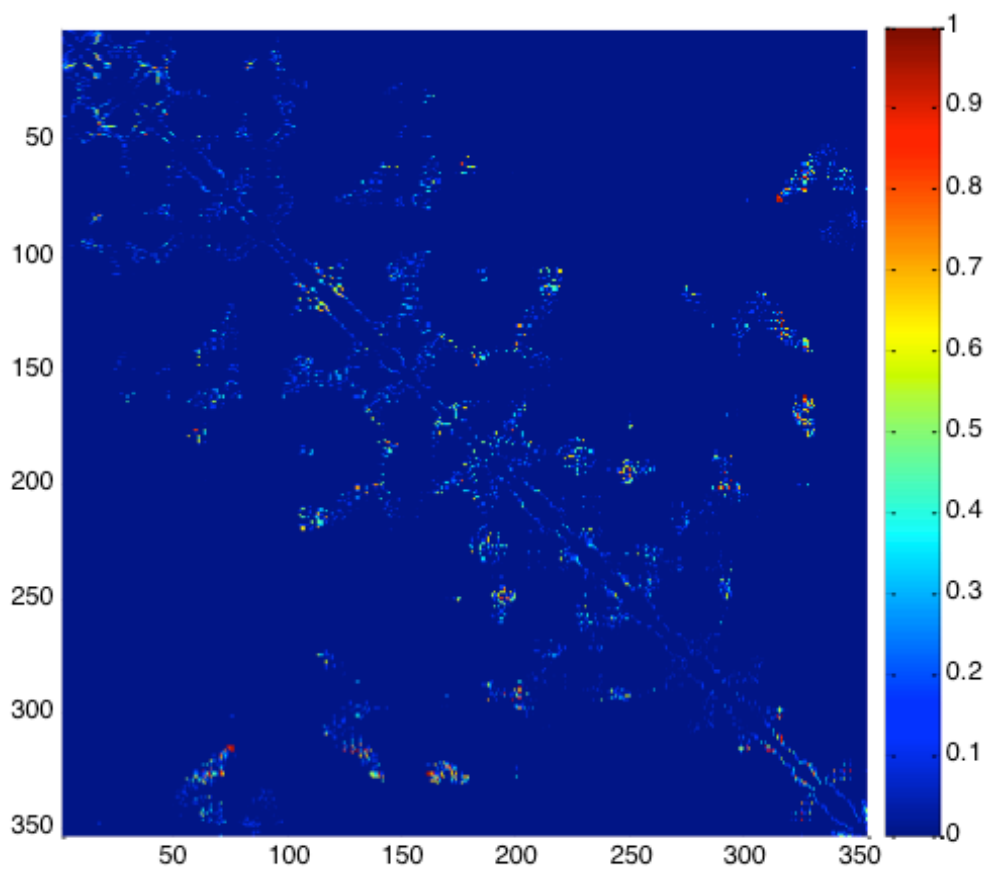


**Figure 19. Map difference between contact maps of phosphorylated wild type and mutant ERK2.** Each spot in this matrix indicates the absolute difference of the contact values from the contact maps of phosphorylated wild type and mutant ERK2. The color scale is from blue (0) to red (1), blue indicating no difference between the two contact maps.

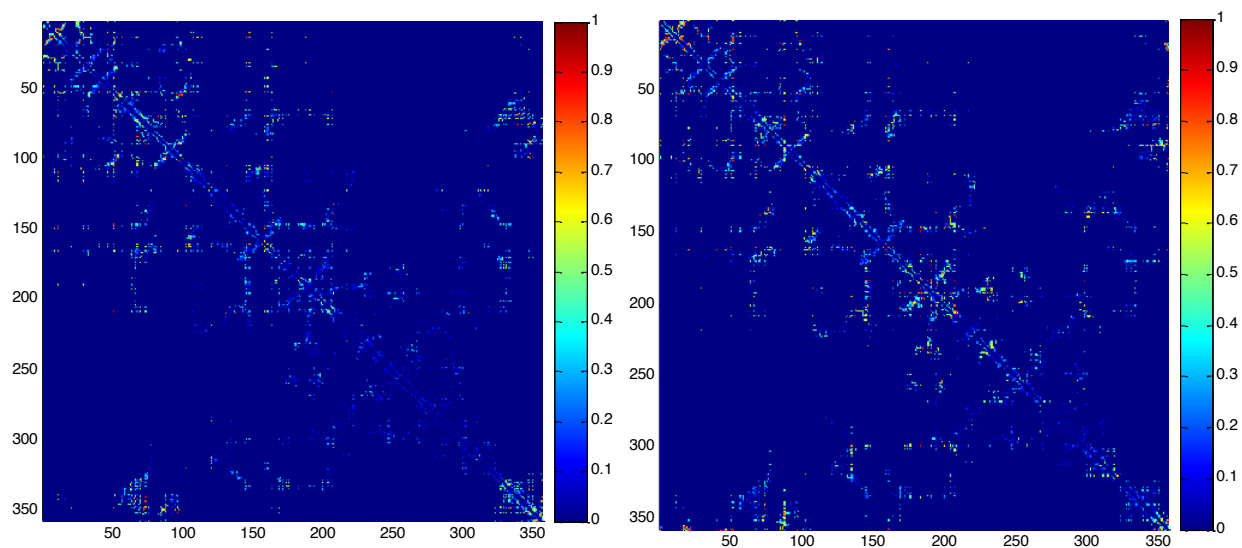


**Figure 20. Correlation matrices of unphosphorylated wild type (left) and mutant ERK2 (right).** Each spot in this matrix indicates the correlation between two residues, scaled from 0 to 1. The color scale is from blue (0) to red (1), blue indicating no correlation.

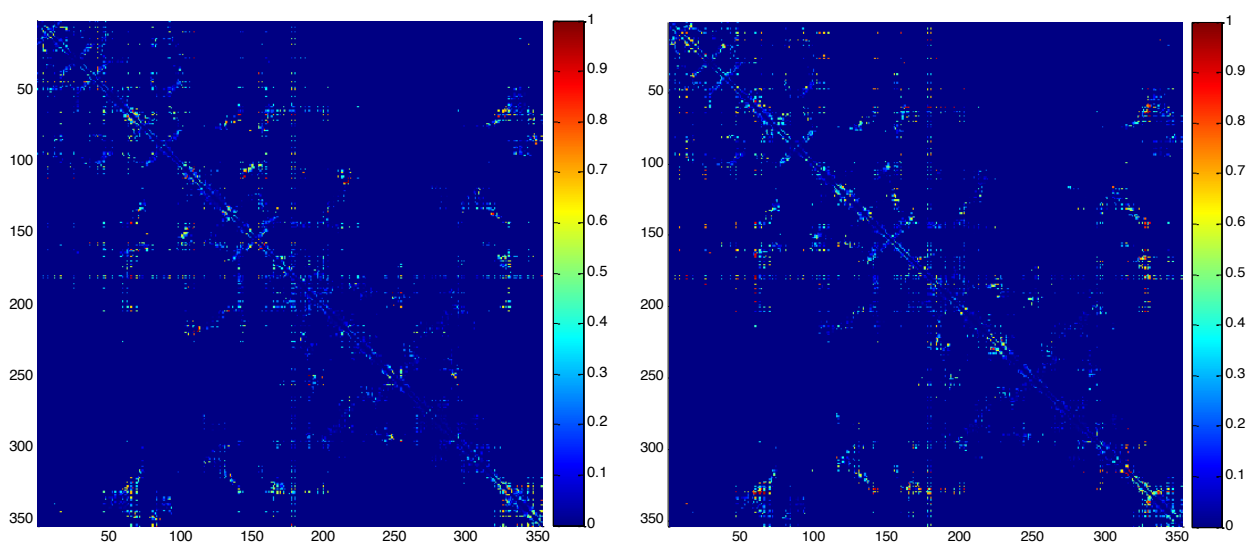


**Figure 21. Correlation matrices of phosphorylated wild type (left) and mutant ERK2 (right).** Each spot in this matrix indicates the correlation between two residues, scaled from 0 to 1. The color scale is from blue (0) to red (1), blue indicating no correlation.

## DISCUSSION

Crystallographic and computational data both indicate a greater flexibility of the docking loop in ERK2 E320K as compared to wild type. This structural disturbance lends to reduced protein-protein interactions as seen in both yeast two-hybrid and SILAC experiments.

Interference with the interaction between ERK2 and its dual-specific phosphatase, MKP-3, has an impact on its activity. Unphosphorylated ERK2 E320K has a reduced ability to activate MKP-3 through a binding event that induces a conformational change of the phosphatase, and phosphorylated ERK2 E320K is not as readily dephosphorylated. Both of these factors, that ultimately resist dephosphorylation, contribute to the mutant form of the protein being more active.

I began a yeast two-hybrid screen of ERK2 interactions with its substrate ERF. ERF does not contain a D domain, but instead binds to ERK2 at its FXF motif,<sup>137</sup> of which it contains two. I subcloned ERF wild type and mutant forms of either one or the other or both of the FXF motifs. Unfortunately, this screen still requires trouble-shooting (most likely with varying concentrations of 3-AT) as ERK2 wild type still interacted with ERF having both FXF motifs mutated. Such a screen could help to determine whether it is only interactions that rely on the CD domain of ERK2 for docking are affected by the E320K mutation.

I thought the SILAC experiment was a potentially powerful approach to both identifying and quantifying differences in interactions between wild type and mutant ERK2. In order to give a reliable result, however, the expression levels of both proteins would first need to be adjusted.

---

<sup>137</sup> Polychronopoulos, S.; Verykokakis, M.; Yazicioglu, M. N.; Sakarellos-Daitsiotis, M.; Cobb, M. H.; Mavrothalassitis, G. *J. Biol. Chem.* **2006**, *281*, 25601.

The experiment would then need to be repeated in triplicate in order to assure reproducibility. In so doing, however, this becomes an expensive undertaking.

What is perhaps most intriguing to me however is the possible effect the mutation in the docking loop has allosterically on the activation loop. This is suggested both from the partial solution of the crystal structure and also from residue-residue correlation analysis. This idea is related to observation that long-range conformational changes are induced by docking interactions, particularly in the activation loop.<sup>138</sup> This could point to a potential change in autoactivation of ERK2 on the part of the mutant kinase. I therefore plan to use kinase assays to assess whether there is a change in autoactivation. I had begun this study however I am still troubleshooting to assure that I am eliminating basal levels of phosphorylation before initiating the assay.

---

<sup>138</sup> Zhou, T.; Sun, L.; Humphreys, J.; Goldsmith, E. J. *Structure* **2006**, *14*, 1011.

## CHAPTER THREE

### Vanadium Catalyzed C-H Benzylic Oxidation<sup>139</sup>

#### ABSTRACT

The functionalization of  $sp^3$ -hybridized C-H bonds is of great importance in chemistry so as to harness simple hydrocarbon building blocks in the synthesis of more complex molecules. The interest in accessing simple substrates depreciates however when a complex, or expensive, system is then required to functionalize them. Thus, there is a real importance in having a practical system for the oxidation of C-H bonds.

While vanadium complexes have been used to catalyze olefin and alcohol oxidation, the application to C-H oxidation has not been well studied. In the course of screening potential catalysts, I found that commercially available  $Cp_2VCl_2$  catalyzes benzylic C-H oxidation selectively and effectively, without giving any aromatic oxidation products.

#### INTRODUCTION

The application of transition metal-catalyzed C-H oxidation to organic synthesis has received increasing attention in recent years.<sup>140</sup> Much of this research into the design of a catalyst system for C-H

---

<sup>139</sup> This chapter describes work I did in Chuo Chen's lab and published as: Xia, J.; Cormier, K. W.; Chen, C. *Chem. Sci.* **2012**, *3*, 2240. Adapted with permission from the Royal Society of Chemistry.

<sup>140</sup> (a) Chen, K.; Baran, P.S., *Nature*, **2009**, *459*, 824; (b) Ishihara, Y.; Baran, P. S. *Synlett*, **2010**, 1733; (c) Gutekunst, W. R.; Baran, P. S. *Chem. Soc. Rev.*, **2011**, *40*, 1976; (d) Newhouse, T.; Baran, P. S.

oxidation has been inspired by nature, with enzymes like cytochrome P450 and methane monooxygenase, for example, have offered templates for iron-catalyzed systems.<sup>141</sup> A synthetic variant to nature's enzymes can offer the advantage of having a broader scope or a more defined selectivity than their natural counterpart. Although many biomimetic<sup>142</sup> and non-biomimetic<sup>143</sup> methods have been

*Angew. Chem. Int. Ed.* **2011**, *50*, 3362; (e) Brückl, T.; Baxter, R. D.; Ishihara, Y.; Baran, P. S. *Acc. Chem. Res.* **2012**, *45*, 826; (f) Chen, M. S.; White, M. C. *Science*, **2007**, *318*, 783; (g) Chen, M. S.; White, M. C. *Science*, **2010**, *327*, 566.

<sup>141</sup> Que, Jr., L.; Tolman, W. B. *Nature* **2008**, *455*, 333.

<sup>142</sup> For reviews, see: (a) Que, Jr., L.; Tolman, W. B. *Angew. Chem. Int. Ed.* **2002**, *41*, 1114; (b) Que, Jr., L.; Tolman, W. B. *Nature* **2008**, *455*, 333; (c) Barton, D. H. R.; Doller, D. *Acc. Chem. Res.*, **1992**, *25*, 504; (d) Eames, J.; Watkinson, M. *Angew. Chem. Int. Ed.* **2001**, *40*, 3567; (e) Punniyamurthy, T.; Rout, L. *Coord. Chem. Rev.*, **2008**, *252*, 134; (f) Wendlandt, A. E.; Suess, A. M.; Stahl, S. S. *Angew. Chem. Int. Ed.* **2011**, *50*, 11062.

For examples of Fe systems, see: (g) Leising, R. A.; Kim, J.; Perez, M. A.; Que, Jr., L. *J. Am. Chem. Soc.* **1993**, *115*, 9524; (h) Kim, C.; Chen, K.; Kim, J.; Que, Jr., L. *J. Am. Chem. Soc.* **1997**, *119*, 5964; (i) Chen, K.; Que, L. *Chem. Commun.* **1999**, 1375; (j) Gómez, L., Garcia-Bosch, I.; Company, A.; Benet-Buchholz, J.; Polo, X.; Sala, X.; Ribas, X.; Costas, M. *Angew. Chem. Int. Ed.*, **2009**, *48*, 5720; (k) Makhlynets, O. V.; Rybak-Akimova, E. V. *Chem. Eur. J.* **2010**, *16*, 13995; (l) Paradine, S. M.; White, M. C. *J. Am. Chem. Soc.* **2012**, *134*, 2036.

For examples of the Mn systems, see: (l) Groves, J. T.; Viski, P. *J. Org. Chem.*, **1990**, *55*, 3628; (m) Tetard, D.; Verlhac, J.-B. *J. Mol. Catal. A: Chem.*, **1996**, *113*, 223; (n) Hamachi, K.; Irie, R.; Katsuki, T. *Tetrahedron Lett.*, **1996**, *37*, 4979; (o) Hull, J. F.; Balcells, D.; Sauer, E. L. O.; Raynaud, C.; Brudvig, G. W.; Crabtree, R. H.; Eisenstein, O. *J. Am. Chem. Soc.* **2010**, *132*, 7605; (p) Kim, J.; Ashenhurst, J. A.; Movassaghi, M. *Science* **2009**, *324*, 238.

For examples of Cu systems, see: (q) Itoh, S.; Kondo, T.; Komatsu, M.; Ohshiro, Y.; Li, C.; Kanehisa, N.; Kai, Y.; Fukuzumi, S. *J. Am. Chem. Soc.* **1995**, *117*, 4714; (r) Schönecker, B.; Zheldakova, T.; Liu, Y.; Kötteritzsch, M.; Günther, W.; Görls, H. *Angew. Chem. Int. Ed.* **2003**, *43*, 3240; (s) Chen, X.; Hao, X.-S.; Goodhue, C. E.; Yu, J.-Q. *J. Am. Chem. Soc.* **2006**, *128*, 6790; (t) Li, C.-J. *Acc. Chem. Res.* **2009**, *42*, 335; (u) Ni, Z.; Zhang, Q.; Xiong, T.; Zheng, Y.; Li, Y.; Zhang, H.; Zhang, J.; Liu, Q. *Angew. Chem. Int. Ed.* **2012**, *51*, 1244; (v) Michaudel, Q.; Thevenet, D.; Baran, P. S. *J. Am. Chem. Soc.* **2012**, *134*, 2547.

<sup>143</sup> For examples of Cr systems, see: (a) Muzart, J. *Chem. Rev.* **1992**, *92*, 113; (b) Pearson, A. J.; Han, G. R. *J. Org. Chem.* **1985**, *50*, 2791; (c) Chidambaram, N.; Chandrasekaran, S., *J. Org. Chem.*, **1987**, *52*, 5048; (d) Yamazaki, S. *Org. Lett.* **1999**, *1*, 2129; (e) Lee, S.; Fuchs, P. L. *J. Am. Chem. Soc.* **2002**, *124*, 13978.

For examples of Ru systems, see: (f) Tenaglia, A., Terranova, E., and Waegell, B., *Tetrahedron Lett.*, **1989**, *30*, 5271; (g) Lee, J. S.; Cao, H.; Fuchs, P. L. *J. Org. Chem.* **2007**, *72*, 5820; (h) McNeill, E.; Du Bois, J. *J. Am. Chem. Soc.* **2010**, *132*, 10202; (i) Harvey, M. E.; Musaev, D. G.; Du Bois, J. *J. Am. Chem. Soc.*, **2011**, *133*, 17207.

For an example of the Ag system, see: (j) Su, S.; Seiple, I. B.; Young, I. S.; Baran, P. S. *J. Am. Chem. Soc.*, **2008**, *130*, 16490.

For examples of Pd systems, see: (k) Muzart, J.; Pale, P.; Pete, J.-P. *Tetrahedron Lett.* **1982**, *23*, 3577; (l) Yu, J.-Q.; Corey, E. J. *J. Am. Chem. Soc.* **2003**, *125*, 3232; (m) Zhang, Y.-H.; Yu, J.-Q. *J. Am. Chem.*

reported, selective and efficient C–H oxidation is still difficult to achieve. Besides the inherent unreactivity of the substrate, the catalysts themselves pose the problem of rapid deactivation, often due to their being oxidized under the reaction conditions, which leads to low turnover numbers. In the case of benzylic oxidation of arylalkanes, competitive aromatic oxidations often further complicate the selectivity of the reaction.

The previously reported vanadium-catalyzed C–H oxidation has focused mainly on oxidative coupling of phenols.<sup>144</sup> The first C–H hydroxylation reaction by vanadium-complexes was reported by Mimoun, who found that oxidation of cyclohexane by (pic)VO(O<sub>2</sub>)·2H<sub>2</sub>O gave cyclohexanol and cyclohexanone, and oxidation of toluene gave a mixture of cresols along with a small amount of benzyl

*Soc.* **2009**, *131*, 14654; (n) Emmert, M. H.; Cook, A. K.; Xie, Y. J.; Sanford, M. S. *Angew Chem. Int. Ed.* **2011**, *50*, 9409; (o) Covell, D. J.; White, M. C. *Angew. Chem. Int. Ed.* **2008**, *47*, 6448; (p) Chuang, G. J.; Wang, W.; Lee, E.; Ritter, T. *J. Am. Chem. Soc.*, **2011**, *133*, 1760; (q) Huang, C.; Ghavtadze, N.; Chattopadhyay, B.; Gevorgyan, V. *J. Am. Chem. Soc.* **2011**, *133*, 17630.

For reviews of Pt systems, see: (r) Shilov, A. E.; Shul'pin, G. B. *Chem. Rev.* **1997**, *97*, 2879; (s) Stahl, S. S.; Labinger, J. A.; Bercaw, J. E. *Angew. Chem. Int. Ed.* **1998**, *37*, 2180; (t) Crabtree, R. H. *J. Chem. Soc., Dalton Trans.* **2001**, 2437; (u) Fekl, U.; Goldberg, K. I. *Adv. Inorg. Chem.* **2003**, *54*, 259; (v) Lersch, M.; Tilset, M. *Chem. Rev.* **2005**, *105*, 2471.

For examples of Os systems, see: (w) Bales, B. C.; Brown, P.; Dehestani, A.; Mayer, J. M. *J. Am. Chem. Soc.*, **2004**, *127*, 2832; (x) Shul'pin, G. B.; Kirillova, M. V.; Kozlov, Y. N.; Shul'pina, L. S.; Kudinov, A. R.; Pombeiro, A. J. L. *J. Catal.* **2011**, *277*, 164.

For a review of Rh-catalyzed C–H amination, see: (y) Zalatan, D. N.; Du Bois, J. *Top. Curr. Chem.* **2010**, *292*, 347.

For examples of hypervalent halogen systems, see: (z) Breslow, R., In *Comprehensive Organic Synthesis*, Trost, B. M.; Fleming, I. Ed.; Pergamon Press, Oxford, United Kingdom, **1991**, *1997*, 1939–1952; (aa) Nicolaou, K. C.; Baran, P. S.; Zhong, Y.-L. *J. Am. Chem. Soc.* **2001**, *123*, 3183; (bb) Ochiai, M.; Miyamoto, K.; Kaneaki, T.; Hayashi, S.; Nakanishi, W. *Science* **2011**, *332*, 448; (cc) Zhao, Y.; Yim, W.-L.; Tan, C. K.; Yeung, Y.-Y. *Org. Lett.* **2011**, *13*, 4308.

For examples of dioxirane systems, see: (dd) Mello, R.; Fiorentino, M.; Fusco, C.; Curci, R. *J. Am. Chem. Soc.* **1989**, *111*, 6749; (ee) Yang, D.; Wong, M.-K.; Wang, X.-C.; Tang, Y.-C. *J. Am. Chem. Soc.* **1998**, *120*, 6611.

For examples of the oxaziridine systems, see: (ff) DesMarteau, D. D.; Donadelli, A.; Montanari, V.; Petrov, V. A.; Resnati, G. *J. Am. Chem. Soc.* **1993**, *115*, 4897; (gg) Brodsky, B. H.; Du Bois, J. *J. Am. Chem. Soc.*, **2005**, *127*, 15391.

<sup>144</sup> For reviews of V-catalyzed reactions, see: (a) Butler, A.; Clague, M. J.; Meister, G. E. *Chem. Rev.* **1994**, *94*, 625; (b) Hirao, T. *Chem. Rev.*, **1997**, *97*, 2707–2724; (c) Conte, V.; Di Furia, F.; Licini, G. *Appl. Catal., A* **1997**, *157*, 335; (d) Ligtenbarg, A. G. J.; Hage, R.; Feringa, B. L. *Coord. Chem. Rev.* **2003**, *237*, 89; (e) da Silva, J. A. L.; da Silva, J. J. R. F.; Pombeiro, A. J. L. *Coord. Chem. Rev.* **2011**, *255*, 2232.

alcohol and benzaldehyde.<sup>145</sup> The reactivity and selectivity of this catalyst are much the same as those of the commonly used C–H oxidizing iron catalyst  $[\text{Fe}(\text{BPMEN})(\text{CH}_3\text{CN})_2][\text{ClO}_4]_2$ <sup>146</sup> that I had worked with before turning to vanadium. Vanadium(V) peroxo complexes are capable of oxidizing aliphatic and aromatic hydrocarbons. Di Furia and Modena subsequently determined the mechanism to be a radical chain reaction mediated by a superoxovanadium species  $(\text{pic})\text{VO}_3^{\cdot-}$ .<sup>147</sup> Meanwhile, a free hydroxyl radical-mediated mechanism was also proposed by Shul'pin.<sup>148</sup> Notably, Talsi has provided evidence for the production of *t*-butylperoxyl radical by  $\text{VO}(\text{acac})_2/\text{TBHP}$ .<sup>149</sup> This free-radical type reactivity toward rapid hydrocarbon oxidation was observed in several related vanadium catalyst systems.<sup>150</sup> With modest yields and regioselectivities, the synthetic utility of most reported vanadium catalysts is rather limited. One of the major interests then of the reaction I developed is the selectivity for benzylic C–H oxidation without any competing aromatic oxidation.

---

<sup>145</sup> (a) Mimoun, H.; Saussine, L.; Daire, E.; Postel, M.; Fischer, J.; Weiss, R. *J. Am. Chem. Soc.* **1983**, *105*, 3101; (b) Mimoun, H.; Chaumette, P.; Mignard, M.; Saussine, L. *New J. Chem.* **1983**, *7*, 467; (c) Mimoun, H.; Mignard, M.; Brechot, P.; Saussine, L. *J. Am. Chem. Soc.* **1986**, *108*, 3711.

<sup>146</sup> (a) Chen, K.; Que, L. *Chem. Commun.* **1999**, 1375; (b) Makhlynets, O. V.; Rybak-Akimova, E. V. *Chem. Eur. J.* **2010**, *16*, 13995.

<sup>147</sup> (a) Bonchio, M.; Conte, V.; Di Furia, F.; Modena, G. *J. Org. Chem.* **1989**, *54*, 4368; (b) Bianchi, M.; Bonchio, M.; Conte, V.; Coppa, F.; Di Furia, F.; Modena, G.; Moro, S.; Standen, S. *J. Mol. Catal.* **1993**, *83*, 107; (c) Bonchio, M.; Conte, V.; Di Furia, F.; Modena, G.; Moro, S.; Edwards, J. O. *Inorg. Chem.* **1994**, *33*, 1631; (d) Bonchio, M.; Conte, V.; Di Furia, F.; Modena, G.; Moro, S. *J. Org. Chem.* **1994**, *59*, 6262.

<sup>148</sup> (a) Shul'pin, G. B.; Attanasio, D.; Suber, L. *J. Catal.* **1993**, *142*, 147; (b) Nizova, G. V.; Shul'pin, G. B. *Russ. Chem. Bull.* **1994**, *43*, 1146.

<sup>149</sup> (a) Talsi, E. P.; Chinakov, V. D.; Babenko, V. P.; Zamaraev, K. I. *J. Mol. Catal.* **1993**, *81*, 235; (b) Talsi, E. P.; Shalyaev, K. V. *J. Mol. Catal.* **1994**, *92*, 245.

<sup>150</sup> (a) Moiseev, I. I.; Gekhman, A. E.; Shishkin, D. I. *New J. Chem.* **1989**, *13*, 683; (b) Gekhman, A. E.; Stolyarov, I. P.; Ershova, N. V.; Moiseeva, N. I.; Moiseev, I. I. *Doklady Chem.* **2001**, *378*, 150; (c) Reis, P. M.; Silva, J. A. L.; Silva, J. J. R. F. d.; Pombeiro, A. J. L. *Chem. Commun.* **2000**, 1845; (d) Silva, T. F. S.; Kirillova, K. V. L. M. V.; Silva, M. F. G. d.; Martins, L. M. D. R. S.; Pombeiro, A. J. L. *Adv. Synth. Catal.* **2010**, *352*, 171.

Vanadium complexes are well-known for their ability to transfer an oxygen (in directed epoxidation)<sup>151</sup> or halogen atom (by halogenase)<sup>152</sup> to olefins. Considering the transition states of metal-catalyzed olefin and C–H oxidation (Figure 1), the idea was that vanadium complexes could also be good catalysts for C–H oxidation, even though a vanadium hydroxylase remains elusive. Studying the Sharpless epoxidation in fact gave the idea to try the same conditions for the oxidation of arylalkanes.

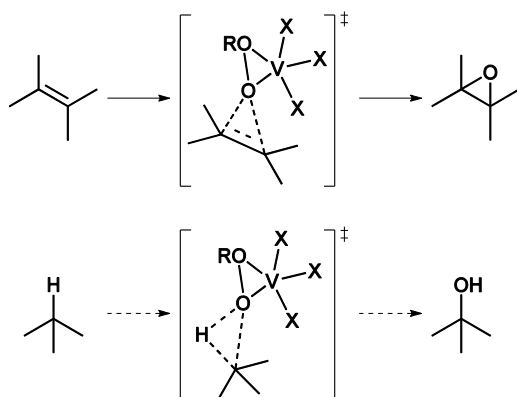


**Figure 1. Olefin vs. C–H oxidation.**

Arylalkanes were the initial focus as substrates, which would complement the substrate scope of Mimoun's complex and those of the prevalent iron catalysts. The thought too was that the benzylic position presents itself as activated by the aromatic ring thus making it more accessible for oxidation allowing for the goal of achieving selective benzylic C(sp<sup>3</sup>)–H oxidation by suppressing aromatic C(sp<sup>2</sup>)–H oxidation and non-metal-based radical oxidation. This consideration relies on the fact that selectivity in a reaction can also be determined by the substrate and does not rely solely on the catalyst.

<sup>151</sup> (a) Sharpless, K. B.; Verhoeven, T. R. *Aldrichimica Acta*, **1979**, *12*, 63; (b) Fukuyama, T.; Vranesic, B.; Negri, D. P.; Y. Kishi, Y. *Tetrahedron Lett.* **1978**, *19*, 2741; (c) Mihelich, E. D.; Daniels, K.; Eickhoff, D. J. *J. Am. Chem. Soc.* **1981**, *103*, 7690; (d) Zhang, W.; Basak, A.; Kosugi, Y.; Hoshino, Y.; Yamamoto, H. *Angew. Chem. Int. Ed.* **2005**, *44*, 4389.

<sup>152</sup> (a) Butler, A.; Sandy, M. *Nature*, **2009**, *460*, 848; (b) Neumann, C. S.; Fujimori, D. G.; Walsh, C. T. *Chem. Biol.* **2008**, *15*, 99; (c) Vaillancourt, F. H.; Yeh, E.; Vosburg, D. A.; Garneau-Tsodikova, S.; Walsh, C. T. *Chem. Rev.* **2006**, *106*, 3364.

## EXPERIMENTAL PROCEDURES

All reactions were performed in glassware under argon. Organic solutions were concentrated by rotary evaporator at ca. 30 mmHg. Flash column chromatography was performed as described by Still,<sup>153</sup> employing EMD silica gel 60 (230–400 mesh ASTM). TLC analyses were performed on EMD 250 m Silica Gel 60 F254 plates and visualized by quenching of UV fluorescence ( $\lambda_{\text{max}} = 254 \text{ nm}$ ), or by staining ceric ammonium molybdate. <sup>1</sup>H and <sup>13</sup>C NMR spectra were recorded on a Varian Inova-500 or Inova-400. Chemical shifts for <sup>1</sup>H and <sup>13</sup>C NMR spectra are reported in ppm ( $\delta$ ) relative to the <sup>1</sup>H and <sup>13</sup>C signals in the solvent (CDCl<sub>3</sub>:  $\delta$  7.26, 77.00 ppm; DMSO-d<sub>6</sub>:  $\delta$  2.50 ppm; CD<sub>3</sub>CN:  $\delta$  1.94 ppm) and the multiplicities are presented as follows: s = singlet, d = doublet, t = triplet, m = multiplet. Mass spectra were acquired on an Agilent 1200 LC-MS or VG 70-VSE. Data collection on 70-VSE (purchased in part with a grant from the Division of Research Resources, National Institutes of Health RR 04648) was serviced by the Mass Spectrometry Laboratory at the University of Illinois at Urbana-Champaign. Gas Chromatography (GC) was performed on an Agilent 6890N GC.

### *General Procedure for the Cp<sub>2</sub>VCl<sub>2</sub>/TBHP-catalyzed benzylic oxidation reaction*

To a 4 mL vial charged with vanadocene dichloride (2.5 mg, 0.01 mmol, 0.01 equiv) was added tert-butyl hydroperoxide (70% in water, 720  $\mu$ L, 5.0 mmol, 5.0 equiv). The solution was stirred at 30°C for 30 min before the substrate (1.0 mmol, 1.0 equiv) was added. After reacting at 30°C for 5 days, the reaction mixture was purified directly by flash column chromatography. Alternatively, the reaction mixture was transferred to a 16 mL vial, diluted with 10 mL ethyl acetate, quenched with solid sodium thiosulfate (700 mg, 5.5 mmol, 5.5 equiv) for 1 hour, filtered, washed with ethyl acetate, concentrated, and purified by flash column chromatography.

---

<sup>153</sup> Still, W. C.; Kahn, M.; Mitra, A. *J. Org. Chem.* **1978**, *43*, 2923.

## RESULTS

Having previously worked on iron as a catalyst for C-H oxidation and found that free radicals were produced in solution, making the selectivity of the reaction more difficult to harness, I turned to investigating the oxidative ability of vanadium catalysts. Through the screening of all the vanadium catalysts commercially available from Strem Chemicals Inc., in combination with several known oxidants, I discovered that  $\text{VO}(\text{acac})_2/\text{TBHP}$  could oxidize ethylbenzene to the ketone selectively and effectively at 30 °C when no solvent was used (Table 1, entry 1). This reaction system is commonly used for Sharpless epoxidation of alkenes. Based on  $^1\text{H}$  NMR analysis and unlike Mimoun's complex, the reaction did not give any aromatic oxidation products, nor was there a reaction with cyclohexane as judged by gas chromatography. A number of other vanadium catalysts were also found to promote this same benzylic oxidation. For example,  $\text{VOF}_3$  and  $\text{VOCl}_3$  showed comparable reactivity and selectivity, while  $\text{VO}(\text{O}^i\text{Pr})_3$  and  $\text{V}_2\text{O}_5$  were less effective (entries 2–5). The best results were obtained with vanadocene dichloride (entry 6). Using 1 mol %  $\text{Cp}_2\text{VCl}_2$  and 5 equiv TBHP, oxidation of ethylbenzene at 30°C gave acetophenone in 87–90% isolated yield. The only detectable byproducts in the crude reaction mixture as determined by GC and  $^1\text{H}$  NMR were 1–2% of benzylic peroxide  $\text{PhCH}(\text{OO}^t\text{Bu})\text{CH}_3$  and benzaldehyde.

Significantly lower turnover numbers were observed at higher temperature, indicating that the active catalyst is thermally unstable. In this vane I tried both conventional heating and microwave reaction conditions, though the benefits of the latter were incremental and required great precaution as the mixture is potentially explosive.

Reducing the amount of TBHP or the reaction time also led to a significant decrease of conversion (entries 7–9). While no solvent is required, acetonitrile could be used to dissolve the

substrates (entry 10). In the screening of solvents, I was also attentive to the possibility of the solvent being oxidized. Among all the oxidants examined, TBHP is the only effective oxidant (entries 11 and 12). There was no reaction in the absence of the catalyst or oxidant. While the initial screening was performed under dry and inert conditions, it was soon found that the reaction could be conducted under argon or ambient atmosphere. This further adds to the attractiveness of the reaction.

Initially thinking that water in the reaction mixture may lead to catalyst deactivation, I tried using anhydrous TBHP both in n-hexane and decane but found that the rate of oxidation is lower. Using these anhydrous forms of TBHP was also inspired by Sharpless's alkene epoxidation work. Other ineffective oxidants that I screened included:  $O_2$ , PhIO,  $PhI(OAc)_2$ ,  $PhI(TFA)_2$ , DDQ, NMO, Oxone, TBA-Oxone,  $(NH_4)_2S_2O_8$ ,  $K_2S_2O_8$ , m-CPBA, benzoyl peroxide,  $NaIO_4$  and  $H_5IO_6$ . At room temperature, PhIO promoted a slow background benzylic oxidation without any catalyst present.

Reaction scheme: 1-phenylethane (**1**) is oxidized to acetophenone (**2**) using 1 mol % catalyst and an oxidant, conducted neat at 30 °C.

Entry	Catalyst	Oxidant	Time	Yield <sup>b</sup>
1	VO(acac) <sub>2</sub>	5 equiv TBHP(aq)	5 days	82%
2	VOF <sub>3</sub>	5 equiv TBHP(aq)	5 days	79%
3	VOCl <sub>3</sub>	5 equiv TBHP(aq)	5 days	79%
4	VO(O <sup>i</sup> Pr) <sub>3</sub>	5 equiv TBHP(aq)	5 days	61%
5	V <sub>2</sub> O <sub>5</sub>	5 equiv TBHP(aq)	5 days	27%
<b>6</b>	<b>Cp<sub>2</sub>VCl<sub>2</sub></b>	<b>5 equiv TBHP(aq)</b>	<b>5 days</b>	<b>87–90%<sup>c</sup></b>
7	Cp <sub>2</sub> VCl <sub>2</sub>	4 equiv TBHP(aq)	5 days	54%
8	Cp <sub>2</sub> VCl <sub>2</sub>	3 equiv TBHP(aq)	5 days	25%
9	Cp <sub>2</sub> VCl <sub>2</sub>	5 equiv TBHP(aq)	3 days	61%
10 <sup>d</sup>	Cp <sub>2</sub> VCl <sub>2</sub>	5 equiv TBHP(aq)	5 days	84%
11	Cp <sub>2</sub> VCl <sub>2</sub>	5 equiv H <sub>2</sub> O <sub>2</sub> (aq)	5 days	0%
12	Cp <sub>2</sub> VCl <sub>2</sub>	5 equiv NaClO(aq)	5 days	0%

<sup>a</sup> All reactions were conducted with 1 mmol of **1**. <sup>b</sup> Determined by GC using dodecane as the external standard with calibration. <sup>c</sup> Isolated yields from 4 runs, 86% GC yield. <sup>d</sup> With 0.2 mL of CH<sub>3</sub>CN.

**Table 1. Development of the vanadium-catalyzed benzylic oxidation.<sup>a</sup>**

This benzylic oxidation exhibits good substrate scope as shown in Table 2. Substrates were chosen that would affect the electronics of the aromatic ring, thus potentially offering insights into the mechanism of the reaction by Hammett plots. Here we expect that having an electron-donating group on the aromatic ring will boost reactivity. However, such a correlation between the electronic effects and reactivity was not exhibited. It was found instead that the 4-position of the phenyl ring tolerated a variety of substituents (fluoro, chloro, acetyl, cyano, or methoxyl) with different electronic properties

(entries 1–6). The desired ketones were all obtained in good yields except for the oxidation of 4-ethylanisole (entry 6). Nor was the 3-position sensitive to electronic perturbation (cyano, carboxyl, bromo, or methoxyl). The desired ketone products were all formed in good yields (entries 7–10). However, in the presence of a substituent at the 2-position (chloro or methoxyl), the ketone formation was less efficient (entries 11 and 12).

1 mol %  $\text{Cp}_2\text{VCl}_2$   
5 equiv TBHP(aq)  
neat, 30 °C, 5 days

Entry	Ar R Yield <sup>b</sup>	Product	Entry	Ar R Yield <sup>b</sup>	Product
1	Ph CH <sub>3</sub> 90%		11	2-Cl-Ph CH <sub>3</sub> 52%	
2	4-F-Ph CH <sub>3</sub> 91%		12	2-MeO-Ph CH <sub>3</sub> 68%	
3	4-Cl-Ph CH <sub>3</sub> 86%		13	4-Et-Ph CH <sub>3</sub> 86% <sup>c</sup>	
4	4-Me(O)C-Ph CH <sub>3</sub> 89%		14	4-Ph-Ph H 54% 60% <sup>d</sup>	
5	4-NC-Ph CH <sub>3</sub> 77%		15	Ph <i>n</i> -C <sub>7</sub> H <sub>15</sub> 57%	
6	4-MeO-Ph CH <sub>3</sub> 57%		16	4-Br-Ph <i>n</i> -C <sub>6</sub> H <sub>13</sub> 51%	
7	3-NC-Ph CH <sub>3</sub> 85%		17	4-MeO-Ph <i>n</i> -C <sub>2</sub> H <sub>5</sub> 49%	
8	3-HO <sub>2</sub> C-Ph CH <sub>3</sub> 91%		18	3-MeO-Ph <i>n</i> -C <sub>6</sub> H <sub>13</sub> 50%	
9	3-Br-Ph CH <sub>3</sub> 90%		19	Ph CH <sub>2</sub> - C(OH)(CH <sub>3</sub> ) <sub>2</sub> 50% <sup>e</sup>	
10	3-MeO-Ph CH <sub>3</sub> 80%		20	Ph Ph 95%	

<sup>a</sup> All reactions were conducted with 1 mmol of the substrate. <sup>b</sup> Isolated yield. <sup>c</sup> With 2 mol%  $\text{Cp}_2\text{VCl}_2$  and 10 equiv TBHP. <sup>d</sup> With acetonitrile (0.2 mL). <sup>e</sup> Yield obtained after TBS protection of the alcohol.

**Table 2. Scope of the  $\text{Cp}_2\text{VCl}_2$ -catalyzed benzylic oxidation.<sup>a</sup>**

A series of different side-chains was also been found to undergo oxidation with no competing aromatic oxidation. Extending the length of the side-chain reduced the catalyst efficiency (entries 15–18). Oxidation of phenyloctane (entry 15) gave 57% yield of the desired ketone and 13% yield of the recovered starting material. In fact, I had been using phenyloctane in the very initial stages of screening as it lends itself to determining the selectivity of oxidation at the benzylic position over the other  $sp^3 C-H$  bonds present in the molecule. It is also not volatile making it easier to determine the mass balance of the reaction. The major byproducts were 9% yield of the benzylic tert-butylperoxide and 10% yield of benzoic acid. We also isolated 3%, 1% and 1% yield of the 1,4-, 1,5- and 1,6-diketone as minor byproducts. Phenolic and alcohol products were not observed in the crude  $^1H$  NMR spectra. The mass balance of these materials is 94%. The diketones were most likely derived from an intramolecular hydrogen abstraction reaction of the benzylic radical. This was determined after subjecting the benzylic ketone to the reaction conditions and not observing any diketones.

This new oxidation method can be used as an alternative approach for aldol synthesis. For example, 2-methyl-4-phenyl-2-butanol was oxidized cleanly to afford the corresponding ketone in 50% yield (entry 19). This particular substrate, with its hydroxyl group two carbons away from the site of oxidation, was also explored as a potential directing group that could be a further means to boost the reactivity. Finally, oxidation of the highly activated diphenylmethane also proceeded effectively (entry 20).

I envision that this reaction likely proceeds through a two-step oxidation where a benzylic C–H oxidation would first give rise to a benzylic alcohol that is then oxidized to the ketone. Since vanadium-catalyzed oxidation of secondary alcohols to ketones is a known process and its mechanism has been investigated,<sup>154</sup> the first step is where mechanistic study is needed.

---

<sup>154</sup> (a) Hanson, S. K.; Baker, R. T.; Gordon, J. C.; Scott, B. L.; Silks, L. A.; Thorn, D. L. *J. Am. Chem. Soc.* 2010, *132*, 17804–16; (b) Kirihara, M.; Ochiai, Y.; Takahata, S. T. H.; Nemoto, H. *Chem. Commun.* 1999, 1387–88; (c) Maeda, Y.; Kakiuchi, N.; Matsumura, S.; Nishimura, T.; Kawamura, T.;

The available evidence suggests that this vanadium-catalyzed benzylic oxidation reaction occurred through a C–H abstraction mechanism (Figure 2). The  $\text{Cp}_2\text{VCl}_2$  solution quickly turned from green to orange upon addition of TBHP, indicating a valence change from V(IV) to V(V). Since  $\text{VOX}_3$  also catalyzed benzylic oxidation effectively, the reactive species generated from  $\text{Cp}_2\text{VCl}_2/\text{TBHP}$  is likely to be II, the valence tautomer of I. (Alternatively, the reactive species could be  $\text{Cp}_2\text{V}(\text{O})(\text{OO}^t\text{Bu})$ ). It has been shown that the one-electron oxidation of  $\text{VO}(\text{acac})_2$  by TBHP in alcohol gives  $\text{VO}(\text{OR})_3$  without radical chain decomposition of TBHP.<sup>155</sup> II abstracts a proton to give the benzylic radical and III. Subsequent rebound affords the benzylic alcohol, which is further oxidized to ketone. Reaction of IV with TBHP regenerates I/II.

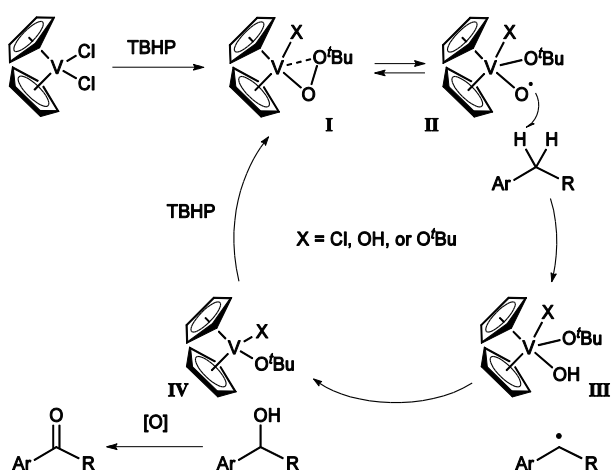
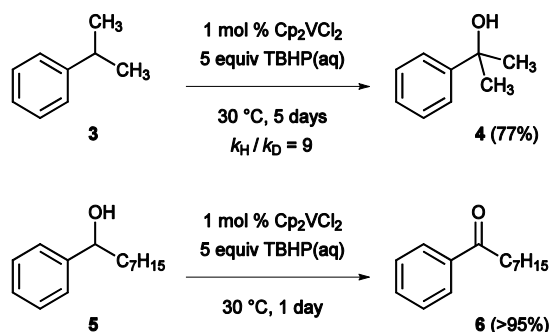


**Figure 2. Proposed mechanism of the  $\text{Cp}_2\text{VCl}_2$ -catalyzed benzylic oxidation.**

Uemura, S. *J. Org. Chem.* **2002**, *67*, 6718–24; (d) Velusamy, S.; Punniyamurthy, T. *Org. Lett.* **2004**, *6*, 217–19; (e) Radosevich, A. T.; Musich, C.; Toste, F. D. *J. Am. Chem. Soc.* **2005**, *127*, 1090–91; (f) Weng, S.-S.; Shen, M.-W.; Kao, J.-Q.; Munot, Y. S.; Chen, C.-T. *Proc. Natl. Acad. Sci. U.S.A.* **2006**, *103*, 3522–27; (g) Jiang, N.; Ragauskas, A. J. *J. Org. Chem.* **2007**, *72*, 7030–33.

<sup>155</sup> S. Cenci, F. Di Furia, G. Modena, R. Curci and J. O. Edwards *J. Chem. Soc. Perkin Trans. 2*, **1978**, 979–984.



**Scheme 1. Evidence for the intermediacy of a benzylic alcohol.**

The intermediacy of a benzylic alcohol in the reaction was proved by the fact that benzylic alcohol **4** is produced with 77% isolated yield when cumene (**3**) is subjected to the oxidation conditions. (Scheme 1). To then demonstrate that benzylic alcohols can be oxidized to ketones, we treated alcohol **5** with the same oxidation conditions and found that ketone **6** was quantitatively obtained in 1 day. The alcohol to ketone oxidation step is thus fast compared to the first step of the reaction. Theoretically, the possibility that the ketone was derived from the oxidation of a benzylic peroxide remained, so Jibao Xia, a post-doctoral fellow in the Chen lab, submitted some of the PhCH(OO<sup>t</sup>Bu)C<sub>7</sub>H<sub>15</sub> minor product he had isolated from the reaction of PhCHC<sub>7</sub>H<sub>15</sub> to the standard reaction conditions. The benzylic peroxide was stable to Cp<sub>2</sub>VCl<sub>2</sub> or TBHP alone. Treating it with the standard oxidation conditions gave **6** cleanly but only in 30% yield after 6 days. It was therefore concluded that ketone **6** was formed predominantly through oxidation of **5** instead of decomposition or oxidation of the benzylic peroxide.

Alternatively, this reaction could proceed through a free radical chain mechanism, with either a superoxovanadium or an alkoxy/hydroxyl radical as the chain carrier. For iron-catalyzed C–H hydroxylation reactions, the role of alkoxy or hydroxyl radical, generated from the metal-catalyzed Haber–Weiss decomposition of peroxides, is often under debate.<sup>156</sup> While it is difficult to unequivocally

<sup>156</sup> (a) Kim, J.; Harrison, R. G.; Kim, C.; Que, L., Jr. *J. Am. Chem. Soc.* 1996, 118, 4373–79; (b) Chen, K.; Que, L., Jr. *J. Am. Chem. Soc.* 2001, 123, 6327–37; (c) MacFaul, P. A.; Ingold, K. U.; Wayner, D.

exclude this possibility, the following observations suggest that our benzylic C–H oxidation reaction is not mediated by  $t\text{BuO}\cdot$  or  $t\text{BuOO}\cdot$ , the Haber–Weiss decomposition products of TBHP.

First, since the vanadium-catalyzed benzylic oxidation reaction is quite a slow reaction, taking several days, it is unlikely that a free alkoxy or hydroxyl radical-mediated chain mechanism is at work.<sup>157</sup> Although it is possible that the low reaction rate is due to a slow generation of free radicals, kinetic isotope effect (KIE) studies performed by Jibao Xia, show that the C–H cleavage instead of the reactive species generation is the rate-limiting step. Second, the  $\text{Cp}_2\text{VCl}_2$ -catalyzed oxidation reaction did not yield any benzylic hydroperoxide (ROOH), the common Fenton reaction product derived from trapping of the evolved  $\text{O}_2$  by the radical intermediates. Third, no reaction occurred when  $\text{H}_2\text{O}_2$  and  $\text{NaClO}$  were used as the oxidants, both commonly used to generate radicals. Substituting  $\text{FeCl}_2$  or  $\text{CuCl}_2$  for  $\text{Cp}_2\text{VCl}_2$  in an attempt to induce the Fenton oxidation of phenyloctane also gave less than 5% yield of **6**. Fourth, cyclohexane, known to be oxidized by  $\text{RO}\cdot$  or  $\text{ROO}\cdot$ , failed to react under our conditions. Olefins are also relatively inert under these conditions. Fifth, addition of the radical inhibitor BHT (2 mol %) in order to suppress the radical initiation had no significant effects on the oxidation of phenyloctane, indicating that the reaction is not a radical chain reaction mediated by  $t\text{BuO}\cdot$  generated from catalyst activation (for example,  $\text{I/II} \rightarrow \text{Cp}_2\text{V}(\text{O})\text{X} + t\text{BuO}\cdot$ ). Sixth, addition of radical trap  $\text{BrCCl}_3$  (1 equiv) in an attempt to capture this benzylic radical failed, indicating that the rebound of III and the benzylic radical is relatively fast and possibly occurs in the solvent cage. This C–H abstraction/rebound may proceed in a nearly concerted asynchronous manner as shown in Fig. 3.

---

D. M.; Que, L., Jr. *J. Am. Chem. Soc.* **1997**, *119*, 10594–98; (d) Chen, K.; Costas, M.; Kim, J.; Tipton, A. K.; Que, L., Jr. *J. Am. Chem. Soc.* **2002**, *124*, 3026–35; (e) Stavropoulos, P.; Çelenligil-Çetin, R.; Tapper, A. E. *Acc. Chem. Res.* **2001**, *34*, 745–52.

<sup>157</sup> (a) MacFaul, P. A.; Ingold, K. U.; Wayner, D. D. M.; Que, Jr., L. *J. Am. Chem. Soc.* **1997**, *119*, 10594.

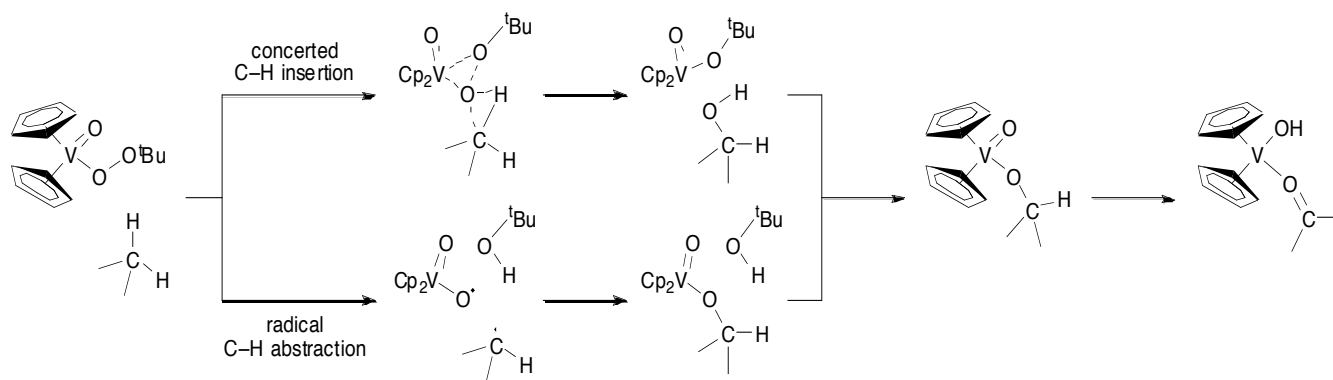


**Figure 3. The two possible pathways for the C-H oxidation step: concerted C-H insertion or a radical C-H abstraction mechanism.**

## DISCUSSION

The reaction that I developed offers an effective and selective means to catalyze benzylic C-H oxidation with a commercially available catalyst. Using 1 mol % Cp<sub>2</sub>VCl<sub>2</sub> and 5 equiv TBHP, the benzylic C(sp<sup>3</sup>)-H groups can be oxidized at 30°C in good yields without aromatic C(sp<sup>2</sup>)-H oxidation. The selectivity of this catalyst system is complementary to that of Mimoun's complex and iron catalysts. The catalyst loading required for this reaction is also significantly lower than most other systems and does not require multiple additions of catalyst.

The oxidation by this vanadium system could be a first step towards another elusive functionalization, namely halogenation of sp<sup>3</sup>-hybridized C-H bonds. Indeed, in nature vanadium numbers among halogenation catalysts that proceeding through an oxidative mechanism.<sup>158</sup>

A next step that I see for furthering this research would be the development of a still better catalyst that has an increased number of turnovers and that could induce enantioselectivity.

<sup>158</sup> Vaillancourt, F. H.; Yeh, E.; Vosburg, D. A.; Garneau-Tsodikova, S.; Walsh, C. T. *Chem. Rev.* **2006**, *106*, 3364.

A first approach to greater reactivity could be the exploration of the effects of substitutions on the cyclopentadienyl rings.<sup>159</sup>

Besides empirically studying the mechanism, the mechanism could be studied computationally by carrying out single point energy calculations to accurately assess the activation barriers of the pathways, helping to discriminate between a radical C–H abstraction or a concerted C–H insertion for the first mechanistic step.

---

<sup>159</sup> Cormier, K. W.; Lewis, M. *Polyhedron* **2009**, *28*, 3120.

## CHAPTER FOUR

# Computational Study of a Mn-catalyzed Oxidative Radical Cyclization<sup>160</sup>

### ABSTRACT

As a means to discriminate between possible reaction mechanisms, computational methods in chemistry can be both predictive and descriptive. Predicting the outcome of a reaction saves time and effort. This is evermore crucial when the chemical target is complex molecule that requires multiple steps for its assembly. Pyrrole–imidazole alkaloids are just such targets, having unique and complex structures that have challenged chemists for decade because of their densely functionalized skeletons and high nitrogen and halogen contents. In completing the total synthesis of these compounds, members of the Chen lab have used a biomimetic route for the construction of the core skeleton. The development of this synthetic strategy was facilitated by computational studies and the mechanism of the reaction further understood by these methods.

### INTRODUCTION

Pyrrole–imidazole alkaloids make up a family of complex natural products that are formed by the dimerization of oroidin (**1**). Romo and Molinski have studied the biosynthesis of

---

<sup>160</sup> The computational study that I describe in this chapter was published as part of a publication: Wang, X.; Wang, X.; Tan, X.; Lu, J.; Cormier, K. W.; Ma, Z.; Chen, C. *J. Am. Chem. Soc.* **2012**, *134*, 18834. Adapted with permission from the American Chemical Society.

the dimers by converting the synthetic, non-natural oroidin derivative dichloroclathrocin into dimeric non-natural pyrrole-imidazole alkaloids. This they achieved using enzymes extracted from *Stylissa caribica*, the bacteria from Caribbean marine sponges that produce the natural products.<sup>161</sup> They use these same cell-free enzymatic transformations to support their hypothesis that the dimerization of oroidins is governed by enzymatic single electron transfers.

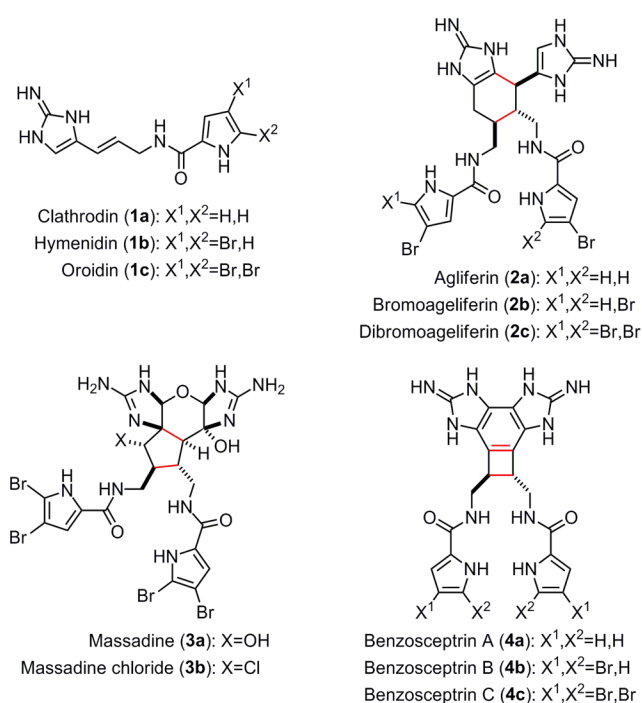


**Figure 1. Structures of selected pyrrole-imidazole alkaloids.**

<sup>161</sup> (a) Stout, E. P.; Wang, Y.-G.; Romo, D.; Molinski, T. F. *Angew. Chem., Int. Ed.* **2012**, *51*, 4877; (b) Stout, E. P.; Morinaka, B. I.; Wang, Y.-G.; Romo, D.; Molinski, T. F. *J. Nat. Prod.* **2012**, *75*, 527.

Enzymes that facilitate single electron transfer are ubiquitous in nature, ranging from the cytochromes, ferridoxin, xanthine oxidase, succinate dehydrogenase, rubredoxin, and others. These are all metal-containing enzymes that can readily switch between oxidation states by donating or accepting an electron. This transfer of an electron can be either induced photochemically or chemically, hence the two major classifications of electron transfer reactions.

Previous work in the Chen lab, using a small-molecule model system, supports the idea that cycloaddition could proceed through a radical mechanism by a single electron transfer oxidation of **1**.<sup>162</sup> Both the [4+2] and [3+2] dimerization products can be obtained in this way.<sup>163</sup> This biomimetic approach was then used to complete the total synthesis of the natural product ageliferin.<sup>164</sup> Manganese (III) was used to promote the radical oxidative cyclization of a  $\beta$ -ketoester. Furthermore, the control of a [4+2] or [3+2] dimer product was developed through an understanding of the mechanism of the cycloaddition using computational methods.

---

<sup>162</sup> Tan, X.; Chen, C. *Angew. Chem., Int. Ed.* **2006**, *45*, 4345.

<sup>163</sup> (a) Ma, Z.; Lu, J.; Wang, X.; Chen, C. *Chem. Commun.* 2011, 47, 427–429; (b) Lu, J.; Tan, X.; Chen, C. *J. Am. Chem. Soc.* **2007**, *129*, 7768.

<sup>164</sup> (a) Wang, X.; Ma, Z.; Lu, J.; Tan, X.; Chen, C. *J. Am. Chem. Soc.* **2011**, *133*, 15350; (b) Wang, X.; Wang, X.; Tan, X.; Lu, J.; Cormier, K. W.; Ma, Z.; Chen, C. *J. Am. Chem. Soc.* **2012**, *134*, 18834.

## EXPERIMENTAL PROCEDURES

### Computational Details

The preliminary computations were performed by Dr. Chen on Spartan 04 suite of programs<sup>165</sup> using UHF/6-31G\*, UB3LYP/6-31G\*\*//UHF/6-31G\* and UB3LYP/6-31G\*\*.<sup>166</sup>

Using the geometries from Spartan at the UB3LYP/6-31G\*\* level of theory as starting geometries, I performed further optimized on Gaussian 03<sup>167</sup> or 09<sup>168</sup> suite of programs using the

---

<sup>165</sup> Spartan'04, Wavefunction, Inc., Irvine, CA. The calculation methods used in Spartan'04 have been documented in: Kong, J.; White, C. A.; Krylov, A. I.; Sherill, C. D.; Adamson, R. D.; Furlani, T. R.; Lee, M. S.; Lee, A. M.; Gwaltney, S. R.; Adams, T. R.; Ochsenfeld, C.; Gilbert, A. T. B.; Kedziora, G. S.; Rassolov, V. A.; Maurice, D. R.; Nair, N.; Shao, Y.; Besley, N. A.; Maslen, P. E.; Dombroski, J. P.; Daschel, H.; Zhang, W.; Korambath, P. P.; Baker, J.; Byrd, E. F. C.; Van, Voorhis, T.; Oumi, M.; Hirata, S.; Hsu, C.-P.; Ishikawa, N.; Florian, J.; Warshel, A.; Johnson, B. G.; Gill, P. M. W.; Head-Gordon, M.; Pople, J. A. *J. Computational Chem.* **2000**, *21*, 1532.

<sup>166</sup> (a) Wong, M. W.; Radom, L. *J. Phys. Chem.* **1995**, *99*, 8582; (b) Leach, A. G.; Wang, R.; Wohlhieter, G. E.; Khan, S. I.; Jung, M. E.; Houk, K. N. *J. Am. Chem. Soc.* **2003**, *125*, 4271.

<sup>167</sup> Gaussian 03, Revision E.01, M. J. Frisch; Trucks, G. W.; Schlegel, H. B.; Scuseria, G. E.; Robb, M. A.; Cheeseman, J. R.; Montgomery, Jr., J. A.; Vreven, T.; Kudin, K. N.; Burant, J. C.; Millam, J. M.; Iyengar, S. S.; Tomasi, J.; Barone, V.; Mennucci, B.; Cossi, M.; Scalmani, G.; Rega, N.; Petersson, G. A.; Nakatsuji, H.; Hada, M.; Ehara, M.; Toyota, K.; Fukuda, R.; Hasegawa, J.; Ishida, M.; Nakajima, T.; Honda, Y.; Kitao, O.; Nakai, H.; Klene, M.; Li, X.; Knox, J. E.; Hratchian, H. P.; Cross, J. B.; Bakken, V.; Adamo, C.; Jaramillo, J.; Gomperts, R.; Stratmann, R. E.; Yazyev, O.; Austin, A. J.; Cammi, R.; Pomelli, C.; Ochterski, J. W.; Ayala, P. Y.; Morokuma, K.; Voth, G. A.; Salvador, P.; Dannenberg, J. J.; Zakrzewski, V. G.; Dapprich, S.; Daniels, A. D.; Strain, M. C.; Farkas, O.; Malick, D. K.; Rabuck, A. D.; Raghavachari, K.; Foresman, J. B.; Ortiz, J. V.; Cui, Q.; Baboul, A. G.; Clifford, S.; Cioslowski, J.; Stefanov, B. B.; Liu, G.; Liashenko, A.; Piskorz, P.; Komaromi, I.; Martin, R. L.; Fox, D. J.; Keith, T.; Al-Laham, M. A.; Peng, C. Y.; Nanayakkara, A.; Challacombe, M.; Gill, P. M. W.; Johnson, B.; Chen, W.; Wong, M. W.; Gonzalez, C.; Pople, J. A. Gaussian, Inc., Wallingford CT, 2004.

<sup>168</sup> Gaussian 09, Revision A.02, Frisch, M. J.; Trucks, G. W.; Schlegel, H. B.; Scuseria, G. E.; Robb, M. A.; Cheeseman, J. R.; Scalmani, G.; Barone, V.; Mennucci, B.; Petersson, G. A.; Nakatsuji, H.; Caricato, M.; Li, X.; Hratchian, H. P.; Izmaylov, A. F.; Bloino, J.; Zheng, G.; Sonnenberg, J. L.; Hada, M.; Ehara, M.; Toyota, K.; Fukuda, R.; Hasegawa, J.; Ishida, M.;

UB3LYP functional and 6-311G\*\* basis set with spin annihilation, giving no spin contamination.<sup>169</sup> I subjected all optimized geometries to frequency analysis and characterized them as a minimum (no imaginary frequencies) or as a saddle point (single imaginary frequency) on the potential energy surface. I verified transition states by imaginary frequency animation with the desired vibrational modes. I derived the zero-point-energy (ZPE) values using unscaled frequencies. I calculated thermodynamic properties assuming an ideal gas at 298.15 K. In the calculations of the reaction pathways for manganese catalyzed radical cycloaddition reaction, the manganese can itself be ignored since it is not bound to the substrate.<sup>170</sup>

## RESULTS

Nature uses the same oroidin building block to produce structurally diverse pyrrole-imidazole alkaloids. Taking a biomimetic approach then, the goal is to construct different members of this family of compounds, having different core skeletons, from the same starting

---

Nakajima, T.; Honda, Y.; Kitao, O.; Nakai, H.; Vreven, T.; Montgomery, Jr., J. A.; Peralta, J. E.; Ogliaro, F.; Bearpark, M.; Heyd, J. J.; Brothers, E.; Kudin, K. N.; Staroverov, V. N.; Kobayashi, R.; Normand, J.; Raghavachari, K.; Rendell, A.; Burant, J. C.; Iyengar, S. S.; Tomasi, J.; Cossi, M.; Rega, N.; Millam, J. M.; Klene, M.; Knox, J. E.; Cross, J. B.; Bakken, V.; Adamo, C.; Jaramillo, J.; Gomperts, R.; Stratmann, R. E.; Yazyev, O.; Austin, A. J.; Cammi, R.; Pomelli, C.; Ochterski, J. W.; Martin, R. L.; Morokuma, K.; Zakrzewski, V. G.; Voth, G. A.; Salvador, P.; Dannenberg, J. J.; Dapprich, S.; Daniels, A. D.; Farkas, O.; Foresman, J. B.; Ortiz, J. V.; Cioslowski, J.; Fox, D. J. Gaussian, Inc., Wallingford CT, 2009.

<sup>169</sup> (a) Becke, A. D., *J. Chem. Phys.* **1993**, *98*, 5648; (b) Lee, C. T.; Yang, W. T.; Parr, R. G. *Phys. Rev. B.* **1988**, *37*, 785.

<sup>170</sup> Curran, D. P.; Morgan, T. M.; Schwartz, C. E.; Snider, B. B.; Dombroski, M. A. *J. Am. Chem. Soc.* **1991**, *113*, 6607-6617.

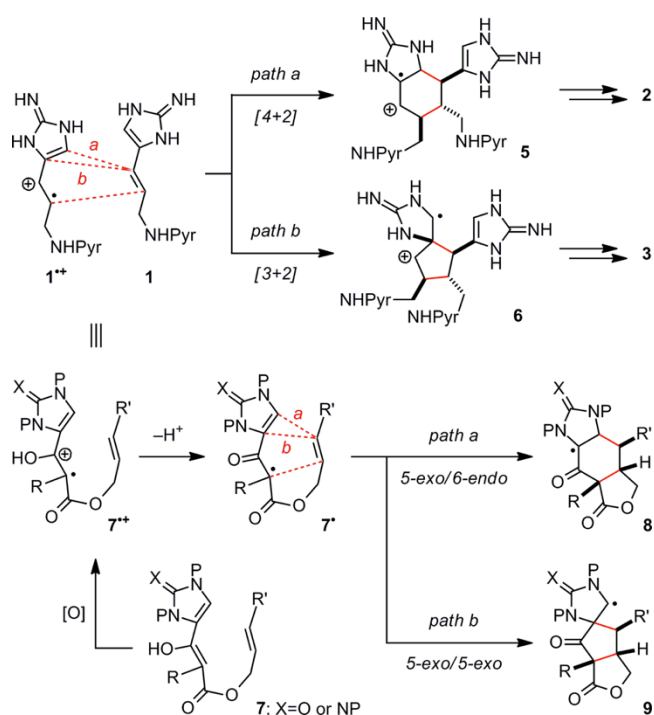
materials. More precisely, a common route to both ageliferin (**2**) and massadine (**3**) was sought. Ageliferin is the product of a [4+2] addition; massadine of a [3+2]. (Scheme 1) This goal can be achieved by realizing the electronic properties that govern the dimerization that takes place in the cycloaddition. Taking into consideration the Bürgi-Dunitz angle of attack, the trends in addition reactions have been summarized as Baldwin's rules that help to predict the regioselectivity of ring closures.<sup>171</sup> In order to facilitate interaction, the otherwise monomer components of the core skeleton were tethered, rendering the reaction intramolecular. The core skeleton is then the product of two radical cyclizations. The regioselectivity of the first of these is 5-exo despite the 6-endo product being normally kinetically favored for  $\alpha$ -acyl radical cyclizations. Houk, however, has shown that planarity of the  $\alpha$ -acyl radical is maintained in the transition state, leading to the 5-exo product instead.<sup>172</sup> It is, however, the regioselectivity of the second cyclization that is of greatest interest since it determines which of the two core structures is constructed. From model studies done previously in the lab, the ageliferin skeleton (**12**) was the only product of the Mn(OAc)<sub>3</sub> catalyzed oxidation of **11**.<sup>173</sup>

---

<sup>171</sup> Anslyn, E. V.; Dougherty, D. A. *Modern Physical Organic Chemistry*, Sausalito, CA: University Science Books, 2006.

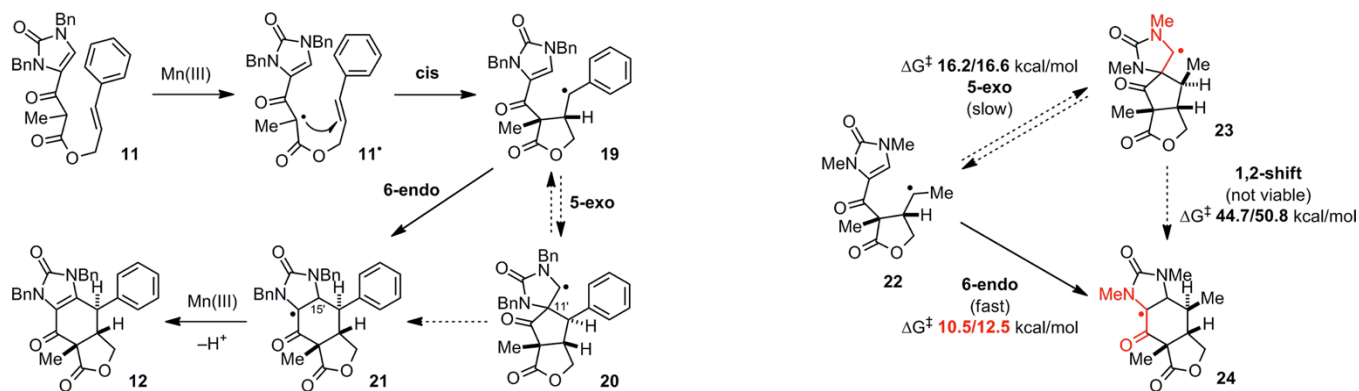
<sup>172</sup> (a) Spellmeyer, D. C.; Houk, K. N. *J. Org. Chem.* **1987**, *52*, 959; (b) Broeker, J. L.; Houk, K. N. *J. Org. Chem.* **1991**, *56*, 3651; (c) Leach, A. G.; Wang, R.; Wohlhieter, G. E.; Khan, S. I.; Jung, M. E.; Houk, K. N. *J. Am. Chem. Soc.* **2003**, *125*, 4271;

<sup>173</sup> Tan, X.; Chen, C. *Angew. Chem., Int. Ed.* **2006**, *45*, 4345.



**Scheme 1. A divergent biomimetic approach for the synthesis of [4+2] and [3+2] dimers.**

As illustrated in Scheme 2, there are three possible pathways that determine the regioselectivity and could explain getting **12** from **11**, after the first radical cyclization gives **19** and a final hydrogen abstraction takes **21** to **12**. First, a 6-endo cyclization would give **21** directly from **19**. Second, a 5-exo cycloaddition to give **20** that then undergoes a 1,2-shift to give **21**. The third possibility is that **19** undergoes a 5-exo cycloaddition, but the reaction is reversible such that the 6-endo thermodynamic product is had. Since the final hydrogen abstraction to give **12** does not maintain the stereochemistry at C11' and C15', both diastereomers need to be considered in each of the three pathways.



**Scheme 2. Proposed mechanism for the Mn(III)-promoted oxidative 5-exo/6-endo radical cyclization**

Depending on the stereochemistry at C11' and C15', the energy barrier of the 6-endo cyclization was either 5.7 or 4.1 kcal/mol lower in energy than that of the 5-exo cyclization. Additionally, the 6-endo reaction that gives the [4+2] cycloaddition product is 16.7 or 11.4 kcal/mol more stable than the 5-exo reaction's [3+2] product. The possibility of a 1,2-shift is ruled out by the fact that the activation barrier for this transformation is forbiddenly high at 44.7 or 50.8 kcal/mol. These results are shown illustrated in Figure 3.

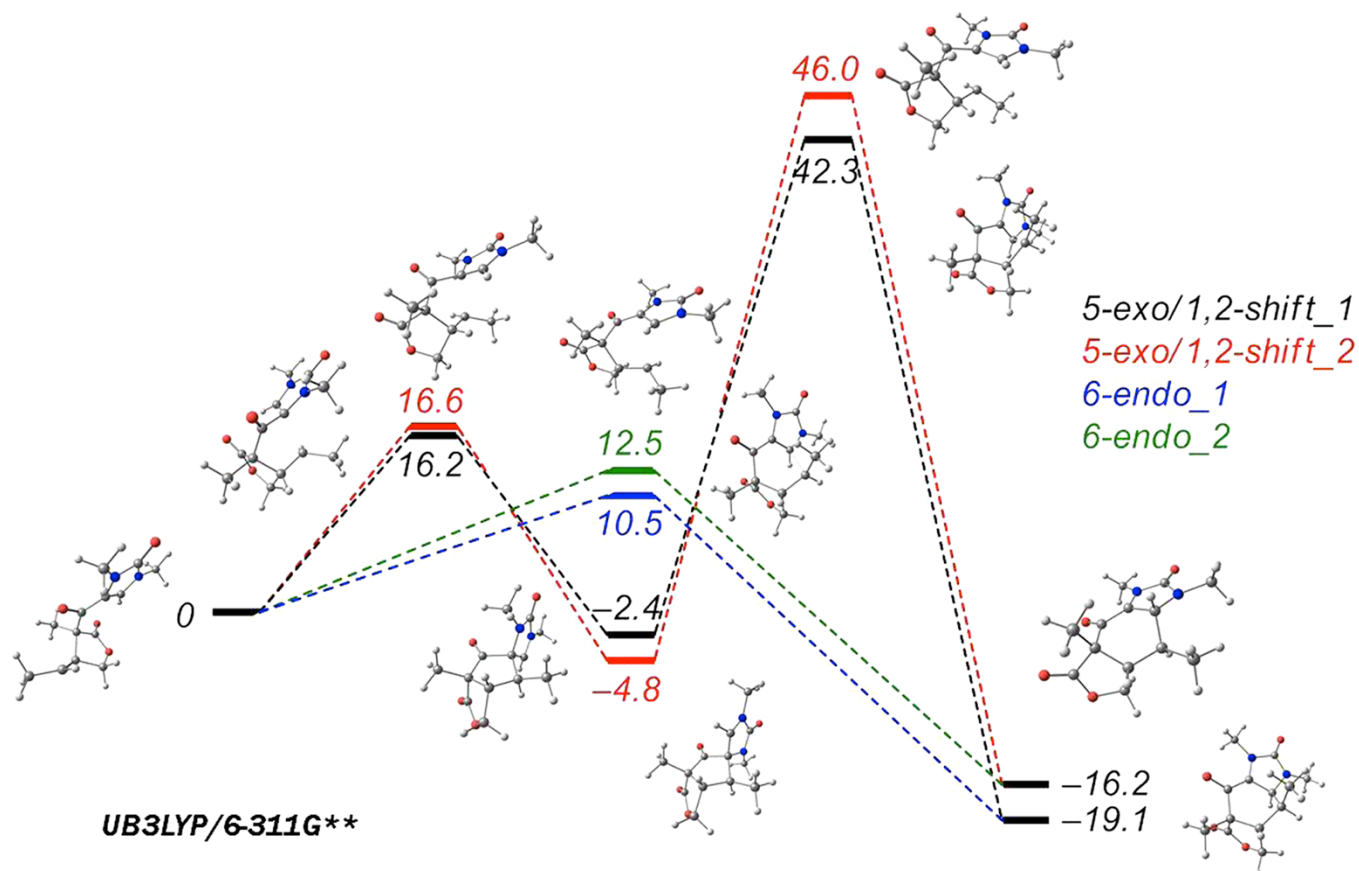


**Figure 2.** Energy diagram for the 6-endo and 5-exo cyclizations of **22**, and the 1,2-shift of **23**.

These results are in agreement with reported electron spin resonance (ESR) spectroscopy data and **24** is predicted to be 16.8 kcal/mol more stable than **23**.<sup>174</sup> The study also suggests that there is a 10.8 kcal/mol stabilization of  $\alpha$ -amino- $\alpha$ -carbonylmethyl radicals attributable to a synergistic captodative substituent effect. The captodative effect refers to the fact that both electron donating and electron withdrawing groups stabilize the radical when placed on the radical center, a concept that can be understood using resonance theory. The captodative effect

<sup>174</sup> Welle, F. M.; Beckhaus, H.-D.; Rüdhardt, C. *J. Org. Chem.* **1997**, *62*, 552.

leads to addition being strongly directing towards  $\beta$  addition of the radical to the center that gives the stabilized radical, a principle that has been used to control regioselectivity in synthetic routes.<sup>175</sup>

Given these results, there was an interest in determining whether the captodative effect could be used to switch the regioselectivity of the radical cyclization to give the 5-exo product. To this end, an electron withdrawing group, either  $-\text{Cl}$  or  $-\text{CN}$  was placed at C15'. Both of these substituents cause a lowering of the activation barrier for the 5-exo pathway but do not affect the activation barrier of the 6-endo pathway. (Figure 4). For unsubstituted **22**, the 6-endo pathway is favored by 4.1 kcal/mol, whereas for the chloro- (**25**) and cyano- (**26**) substituted compounds the 5-exo pathway is favored by 3.7 and 6.2 kcal/mol respectively.

---

<sup>175</sup> Viehe, H. G.; Janousek, Z.; Merenyi, R. *Acc. Chem. Res.* **1985**, *18*, 148.

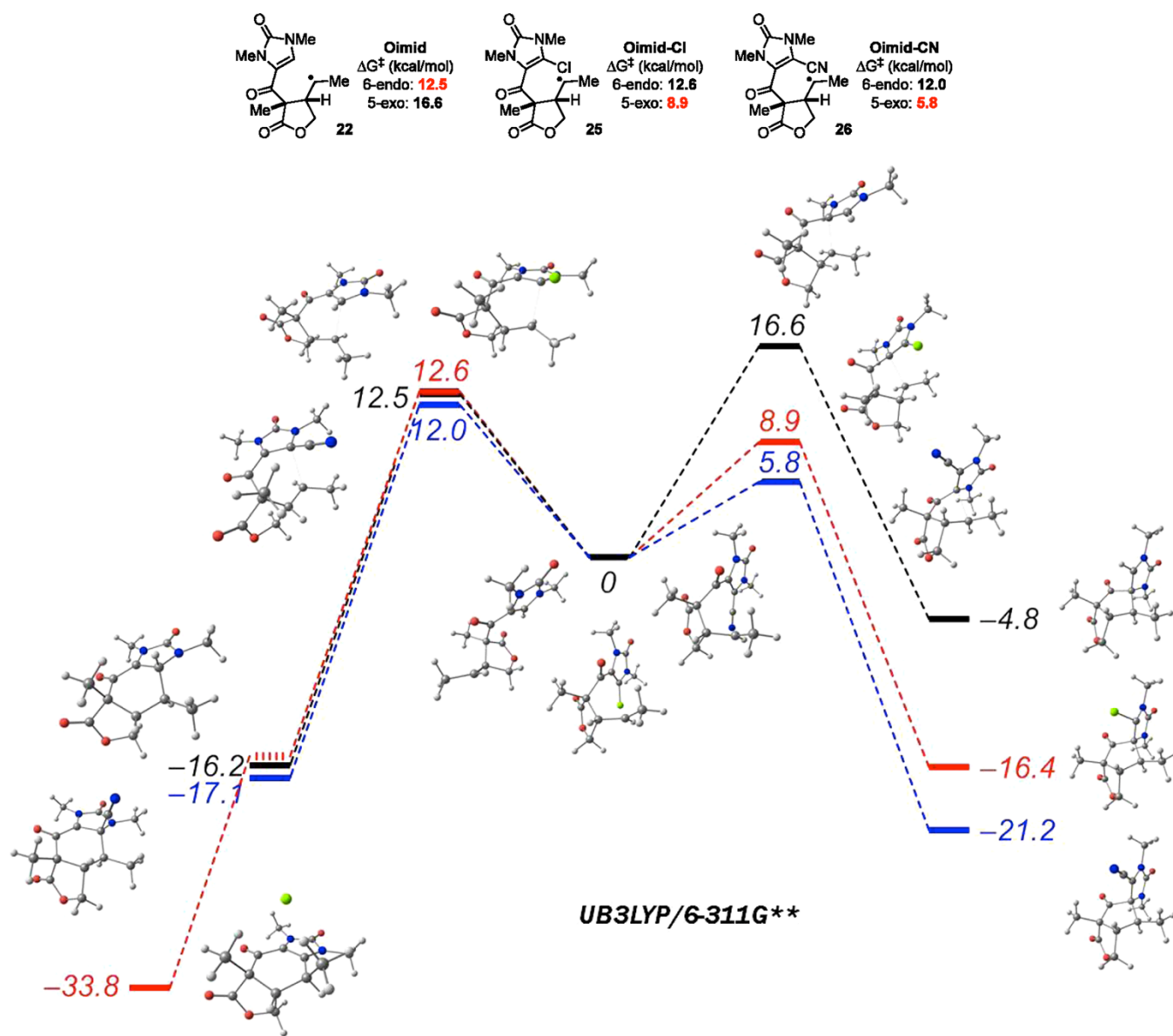


Figure 4. Energy diagram for the 6-endo versus 5-exo cyclization for 22, 25, and 26.

These results were confirmed experimentally. Also experimentally, the cyano-substituted compound, with its predicted stronger captodative effect, gave solely the 5-exo product.

## DISCUSSION

By pairing computational studies to experimental model studies, a synthetic route towards pyrrole-imidazole alkaloids through the dimerization of their oroidin precursors has been achieved. This synthetic route mimics the proposed single electron transfer mechanism that is operational in nature. By understanding the electronics at play in the radical cyclization reaction, the regioselectivity can be controlled such that the route can diverge to give either the [4+2] core skeleton of ageliferin or the [3+2] core skeleton of massadine. I consider this work a beautiful example of the potentially powerful cooperation that can exist between *in silico* studies and work at the bench.

## CHAPTER FIVE

### Conclusions and Recommendations

The ERK2 E320K mutation disrupts interactions with other proteins, most obviously with those having D domains that thus bind to the CD domain of ERK2. Because the dual phosphatase MKP-3 is one such D domain containing interactor with ERK2, the mutation has an impact on the activity of the kinase. Because the kinase and phosphatase do not interact as well, ERK2 E320K remains active longer. Additionally, it is less capable of inducing the conformational change that renders MKP-3 active.

In trying to understand how this mutation contributes to cancer, this characteristic of remaining active longer should be measured against its reduced ability to bind to its substrates. Does the signaling of cellular processes through phosphorylation still take place to the same degree, but perhaps now more transitionally as a Michaelis complex? To this end, it would be interesting to determine the  $K_D$  for ERK2 wild type and mutant with various substrates. It would also be interesting to do kinetic studies, using RSK or another D domain-containing substrates of ERK2. Gel filtration could also be used to get an additional assessment of the effect of the mutation on the complexation of MKP-3 with both phosphorylated and unphosphorylated ERK2.

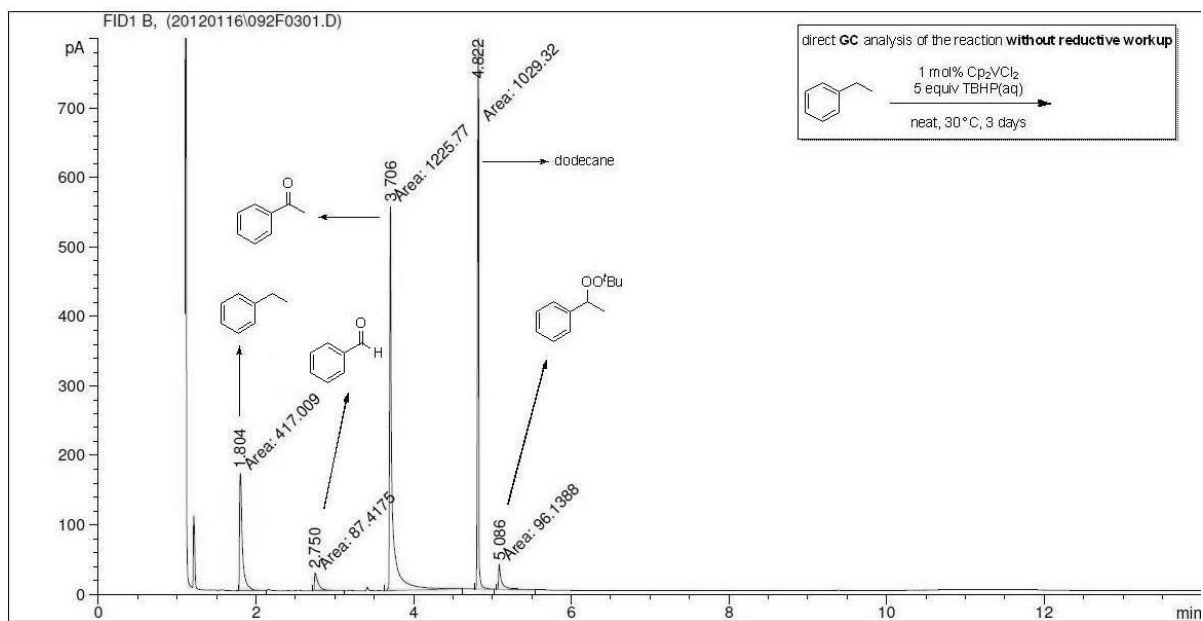
As shown, there is also evidence of allosteric interactions between the CD region and the activation loop. The correlation between these two regions may have an impact on the autoactivation of the kinase, and a comparative study of autophosphorylation in ERK2 E320K may give insights into the mechanisms at play in the wild type. More generally, from a physical chemist's perspective, the structure of ERK2 E320K may reveal something of conformational

transitions. Since the structure is not drastically different from the wild type, the structure of the mutant represents a conformation of the wild type that is accessible on the potential energy surface should a given activation barrier be overcome.

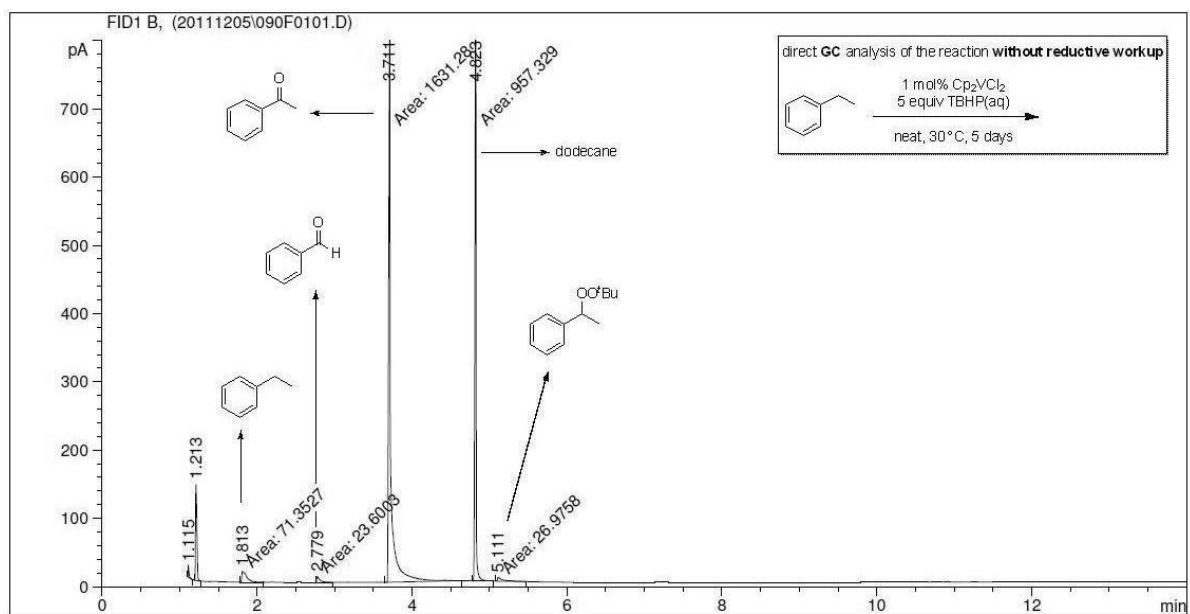
## **APPENDIX A**

### **Supplemental Information for Chapter Three**

The crude  $^1\text{H}$  NMR spectra of all the oxidation reactions and the GC chromatograms of the oxidation of ethylbenzene were carefully analyzed. No aromatic oxidation products were detected. The GC chromatograms of the oxidation of ethylbenzene after 3 days (Figure S1) and 5 days (Figure S2) and the  $^1\text{H}$  NMR spectra of the oxidation of ethylbenzene (Figure S3) and phenyloctane (Figure S4) after 5 days are shown below.

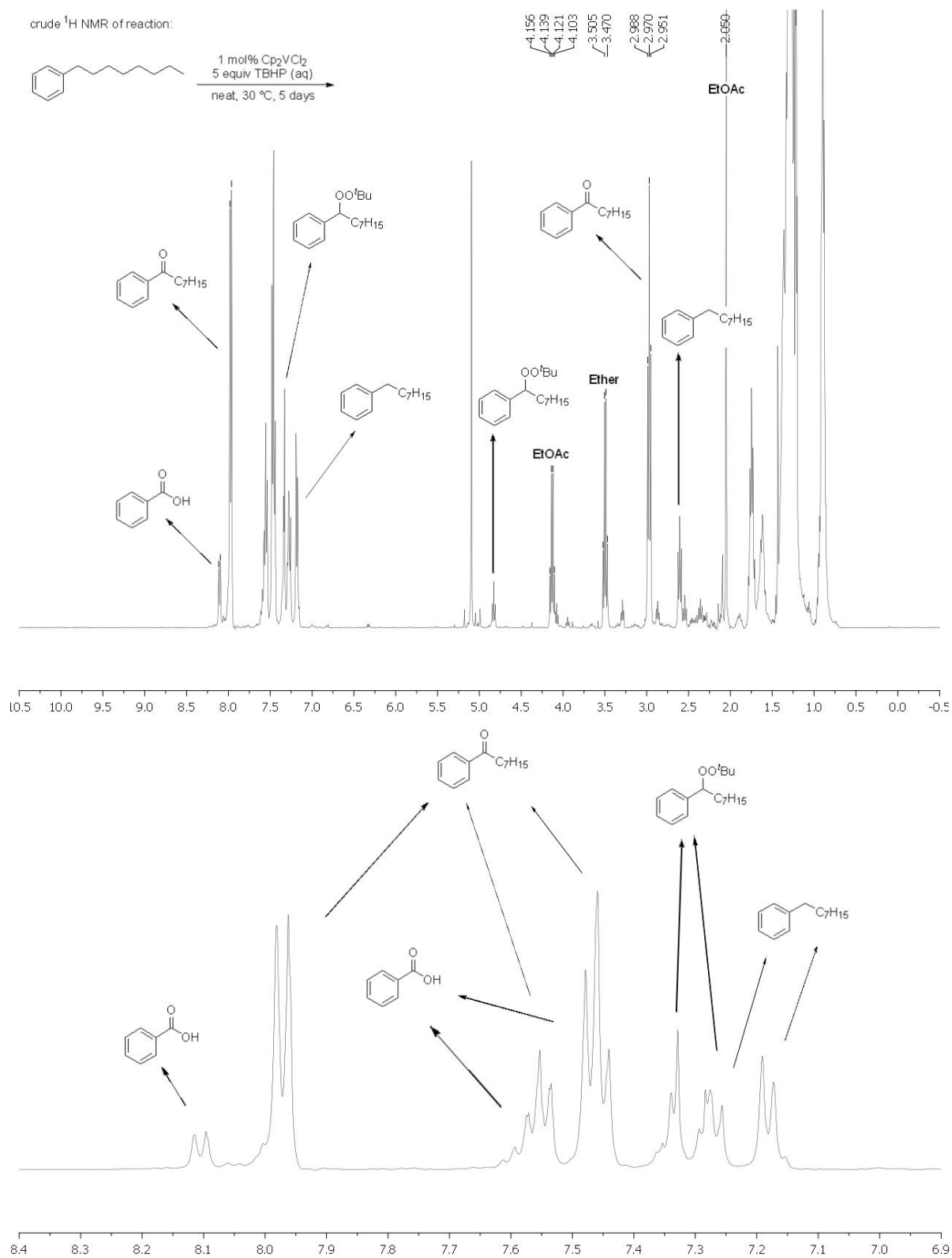


**Figure S1** GC chromatogram of the oxidation of ethylbenzene after 3 days

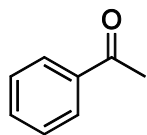


**Figure S2** GC chromatogram of the oxidation of ethylbenzene after 5 days

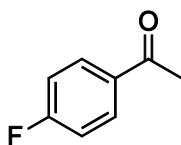




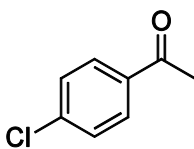
**Figure S4**  $^1\text{H}$  NMR spectra of the oxidation of phenyloctane after 5 days

**Characterization Data**

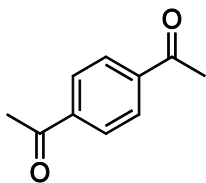
Acetophenone. Oxidation of ethylbenzene (105.2 mg, 1.0 mmol, 1.0 equiv) according to the general procedure and purified directly by flash column chromatography (7% diethyl ether/pentane) gave acetophenone (108 mg, 90% yield) as a colorless oil.  $^1\text{H NMR}$  (400 MHz,  $\text{CDCl}_3$ )  $\delta$  7.95-7.97 (m, 2H), 7.55-7.59 (m, 1H), 7.45-7.48 (m, 2H), 2.61 (s, 3H);  $\text{MS}(\text{ESI})^+$  calcd for  $\text{C}_8\text{H}_8\text{O}$  ( $\text{M}+\text{H}$ ) $^+$  121.1, found 121.1.



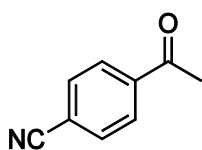
1-(4-Fluorophenyl)ethanone. Oxidation of 1-ethyl-4-fluorobenzene (124.1 mg, 1.0 mmol, 1.0 equiv) according to the general procedure and purified directly by flash column chromatography (7% diethyl ether/pentane) gave 1-(4-fluorophenyl)ethanone (125 mg, 91% yield) as a colorless oil.  $^1\text{H NMR}$  (400 MHz,  $\text{CDCl}_3$ )  $\delta$  7.97-8.00 (m, 2H), 7.11-7.15 (m, 2H), 2.59 (s, 3H);  $\text{MS}(\text{ESI})^+$  calcd for  $\text{C}_8\text{H}_8\text{FO}$  ( $\text{M}+\text{H}$ ) $^+$  139.0, found 139.1.



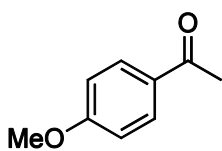
1-(4-Chlorophenyl)ethanone. Oxidation of 1-chloro-4-ethylbenzene (138.0 mg, 1.0 mmol, 1.0 equiv) according to the general procedure and purified by flash column chromatography (2% ethyl acetate/hexanes) gave 1-(4-chlorophenyl)ethanone (131 mg, 86% yield) as a colorless oil.  $^1\text{H NMR}$  (400 MHz,  $\text{CDCl}_3$ )  $\delta$  7.89 (d,  $J = 8.5$  Hz, 2H), 7.43 (d,  $J = 8.5$  Hz, 2H), 2.59 (s, 3H);  $\text{MS}(\text{ESI})^+$  calcd for  $\text{C}_8\text{H}_8\text{ClO}$  ( $\text{M}+\text{H}$ ) $^+$  155.0, found 155.1.



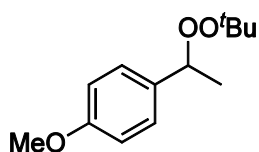
1,1'-(1,4-Phenylene)diethanone. Oxidation of 1-(4-ethylphenyl)ethanone (148.2 mg, 1.0 mmol, 1.0 equiv) according to the general procedure and purified by flash column chromatography (15% ethyl acetate/hexanes) to give 1,1'-(1,4-phenylene)diethanone (144 mg, 89% yield) as a white solid.  $^1\text{H NMR}$  (400 MHz,  $\text{CDCl}_3$ )  $\delta$  8.03 (s, 4H), 2.65 (s, 6H);  $\text{MS}(\text{ESI})^+$  calcd for  $\text{C}_{10}\text{H}_{11}\text{O}_2$  ( $\text{M}+\text{H}$ ) $^+$  163.1, found 163.1.



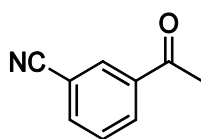
4-Acetylbenzotrile. Oxidation of 4-ethylbenzotrile (129.7 mg, 1.0 mmol, 1.0 equiv) according to the general procedure and purified by flash column chromatography (10% ethyl acetate/hexanes) gave 4-acetylbenzotrile (110 mg, 77% yield) as a colorless oil.  $^1\text{H NMR}$  (400 MHz,  $\text{CDCl}_3$ )  $\delta$  8.04 (d,  $J = 8.4$  Hz, 2H), 7.78 (d,  $J = 8.4$  Hz, 2H), 2.65 (s, 3H);  $\text{MS}(\text{ESI})^+$  calcd for  $\text{C}_9\text{H}_8\text{NO}$  ( $\text{M}+\text{H}$ ) $^+$  146.1, found 146.2.



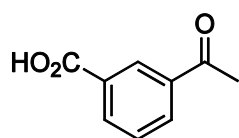
1-(4-Methoxyphenyl)ethanone. Oxidation of 1-ethyl-4-methoxybenzene (136.2 mg, 1.0 mmol, 1.0 equiv) according to the general procedure and purified by flash column chromatography (5% ethyl acetate/hexanes) gave 1-(4-methoxyphenyl)-ethanone (81 mg, 54% yield) as a colorless oil, and 1-(1-(tert-butylperoxy)ethyl)-4-methoxybenzene (65 mg, 29% yield) as a colorless oil.  $^1\text{H NMR}$  (400 MHz,  $\text{CDCl}_3$ )  $\delta$  7.93 (d,  $J = 8.7$  Hz, 2H), 6.93 (d,  $J = 8.7$  Hz, 2H), 3.87 (s, 3H), 2.55 (s, 3H);  $\text{MS}(\text{ESI})^+$  calcd for  $\text{C}_9\text{H}_{11}\text{O}_2$  ( $\text{M}+\text{H}$ ) $^+$  151.1, found 151.2.



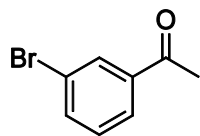
1-(1-(tert-Butylperoxy)ethyl)-4-methoxybenzene.  $^1\text{H}$  NMR (400 MHz,  $\text{CDCl}_3$ )  $\delta$  7.29 (d,  $J = 8.3$  Hz, 2H), 6.88 (d,  $J = 8.3$  Hz, 2H), 4.95 (q,  $J = 6.5$  Hz, 1H), 3.80 (s, 3H), 1.48 (d,  $J = 6.5$  Hz, 3H), 1.21 (s, 9H);  $^{13}\text{C}$  NMR (100 MHz,  $\text{CDCl}_3$ ):  $\delta$  20.1, 26.5, 55.2, 80.0, 81.1, 113.6, 128.1, 134.0, 159.2; MS(ESI) $^+$  calcd for  $\text{C}_{13}\text{H}_{20}\text{O}_3\text{Na}$  ( $\text{M}+\text{Na}$ ) $^+$  247.1, found 247.2.



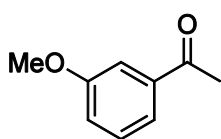
3-Acetylbenzotrile. Oxidation of 3-ethylbenzotrile (131.2 mg, 1.0 mmol, 1.0 equiv) according to the general procedure and purified by flash column chromatography (20% ethyl acetate/hexanes) gave 3-acetylbenzotrile (123 mg, 85% yield) as a white solid.  $^1\text{H}$  NMR (400 MHz,  $\text{CDCl}_3$ )  $\delta$  8.24 (s, 1H), 8.18 (d,  $J = 7.9$  Hz, 1H), 7.85 (d,  $J = 7.7$  Hz, 1H), 7.62 (dd,  $J = 7.9, 7.7$  Hz, 1H), 2.64 (s, 3H); MS(ESI) $^+$  calcd for  $\text{C}_9\text{H}_8\text{NO}$  ( $\text{M}+\text{H}$ ) $^+$  146.1, found 146.1.



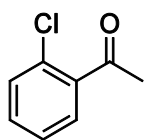
3-Acetylbenzoic acid. Oxidation of 3-ethylbenzoic acid (151.0 mg, 1.0 mmol, 1.0 equiv) according to the general procedure and purified by flash column chromatography (5% methanol/dichloromethane) gave 3-acetylbenzoic acid (150 mg, 91% yield) as a white solid.  $^1\text{H}$  NMR (400 MHz,  $\text{DMSO-d}_6$ )  $\delta$  13.35 (brs, 1H), 8.45 (s, 1H), 8.17-8.20 (m, 2H), 7.67 (dd,  $J = 7.7, 7.7$  Hz, 1H), 2.63 (s, 3H); MS(ESI) $^+$  calcd for  $\text{C}_9\text{H}_9\text{O}_3$  ( $\text{M}+\text{H}$ ) $^+$  165.0, found 165.1.



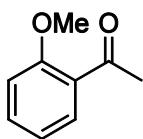
1-(3-Bromophenyl)ethanone. Oxidation of 1-bromo-3-ethylbenzene (186.0 mg, 1.0 mmol, 1.0 equiv) according to the general procedure and purified directly by flash column chromatography (5% diethyl ether/pentane) gave 1-(3-bromophenyl)ethanone (179 mg, 90% yield) as a colorless oil.  $^1\text{H}$  NMR (400 MHz,  $\text{CDCl}_3$ )  $\delta$  8.08 (dd,  $J = 1.2, 1.6$  Hz, 1H), 7.88 (d,  $J = 7.8$  Hz, 1H), 7.69 (dd,  $J = 0.8, 7.9$  Hz, 1H), 7.35 (dd,  $J = 7.9, 7.8$  Hz, 1H), 2.60 (s, 3H); MS(ESI) $^+$  calcd for  $\text{C}_8\text{H}_8\text{BrO}$  ( $\text{M}+\text{H}$ ) $^+$  199.0, found 199.0.



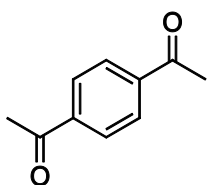
1-(3-Methoxyphenyl)ethanone. Oxidation of 1-ethyl-3-methoxybenzene (133.0 mg, 1.0 mmol, 1.0 equiv) according to the general procedure and purified directly by flash column chromatography (5% diethyl ether/pentane) gave 1-(3-methoxyphenyl)ethanone (117 mg, 80% yield) as a colorless oil.  $^1\text{H}$  NMR (400 MHz,  $\text{CDCl}_3$ )  $\delta$  7.53-5.55 (m, 1H), 7.48-7.49 (m, 1H), 7.37 (dd,  $J = 8.0, 7.6$  Hz, 1H), 7.10-7.13 (m, 1H), 3.86 (s, 3H), 2.60 (s, 3H); MS(ESI) $^+$  calcd for  $\text{C}_9\text{H}_{11}\text{O}_2$  ( $\text{M}+\text{H}$ ) $^+$  151.1, found 151.1.



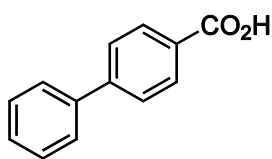
1-(2-Chlorophenyl)ethanone. Oxidation of 1-chloro-2-ethylbenzene (140.2 mg, 1.0 mmol, 1.0 equiv) according to the general procedure and purified directly by flash column chromatography (3% diethyl ether/pentane) gave 1-(2-chlorophenyl)ethanone (80 mg, 52% yield) as a colorless oil.  $^1\text{H}$  NMR (400 MHz,  $\text{CDCl}_3$ )  $\delta$  7.55 (dd,  $J = 1.6, 7.6$  Hz, 1H), 7.30-7.41 (m, 3H), 2.65 (s, 3H); MS(ESI) $^+$  calcd for  $\text{C}_8\text{H}_8\text{ClO}$  ( $\text{M}+\text{H}$ ) $^+$  155.0, found 155.1.



1-(2-Methoxyphenyl)ethanone. Oxidation of 1-ethyl-2-methoxybenzene (138.0 mg, 1.0 mmol, 1.0 equiv) according to the general procedure and purified directly by flash column chromatography (3% diethyl ether/pentane) gave 1-(2-methoxyphenyl)ethanone (103 mg, 68% yield) as a colorless oil.  $^1\text{H NMR}$  (400 MHz,  $\text{CDCl}_3$ )  $\delta$  7.73 (dd,  $J = 1.8, 7.7$  Hz, 1H), 7.44-7.49 (m, 1H), 6.96-7.01 (m, 2H), 3.91 (s, 3H), 2.61 (s, 3H); MS(ESI) $^+$  calcd for  $\text{C}_9\text{H}_{11}\text{O}_2$  (M+H) $^+$  151.1, found 151.1.



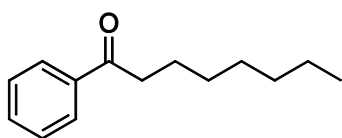
1,1'-(1,4-Phenylene)diethanone. Oxidation of 1,4-diethylbenzene (133.8 mg, 1.0 mmol, 1.0 equiv) according to the general procedure but with 2 mol % vanadocene dichloride (5.0 mg, 0.02 mmol, 0.02 equiv) and 10 equiv tert-butyl hydroperoxide (70% in water, 1440  $\mu\text{L}$ , 10.0 mmol, 10.0 equiv), and purified by flash column chromatography (15% ethyl acetate/hexanes) gave 1,1'-(1,4-phenylene)diethanone (140 mg, 86% yield) as a white solid.  $^1\text{H NMR}$  (400 MHz,  $\text{CDCl}_3$ )  $\delta$  8.03 (s, 4H), 2.65 (s, 6H); MS(ESI) $^+$  calcd for  $\text{C}_{10}\text{H}_{11}\text{O}_2$  (M+H) $^+$  163.1, found 163.1.



[1,1'-Biphenyl]-4-carboxylic acid. Oxidation of 4-methyl-1,1'-biphenyl (168.5 mg, 1.0 mmol, 1.0 equiv) according to the general procedure and purified by flash column chromatography (4% ethyl acetate/hexanes) gave [1,1'-biphenyl]-4-carboxylic acid (108 mg, 54% yield) as a white solid. In a separate run with an addition of acetonitrile (0.2 mL) as solvent, the acid product was isolated in 60% yield.  $^1\text{H NMR}$  (400 MHz,  $\text{DMSO-d}_6$ )  $\delta$  12.99 (brs, 1H), 8.02 (d,  $J = 8.2$  Hz, 2H), 7.80

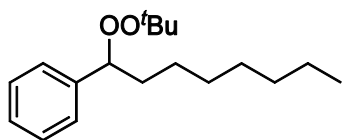
(d,  $J = 8.2$  Hz, 2H), 7.73 (d,  $J = 7.6$  Hz, 2H), 7.50 (dd,  $J = 7.6, 7.6$  Hz, 2H), 7.40-7.44 (m, 1H);

MS(ESI)<sup>+</sup> calcd for C<sub>13</sub>H<sub>11</sub>O<sub>2</sub> (M+H)<sup>+</sup> 199.1, found 199.2.



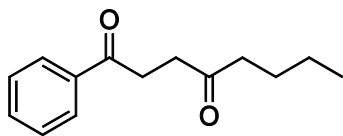
1-Phenyloctan-1-one. Oxidation of 1-phenyloctane (190.3 mg, 1.0 mmol, 1.0 equiv) according to the general procedure and purified by flash column chromatography (1→4% ethyl acetate/hexanes)

gave 1-phenyloctan-1-one (116 mg, 57% yield) as a colorless oil, (1-(tert-butylperoxy)octyl)benzene (26 mg, 9% yield) as a colorless oil, 1-phenyloctane-1,4-dione (7 mg, 3% yield) as a colorless oil, 1-phenyloctane-1,5-dione (2 mg, 1% yield) as a colorless oil, 1-phenyloctane-1,6-dione (2 mg, 1% yield) as a colorless oil, benzoic acid (11 mg, 10% yield), and recovered 1-phenyloctane (25 mg, 13% yield). <sup>1</sup>H NMR (400 MHz, CDCl<sub>3</sub>) δ 7.96-7.94 (m, 2H), 7.52-7.56 (m, 1H), 7.43-7.46 (m, 2H), 2.95 (t,  $J = 7.4$  Hz, 2H), 1.70-1.77 (m, 2H), 1.26-1.35 (m, 8H), 0.88 (t,  $J = 6.6$  Hz, 3H); MS(ESI)<sup>+</sup> calcd for C<sub>14</sub>H<sub>21</sub>O (M+H)<sup>+</sup> 205.2, found 205.1.

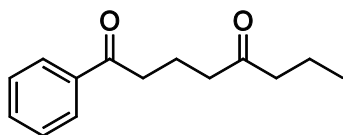


(1-(tert-Butylperoxy)octyl)benzene. <sup>1</sup>H NMR (400 MHz, CDCl<sub>3</sub>) δ 7.27- 7.36 (m, 5H), 4.82 (t,  $J = 6.9$  Hz, 1H), 1.86-1.91 (m, 1H), 1.61-1.67 (m, 1H), 1.21-1.27 (m, 10H), 1.21 (s, 9H),

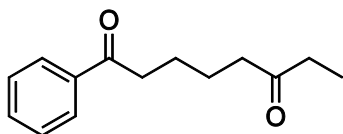
0.88 (t,  $J = 6.9$  Hz, 3H); <sup>13</sup>C NMR (125 MHz, CDCl<sub>3</sub>): δ 14.1, 22.6, 25.9, 26.5, 29.1, 29.6, 31.8, 35.1, 80.1, 86.1, 126.9, 127.4, 128.1, 141.9; MS(ESI)<sup>+</sup> calcd for C<sub>18</sub>H<sub>31</sub>O<sub>2</sub> (M+H)<sup>+</sup> 279.2, found 279.2.



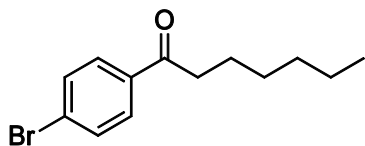
1-Phenyloctane-1,4-dione.  $^1\text{H}$  NMR (400 MHz,  $\text{CDCl}_3$ )  $\delta$  7.97-7.99 (m, 2H), 7.55-7.58 (m, 1H), 7.44-7.48 (m, 2H), 3.28 (t,  $J$  = 6.3 Hz, 2H), 2.86 (t,  $J$  = 6.3 Hz, 2H), 2.53 (t,  $J$  = 7.5 Hz, 2H), 1.57-1.63 (m, 2H), 1.32-1.37 (m, 2H), 0.92 (t,  $J$  = 7.3 Hz, 3H); MS(ESI) $^+$  calcd for  $\text{C}_{14}\text{H}_{19}\text{O}_2$  ( $\text{M}+\text{H}$ ) $^+$  219.1, found 219.1.



1-Phenyloctane-1,5-dione.  $^1\text{H}$  NMR (400 MHz,  $\text{CDCl}_3$ )  $\delta$  7.95-7.97 (m, 2H), 7.54-7.58 (m, 1H), 7.44-7.48 (m, 2H), 3.01 (t,  $J$  = 7.0 Hz, 2H), 2.54 (t,  $J$  = 7.0 Hz, 2H), 2.39 (t,  $J$  = 7.4 Hz, 2H), 2.00-2.04 (m, 2H), 1.55-1.63 (m, 2H), 0.91 (t,  $J$  = 7.4 Hz, 3H); MS(ESI) $^+$  calcd for  $\text{C}_{14}\text{H}_{19}\text{O}_2$  ( $\text{M}+\text{H}$ ) $^+$  219.1, found 219.0.

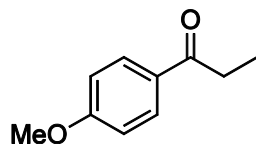


1-Phenyloctane-1,6-dione.  $^1\text{H}$  NMR (500 MHz,  $\text{CDCl}_3$ )  $\delta$  7.94-7.96 (m, 2H), 7.54-7.57 (m, 1H), 7.45-7.48 (m, 2H), 2.99 (t,  $J$  = 7.1 Hz, 2H), 2.47 (t,  $J$  = 7.3 Hz, 2H), 2.43 (q,  $J$  = 7.4 Hz, 2H), 1.65-1.77 (m, 4H), 1.05 (t,  $J$  = 7.3 Hz, 3H); MS(ESI) $^+$  calcd for  $\text{C}_{14}\text{H}_{19}\text{O}_2$  ( $\text{M}+\text{H}$ ) $^+$  219.1, found 219.1.

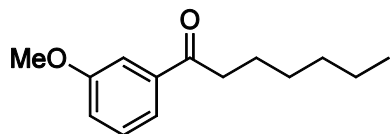


1-(4-Bromophenyl)heptan-1-one. Oxidation of 1-bromo-4-heptylbenzene (254.6 mg, 1.0 mmol, 1.0 equiv) according to the general procedure and purified by flash column chromatography (2% ethyl acetate/hexanes) gave 1-(4-bromophenyl)heptan-1-one (137 mg, 51%

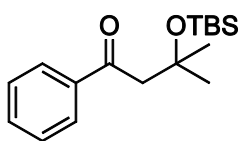
yield) as a white solid.  $^1\text{H NMR}$  (400 MHz,  $\text{CDCl}_3$ )  $\delta$  7.82 (d,  $J = 8.5$  Hz, 2H), 7.60 (d,  $J = 8.5$  Hz, 2H), 2.92 (t,  $J = 7.4$  Hz, 2H), 1.68-1.75 (m, 2H), 1.29-1.39 (m, 6H), 0.89 (t,  $J = 6.7$  Hz, 3H);  $\text{MS}(\text{ESI})^+$  calcd for  $\text{C}_{13}\text{H}_{18}\text{BrO}$  ( $\text{M}+\text{H}$ ) $^+$  269.0, found 269.1.



1-(4-Methoxyphenyl)propan-1-one. Oxidation of 1-methoxy-4-propylbenzene (150.0 mg, 1.0 mmol, 1.0 equiv) according to the general procedure and purified by flash column chromatography (2% ethyl acetate/hexanes) gave 1-(4-methoxyphenyl)propan-1-one (81 mg, 49% yield) as a colorless oil.  $^1\text{H NMR}$  (400 MHz,  $\text{CDCl}_3$ )  $\delta$  7.95 (d,  $J = 8.9$  Hz, 2H), 6.93 (d,  $J = 8.9$  Hz, 2H), 3.86 (s, 3H), 2.95 (q,  $J = 7.3$  Hz, 2H), 1.21 (t,  $J = 7.3$  Hz, 3H);  $\text{MS}(\text{ESI})^+$  calcd for  $\text{C}_{10}\text{H}_{13}\text{O}_2$  ( $\text{M}+\text{H}$ ) $^+$  165.1, found 165.1.

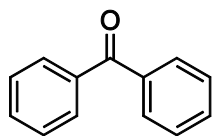


1-(3-Methoxyphenyl)heptan-1-one. Oxidation of 1-heptyl-3-methoxybenzene (205.8 mg, 1.0 mmol, 1.0 equiv) according to the general procedure and purified by flash column chromatography (5% ethyl acetate/hexanes) gave 1-(3-methoxyphenyl)heptan-1-one (113 mg, 50% yield) as a white solid.  $^1\text{H NMR}$  (400 MHz,  $\text{CDCl}_3$ )  $\delta$  7.53 (d,  $J = 7.8$  Hz, 1H), 7.49 (d,  $J = 2.0$  Hz, 1H), 7.36 (dd,  $J = 7.8, 8.0$  Hz, 1H), 7.09 (dd,  $J = 2.0, 8.0$  Hz, 1H), 3.85 (s, 3H), 2.94 (t,  $J = 7.4$  Hz, 2H), 1.69-1.76 (m, 2H), 1.31-1.39 (m, 6H), 0.89 (t,  $J = 6.7$  Hz, 3H);  $\text{MS}(\text{ESI})^+$  calcd for  $\text{C}_{14}\text{H}_{21}\text{O}_2$  ( $\text{M}+\text{H}$ ) $^+$  221.1, found 221.1.



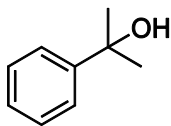
3-((tert-Butyldimethylsilyl)oxy)-3-methyl-1-phenylbutan-1-one. Oxidation of 2-methyl-4-phenylbutan-2-ol (165.0 mg, 1.0 mmol, 1.0 equiv)

according to the general procedure and purified by flash column chromatography (5→15% ethyl acetate/hexanes) gave an inseparable mixture of recovered starting material and the benzylic oxidation product 3-hydroxy-3-methyl-1-phenylbutan-1-one (121 mg), and benzoic acid (11 mg, 9% yield). This mixture was dissolved in methylene chloride (3 mL) and treated with tert-butyl dimethylsilyl trifluoromethanesulfonate (211.4 mg, 0.8 mmol) and 2,6-lutidine (186  $\mu$ L, 1.6 mmol) to afford 3-((tert-butyl dimethylsilyl)oxy)-3-methyl-1-phenylbutan-1-one (146 mg, 50% yield for two steps) as a colorless oil, and 3-((tert-butyl dimethylsilyl)oxy)-3-methyl-1-phenylbutane (45 mg, 16% yield) as a colorless oil after flash column chromatography (1→5% ethyl acetate/hexanes).  $^1\text{H}$  NMR (400 MHz,  $\text{CDCl}_3$ )  $\delta$  7.96 (d,  $J = 7.6$  Hz, 2H), 7.50 (dd,  $J = 7.3$ , 7.3 Hz, 1H), 7.41 (dd,  $J = 7.6$ , 7.3 Hz, 2H), 3.09 (s, 2H), 1.40 (s, 6H), 0.73 (s, 9H), 0.03 (s, 6H);  $^{13}\text{C}$  NMR (100 MHz,  $\text{CDCl}_3$ ):  $\delta$  2.1, 17.8, 25.6, 30.3, 51.7, 73.6, 128.3, 128.6, 132.6, 138.4, 199.2; MS(ESI) $^+$  calcd for  $\text{C}_{17}\text{H}_{28}\text{O}_2\text{SiNa}$  ( $\text{M}+\text{Na}$ ) $^+$  315.2, found 315.1.



Benzophenone. Oxidation of diphenylmethane (165.0 mg, 1.0 mmol, 1.0 equiv) according to the general procedure and purified by flash column

chromatography (2% ethyl acetate/hexanes) gave benzophenone (170 mg, 95% yield) as a white solid.  $^1\text{H}$  NMR (400 MHz,  $\text{CDCl}_3$ )  $\delta$  7.81 (d,  $J = 7.2$  Hz, 4H), 7.59 (dd,  $J = 7.4$ , 7.3 Hz, 2H), 7.49 (dd,  $J = 7.7$ , 7.5 Hz, 4H); MS(ESI) $^+$  calcd for  $\text{C}_{13}\text{H}_{10}\text{O}$  ( $\text{M}+\text{H}$ ) $^+$  183.1, found 183.1.



2-Phenylpropan-2-ol. Oxidation of cumene (120.0 mg, 1.0 mmol, 1.0 equiv)

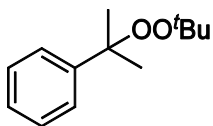
according to the general procedure and purified directly by flash column

chromatography (3→50% diethyl ether/pentane) gave 2-phenylpropan-2-ol (105 mg, 77% yield)

as a colorless oil and (2-(tert-butylperoxy)propan-2-yl)benzene (26 mg, 13% yield) as a colorless

oil.  $^1\text{H}$  NMR (400 MHz,  $\text{CDCl}_3$ )  $\delta$  7.49 (d,  $J = 8.0$  Hz, 2H), 7.34 (dd,  $J = 8.0, 7.2$  Hz, 2H), 7.22-

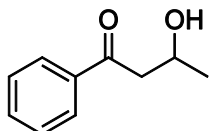
7.26 (m, 1H), 1.96 (brs, 1H), 1.58 (s, 6H); MS(EI) $^+$  calcd for  $\text{C}_9\text{H}_{12}\text{O}$  ( $\text{M}$ ) $^+$  136.1, found 136.1.



(2-(tert-Butylperoxy)propan-2-yl)benzene.  $^1\text{H}$  NMR (400 MHz,  $\text{CDCl}_3$ )  $\delta$

7.47 (d,  $J = 7.4$  Hz, 2H), 7.31-7.35 (m, 2H), 7.21-7.26 (m, 1H), 1.57 (s,

6H), 1.23 (s, 9H); MS(EI) $^+$  calcd for  $\text{C}_{13}\text{H}_{20}\text{O}_2$  ( $\text{M}$ ) $^+$  208.1, found 208.2.



3-Hydroxy-1-phenylbutan-1-one. Oxidation of 4-phenylbutan-2-ol (150.2

mg, 1.0 mmol, 1.0 equiv) according to the general procedure for 3 days and

purified by flash column chromatography (10→30% ethyl acetate/hexanes) gave 3-hydroxy-1-

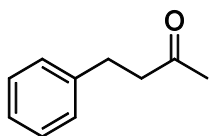
phenylbutan-1-one (43 mg, 26% yield) as a colorless oil, 1-phenylbutane-1,3-dione

(16 mg, 11%) as a colorless oil, and benzoic acid (22 mg, 18% yield).  $^1\text{H}$  NMR (400 MHz,

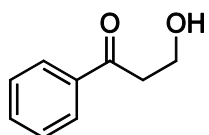
$\text{CDCl}_3$ )  $\delta$  7.94 (d,  $J = 7.4$  Hz, 2H), 7.57 (m, 1H), 7.46 (m, 2H), 4.36-4.44 (m, 1H), 3.40 (brs, 1H),

3.16 (dd,  $J = 2.9, 17.7$  Hz, 1H), 3.04 (dd,  $J = 8.8, 17.7$  Hz, 1H), 1.29 (d,  $J = 6.4$  Hz, 3H);

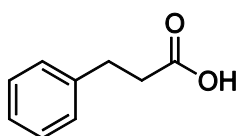
MS(ESI) $^+$  calcd for  $\text{C}_{10}\text{H}_{13}\text{O}_2$  ( $\text{M}+\text{H}$ ) $^+$  165.1, found 165.1.



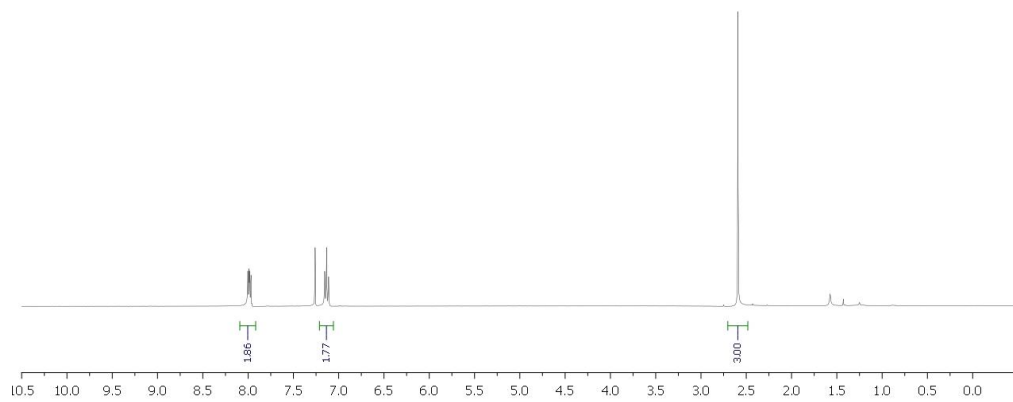
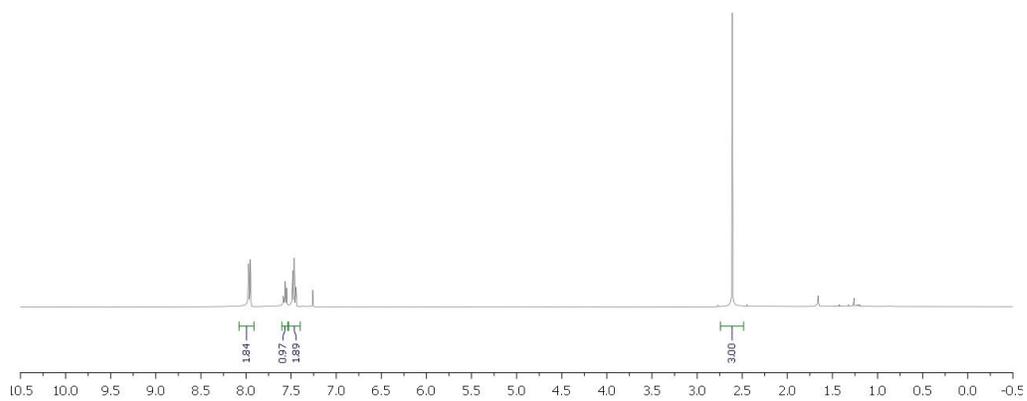
4-Phenylbutan-2-one.  $^1\text{H NMR}$  (400 MHz,  $\text{CDCl}_3$ )  $\delta$  7.26-7.31 (m, 2H), 7.18-7.21 (m, 3H), 2.90 (d,  $J = 7.6$  Hz, 2H), 2.77 (d,  $J = 7.6$  Hz, 2H), 2.14 (s, 3H); MS(ESI) $^+$  calcd for  $\text{C}_{10}\text{H}_{13}\text{O}$  ( $\text{M}+\text{H}$ ) $^+$  149.1, found 149.1.

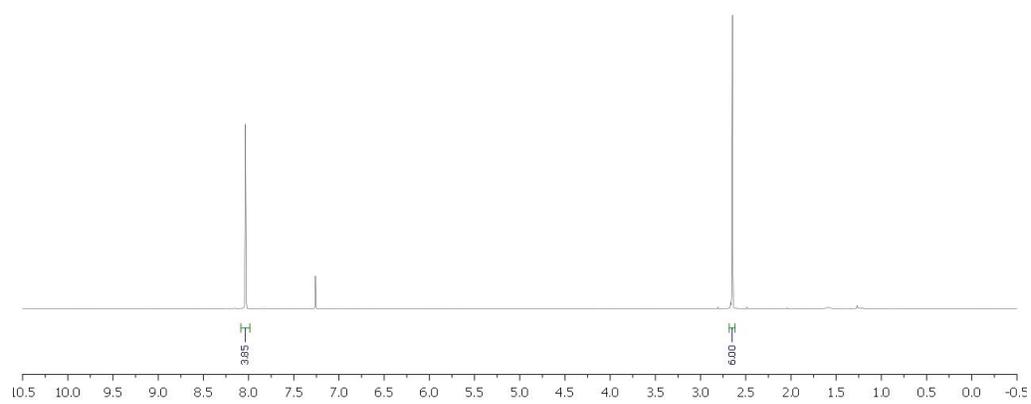
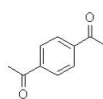
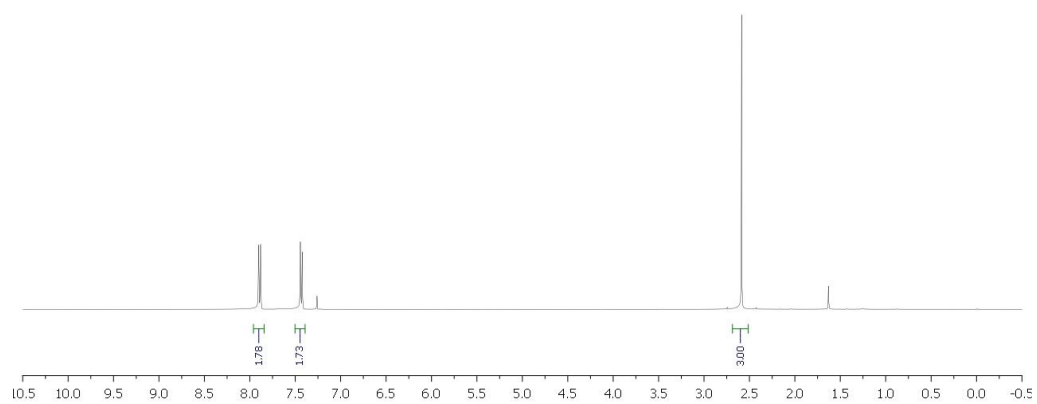
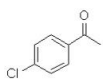


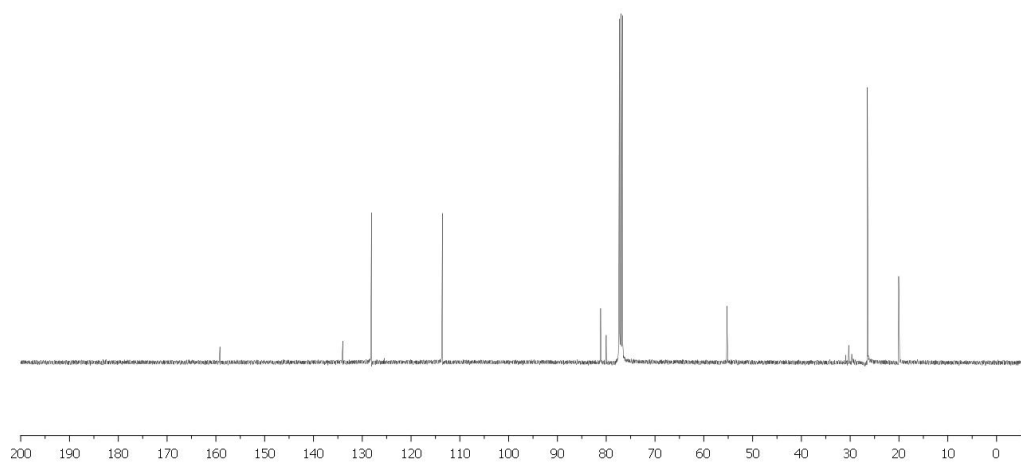
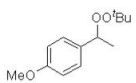
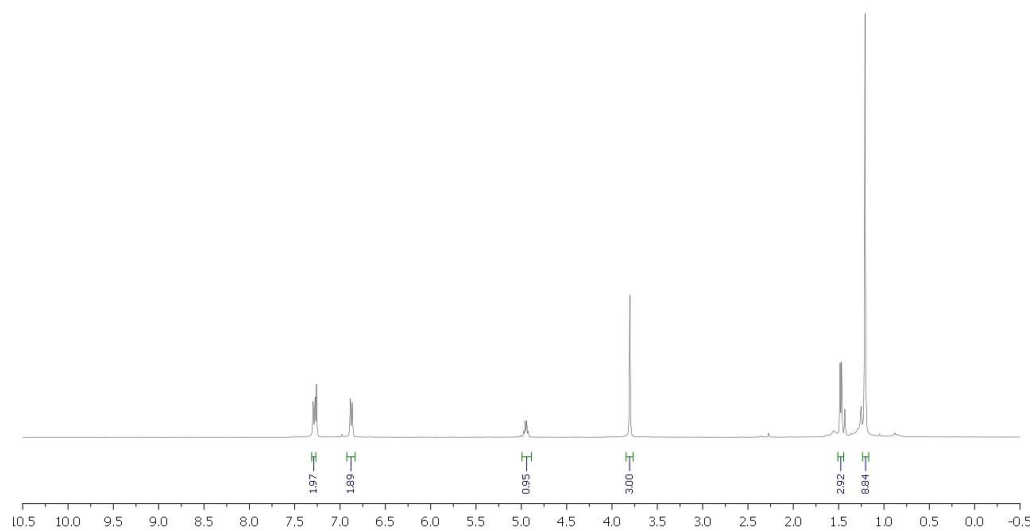
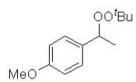
3-Hydroxy-1-phenylpropan-1-one. Oxidation of 3-phenylpropan-1-ol (136.2 mg, 1.0 mmol, 1.0 equiv) according to the general procedure for 3 days and purified by flash column chromatography (10 $\rightarrow$ 25% ethyl acetate/hexanes) gave 3-hydroxy-1-phenylpropan-1-one (51 mg, 34% yield) as a colorless oil, 3-phenylpropanoic acid (13 mg, 9%) as a colorless oil, and benzoic acid (15 mg, 12% yield).  $^1\text{H NMR}$  (400 MHz,  $\text{CDCl}_3$ )  $\delta$  7.97 (d,  $J = 7.8$  Hz, 2H), 7.59 (dd,  $J = 7.3, 7.5$  Hz, 1H), 7.48 (dd,  $J = 7.8, 7.5$  Hz, 2H), 4.03-4.04 (m, 2H), 3.24 (t,  $J = 5.3$  Hz, 3H), 2.68 (brs, 1H); MS(ESI) $^+$  calcd for  $\text{C}_9\text{H}_{11}\text{O}_2$  ( $\text{M}+\text{H}$ ) $^+$  151.1, found 151.1.

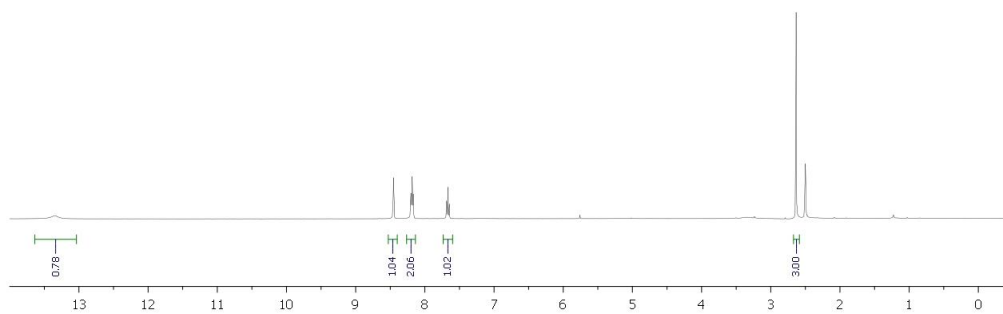
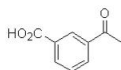
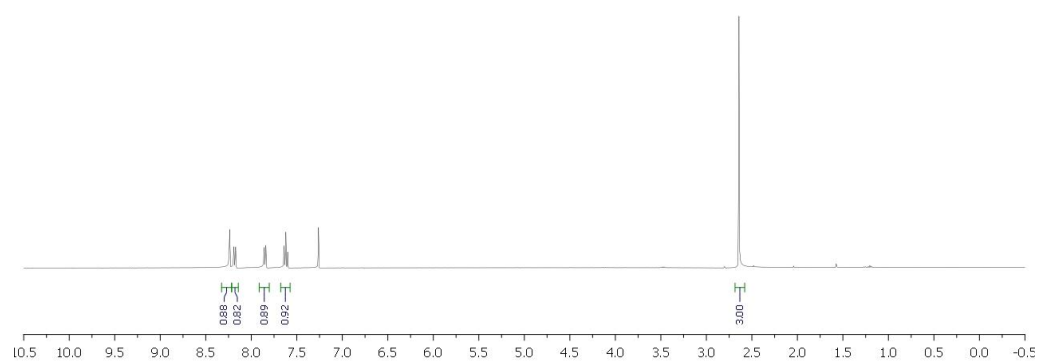
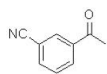


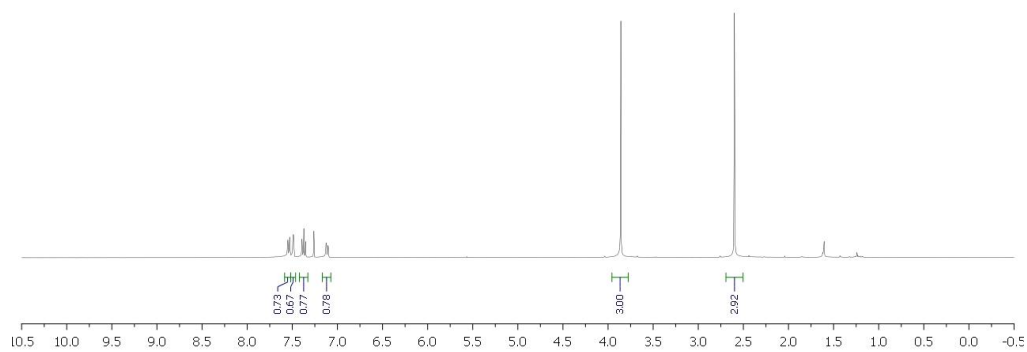
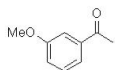
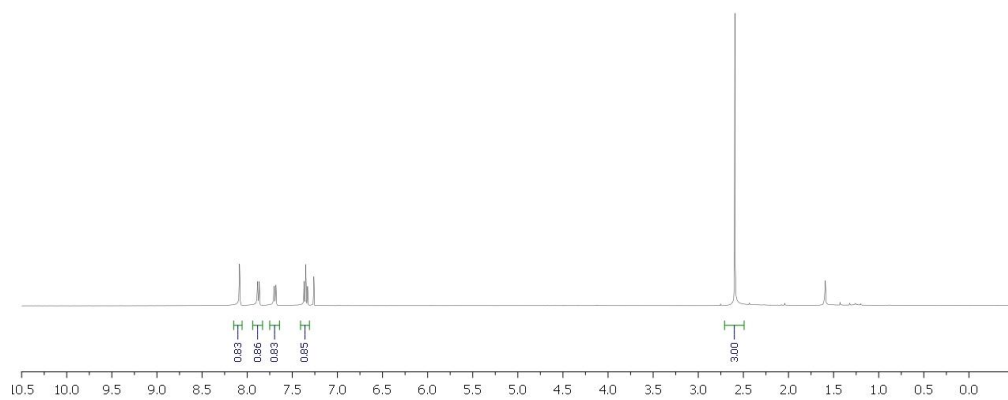
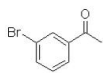
3-Phenylpropanoic acid.  $^1\text{H NMR}$  (400 MHz,  $\text{CDCl}_3$ )  $\delta$  7.21-7.33 (m, 5H), 2.97 (t,  $J = 7.8$  Hz, 2H), 2.70 (t,  $J = 7.8$  Hz, 2H); MS(ESI) $^+$  calcd for  $\text{C}_9\text{H}_{11}\text{O}_2$  ( $\text{M}+\text{H}$ ) $^+$  151.1, found 151.1.

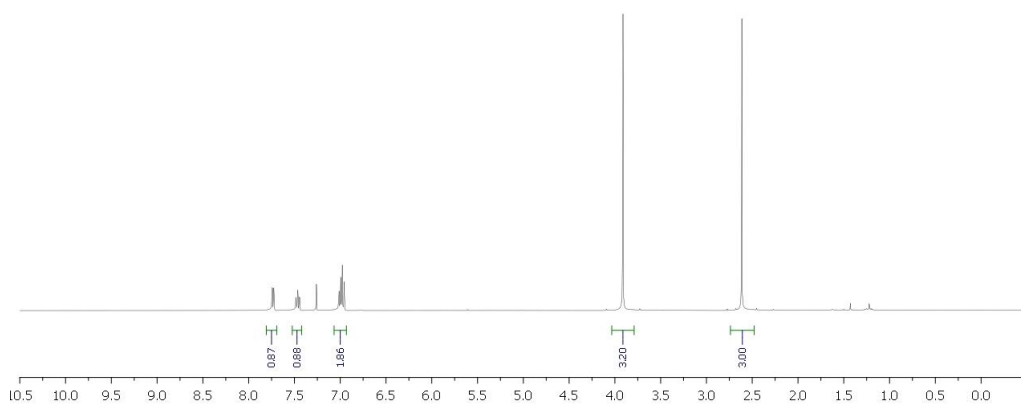
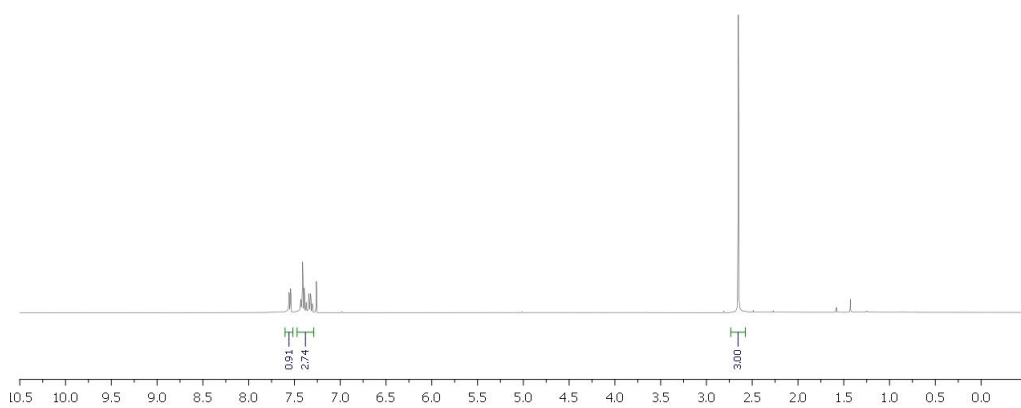


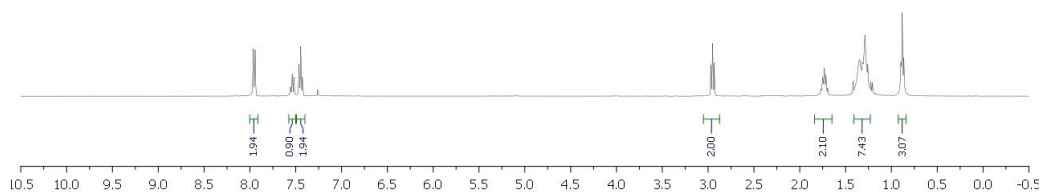
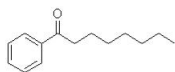
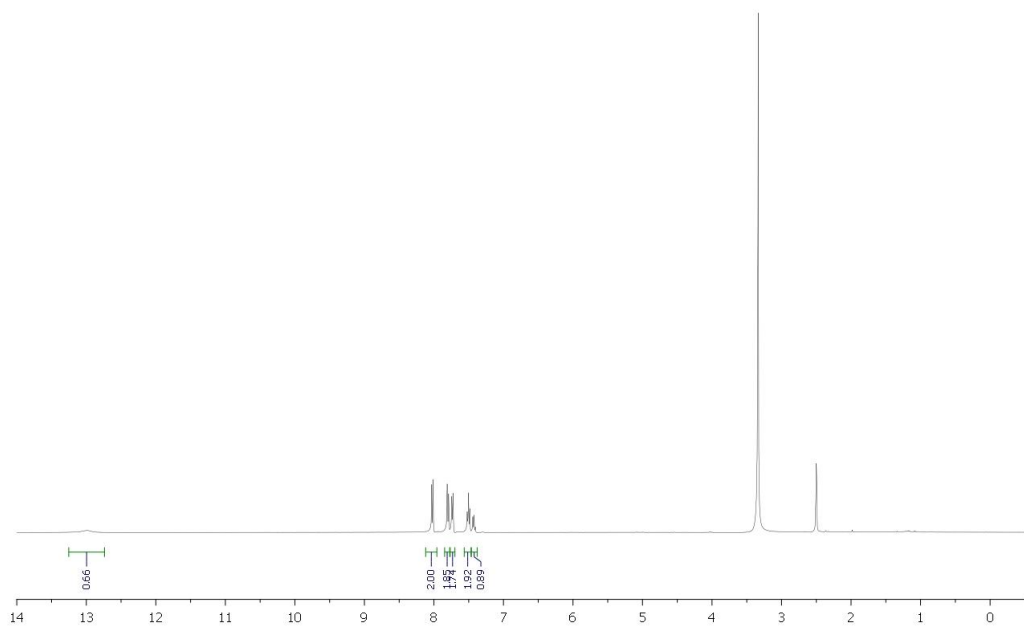
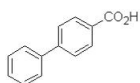


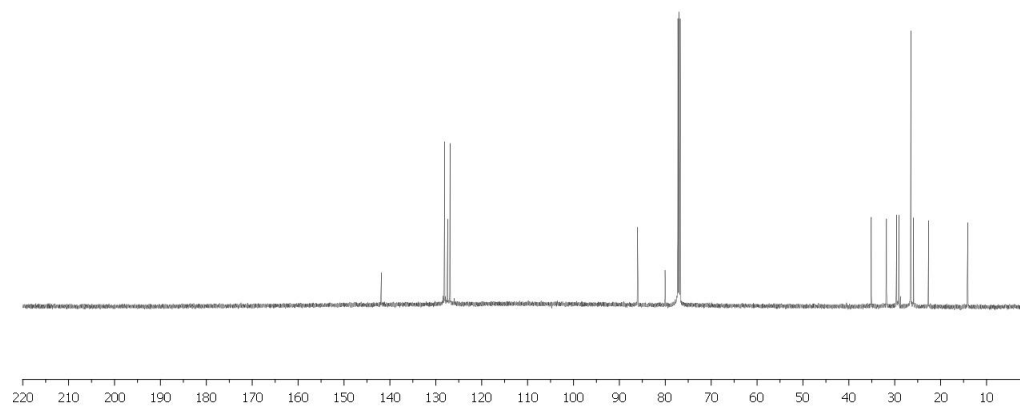
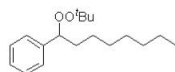
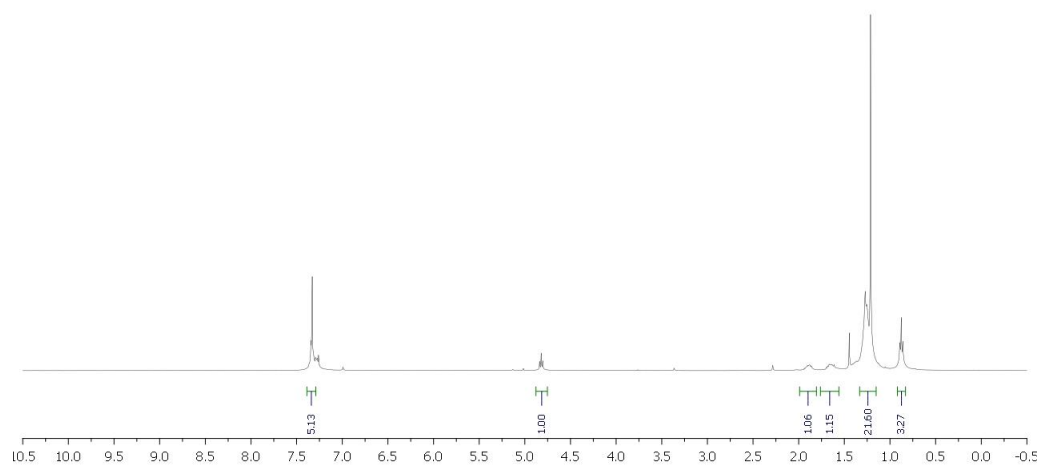
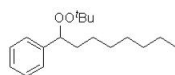


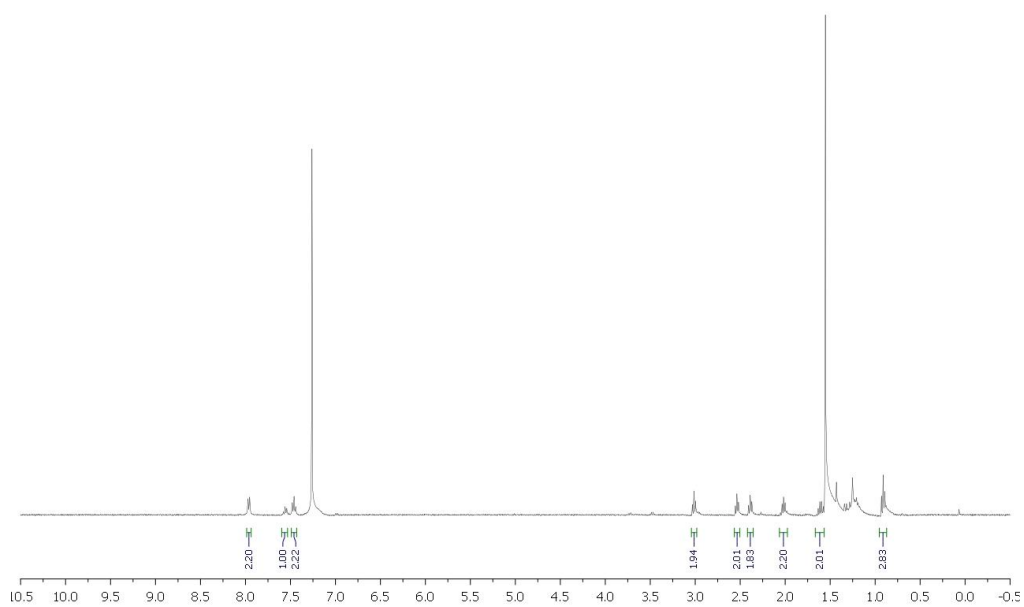
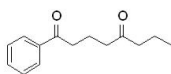
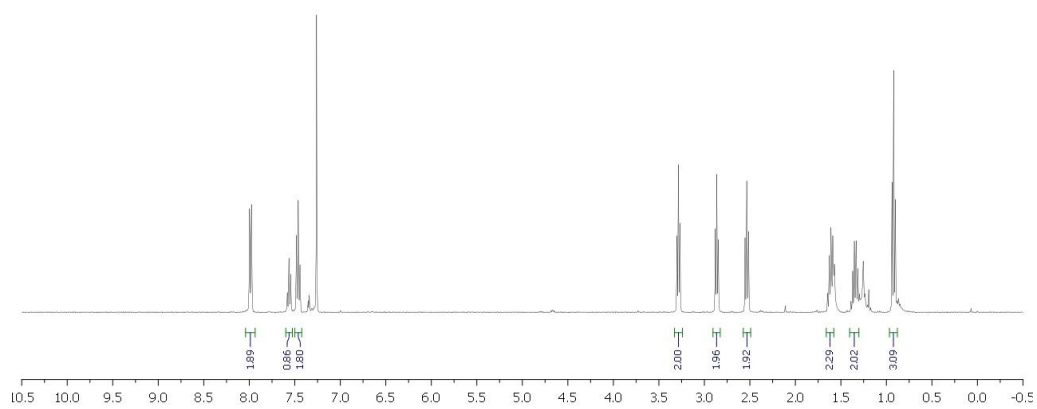
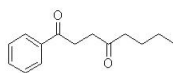


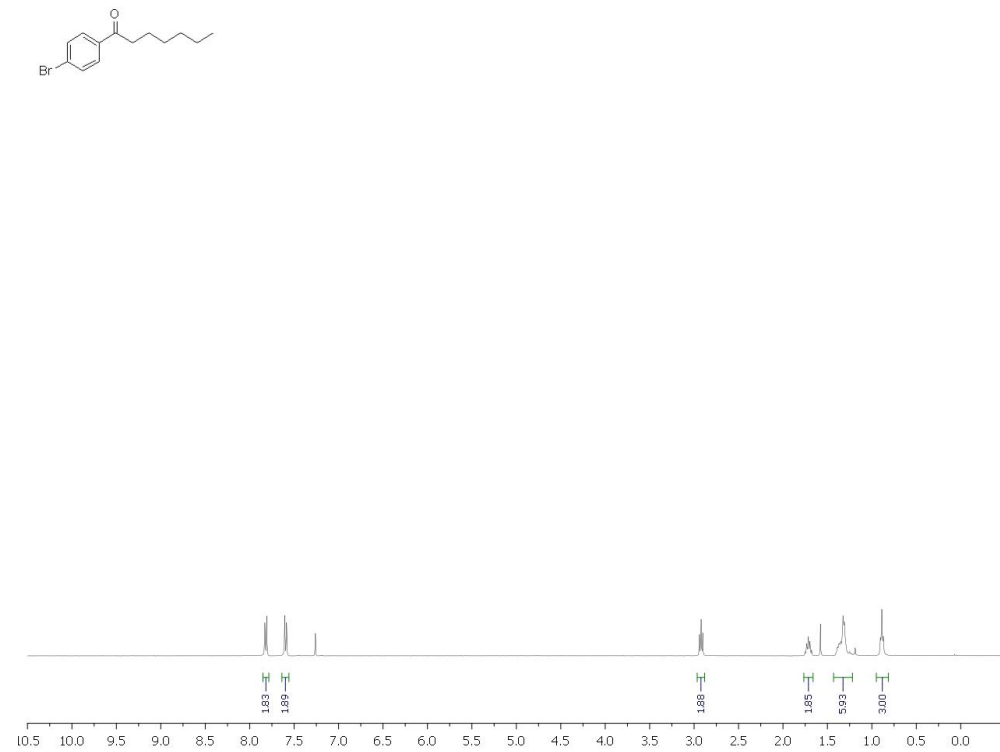
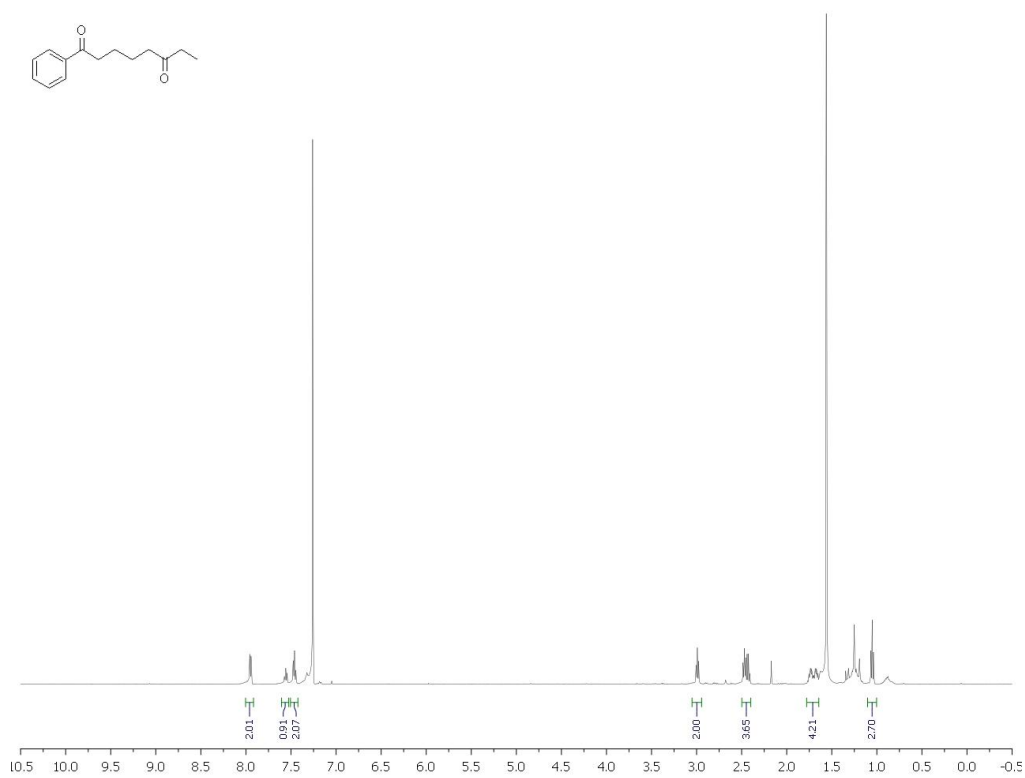


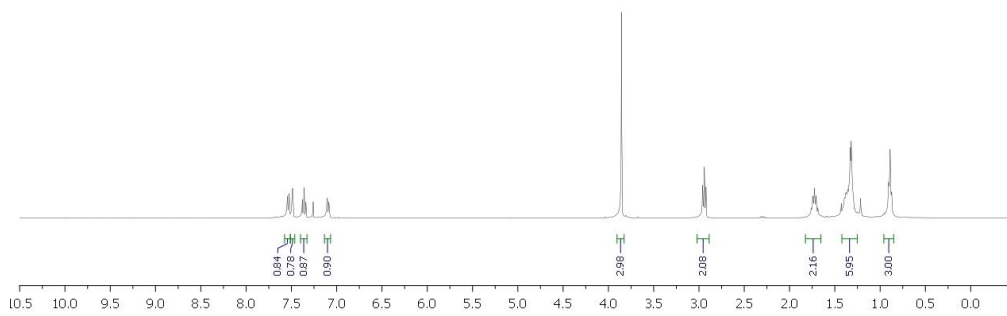
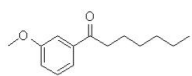
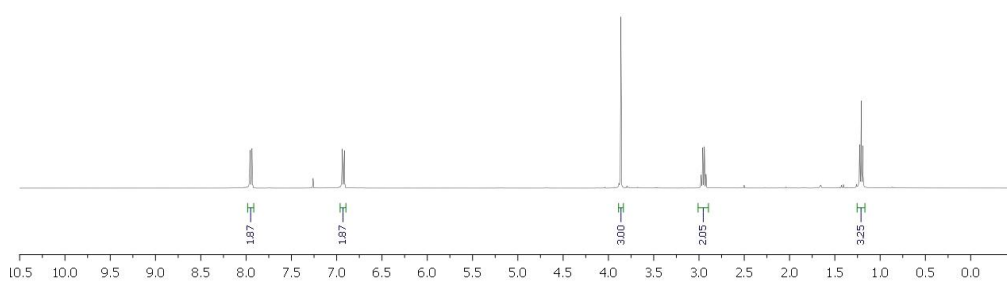
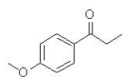


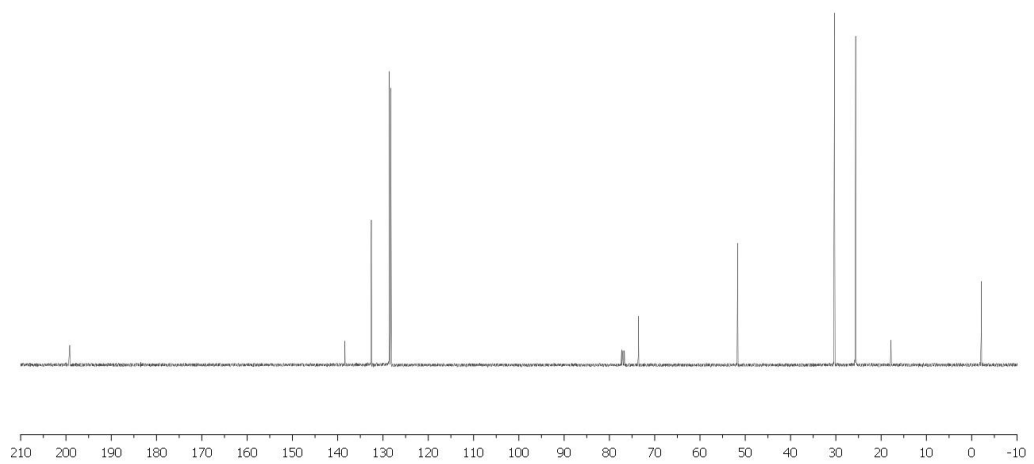
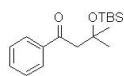
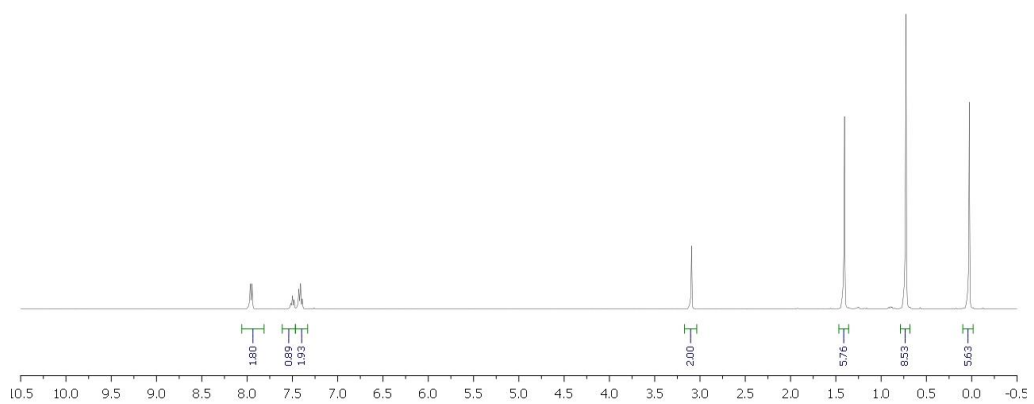
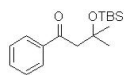


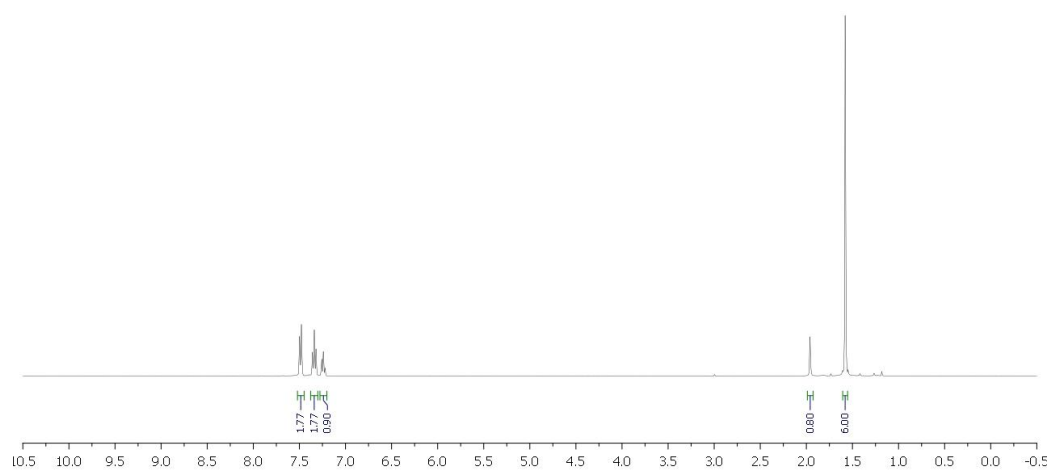
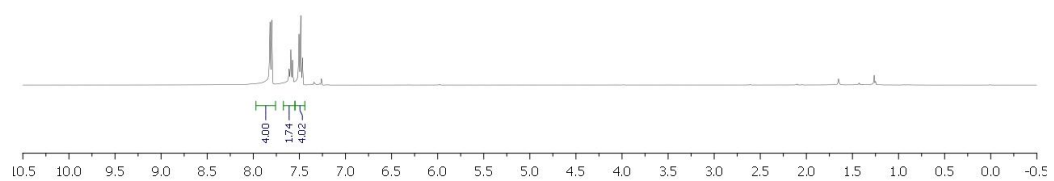
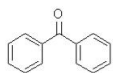


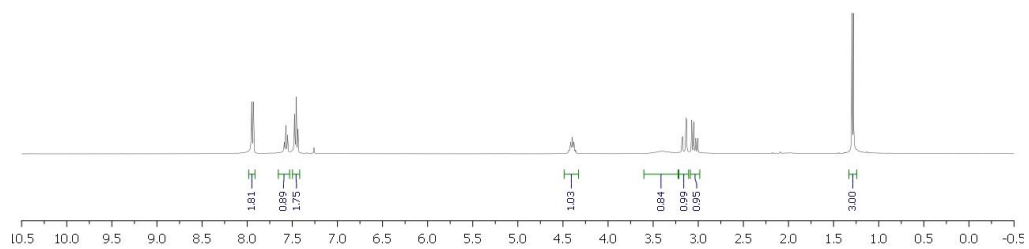
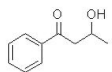
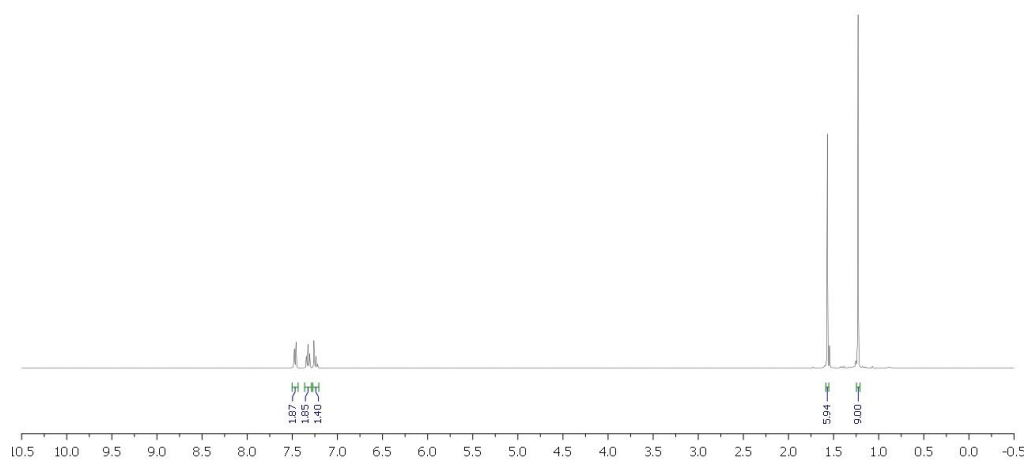
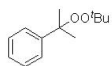


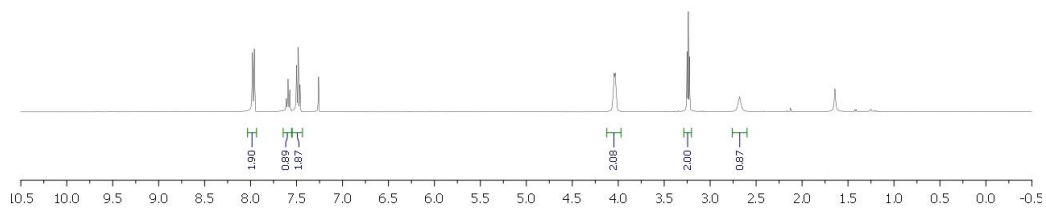
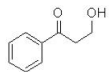
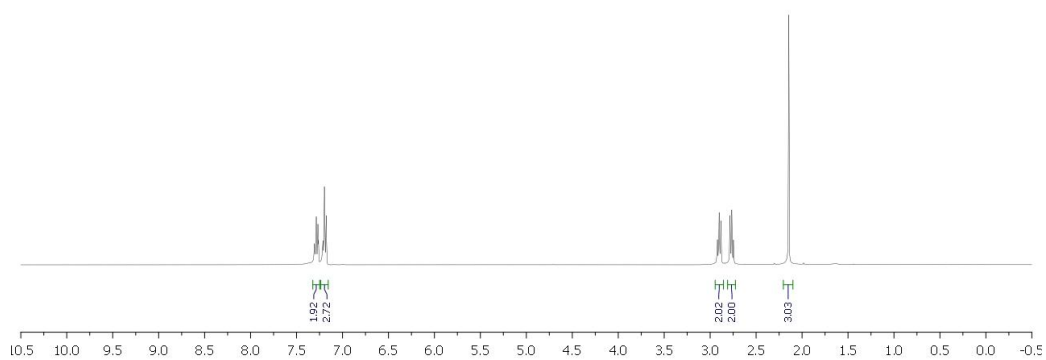
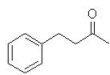


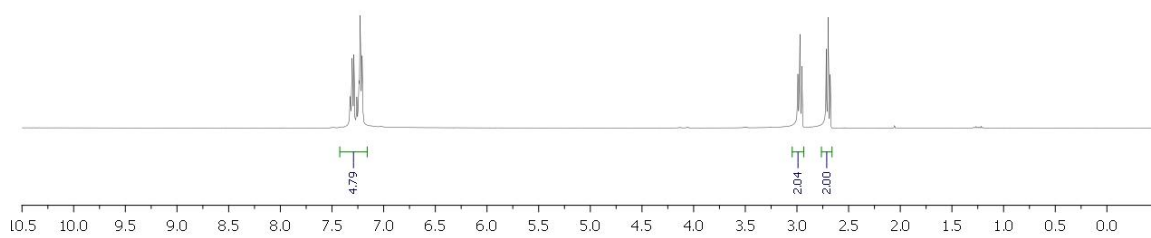
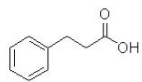












## APPENDIX B

### Supplemental Information for Chapter Four

**Table S1.** Comparison of SCFE energies (kcal/mol) computed at various levels of theory and basis set

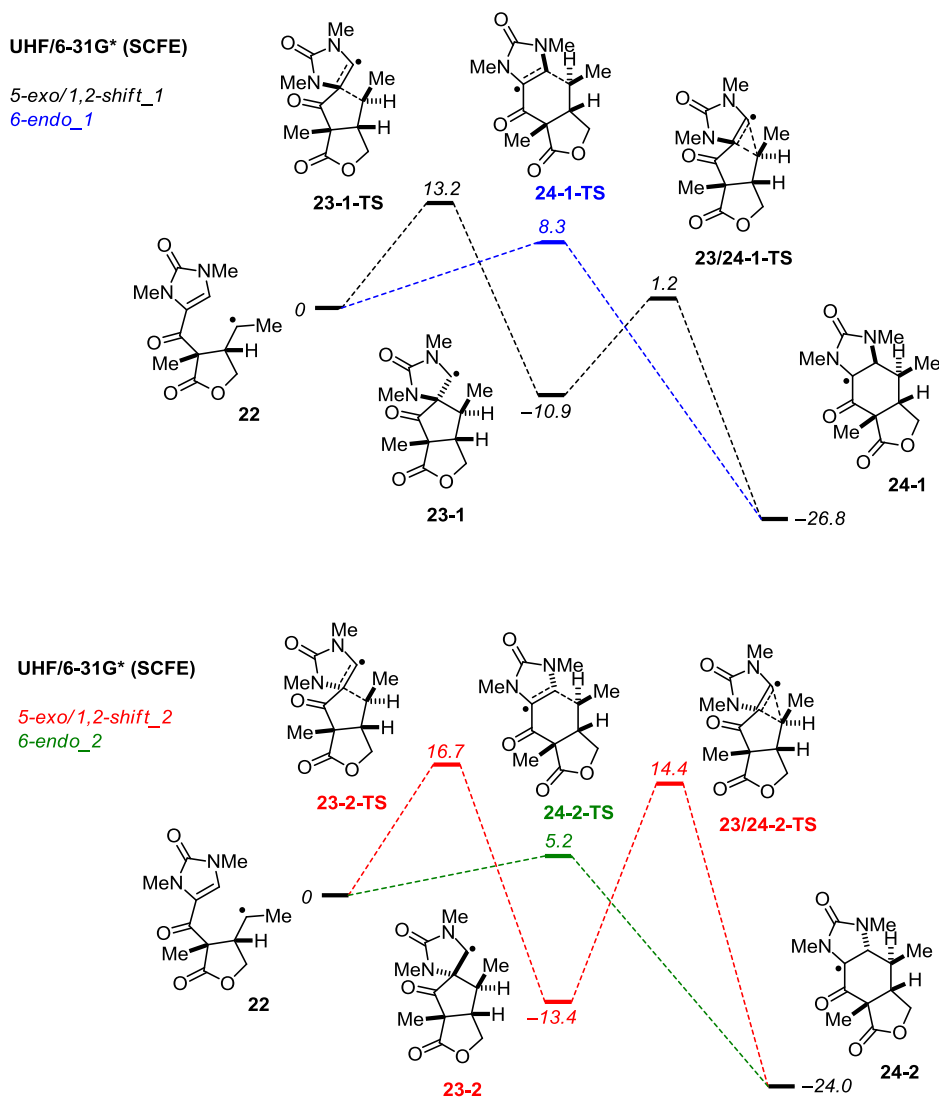
	<b>22</b>	<b>23-1-TS</b>	<b>23-1</b>	<b>23/24-1-TS</b>	<b>24-1</b>	<b>24-1-TS</b>
UHF/6-31G*	0	13.2	-10.9	1.2	-26.8	8.3
UB3LYP/6-31G**//UHF/6-31G*	0	10.8	-7.2	1.2	-27.8	-1.2
UB3LYP/6-31G**	0	13.4	-7.2	1.2	-26.2	7.2
UB3LYP/6-311G**	0	14.5	-5.8	40.9	-24.0	8.6
	<b>22</b>	<b>23-2-TS</b>	<b>24-2</b>	<b>23/24-2-TS</b>	<b>24-2</b>	<b>24-2-TS</b>
UHF/6-31G*	0	16.7	-13.4	14.4	-24.0	5.2
UB3LYP/6-31G**//UHF/6-31G*	0	13.3	-10.5	9.6	-25.2	-3.9
UB3LYP/6-31G**	0	14.7	-9.4	9.1	-23.6	9.0
UB3LYP/6-311G**	0	15.6	-7.9	44.9	-21.1	10.6

**Table S2.** Comparison of SCFE barriers (kcal/mol) computed at various levels of theory and basis set

	<b>5-exo-1</b>	<b>6-endo-1</b>	<b>1,2-shift-1</b>
UHF/6-31G*	13.2	8.3	12.1
UB3LYP/6-31G**//UHF/6-31G*	10.8	-1.2	8.4
UB3LYP/6-31G**	13.4	7.2	8.4
UB3LYP/6-311G**	14.5	8.6	46.6
	<b>5-exo-2</b>	<b>6-endo-2</b>	<b>1,2-shift-2</b>
UHF/6-31G*	16.7	5.2	27.8
UB3LYP/6-31G**//UHF/6-31G*	13.3	-3.9	20.1
UB3LYP/6-31G**	14.7	9.0	18.5
UB3LYP/6-311G**	15.6	10.6	52.8

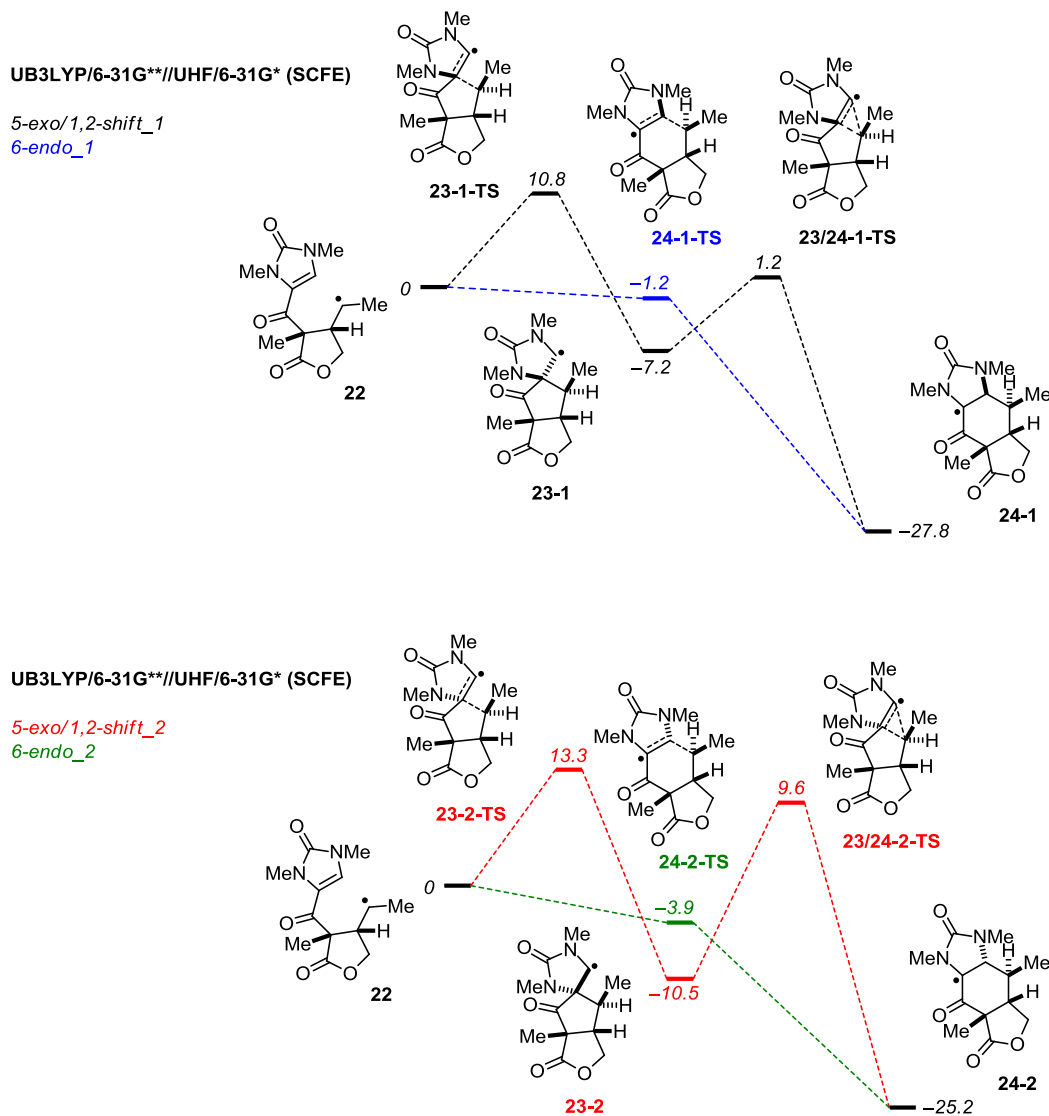
**Table S3.** Computed energies (kcal/mol) in gas phase at 298.15 K by UB3LYP/6-311G\*\*

	<b>22</b>	<b>23-1-TS</b>	<b>23-1</b>	<b>23/24-1-TS</b>	<b>24-1</b>	<b>24-1-TS</b>
SCFE	-574942.72	-574928.19	-574948.46	-574901.82	-574966.70	-574934.16
$\Delta$ SCFE	0	14.5	-5.7	40.9	-24.0	8.6
ZPE	181.63	181.40	183.02	181.02	184.36	181.61
H <sub>tot</sub>	-574748.11	-574734.46	-574753.20	-574708.51	-574770.30	-574740.28
$\Delta$ H	0	13.7	-5.1	39.6	-22.2	7.8
G <sub>tot</sub>	-574792.34	-574776.16	-574794.72	-574750.05	-574811.45	-574781.84
$\Delta$ G	0	16.2	-2.4	42.3	-19.1	10.5
	<b>22</b>	<b>23-2-TS</b>	<b>23-2</b>	<b>23/24-2-TS</b>	<b>24-2</b>	<b>24-2-TS</b>
SCFE	-574942.72	-574927.11	-574950.63	-574897.86	-574963.85	-574932.10
$\Delta$ SCFE	0	15.6	-7.9	44.9	-21.1	10.6
ZPE	181.63	181.03	182.90	180.98	184.41	181.64
H <sub>tot</sub>	-574748.11	-574733.60	-574755.40	-574704.56	-574767.43	-574738.12
$\Delta$ H	0	14.5	-7.3	43.5	-19.3	10.0
G <sub>tot</sub>	-574792.34	-574775.77	-574797.09	-574746.35	-574808.52	-574779.86
$\Delta$ G	0	16.6	-4.8	46.0	-16.2	12.5

**Figure S1.** SCF energy diagrams of the 5-exo and 6-endo cyclization of **22** calculated with UHF/6-31G\*.

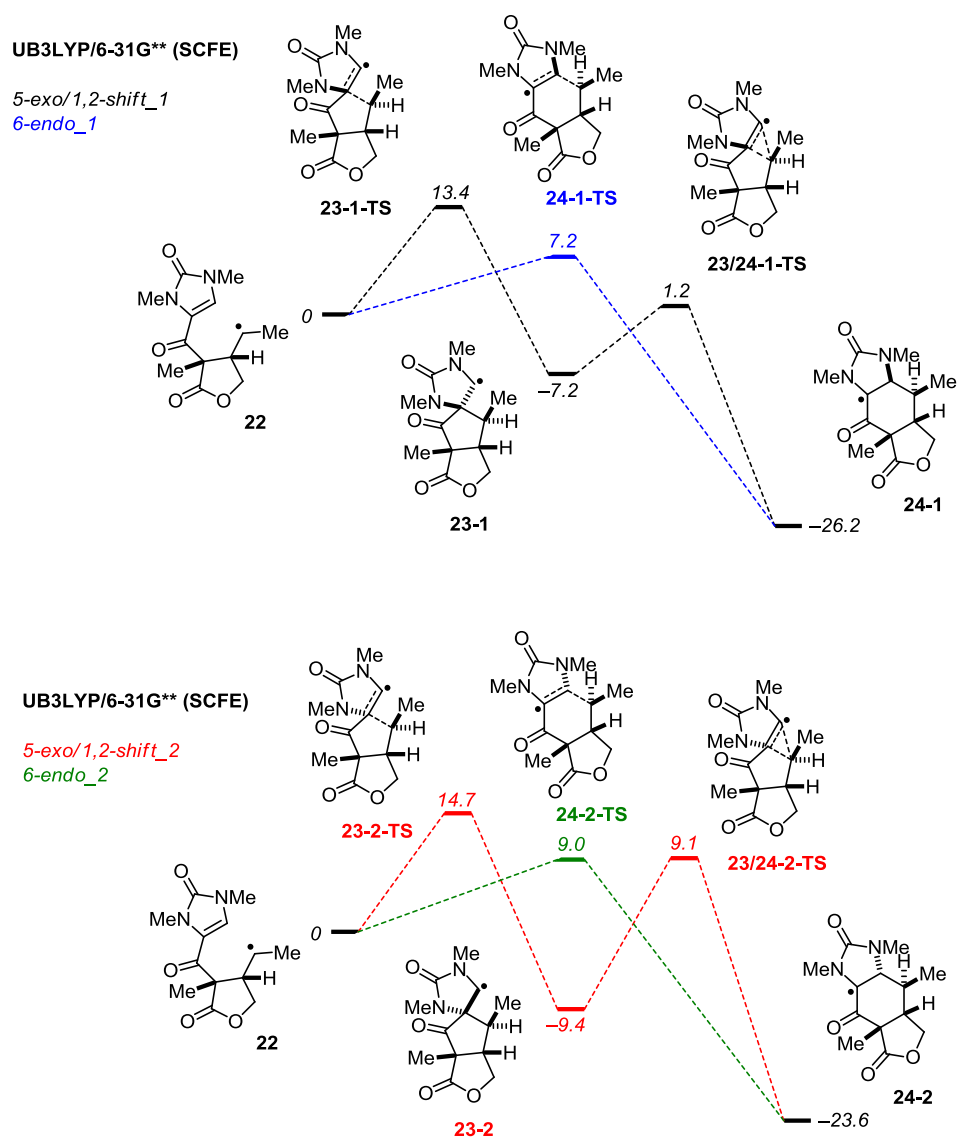
SCFE (kcal/mol)	<b>22</b>	<b>23-1-TS</b>	<b>23-1</b>	<b>23/24-1-TS</b>	<b>24-1</b>	<b>24-1-TS</b>
	0	13.2	-10.9	1.2	-26.8	8.3
SCFE (kcal/mol)	<b>22</b>	<b>23-2-TS</b>	<b>23-2</b>	<b>23/24-2-TS</b>	<b>24-2</b>	<b>24-2-TS</b>
	0	16.7	-13.4	14.4	-24.0	5.2

**Figure S2.** SCF energy diagrams of the 5-exo and 6-endo cyclization of **22** calculated with UB3LYP/6-31G\*\*//UHF/6-31G\*.



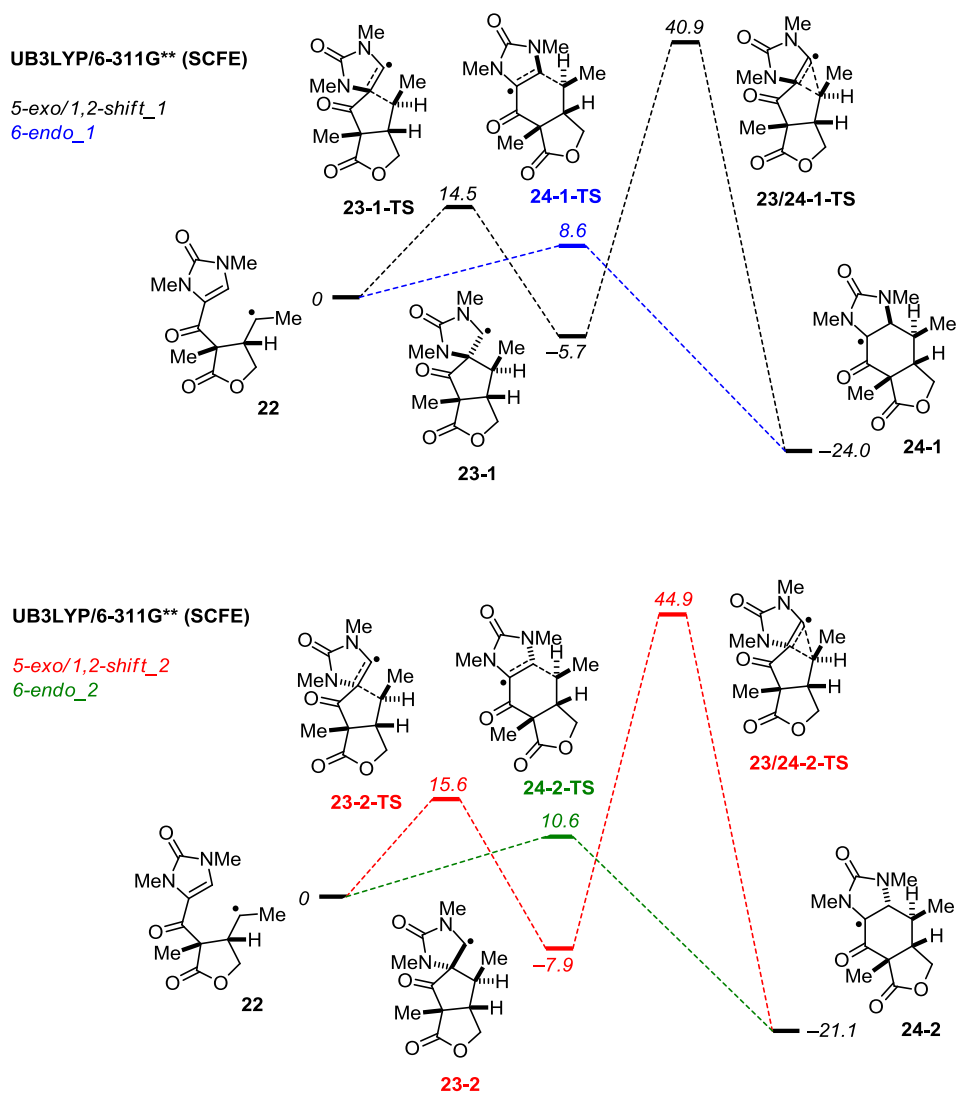
SCFE (kcal/mol)	<b>22</b>	<b>23-1-TS</b>	<b>23-1</b>	<b>23/24-1-TS</b>	<b>24-1</b>	<b>24-1-TS</b>
	0	10.8	-7.2	1.2	-27.8	-1.2
SCFE (kcal/mol)	<b>22</b>	<b>23-2-TS</b>	<b>23-2</b>	<b>23/24-2-TS</b>	<b>24-2</b>	<b>24-2-TS</b>
	0	13.3	-10.5	9.6	-25.2	-3.9

**Figure S3.** SCFE energy diagrams of the 5-exo and 6-endo cyclization of **22** calculated with UB3LYP/6-31G\*\*.



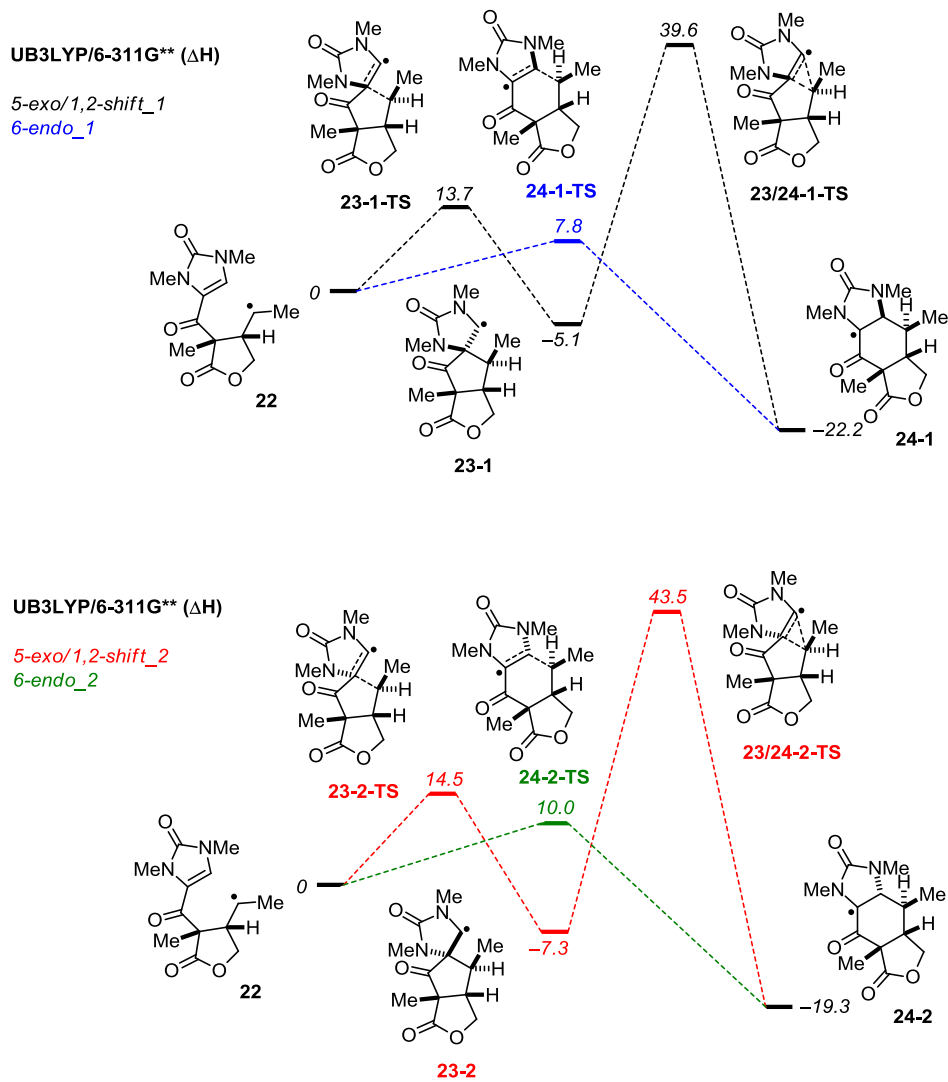
SCFE (kcal/mol)	<b>22</b>	<b>23-1-TS</b>	<b>23-1</b>	<b>23/24-1-TS</b>	<b>24-1</b>	<b>24-1-TS</b>
	0	13.4	-7.2	1.2	-26.2	7.2
SCFE (kcal/mol)	<b>22</b>	<b>23-2-TS</b>	<b>23-2</b>	<b>23/24-2-TS</b>	<b>24-2</b>	<b>24-2-TS</b>
	0	14.7	-9.4	9.1	-23.6	9.0

**Figure S4.** SCF energy diagrams of the 5-exo and 6-endo cyclization of **22** calculated with UB3LYP/6-311G\*\*.



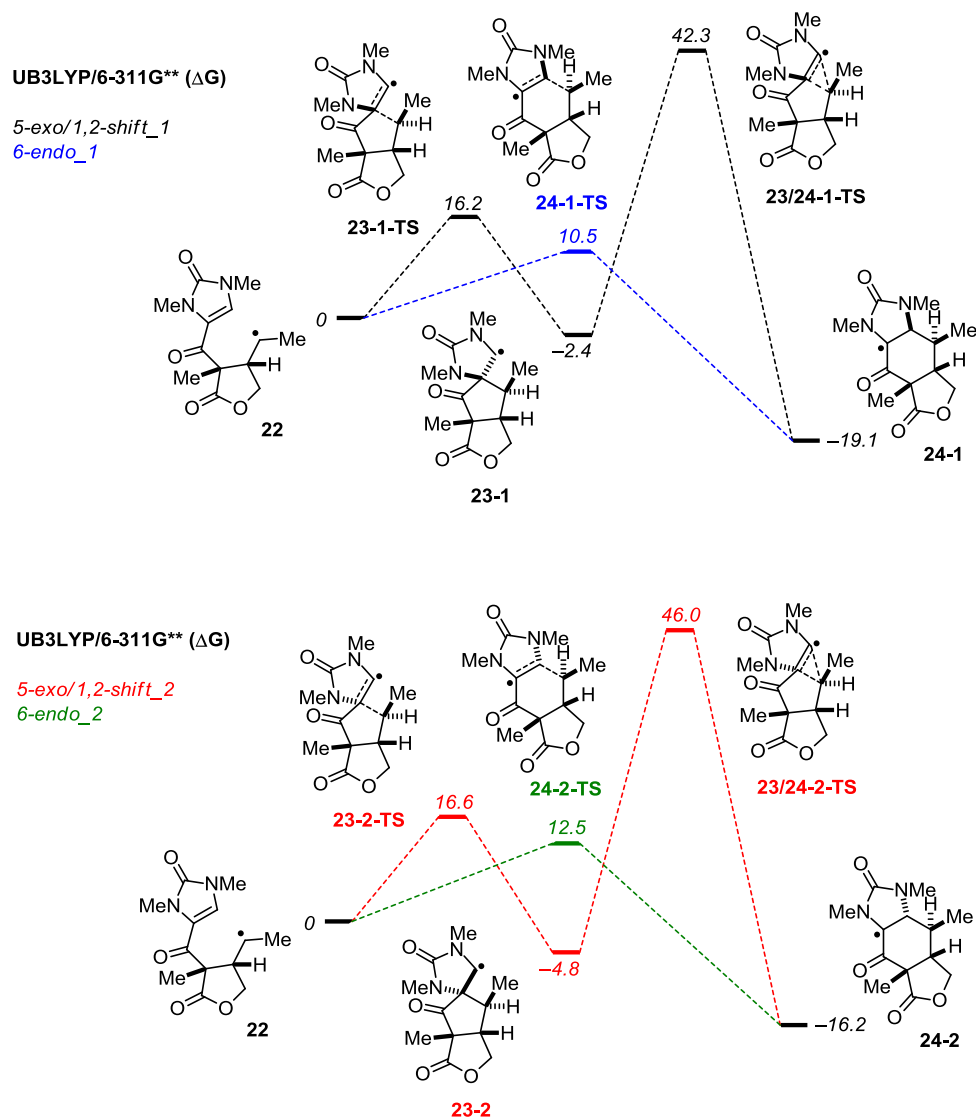
	<b>22</b>	<b>23-1-TS</b>	<b>23-1</b>	<b>23/24-1-TS</b>	<b>24-1</b>	<b>24-1-TS</b>
SCFE (kcal/mol)	0	14.5	-5.7	40.9	-24.0	8.6
	<b>22</b>	<b>23-2-TS</b>	<b>23-2</b>	<b>23/24-2-TS</b>	<b>24-2</b>	<b>24-2-TS</b>
SCFE (kcal/mol)	0	15.6	-7.9	44.9	-21.1	10.6

**Figure S5.** Reaction enthalpy diagrams of the 5-exo and 6-endo cyclization of **22** calculated with UB3LYP/6-311G\*\*.



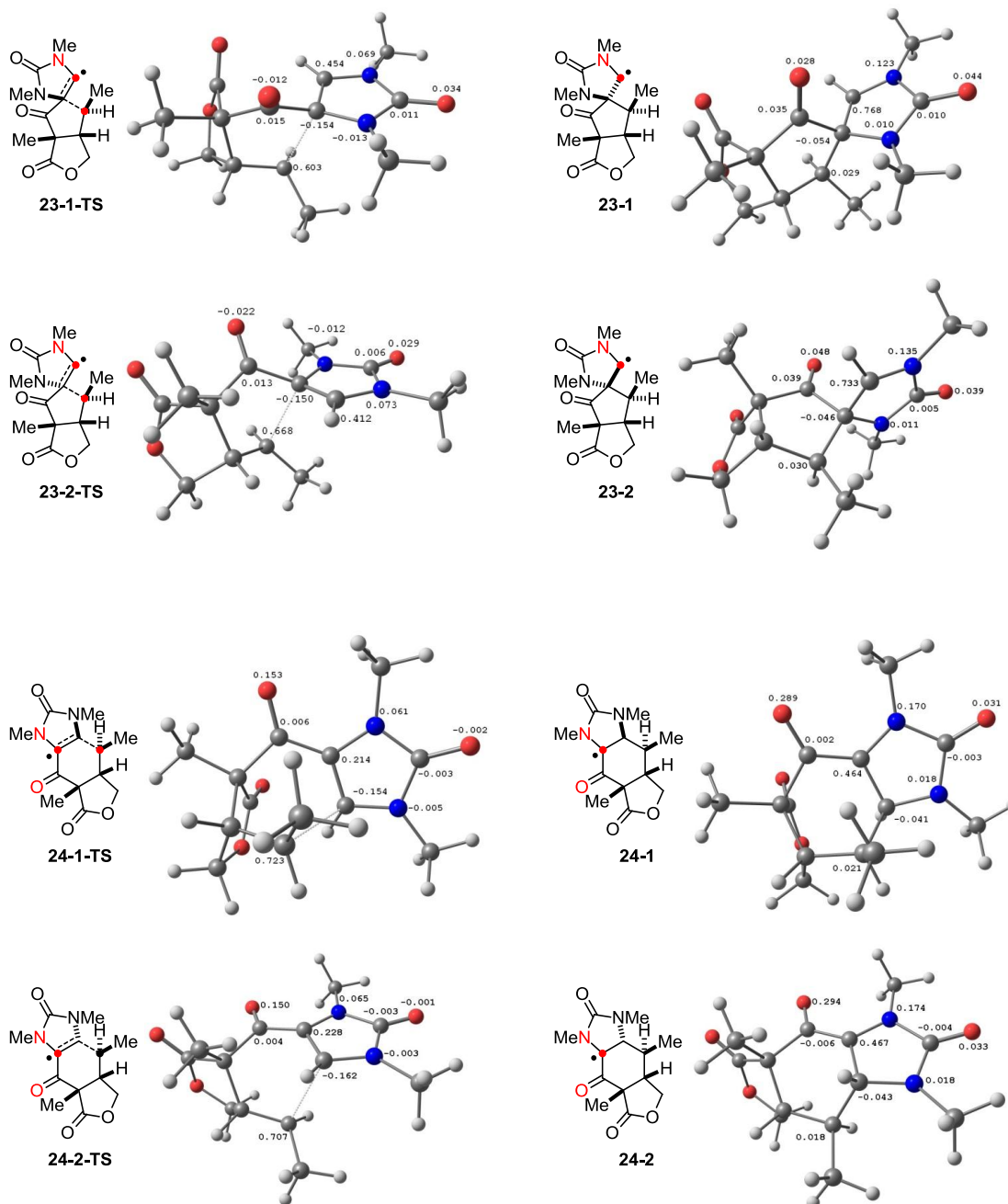
$\Delta H$ (kcal/mol)	<b>22</b>	<b>23-1-TS</b>	<b>23-1</b>	<b>23/24-1-TS</b>	<b>24-1</b>	<b>24-1-TS</b>
	0	13.7	-5.1	39.6	-22.2	7.8
$\Delta H$ (kcal/mol)	<b>22</b>	<b>23-2-TS</b>	<b>23-2</b>	<b>23/24-2-TS</b>	<b>24-2</b>	<b>24-2-TS</b>
	0	14.5	-7.3	43.5	-19.3	10.0

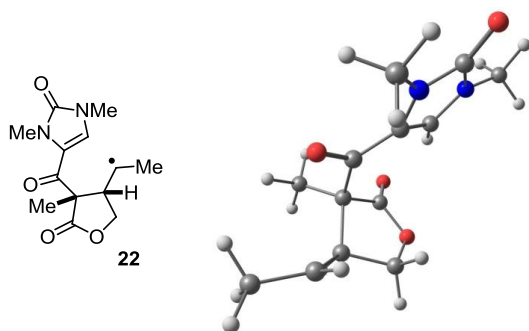
**Figure S6.** Reaction free energy diagrams of the 5-exo and 6-endo cyclization of **22** at 298.15K calculated with UB3LYP/6-311G\*\*.



$\Delta G$ (kcal/mol)	<b>22</b>	<b>23-1-TS</b>	<b>23-1</b>	<b>23/24-1-TS</b>	<b>24-1</b>	<b>24-1-TS</b>
	0	16.2	-2.4	42.3	-19.1	10.5
$\Delta G$ (kcal/mol)	<b>22</b>	<b>23-2-TS</b>	<b>23-2</b>	<b>23/24-2-TS</b>	<b>24-2</b>	<b>24-2-TS</b>
	0	16.6	-4.8	46.0	-16.2	12.5

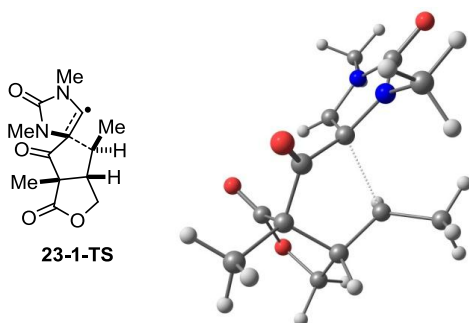
**Figure S7.** Atomic spin densities of the transition states and intermediates of the 5-exo and 6-endo cyclization of **22**. Positions of high spin density were labeled in red.





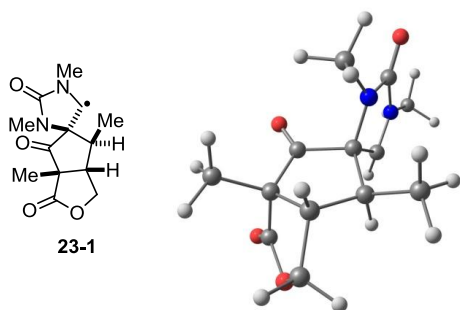
Zero-point correction=	0.289454 (Hartree/Particle)
Thermal correction to Energy=	0.309182
Thermal correction to Enthalpy=	0.310127
Thermal correction to Gibbs Free Energy=	0.239646
Sum of electronic and zero-point Energies=	-915.940090
Sum of electronic and thermal Energies=	-915.920361
Sum of electronic and thermal Enthalpies=	-915.919417
Sum of electronic and thermal Free Energies=	-915.989897

C	3.295160000	1.089549000	0.039267000
O	4.259401000	1.811548000	0.210049000
N	3.299996000	-0.317177000	0.010118000
N	1.973475000	1.437385000	-0.155672000
C	1.176819000	0.278736000	-0.277759000
C	2.036876000	-0.789962000	-0.178578000
H	1.839954000	-1.842182000	-0.278054000
C	4.518494000	-1.095591000	0.157700000
H	5.333804000	-0.387114000	0.295978000
H	4.705329000	-1.694886000	-0.735992000
H	4.454517000	-1.751116000	1.028704000
C	1.563305000	2.837000000	-0.133517000
H	2.466648000	3.415766000	0.054924000
H	0.837336000	3.016674000	0.660406000
H	1.117362000	3.126872000	-1.082715000
C	-0.243956000	0.341379000	-0.589881000
O	-0.761290000	1.404536000	-0.908698000
C	-1.198305000	-0.886830000	-0.513830000
C	-2.250550000	-0.663369000	0.658808000
H	-3.087694000	-1.325732000	0.401472000
C	-1.850599000	-1.069042000	-1.890509000
H	-2.294789000	-0.129614000	-2.217808000
H	-2.624536000	-1.839166000	-1.848744000
H	-1.103923000	-1.384434000	-2.621898000
C	-0.559998000	-2.199421000	-0.052138000
O	0.006069000	-3.013103000	-0.732188000
O	-0.726722000	-2.372923000	1.280025000
C	-1.501713000	-1.289407000	1.840641000
H	-0.817385000	-0.579351000	2.315095000
H	-2.160461000	-1.714698000	2.596418000
C	-2.782811000	0.694018000	0.926854000
H	-2.180098000	1.368519000	1.526556000
C	-3.953845000	1.260488000	0.203786000
H	-4.646057000	0.481031000	-0.129489000
H	-3.630514000	1.815466000	-0.689720000
H	-4.509298000	1.967151000	0.828387000



Imaginary Frequency=	-437.7573 cm <sup>-1</sup>
Zero-point correction=	0.289076 (Hartree/Particle)
Thermal correction to Energy=	0.307796
Thermal correction to Enthalpy=	0.308740
Thermal correction to Gibbs Free Energy=	0.242284
Sum of electronic and zero-point Energies=	-915.917324
Sum of electronic and thermal Energies=	-915.898604
Sum of electronic and thermal Enthalpies=	-915.897659
Sum of electronic and thermal Free Energies=	-915.964116

C	2.963748000	0.345999000	-0.277626000
O	4.068981000	0.849285000	-0.214993000
N	2.645915000	-1.003048000	-0.070768000
N	1.755428000	0.960645000	-0.558380000
C	3.653709000	-2.008107000	0.208480000
H	4.614644000	-1.497226000	0.249743000
H	3.678091000	-2.762773000	-0.582008000
H	3.460187000	-2.496344000	1.166898000
C	1.691061000	2.361685000	-0.946989000
H	1.040859000	2.926406000	-0.277284000
H	1.324670000	2.457569000	-1.968668000
H	2.704675000	2.753405000	-0.873181000
C	-0.516242000	0.189504000	-1.341000000
O	-0.498611000	0.837717000	-2.363271000
C	-1.818240000	-0.371572000	-0.755461000
C	-1.946520000	0.206897000	0.683680000
H	-2.506814000	1.145715000	0.667306000
C	-3.009111000	-0.073996000	-1.677312000
H	-3.075547000	0.998209000	-1.865536000
H	-3.948291000	-0.415697000	-1.235303000
H	-2.876264000	-0.577015000	-2.635961000
C	-1.790651000	-1.885206000	-0.478536000
O	-1.385386000	-2.758216000	-1.191298000
O	-2.344560000	-2.132740000	0.736960000
C	-2.753947000	-0.904628000	1.378467000
H	-2.531951000	-1.001905000	2.440970000
H	-3.832905000	-0.788600000	1.244040000
C	-0.569100000	0.418601000	1.293374000
H	-0.206278000	-0.437689000	1.857979000
C	0.683460000	0.043354000	-0.459612000
C	-0.267051000	1.739723000	1.942621000
H	-0.617530000	2.581723000	1.339082000
H	0.805732000	1.865284000	2.115256000
H	-0.756516000	1.826827000	2.925203000
C	1.300630000	-1.206617000	-0.242184000
H	0.858724000	-2.187169000	-0.234686000

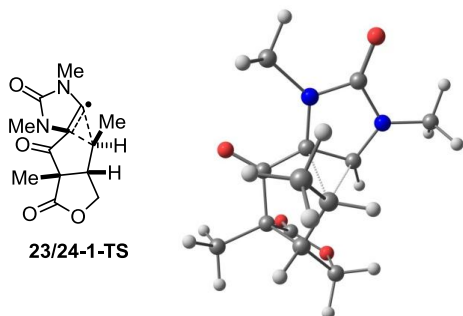


```

Zero-point correction=                0.291664 (Hartree/Particle)
Thermal correction to Energy=         0.310228
Thermal correction to Enthalpy=       0.311172
Thermal correction to Gibbs Free Energy= 0.245004
Sum of electronic and zero-point Energies= -915.947040
Sum of electronic and thermal Energies= -915.928477
Sum of electronic and thermal Enthalpies= -915.927533
Sum of electronic and thermal Free Energies= -915.993700

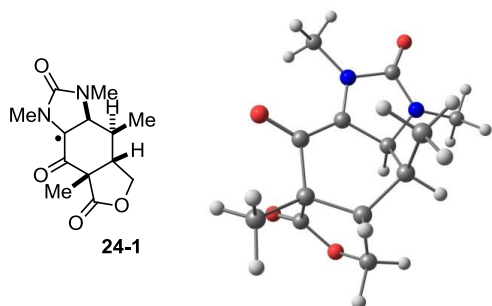
```

C	-2.740269000	0.365983000	-0.742338000
O	-3.638981000	0.670703000	-1.497721000
N	-2.857036000	0.149159000	0.632714000
N	-1.410184000	0.145134000	-1.067283000
C	-4.128720000	0.205655000	1.322490000
H	-4.878189000	0.529620000	0.601949000
H	-4.084182000	0.921782000	2.147468000
H	-4.403601000	-0.777878000	1.715914000
C	-0.897097000	0.633600000	-2.334859000
H	-0.428004000	1.619301000	-2.234611000
H	-1.744428000	0.722774000	-3.013497000
H	-0.175878000	-0.066749000	-2.761621000
C	0.287356000	1.228183000	0.387033000
O	-0.143988000	2.345659000	0.466513000
C	1.770305000	0.842527000	0.405131000
C	1.831914000	-0.564521000	-0.215239000
H	2.034641000	-0.544547000	-1.288986000
C	2.635534000	1.940814000	-0.229282000
H	2.337836000	2.109069000	-1.266693000
H	3.695055000	1.673692000	-0.211704000
H	2.499263000	2.870702000	0.323509000
C	2.283926000	0.580914000	1.840697000
O	2.176017000	1.287393000	2.796651000
O	2.941022000	-0.611765000	1.871894000
C	2.973700000	-1.223374000	0.563839000
H	2.848954000	-2.297624000	0.704320000
H	3.953308000	-1.033685000	0.116685000
C	0.452978000	-1.206798000	0.095116000
H	0.504900000	-1.565676000	1.130890000
C	-0.590026000	-0.050473000	0.130806000
C	0.077879000	-2.394451000	-0.785787000
H	0.015782000	-2.117443000	-1.840032000
H	-0.892087000	-2.799800000	-0.490026000
H	0.816955000	-3.195333000	-0.691116000
C	-1.650228000	-0.233856000	1.176725000
H	-1.473427000	-0.160692000	2.240450000



Imaginary Frequency=	-1212.5947 cm <sup>-1</sup>
Zero-point correction=	0.288468 (Hartree/Particle)
Thermal correction to Energy=	0.307122
Thermal correction to Enthalpy=	0.308066
Thermal correction to Gibbs Free Energy=	0.241857
Sum of electronic and zero-point Energies=	-915.875905
Sum of electronic and thermal Energies=	-915.857251
Sum of electronic and thermal Enthalpies=	-915.856307
Sum of electronic and thermal Free Energies=	-915.922515

C	-2.814803000	0.224897000	-0.420920000
O	-3.941538000	0.143496000	-0.856394000
N	-2.378027000	-0.220451000	0.834125000
N	-1.693188000	0.747155000	-1.055429000
C	-3.260711000	-0.866061000	1.786180000
H	-4.261771000	-0.858607000	1.357626000
H	-3.269247000	-0.320778000	2.734235000
H	-2.955481000	-1.900174000	1.971332000
C	-1.780029000	1.299199000	-2.405225000
H	-1.378893000	2.308889000	-2.423160000
H	-2.834496000	1.290110000	-2.677379000
H	-1.219679000	0.689102000	-3.116864000
C	0.691614000	1.321519000	-0.516087000
O	0.825102000	2.167714000	-1.412901000
C	1.897257000	0.740597000	0.251047000
C	1.687902000	-0.796235000	0.362468000
H	2.439641000	-1.325405000	-0.230962000
C	3.213332000	1.174734000	-0.404013000
H	3.236371000	0.863169000	-1.449492000
H	4.072524000	0.742781000	0.117264000
H	3.292881000	2.260661000	-0.374192000
C	1.885301000	1.220923000	1.711749000
O	1.935502000	2.344254000	2.113893000
O	1.783843000	0.152474000	2.564809000
C	1.907644000	-1.094002000	1.857889000
H	1.170273000	-1.783799000	2.273130000
H	2.906396000	-1.493371000	2.050747000
C	0.312451000	-1.196667000	-0.172156000
H	-0.149924000	-1.979214000	0.428645000
C	-0.545490000	0.615150000	-0.249975000
C	0.231369000	-1.581558000	-1.634951000
H	0.736283000	-0.860985000	-2.280517000
H	-0.805580000	-1.681019000	-1.963372000
H	0.706068000	-2.562998000	-1.765335000
C	-1.038296000	0.046918000	1.007034000
H	-0.603600000	0.165580000	1.987152000

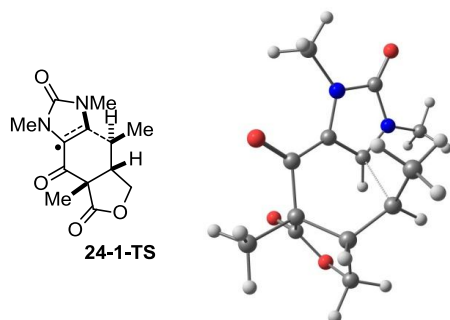


```

Zero-point correction=                0.293801 (Hartree/Particle)
Thermal correction to Energy=         0.312027
Thermal correction to Enthalpy=       0.312971
Thermal correction to Gibbs Free Energy= 0.247395
Sum of electronic and zero-point Energies= -915.973956
Sum of electronic and thermal Energies= -915.955730
Sum of electronic and thermal Enthalpies= -915.954785
Sum of electronic and thermal Free Energies= -916.020362

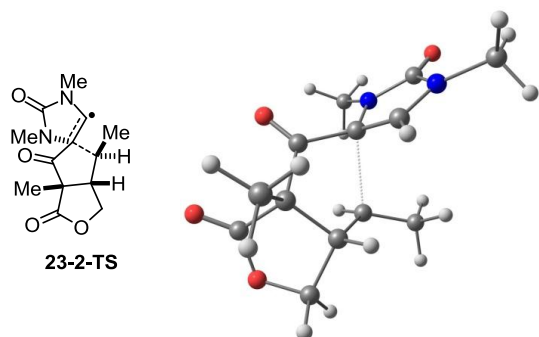
```

C	-2.844797000	0.377822000	0.221572000
O	-4.042188000	0.547352000	0.194505000
N	-2.154513000	-0.809044000	0.287355000
N	-1.870149000	1.409383000	0.178556000
C	-2.814809000	-2.059924000	0.600744000
H	-3.888577000	-1.900616000	0.510845000
H	-2.586438000	-2.385401000	1.622761000
H	-2.513471000	-2.847273000	-0.095241000
C	-2.244331000	2.810320000	0.032993000
H	-3.332035000	2.845432000	0.004824000
H	-1.818838000	3.223591000	-0.880880000
H	-1.868744000	3.387249000	0.878812000
C	0.620167000	1.541232000	0.006479000
O	0.727703000	2.728754000	-0.322987000
C	1.860533000	0.627150000	0.167268000
C	1.667777000	-0.849785000	-0.315250000
H	2.223500000	-0.997588000	-1.243438000
C	3.085760000	1.300311000	-0.473110000
H	2.919005000	1.443964000	-1.542516000
H	3.984266000	0.692307000	-0.335714000
H	3.247181000	2.277961000	-0.021795000
C	2.136655000	0.473349000	1.680009000
O	2.190959000	1.340140000	2.500329000
O	2.326802000	-0.838861000	1.995108000
C	2.355463000	-1.652830000	0.810550000
H	1.848321000	-2.589196000	1.046863000
H	3.399999000	-1.872753000	0.573353000
C	0.202289000	-1.295201000	-0.583389000
H	0.150094000	-2.375879000	-0.408296000
C	-0.614495000	0.891533000	0.268576000
C	-0.723439000	-0.595767000	0.442007000
H	-0.417716000	-0.904871000	1.455421000
C	-0.223342000	-1.032305000	-2.033478000
H	-0.122850000	0.021690000	-2.304678000
H	-1.263506000	-1.321593000	-2.197364000
H	0.399766000	-1.612650000	-2.718795000



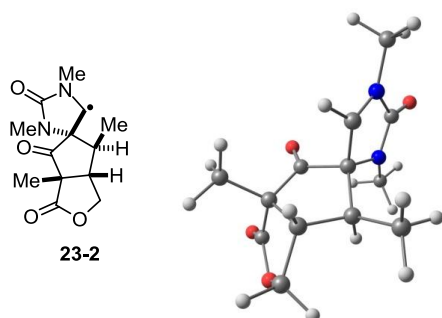
Imaginary Frequency=	-332.2361 cm <sup>-1</sup>
Zero-point correction=	0.289417 (Hartree/Particle)
Thermal correction to Energy=	0.308031
Thermal correction to Enthalpy=	0.308976
Thermal correction to Gibbs Free Energy=	0.242738
Sum of electronic and zero-point Energies=	-915.926498
Sum of electronic and thermal Energies=	-915.907884
Sum of electronic and thermal Enthalpies=	-915.906940
Sum of electronic and thermal Free Energies=	-915.973177

C	-2.940707000	0.303583000	0.282724000
O	-4.136124000	0.401238000	0.089955000
N	-2.240529000	-0.856691000	0.644679000
N	-1.971043000	1.293728000	0.198621000
C	-2.905232000	-2.122801000	0.891216000
H	-2.706777000	-2.473490000	1.906895000
H	-2.578641000	-2.881800000	0.175573000
H	-3.974151000	-1.953477000	0.769530000
C	-2.312970000	2.667362000	-0.150695000
H	-3.392663000	2.691033000	-0.291378000
H	-1.806330000	2.973872000	-1.065263000
H	-2.021925000	3.347827000	0.649106000
C	0.536846000	1.451783000	0.308824000
O	0.606791000	2.641236000	0.012568000
C	1.808655000	0.581694000	0.375295000
C	1.822942000	-0.662518000	-0.608018000
H	2.403030000	-0.367076000	-1.491678000
C	3.042306000	1.476249000	0.151150000
H	2.956874000	1.991082000	-0.806033000
H	3.963455000	0.887750000	0.160350000
H	3.103330000	2.231625000	0.934263000
C	1.970918000	-0.077373000	1.755495000
O	1.803538000	0.424490000	2.827263000
O	2.378473000	-1.370890000	1.612291000
C	2.630157000	-1.677100000	0.226904000
H	2.323671000	-2.709670000	0.062070000
H	3.705180000	-1.595909000	0.047224000
C	0.499813000	-1.214110000	-1.076358000
H	0.357610000	-2.282630000	-0.937336000
C	-0.716399000	0.769312000	0.508960000
C	-0.894969000	-0.592153000	0.750760000
H	-0.258042000	-1.262024000	1.301507000
C	-0.155878000	-0.621859000	-2.284181000
H	-0.157205000	0.471472000	-2.259836000
H	-1.189566000	-0.961198000	-2.391241000
H	0.374561000	-0.915573000	-3.203207000



Imaginary Frequency=	-369.5937 cm <sup>-1</sup>
Zero-point correction=	0.288485 (Hartree/Particle)
Thermal correction to Energy=	0.307430
Thermal correction to Enthalpy=	0.308374
Thermal correction to Gibbs Free Energy=	0.241165
Sum of electronic and zero-point Energies=	-915.916186
Sum of electronic and thermal Energies=	-915.897241
Sum of electronic and thermal Enthalpies=	-915.896297
Sum of electronic and thermal Free Energies=	-915.963505

C	-2.924299000	-0.520869000	0.327511000
O	-4.037249000	-0.990750000	0.190542000
N	-2.579040000	0.837467000	0.291321000
N	-1.728540000	-1.185903000	0.539644000
C	-3.564013000	1.887751000	0.126172000
H	-3.581458000	2.547566000	0.997920000
H	-4.534160000	1.403671000	0.022558000
H	-3.357795000	2.478922000	-0.770160000
C	-1.653041000	-2.637320000	0.585808000
H	-2.674075000	-3.010005000	0.519944000
H	-1.190468000	-2.963419000	1.516081000
H	-1.074897000	-3.022592000	-0.259151000
C	0.602603000	-0.604311000	1.313046000
O	0.617803000	-1.413760000	2.208475000
C	1.855679000	0.140755000	0.807059000
C	1.668752000	0.457619000	-0.699394000
H	1.350551000	1.490673000	-0.866613000
C	2.161908000	1.347598000	1.719321000
H	1.315172000	2.036078000	1.764485000
H	3.032674000	1.900635000	1.356940000
H	2.377647000	0.993531000	2.728629000
C	3.100947000	-0.774922000	0.818334000
O	3.540569000	-1.408075000	1.727359000
O	3.709286000	-0.729737000	-0.402569000
C	3.090708000	0.245010000	-1.259614000
H	3.100925000	-0.152667000	-2.274283000
H	3.688978000	1.161544000	-1.230014000
C	0.645035000	-0.493262000	-1.268294000
H	0.922067000	-1.545460000	-1.201387000
C	-0.646293000	-0.287403000	0.550034000
C	-0.155053000	-0.110023000	-2.472703000
H	-0.624103000	0.871597000	-2.344517000
H	-0.943779000	-0.838570000	-2.677596000
H	0.467189000	-0.050715000	-3.378924000
C	-1.223124000	0.985519000	0.465685000
H	-0.759105000	1.953828000	0.527350000

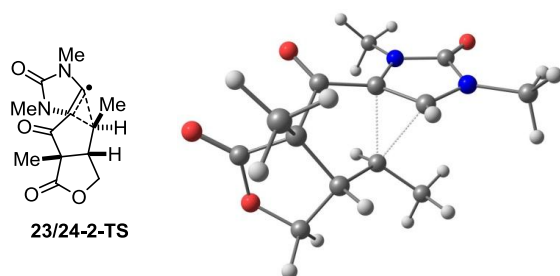


```

Zero-point correction=                0.291464 (Hartree/Particle)
Thermal correction to Energy=         0.310171
Thermal correction to Enthalpy=       0.311115
Thermal correction to Gibbs Free Energy= 0.244687
Sum of electronic and zero-point Energies= -915.950691
Sum of electronic and thermal Energies= -915.931985
Sum of electronic and thermal Enthalpies= -915.931041
Sum of electronic and thermal Free Energies= -915.997469

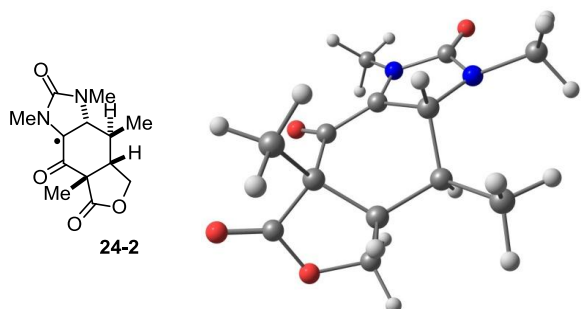
```

C	-2.818287000	0.411005000	-0.582529000
O	-3.864568000	0.748695000	-1.092650000
N	-2.645650000	-0.672230000	0.294747000
N	-1.577820000	1.002067000	-0.718004000
C	-3.752658000	-1.495567000	0.733014000
H	-4.639899000	-1.159696000	0.198289000
H	-3.916379000	-1.390284000	1.810011000
H	-3.565472000	-2.547530000	0.499696000
C	-1.326879000	1.965777000	-1.775432000
H	-2.296049000	2.297046000	-2.145761000
H	-0.767049000	1.516436000	-2.601498000
H	-0.780546000	2.832212000	-1.394454000
C	0.278917000	-0.652554000	-1.102807000
O	-0.155456000	-1.131751000	-2.115050000
C	1.699049000	-0.835342000	-0.546017000
C	1.729183000	-0.042681000	0.776726000
H	1.592792000	-0.680353000	1.654320000
C	2.103350000	-2.317315000	-0.504619000
H	1.428693000	-2.881238000	0.144049000
H	3.124493000	-2.445113000	-0.135532000
H	2.043645000	-2.730429000	-1.512355000
C	2.722229000	-0.069141000	-1.417928000
O	2.899424000	-0.167546000	-2.593174000
O	3.459810000	0.760673000	-0.627360000
C	3.119524000	0.598679000	0.764859000
H	3.152341000	1.586324000	1.225888000
H	3.876080000	-0.037020000	1.232991000
C	0.572489000	0.984930000	0.670762000
H	0.910111000	1.784261000	-0.002527000
C	-0.533101000	0.214345000	-0.088714000
C	0.145873000	1.610926000	1.994582000
H	-0.183912000	0.848478000	2.704208000
H	-0.683865000	2.305431000	1.842625000
H	0.969057000	2.170703000	2.448056000
C	-1.347580000	-0.740388000	0.746991000
H	-0.973890000	-1.640810000	1.212598000



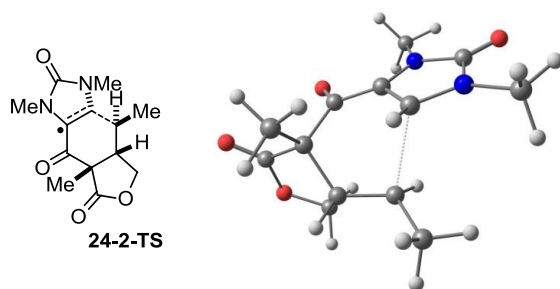
Imaginary Frequency= -1201.6831 cm<sup>-1</sup>  
 Zero-point correction= 0.288416 (Hartree/Particle)  
 Thermal correction to Energy= 0.307094  
 Thermal correction to Enthalpy= 0.308038  
 Thermal correction to Gibbs Free Energy= 0.241446  
 Sum of electronic and zero-point Energies= -915.869637  
 Sum of electronic and thermal Energies= -915.850960  
 Sum of electronic and thermal Enthalpies= -915.850016  
 Sum of electronic and thermal Free Energies= -915.916608

C	0.007384000	0.009755000	-0.002125000
O	0.086956000	0.371434000	1.150250000
N	0.951765000	0.236780000	-1.011106000
N	-1.039719000	-0.682749000	-0.603741000
C	2.196394000	0.939766000	-0.771856000
H	2.256390000	1.853365000	-1.370042000
H	3.053389000	0.301692000	-1.008495000
H	2.225100000	1.199690000	0.285355000
C	-2.281282000	-0.957217000	0.112480000
H	-3.091131000	-0.317946000	-0.251942000
H	-2.096550000	-0.736097000	1.162461000
H	-2.566907000	-1.996313000	-0.027353000
C	0.523562000	-0.294115000	-2.213835000
H	1.230568000	-0.625117000	-2.960025000
C	-0.798686000	-0.873435000	-1.972428000
C	-1.537487000	-1.813541000	-2.789152000
O	-2.349990000	-2.623676000	-2.330883000
C	-1.349581000	-1.565629000	-4.311514000
C	-0.339164000	-2.566544000	-4.902568000
H	-0.743631000	-3.574553000	-4.802120000
H	-0.159370000	-2.373433000	-5.964833000
H	0.619070000	-2.522664000	-4.378787000
C	-2.697136000	-1.752084000	-5.030233000
O	-3.316073000	-2.759855000	-5.170813000
O	-3.125740000	-0.556586000	-5.546042000
C	-2.072055000	0.411483000	-5.548534000
H	-1.653297000	0.467126000	-6.557614000
H	-2.510106000	1.379630000	-5.300936000
C	-1.012319000	-0.062972000	-4.524654000
H	-0.011597000	0.075003000	-4.940205000
C	-1.119121000	0.685086000	-3.206846000
H	-2.152446000	0.722981000	-2.852375000
C	-0.518822000	2.070658000	-3.108533000
H	-1.182675000	2.792327000	-3.603703000
H	0.469789000	2.128296000	-3.568454000
H	-0.436628000	2.390179000	-2.066364000



Zero-point correction=	0.293877 (Hartree/Particle)
Thermal correction to Energy=	0.312075
Thermal correction to Enthalpy=	0.313019
Thermal correction to Gibbs Free Energy=	0.247540
Sum of electronic and zero-point Energies=	-915.969346
Sum of electronic and thermal Energies=	-915.951148
Sum of electronic and thermal Enthalpies=	-915.950204
Sum of electronic and thermal Free Energies=	-916.015684

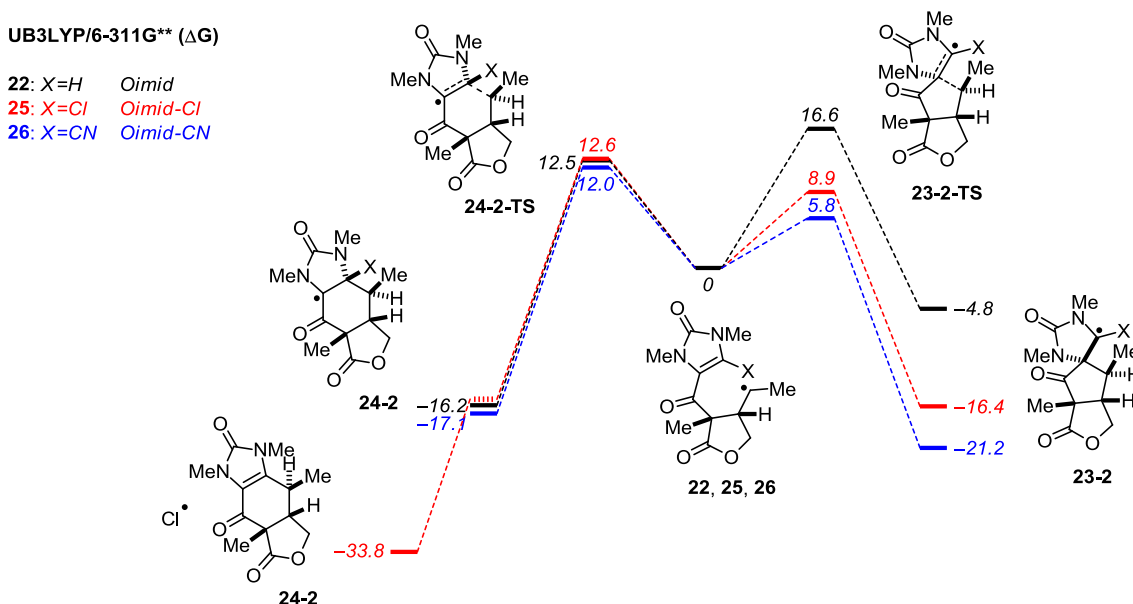
C	-2.779129000	-0.717239000	-0.173719000
O	-3.943840000	-0.988964000	-0.356186000
N	-2.221487000	0.522434000	0.042311000
N	-1.718414000	-1.655409000	-0.142503000
C	-3.071427000	1.648238000	0.392471000
H	-2.826708000	2.021932000	1.392527000
H	-4.102981000	1.297490000	0.382396000
H	-2.977187000	2.466980000	-0.323778000
C	-1.940172000	-3.066618000	-0.434482000
H	-3.013097000	-3.195442000	-0.565963000
H	-1.577887000	-3.681090000	0.388931000
H	-1.405396000	-3.357701000	-1.338832000
C	0.764666000	-1.608866000	0.083818000
O	0.995552000	-2.797408000	-0.170958000
C	1.884364000	-0.584407000	0.397833000
C	1.630178000	0.755456000	-0.347029000
H	2.229905000	1.517550000	0.161749000
C	2.082856000	-0.478334000	1.918732000
H	1.157024000	-0.217793000	2.435941000
H	2.835638000	0.277488000	2.158878000
H	2.435709000	-1.438409000	2.298004000
C	3.199776000	-1.057102000	-0.247063000
O	3.999210000	-1.820104000	0.201283000
O	3.380891000	-0.422895000	-1.441565000
C	2.285826000	0.466632000	-1.708663000
H	1.588743000	-0.030784000	-2.391273000
H	2.689217000	1.353741000	-2.198001000
C	0.170162000	1.285131000	-0.481183000
H	-0.152863000	1.147883000	-1.519340000
C	-0.535841000	-1.037528000	0.127266000
C	-0.799833000	0.424812000	0.367707000
H	-0.656644000	0.684238000	1.430448000
C	0.104164000	2.781611000	-0.147463000
H	0.331635000	2.957384000	0.908712000
H	-0.876390000	3.209578000	-0.359552000
H	0.836777000	3.336516000	-0.739455000



Imaginary Frequency=	-376.9993 cm <sup>-1</sup>
Zero-point correction=	0.289467 (Hartree/Particle)
Thermal correction to Energy=	0.308178
Thermal correction to Enthalpy=	0.309122
Thermal correction to Gibbs Free Energy=	0.242610
Sum of electronic and zero-point Energies=	-915.923152
Sum of electronic and thermal Energies=	-915.904441
Sum of electronic and thermal Enthalpies=	-915.903497
Sum of electronic and thermal Free Energies=	-915.970009

C	-2.887133000	-0.740166000	-0.095649000
O	-4.027094000	-0.973636000	-0.444365000
N	-2.384197000	0.485262000	0.361374000
N	-1.804966000	-1.609165000	-0.054646000
C	-3.231996000	1.649910000	0.538399000
H	-3.141874000	2.041109000	1.554716000
H	-4.258065000	1.329792000	0.362597000
H	-2.979463000	2.437505000	-0.175550000
C	-1.932386000	-2.999811000	-0.477086000
H	-2.976303000	-3.144077000	-0.751754000
H	-1.658629000	-3.672447000	0.334900000
H	-1.284994000	-3.208159000	-1.328224000
C	0.666694000	-1.495732000	0.376390000
O	0.894006000	-2.663579000	0.072384000
C	1.817158000	-0.490308000	0.596369000
C	1.783123000	0.639847000	-0.505877000
H	2.453605000	1.425314000	-0.136276000
C	1.914809000	-0.004705000	2.050805000
H	0.975515000	0.388204000	2.436890000
H	2.678496000	0.772643000	2.141443000
H	2.219800000	-0.842688000	2.679976000
C	3.135684000	-1.211286000	0.235660000
O	3.821969000	-1.865856000	0.960033000
O	3.471016000	-0.947883000	-1.055155000
C	2.497195000	-0.084117000	-1.663721000
H	1.798902000	-0.693831000	-2.245702000
H	3.026836000	0.592979000	-2.333577000
C	0.481358000	1.274146000	-0.912338000
H	-0.035811000	0.810189000	-1.747832000
C	-0.670655000	-0.950177000	0.421108000
C	-1.037490000	0.381790000	0.637182000
H	-0.574284000	1.102194000	1.287121000
C	0.334339000	2.762539000	-0.798566000
H	0.560491000	3.122236000	0.211866000
H	-0.672535000	3.093903000	-1.062293000
H	1.028877000	3.286061000	-1.473604000

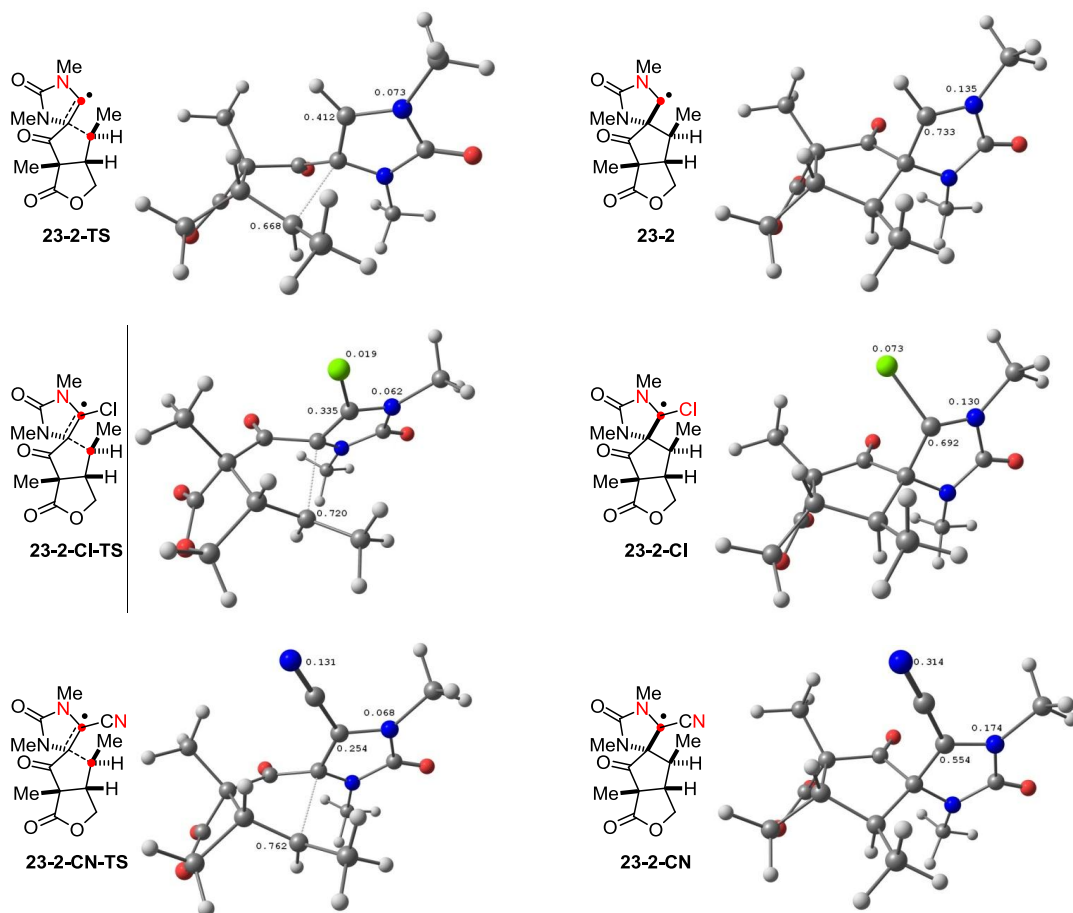
**Figure S8.** Reaction free energy diagrams of the 5-exo and 6-endo cyclization of **22**, **25** and **26** at 298.15K calculated with UB3LYP/6-311G\*\*.

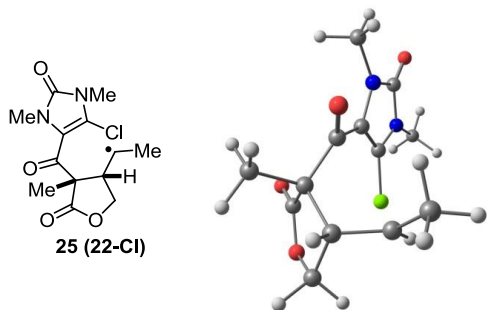


**Table S4.** Computed energies (kcal/mol) in gas phase at 298.15 K by UB3LYP/6-311G\*\*

	<b>24-2-H</b>	<b>24-2-H-TS</b>	<b>22-H</b>	<b>23-2-H-TS</b>	<b>23-2-H</b>
SCFE	-574963.85	-574932.10	-574942.72	-574927.11	-574950.63
ZPE	184.41	181.64	181.63	181.03	182.90
H <sub>tot</sub>	-574767.43	-574738.12	-574748.11	-574733.60	-574755.40
$\Delta H$	-19.3	10.0	0	14.5	-7.3
G <sub>tot</sub>	-574808.52	-574779.86	-574792.34	-574775.77	-574797.09
$\Delta G$	-16.2	12.5	0	16.6	-4.8
	<b>24-2-Cl</b>	<b>24-2-Cl-TS</b>	<b>25 (22-Cl)</b>	<b>23-2-Cl-TS</b>	<b>23-2-Cl</b>
SCFE	-863384.95	-863336.14	-863347.07	-863338.97	-863367.30
ZPE	178.17	175.48	175.39	175.08	177.57
H <sub>tot</sub>	-863193.56	-863147.54	-863157.84	-863150.55	-863176.72
$\Delta H$	-35.7	10.3	0	7.3	-18.9
G <sub>tot</sub>	-863237.51	-863191.12	-863203.72	-863194.77	-863220.07
$\Delta G$	-33.8	12.6	0	8.9	-16.4
	<b>24-2-CN</b>	<b>24-2-CN-TS</b>	<b>26 (22-CN)</b>	<b>23-2-CN-TS</b>	<b>23-2-CN</b>
SCFE	-632852.29	-632820.35	-632830.27	-632825.48	-632855.18
ZPE	183.26	180.89	180.51	180.29	182.65
H <sub>tot</sub>	-632655.93	-632626.12	-632635.53	-632631.53	-632659.12
$\Delta H$	-20.4	9.4	0	4.0	-23.6
G <sub>tot</sub>	-632699.22	-632670.12	-632682.15	-632676.33	-632703.30
$\Delta G$	-17.1	12.0	0	5.8	-21.2

**Figure S9.** Atomic spin densities of the transition states and intermediates of the 5-exo cyclization of **22**, **25** and **26**. Positions of high spin density were labeled in red.



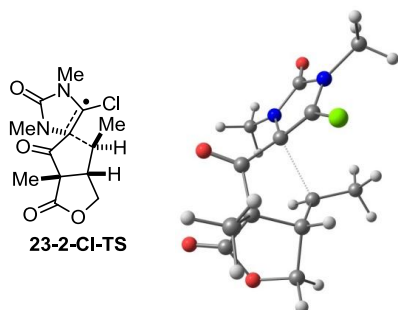


```

Zero-point correction=                0.279506 (Hartree/Particle)
Thermal correction to Energy=         0.300608
Thermal correction to Enthalpy=       0.301552
Thermal correction to Gibbs Free Energy= 0.228440
Sum of electronic and zero-point Energies= -1375.551627
Sum of electronic and thermal Energies= -1375.530525
Sum of electronic and thermal Enthalpies= -1375.529581
Sum of electronic and thermal Free Energies= -1375.602693

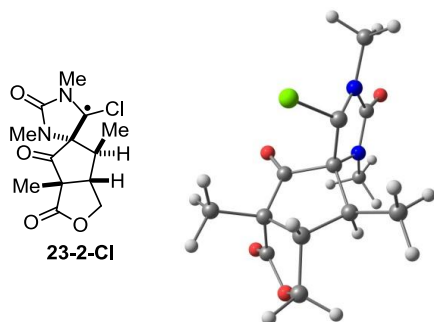
```

C	3.387159000	0.266448000	0.285890000
O	4.543383000	0.555676000	0.526183000
N	2.926179000	-0.975568000	-0.189672000
N	2.256865000	1.045274000	0.389327000
C	1.113347000	0.335917000	-0.050135000
C	1.574219000	-0.912489000	-0.393656000
C	3.822739000	-2.092624000	-0.435272000
H	4.824540000	-1.736795000	-0.200672000
H	3.776325000	-2.402172000	-1.480694000
H	3.574900000	-2.940771000	0.206048000
C	2.365497000	2.464306000	0.717876000
H	1.958509000	3.077222000	-0.087990000
H	3.428894000	2.668596000	0.831798000
H	1.832651000	2.692550000	1.637699000
C	-0.219585000	0.933879000	0.085140000
O	-0.374349000	1.848858000	0.882094000
C	-1.454982000	0.523941000	-0.755760000
C	-2.460139000	-0.380176000	0.055156000
H	-3.269877000	0.264736000	0.408599000
C	-2.154922000	1.831277000	-1.206129000
H	-2.369265000	2.444296000	-0.331943000
H	-3.087242000	1.603260000	-1.729096000
H	-1.510964000	2.391652000	-1.886382000
C	-1.191162000	-0.255069000	-2.045046000
O	-0.377817000	-0.006409000	-2.888079000
O	-2.093131000	-1.259104000	-2.174703000
C	-2.996585000	-1.322866000	-1.055083000
H	-3.041438000	-2.361954000	-0.728427000
H	-3.985227000	-1.019616000	-1.407056000
C	-1.903542000	-1.108639000	1.236655000
H	-1.361534000	-2.031901000	1.069402000
C	-2.036994000	-0.568733000	2.619149000
H	-1.652613000	-1.267280000	3.364639000
H	-3.086679000	-0.354878000	2.866681000
H	-1.499839000	0.382813000	2.739077000
Cl	0.741680000	-2.335658000	-0.874615000



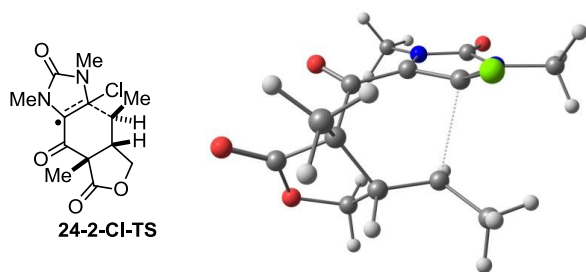
Imaginary Frequency=	-334.7201 cm <sup>-1</sup>
Zero-point correction=	0.279007 (Hartree/Particle)
Thermal correction to Energy=	0.299324
Thermal correction to Enthalpy=	0.300269
Thermal correction to Gibbs Free Energy=	0.229791
Sum of electronic and zero-point Energies=	-1375.539220
Sum of electronic and thermal Energies=	-1375.518903
Sum of electronic and thermal Enthalpies=	-1375.517958
Sum of electronic and thermal Free Energies=	-1375.588436

C	-2.796729000	1.062079000	0.151904000
O	-3.762716000	1.739166000	0.442809000
N	-2.794578000	-0.317611000	-0.111677000
N	-1.476667000	1.450839000	0.028382000
C	-4.003684000	-1.118879000	-0.086692000
H	-4.189812000	-1.574875000	-1.061478000
H	-4.818684000	-0.439905000	0.159425000
H	-3.938809000	-1.902773000	0.671498000
C	-1.046276000	2.821731000	0.252615000
H	-1.941176000	3.404496000	0.463861000
H	-0.546132000	3.212476000	-0.633431000
H	-0.367909000	2.880490000	1.108214000
C	0.651405000	0.568045000	-0.990908000
O	0.701004000	1.384998000	-1.877825000
C	1.875207000	-0.237637000	-0.544372000
C	1.624810000	-0.950631000	0.804485000
H	1.262509000	-1.972117000	0.671555000
C	2.364417000	-1.138271000	-1.700704000
H	2.579653000	-0.517460000	-2.571315000
H	1.601064000	-1.871115000	-1.967732000
H	3.275682000	-1.674799000	-1.425453000
C	3.053395000	0.711787000	-0.186319000
O	3.434074000	1.676223000	-0.773429000
O	3.669970000	0.245373000	0.935686000
C	3.042259000	-0.958394000	1.415438000
H	3.045682000	-0.920114000	2.504370000
H	3.634381000	-1.817382000	1.084836000
C	0.646501000	-0.143888000	1.617146000
C	-0.634156000	0.349133000	-0.227516000
C	-1.505048000	-0.725770000	-0.376131000
H	0.981069000	0.863388000	1.863536000
C	-0.223178000	-0.806297000	2.637554000
H	-0.988938000	-0.123103000	3.014798000
H	0.354191000	-1.146227000	3.511509000
H	-0.724576000	-1.689109000	2.228346000
Cl	-1.173628000	-2.329918000	-0.909201000



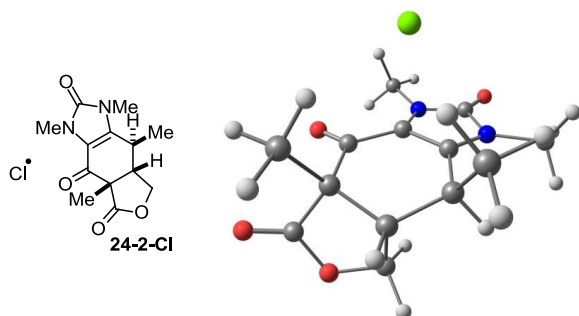
Zero-point correction=	0.282978 (Hartree/Particle)
Thermal correction to Energy=	0.302760
Thermal correction to Enthalpy=	0.303704
Thermal correction to Gibbs Free Energy=	0.234616
Sum of electronic and zero-point Energies=	-1375.580393
Sum of electronic and thermal Energies=	-1375.560612
Sum of electronic and thermal Enthalpies=	-1375.559668
Sum of electronic and thermal Free Energies=	-1375.628756

C	-2.809000000	0.471692000	-0.620772000
O	-3.812442000	0.894181000	-1.148078000
N	-2.751965000	-0.633154000	0.254272000
N	-1.530082000	0.971424000	-0.706175000
C	-3.952364000	-1.303640000	0.720380000
H	-4.787680000	-0.883574000	0.162906000
H	-4.100088000	-1.136398000	1.790853000
H	-3.885893000	-2.376271000	0.530078000
C	-1.177429000	1.951235000	-1.722114000
H	-2.109446000	2.320497000	-2.147058000
H	-0.576370000	1.503851000	-2.519231000
H	-0.633454000	2.792122000	-1.285443000
C	0.279796000	-0.714703000	-1.077668000
O	-0.175588000	-1.221236000	-2.062711000
C	1.736625000	-0.764971000	-0.617511000
C	1.758182000	-0.102744000	0.771839000
H	1.704961000	-0.826854000	1.587132000
C	2.333563000	-2.173721000	-0.759334000
H	1.780856000	-2.884442000	-0.142918000
H	3.384039000	-2.191932000	-0.458549000
H	2.265030000	-2.486075000	-1.802081000
C	2.597713000	0.216444000	-1.453960000
O	2.668798000	0.296022000	-2.642122000
O	3.324965000	1.002675000	-0.614122000
C	3.089651000	0.652129000	0.767039000
H	3.073840000	1.580024000	1.339654000
H	3.922123000	0.034508000	1.114106000
C	0.528213000	0.844971000	0.793323000
H	0.803068000	1.734234000	0.212377000
C	-0.558050000	0.115452000	-0.040019000
C	0.096484000	1.294938000	2.185969000
H	-0.165225000	0.441194000	2.814910000
H	-0.775862000	1.950446000	2.128897000
H	0.897707000	1.852471000	2.679590000
C	-1.484199000	-0.789868000	0.760587000
Cl	-0.960477000	-2.428925000	1.206953000



Imaginary Frequency=	-361.4254 cm <sup>-1</sup>
Zero-point correction=	0.279648 (Hartree/Particle)
Thermal correction to Energy=	0.299605
Thermal correction to Enthalpy=	0.300549
Thermal correction to Gibbs Free Energy=	0.231093
Sum of electronic and zero-point Energies=	-1375.534066
Sum of electronic and thermal Energies=	-1375.514109
Sum of electronic and thermal Enthalpies=	-1375.513165
Sum of electronic and thermal Free Energies=	-1375.582621

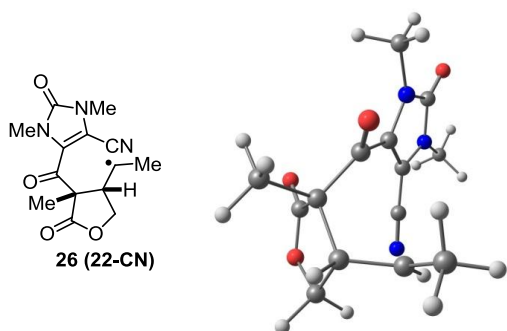
C	-2.777431000	-1.011313000	-0.103703000
O	-3.819195000	-1.395752000	-0.594498000
N	-2.513496000	0.265308000	0.404797000
N	-1.593590000	-1.714058000	0.057182000
C	-3.544305000	1.287925000	0.478040000
H	-3.782416000	1.530116000	1.515501000
H	-4.424334000	0.873682000	-0.011109000
H	-3.229921000	2.194886000	-0.040673000
C	-1.464183000	-3.077394000	-0.453354000
H	-2.433835000	-3.336174000	-0.875226000
H	-1.198028000	-3.762097000	0.348502000
H	-0.695856000	-3.133446000	-1.225285000
C	0.781573000	-1.351269000	0.700321000
O	1.047371000	-2.545732000	0.708508000
C	1.911171000	-0.301195000	0.578849000
C	1.649913000	0.720027000	-0.596002000
H	2.360546000	1.537485000	-0.423439000
C	2.305218000	0.298351000	1.937622000
H	1.469818000	0.754026000	2.458807000
H	3.082877000	1.054510000	1.799553000
H	2.722355000	-0.496790000	2.557439000
C	3.155377000	-1.053212000	0.034864000
O	3.984649000	-1.631512000	0.666528000
O	3.228296000	-0.916846000	-1.316935000
C	2.153838000	-0.099042000	-1.800970000
H	1.366403000	-0.746958000	-2.201017000
H	2.544007000	0.522247000	-2.607043000
C	0.295889000	1.321733000	-0.853976000
H	-0.317142000	0.813478000	-1.593713000
C	-0.608780000	-0.907876000	0.643199000
C	-1.197418000	0.351518000	0.821203000
C	0.132161000	2.806636000	-0.781223000
H	0.515633000	3.214187000	0.158387000
H	-0.912233000	3.109185000	-0.883961000
H	0.689791000	3.301643000	-1.592418000
Cl	-0.885724000	1.525722000	2.083243000



five\_six\_OimidCl

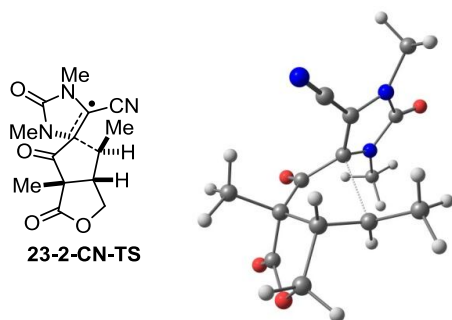
Zero-point correction=	0.283932 (Hartree/Particle)
Thermal correction to Energy=	0.304048
Thermal correction to Enthalpy=	0.304992
Thermal correction to Gibbs Free Energy=	0.234960
Sum of electronic and zero-point Energies=	-1375.607573
Sum of electronic and thermal Energies=	-1375.587457
Sum of electronic and thermal Enthalpies=	-1375.586513
Sum of electronic and thermal Free Energies=	-1375.656546

C	-2.744147000	-0.813558000	-0.470058000
O	-3.903450000	-1.069544000	-0.685190000
N	-2.146984000	0.476871000	-0.545745000
N	-1.709047000	-1.672348000	-0.126627000
C	-2.942994000	1.659859000	-0.840357000
H	-3.124860000	2.232808000	0.070746000
H	-3.894183000	1.315017000	-1.241493000
H	-2.437525000	2.285135000	-1.577297000
C	-1.954934000	-3.065436000	0.245520000
H	-2.974825000	-3.298441000	-0.053687000
H	-1.845133000	-3.172550000	1.325859000
H	-1.244747000	-3.716874000	-0.257495000
C	0.787181000	-1.484637000	0.283209000
O	0.993538000	-2.669484000	0.426059000
C	1.936677000	-0.441607000	0.276628000
C	1.574450000	0.877393000	-0.456783000
H	2.310458000	1.626142000	-0.149239000
C	2.494440000	-0.302684000	1.703639000
H	1.719351000	0.007161000	2.404028000
H	3.311087000	0.423457000	1.715879000
H	2.890082000	-1.267923000	2.020240000
C	3.043236000	-1.001728000	-0.651889000
O	3.895898000	-1.786154000	-0.379284000
O	2.933956000	-0.436076000	-1.890457000
C	1.859084000	0.512202000	-1.923464000
H	0.992353000	0.048649000	-2.408927000
H	2.182977000	1.364317000	-2.522040000
C	0.169478000	1.494315000	-0.263338000
H	-0.050445000	2.081641000	-1.166496000
C	-0.566486000	-0.945129000	0.087890000
C	-0.844428000	0.398999000	-0.207046000
C	0.099224000	2.473881000	0.928805000
H	0.327650000	1.970109000	1.865808000
H	-0.896618000	2.909558000	1.025513000
H	0.811146000	3.286628000	0.764989000
Cl	-1.052461000	-0.302970000	2.672099000



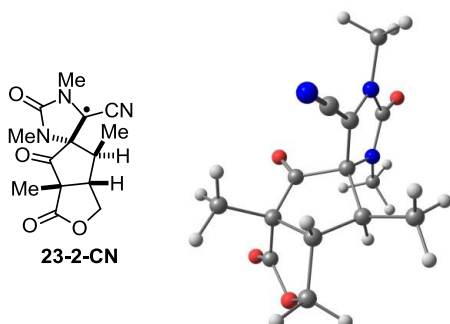
Zero-point correction=	0.287668 (Hartree/Particle)
Thermal correction to Energy=	0.309397
Thermal correction to Enthalpy=	0.310341
Thermal correction to Gibbs Free Energy=	0.236051
Sum of electronic and zero-point Energies=	-1008.191564
Sum of electronic and thermal Energies=	-1008.169836
Sum of electronic and thermal Enthalpies=	-1008.168891
Sum of electronic and thermal Free Energies=	-1008.243181

C	3.381836000	0.403900000	0.012380000
O	4.543111000	0.746013000	0.097287000
N	2.892313000	-0.891353000	-0.139982000
N	2.244535000	1.210559000	0.036376000
C	1.095722000	0.447324000	-0.126551000
C	1.510399000	-0.864237000	-0.230963000
C	3.756235000	-2.059574000	-0.203585000
H	4.778924000	-1.696260000	-0.119175000
H	3.628636000	-2.580789000	-1.154147000
H	3.541849000	-2.746007000	0.618108000
C	2.373008000	2.663625000	0.115372000
H	1.872215000	3.137368000	-0.729427000
H	3.440181000	2.875833000	0.078566000
H	1.941527000	3.039700000	1.040357000
C	-0.248959000	1.061248000	-0.032002000
O	-0.363214000	2.099394000	0.595608000
C	-1.497555000	0.484806000	-0.736504000
C	-2.414134000	-0.387600000	0.209075000
H	-3.308975000	0.210152000	0.410175000
C	-2.298452000	1.684481000	-1.300808000
H	-2.539415000	2.373977000	-0.492641000
H	-3.222408000	1.331813000	-1.765124000
H	-1.715036000	2.212994000	-2.056827000
C	-1.213301000	-0.417323000	-1.941002000
O	-0.430581000	-0.203502000	-2.824042000
O	-2.050294000	-1.473105000	-1.938845000
C	-2.790495000	-1.586671000	-0.708115000
H	-2.520533000	-2.542301000	-0.259137000
H	-3.850807000	-1.594256000	-0.964232000
C	-1.841601000	-0.804279000	1.526384000
H	-1.315554000	-1.749083000	1.587775000
C	-2.043379000	0.016228000	2.754215000
H	-1.573193000	-0.441492000	3.626260000
H	-3.113102000	0.143522000	2.979875000
H	-1.636114000	1.030058000	2.643241000
C	0.772831000	-2.062155000	-0.292616000
N	0.211784000	-3.074006000	-0.312327000



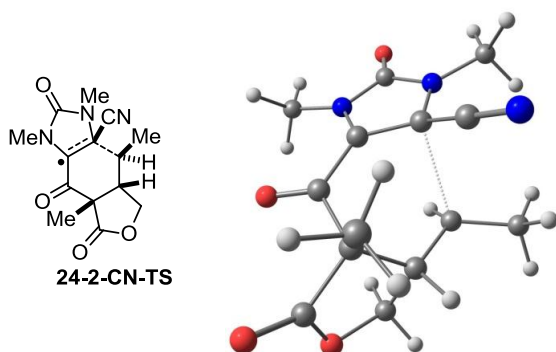
Imaginary Frequency=	-276.5934 cm <sup>-1</sup>
Zero-point correction=	0.287318 (Hartree/Particle)
Thermal correction to Energy=	0.308143
Thermal correction to Enthalpy=	0.309087
Thermal correction to Gibbs Free Energy=	0.237698
Sum of electronic and zero-point Energies=	-1008.184290
Sum of electronic and thermal Energies=	-1008.163465
Sum of electronic and thermal Enthalpies=	-1008.162520
Sum of electronic and thermal Free Energies=	-1008.233909

C	2.898225000	-0.898895000	0.150751000
O	3.894196000	-1.513946000	0.468925000
N	2.806683000	0.453196000	-0.171261000
N	1.594510000	-1.382438000	0.038439000
C	3.960301000	1.334183000	-0.219407000
H	4.108077000	1.725524000	-1.228580000
H	4.824000000	0.737849000	0.070143000
H	3.840963000	2.168180000	0.475698000
C	1.266770000	-2.775549000	0.307943000
H	2.200235000	-3.274502000	0.562247000
H	0.818809000	-3.235777000	-0.571671000
H	0.574482000	-2.852012000	1.150227000
C	-0.613354000	-0.676917000	-0.944706000
O	-0.678677000	-1.586766000	-1.734614000
C	-1.826120000	0.171522000	-0.553603000
C	-1.572593000	0.976787000	0.742808000
H	-1.200147000	1.982461000	0.539176000
C	-2.299147000	1.005107000	-1.768487000
H	-2.511353000	0.334470000	-2.602048000
H	-1.534825000	1.723508000	-2.068315000
H	-3.211769000	1.557083000	-1.531178000
C	-3.019018000	-0.735485000	-0.139097000
O	-3.408993000	-1.733496000	-0.659199000
O	-3.634928000	-0.183052000	0.943596000
C	-2.995241000	1.042346000	1.342709000
H	-3.007364000	1.081454000	2.431453000
H	-3.569022000	1.885455000	0.946908000
C	-0.615105000	0.224386000	1.624017000
C	0.704973000	-0.364428000	-0.277352000
C	1.488285000	0.780095000	-0.472633000
C	1.105731000	2.052921000	-0.911826000
N	0.787436000	3.113186000	-1.262168000
H	-0.920088000	-0.786322000	1.891915000
C	0.257143000	0.934231000	2.604745000
H	1.043235000	0.280336000	2.991720000
H	-0.318868000	1.281058000	3.477077000
H	0.725342000	1.819899000	2.165337000



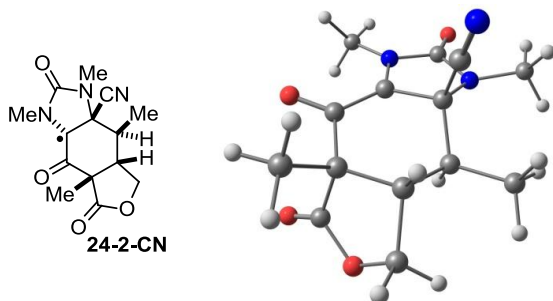
Zero-point correction=	0.291077 (Hartree/Particle)
Thermal correction to Energy=	0.311490
Thermal correction to Enthalpy=	0.312434
Thermal correction to Gibbs Free Energy=	0.242038
Sum of electronic and zero-point Energies=	-1008.227849
Sum of electronic and thermal Energies=	-1008.207436
Sum of electronic and thermal Enthalpies=	-1008.206492
Sum of electronic and thermal Free Energies=	-1008.276888

C	-2.826040000	0.488428000	-0.585328000
O	-3.853943000	0.910979000	-1.061078000
N	-2.722917000	-0.652168000	0.240439000
N	-1.554712000	0.998880000	-0.704611000
C	-3.874034000	-1.449148000	0.621431000
H	-4.745054000	-0.997034000	0.150528000
H	-3.999949000	-1.450689000	1.707090000
H	-3.757679000	-2.477897000	0.272568000
C	-1.253254000	2.036700000	-1.678297000
H	-2.204829000	2.419067000	-2.044153000
H	-0.683148000	1.635581000	-2.520843000
H	-0.696816000	2.856697000	-1.218250000
C	0.304523000	-0.629998000	-1.183448000
O	-0.127760000	-1.038275000	-2.223079000
C	1.733761000	-0.776561000	-0.660156000
C	1.736945000	-0.137137000	0.742561000
H	1.642882000	-0.875554000	1.540528000
C	2.239376000	-2.223251000	-0.787534000
H	1.623561000	-2.896536000	-0.188116000
H	3.275321000	-2.310069000	-0.450461000
H	2.187784000	-2.529207000	-1.833134000
C	2.684514000	0.158482000	-1.451999000
O	2.823662000	0.224637000	-2.634538000
O	3.394909000	0.921408000	-0.577859000
C	3.092077000	0.574232000	0.790130000
H	3.086049000	1.499733000	1.366696000
H	3.887589000	-0.073576000	1.166744000
C	0.533190000	0.842533000	0.752767000
H	0.834987000	1.726888000	0.176656000
C	-0.547288000	0.140432000	-0.108436000
C	0.082403000	1.301696000	2.136531000
H	-0.184273000	0.456634000	2.774709000
H	-0.786021000	1.960845000	2.061498000
H	0.877646000	1.861743000	2.635997000
C	-1.418594000	-0.871922000	0.606870000
C	-0.995666000	-1.903683000	1.423781000
N	-0.602201000	-2.757890000	2.117795000



Imaginary Frequency=	-334.0125 cm <sup>-1</sup>
Zero-point correction=	0.288266 (Hartree/Particle)
Thermal correction to Energy=	0.308576
Thermal correction to Enthalpy=	0.309521
Thermal correction to Gibbs Free Energy=	0.239400
Sum of electronic and zero-point Energies=	-1008.175157
Sum of electronic and thermal Energies=	-1008.154846
Sum of electronic and thermal Enthalpies=	-1008.153902
Sum of electronic and thermal Free Energies=	-1008.224023

C	-2.826104000	-0.983995000	-0.129077000
O	-3.916287000	-1.339398000	-0.521642000
N	-2.455481000	0.293268000	0.278975000
N	-1.674692000	-1.760172000	0.008614000
C	-3.409367000	1.388939000	0.363725000
H	-3.455847000	1.783476000	1.380396000
H	-4.378888000	0.982315000	0.081534000
H	-3.141288000	2.194532000	-0.322722000
C	-1.694569000	-3.176922000	-0.353678000
H	-2.721977000	-3.402197000	-0.634698000
H	-1.385162000	-3.788782000	0.491284000
H	-1.021606000	-3.374120000	-1.186942000
C	0.759113000	-1.486200000	0.438051000
O	1.001100000	-2.666461000	0.215324000
C	1.887586000	-0.447489000	0.541324000
C	1.730707000	0.692706000	-0.541065000
H	2.323427000	1.535816000	-0.171992000
C	2.103756000	0.001843000	1.999275000
H	1.189402000	0.291918000	2.507712000
H	2.793939000	0.848554000	2.037953000
H	2.557412000	-0.829885000	2.540461000
C	3.203095000	-1.130509000	0.082779000
O	3.924613000	-1.812786000	0.742304000
O	3.487692000	-0.793714000	-1.201700000
C	2.473399000	0.060990000	-1.742495000
H	1.797408000	-0.542010000	-2.357050000
H	2.963398000	0.801363000	-2.374546000
C	0.379118000	1.206591000	-0.961308000
H	-0.145503000	0.601171000	-1.696318000
C	-0.616520000	-1.003009000	0.490827000
C	-1.105916000	0.322428000	0.640265000
C	0.178414000	2.685012000	-1.075375000
H	0.371735000	3.194371000	-0.125816000
H	-0.831695000	2.936142000	-1.405599000
H	0.873555000	3.114812000	-1.812894000
C	-0.719301000	1.349949000	1.540058000
N	-0.494666000	2.250454000	2.231059000



Zero-point correction=	0.292048 (Hartree/Particle)
Thermal correction to Energy=	0.311990
Thermal correction to Enthalpy=	0.312934
Thermal correction to Gibbs Free Energy=	0.243941
Sum of electronic and zero-point Energies=	-1008.222283
Sum of electronic and thermal Energies=	-1008.202341
Sum of electronic and thermal Enthalpies=	-1008.201397
Sum of electronic and thermal Free Energies=	-1008.270390

C	-2.860138000	-0.845381000	-0.223599000
O	-3.998549000	-1.162058000	-0.466827000
N	-2.314680000	0.428385000	-0.258999000
N	-1.823580000	-1.734589000	0.138525000
C	-3.209769000	1.581572000	-0.257595000
H	-3.097951000	2.162362000	0.662403000
H	-4.227147000	1.197224000	-0.315840000
H	-3.031064000	2.226338000	-1.118632000
C	-2.019498000	-3.181492000	0.111280000
H	-3.081397000	-3.350787000	-0.056353000
H	-1.699195000	-3.615462000	1.056180000
H	-1.431474000	-3.629165000	-0.691149000
C	0.641887000	-1.624398000	0.483801000
O	0.823410000	-2.824134000	0.708676000
C	1.838968000	-0.671246000	0.324450000
C	1.527528000	0.839522000	0.133389000
H	1.586711000	1.361957000	1.091908000
C	2.828746000	-0.918114000	1.486904000
H	2.378647000	-0.608065000	2.433127000
H	3.761948000	-0.366497000	1.350171000
H	3.055072000	-1.982409000	1.537921000
C	2.575127000	-1.025340000	-0.994908000
O	2.772085000	-2.099382000	-1.472279000
O	3.023991000	0.123920000	-1.575851000
C	2.698256000	1.268859000	-0.771414000
H	2.460438000	2.080974000	-1.455653000
H	3.578191000	1.551492000	-0.188005000
C	0.151249000	1.166612000	-0.509233000
H	0.112359000	0.739238000	-1.517302000
C	-0.653838000	-1.062086000	0.316591000
C	-0.954678000	0.423174000	0.293391000
C	-0.081864000	2.681364000	-0.589693000
H	-0.169036000	3.123620000	0.406487000
H	-0.984770000	2.919330000	-1.150921000
H	0.745428000	3.176623000	-1.099922000
C	-0.990671000	0.941552000	1.689945000
N	-1.025740000	1.355490000	2.766029000

**Figure S9.** Reaction free energy diagrams of the 6-endo cyclization of **23**, **35** and **36** at 298.15K calculated with UB3LYP/6-311G\*\*.

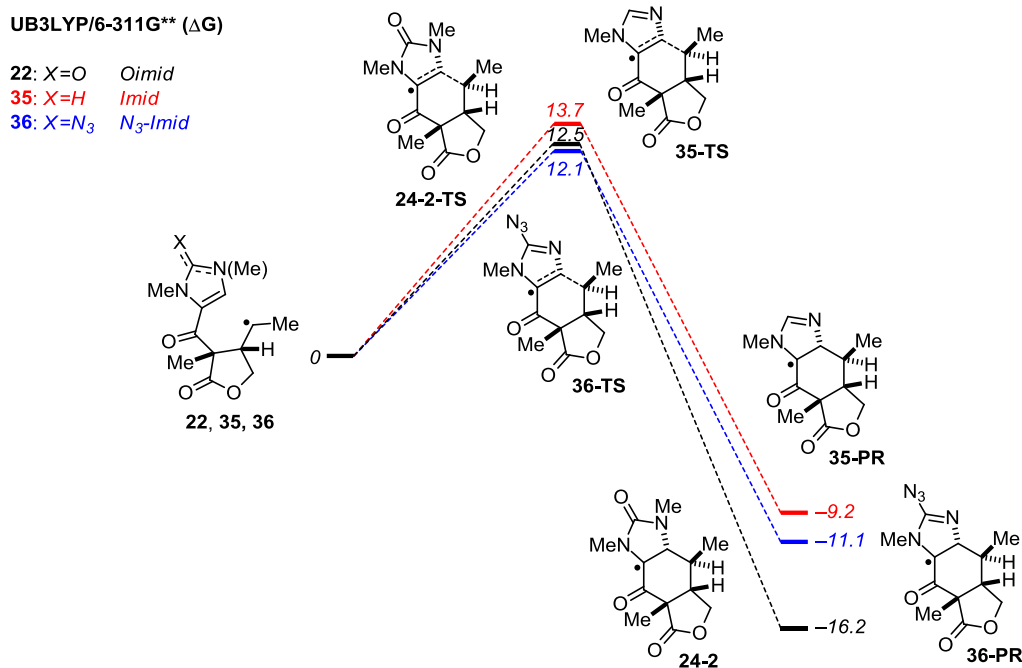
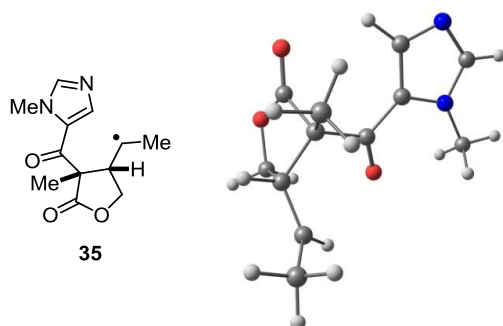


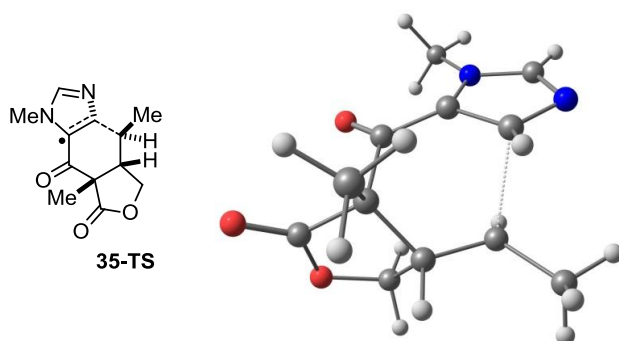
**Table S5.** Computed energies (kcal/mol) in gas phase at 298.15 K by UB3LYP/6-311G\*\*

	<b>23</b>	<b>25-2-TS</b>	<b>25-2</b>
SCFE	-574942.72	-574932.10	-574963.85
ZPE	181.63	181.64	184.41
H <sub>tot</sub>	-574748.11	-574738.12	-574767.43
$\Delta H$	0	10.0	-19.3
G <sub>tot</sub>	-574792.34	-574779.86	-574808.52
$\Delta G$	0	12.5	-16.2
	<b>35</b>	<b>35-TS</b>	<b>35-PR</b>
SCFE	-503035.72	-503023.54	-503048.13
ZPE	161.48	161.50	163.49
H <sub>tot</sub>	-502863.08	-502851.60	-502874.26
$\Delta H$	0	11.5	-11.2
G <sub>tot</sub>	-502902.77	-502889.07	-502911.95
$\Delta G$	0	13.7	-9.2
	<b>36</b>	<b>36-TS</b>	<b>36-PR</b>
SCFE	-605715.62	-605704.77	-605730.29
ZPE	163.28	163.39	165.59
H <sub>tot</sub>	-605539.42	-605529.15	-605552.66
$\Delta H$	0	10.3	-13.2
G <sub>tot</sub>	-605583.18	-605571.13	-605594.25
$\Delta G$	0	12.1	-11.1



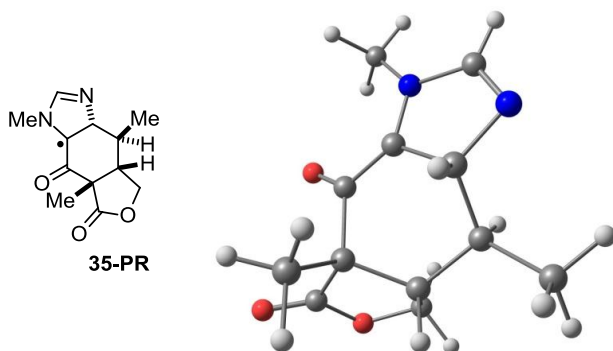
Zero-point correction=	0.257342 (Hartree/Particle)
Thermal correction to Energy=	0.274177
Thermal correction to Enthalpy=	0.275121
Thermal correction to Gibbs Free Energy=	0.211871
Sum of electronic and zero-point Energies=	-801.381106
Sum of electronic and thermal Energies=	-801.364271
Sum of electronic and thermal Enthalpies=	-801.363327
Sum of electronic and thermal Free Energies=	-801.426577

C	3.807479000	-0.197497000	0.137678000
N	3.552612000	0.983238000	0.677361000
N	2.692884000	-0.863847000	-0.236967000
C	1.612640000	-0.045456000	0.109035000
C	2.200624000	1.087718000	0.666443000
H	1.699672000	1.980148000	1.003877000
C	2.679499000	-2.187924000	-0.853752000
H	3.707758000	-2.548842000	-0.889465000
H	2.265870000	-2.139064000	-1.859035000
H	2.073287000	-2.877160000	-0.267185000
C	0.233732000	-0.400394000	-0.215271000
O	-0.008005000	-1.338171000	-0.963445000
C	-0.934162000	0.428050000	0.398433000
C	-2.339138000	-0.123672000	-0.053036000
H	-3.049848000	0.420452000	0.584269000
C	-0.812988000	0.566194000	1.921638000
H	-0.741867000	-0.417953000	2.390800000
H	-1.696397000	1.070941000	2.319634000
H	0.059951000	1.146508000	2.210428000
C	-0.958126000	1.805597000	-0.303010000
O	-0.367578000	2.798198000	0.017078000
O	-1.780354000	1.759634000	-1.375553000
C	-2.455116000	0.478551000	-1.459334000
H	-1.957069000	-0.134895000	-2.211099000
H	-3.483552000	0.675004000	-1.759802000
C	-2.653140000	-1.573836000	0.048829000
H	-2.274668000	-2.235545000	-0.718091000
C	-3.295130000	-2.163762000	1.258017000
H	-3.968871000	-1.455543000	1.752477000
H	-2.555624000	-2.472068000	2.015818000
H	-3.867311000	-3.062498000	1.008831000
H	4.792853000	-0.619263000	0.001660000



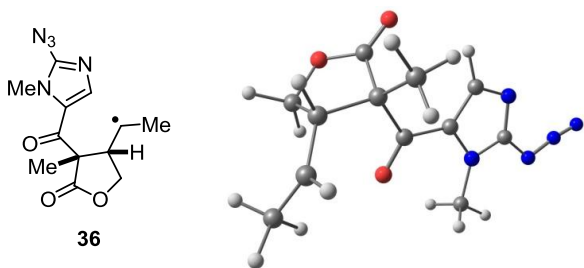
Imaginary Frequency=	-433.8117 cm <sup>-1</sup>
Zero-point correction=	0.257374 (Hartree/Particle)
Thermal correction to Energy=	0.273073
Thermal correction to Enthalpy=	0.274017
Thermal correction to Gibbs Free Energy=	0.214300
Sum of electronic and zero-point Energies=	-801.361674
Sum of electronic and thermal Energies=	-801.345974
Sum of electronic and thermal Enthalpies=	-801.345030
Sum of electronic and thermal Free Energies=	-801.404747

C	-2.695692000	-0.576769000	-0.178384000
N	-2.291796000	0.599900000	0.240584000
N	-1.748917000	-1.550414000	-0.085178000
C	-1.916857000	-2.946083000	-0.480162000
H	-2.939112000	-3.075387000	-0.836609000
H	-1.737578000	-3.603589000	0.369941000
H	-1.211110000	-3.209797000	-1.266265000
C	0.709034000	-1.524301000	0.387717000
O	0.924076000	-2.694557000	0.081799000
C	1.855626000	-0.511962000	0.587282000
C	1.776272000	0.632056000	-0.502813000
H	2.421864000	1.435649000	-0.129883000
C	1.961757000	-0.035378000	2.043906000
H	1.016046000	0.331061000	2.440138000
H	2.705939000	0.760952000	2.131244000
H	2.295046000	-0.870535000	2.662432000
C	3.177192000	-1.206244000	0.196863000
O	3.879723000	-1.869662000	0.897639000
O	3.493871000	-0.913646000	-1.092962000
C	2.499387000	-0.055832000	-1.676460000
H	1.809942000	-0.667711000	-2.266983000
H	3.011515000	0.644009000	-2.336612000
C	0.446450000	1.225945000	-0.892393000
H	-0.055506000	0.739149000	-1.725080000
C	-0.613001000	-0.947564000	0.445151000
C	-0.971745000	0.415365000	0.602152000
H	-0.517996000	1.124030000	1.276193000
C	0.244482000	2.709766000	-0.811779000
H	0.603662000	3.116255000	0.139127000
H	-0.811952000	2.966653000	-0.918275000
H	0.793025000	3.232246000	-1.609408000
H	-3.685647000	-0.794606000	-0.554922000



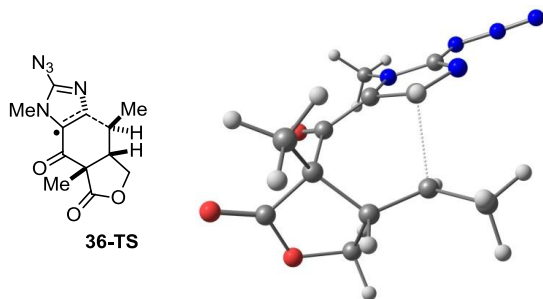
Zero-point correction=	0.260535 (Hartree/Particle)
Thermal correction to Energy=	0.276145
Thermal correction to Enthalpy=	0.277089
Thermal correction to Gibbs Free Energy=	0.217020
Sum of electronic and zero-point Energies=	-801.397697
Sum of electronic and thermal Energies=	-801.382086
Sum of electronic and thermal Enthalpies=	-801.381142
Sum of electronic and thermal Free Energies=	-801.441211

C	-3.292136000	0.031654000	-0.156715000
N	-2.817097000	1.166124000	0.193618000
N	-2.393255000	-1.037004000	-0.153779000
C	-2.693412000	-2.409516000	-0.543889000
H	-3.703194000	-2.440130000	-0.953953000
H	-2.632090000	-3.074495000	0.320175000
H	-1.973274000	-2.751871000	-1.285111000
C	0.098670000	-1.147604000	0.128184000
O	0.298758000	-2.309038000	-0.248728000
C	1.239917000	-0.180092000	0.544673000
C	1.046933000	1.232816000	-0.086973000
H	1.620341000	1.933287000	0.529497000
C	1.391601000	-0.198961000	2.075594000
H	0.456904000	0.051641000	2.581166000
H	2.157101000	0.512901000	2.396457000
H	1.704277000	-1.195650000	2.390469000
C	2.563448000	-0.638563000	-0.090953000
O	3.309788000	-1.480450000	0.306704000
O	2.828731000	0.108931000	-1.200074000
C	1.780497000	1.064538000	-1.428888000
H	1.113512000	0.670202000	-2.202703000
H	2.242277000	1.982339000	-1.794059000
C	-0.397203000	1.791602000	-0.256672000
H	-0.682004000	1.686710000	-1.309997000
C	-1.177406000	-0.531887000	0.226660000
C	-1.403218000	0.920703000	0.529578000
H	-1.280248000	1.141194000	1.601507000
C	-0.509826000	3.270776000	0.122359000
H	-0.242921000	3.426253000	1.172501000
H	-1.531807000	3.624616000	-0.024482000
H	0.158126000	3.885260000	-0.487534000
H	-4.319938000	-0.144437000	-0.453776000



Zero-point correction=	0.260196 (Hartree/Particle)
Thermal correction to Energy=	0.279847
Thermal correction to Enthalpy=	0.280791
Thermal correction to Gibbs Free Energy=	0.211055
Sum of electronic and zero-point Energies=	-965.009094
Sum of electronic and thermal Energies=	-964.989443
Sum of electronic and thermal Enthalpies=	-964.988499
Sum of electronic and thermal Free Energies=	-965.058235

C	3.612166000	-0.100897000	-0.082421000
N	3.483842000	1.217781000	-0.114809000
N	2.433992000	-0.763311000	-0.046339000
C	1.441657000	0.232318000	-0.039133000
C	2.145966000	1.430726000	-0.086373000
H	1.732724000	2.423833000	-0.152597000
C	2.275326000	-2.216550000	0.009855000
H	3.267838000	-2.655163000	0.091379000
H	1.775752000	-2.577245000	-0.887167000
H	1.673840000	-2.493892000	0.874173000
C	0.020971000	-0.086736000	-0.080073000
O	-0.357861000	-1.232689000	-0.284422000
C	-1.026620000	1.045328000	0.150628000
C	-2.489937000	0.495462000	0.040868000
H	-3.101384000	1.338906000	0.404019000
C	-0.772646000	1.802528000	1.461382000
H	-0.751504000	1.108114000	2.305058000
H	-1.572851000	2.526316000	1.633418000
H	0.169627000	2.345235000	1.443816000
C	-1.008750000	1.990194000	-1.070716000
O	-0.319051000	2.955879000	-1.241741000
O	-1.928093000	1.584379000	-1.975666000
C	-2.687340000	0.453289000	-1.477187000
H	-2.290382000	-0.457371000	-1.926720000
H	-3.720479000	0.600411000	-1.790148000
C	-2.878613000	-0.713430000	0.822391000
H	-2.728786000	-0.663723000	1.895628000
C	-3.379861000	-1.985260000	0.228014000
H	-2.557193000	-2.574830000	-0.200602000
H	-4.101763000	-1.816362000	-0.580481000
H	-3.872105000	-2.604237000	0.981691000
N	4.804822000	-0.815732000	-0.074348000
N	5.844262000	-0.138613000	-0.103246000
N	6.860435000	0.347343000	-0.127131000



Imaginary Frequency=	-425.3367 cm <sup>-1</sup>
Zero-point correction=	0.260379 (Hartree/Particle)
Thermal correction to Energy=	0.278924
Thermal correction to Enthalpy=	0.279868
Thermal correction to Gibbs Free Energy=	0.212967
Sum of electronic and zero-point Energies=	-964.991611
Sum of electronic and thermal Energies=	-964.973066
Sum of electronic and thermal Enthalpies=	-964.972122
Sum of electronic and thermal Free Energies=	-965.039023

C	-2.711698000	-0.572279000	-0.126358000
N	-2.305889000	0.607797000	0.289486000
N	-1.765357000	-1.549084000	-0.060740000
C	-1.930699000	-2.948183000	-0.453921000
H	-2.961397000	-3.086734000	-0.773776000
H	-1.709643000	-3.598698000	0.391301000
H	-1.245067000	-3.195649000	-1.262651000
C	0.702146000	-1.508275000	0.375113000
O	0.916844000	-2.674588000	0.053638000
C	1.849737000	-0.498069000	0.580269000
C	1.769429000	0.651248000	-0.503189000
H	2.412227000	1.454859000	-0.125525000
C	1.961156000	-0.028726000	2.039363000
H	1.019008000	0.341995000	2.440127000
H	2.710450000	0.762726000	2.127913000
H	2.291249000	-0.868279000	2.653589000
C	3.170237000	-1.192244000	0.185514000
O	3.870335000	-1.862226000	0.882266000
O	3.489556000	-0.888913000	-1.100883000
C	2.495134000	-0.028620000	-1.680652000
H	1.807232000	-0.637881000	-2.275535000
H	3.007633000	0.675675000	-2.335706000
C	0.437559000	1.241595000	-0.889364000
H	-0.065478000	0.754860000	-1.721597000
C	-0.619984000	-0.936052000	0.450345000
C	-0.980298000	0.422992000	0.620026000
H	-0.513626000	1.131543000	1.284376000
C	0.229542000	2.724143000	-0.803368000
H	0.590572000	3.130064000	0.147060000
H	-0.828044000	2.978377000	-0.905955000
H	0.772824000	3.251325000	-1.601522000
N	-3.981067000	-0.897513000	-0.593216000
N	-4.801932000	0.033135000	-0.620089000
N	-5.640689000	0.780680000	-0.699337000





## BIBLIOGRAPHY

- Adachi, M.; Fukuda, M.; Nishida, E. *EMBO J.* **1999**, *18*, 5347.
- Adachi, M.; Fukuda, M.; Nishida, E. *J. Cell Biol.* **2000**, *148*, 849.
- Adams, P.D.; Afonine, P. V.; Bunkóczi, G.; Chen, V. B.; Davis, I. W.; Echols, N.; Headd, J. J.; Hung, L.-W.; Kapral, G. J.; Grosse-Kunstleve, R. W.; McCoy, A. J.; Moriarty, N. W.; Oeffner, R.; Read, R. J.; Richardson, D. C.; Richardson, J. S.; Terwilliger, T. C.; Zwart, P.H. *Acta Cryst. D.* **2010**, *66*, 213.
- Agrawal, N.; Frederick, M. J.; Pickering, C. R.; Bettegowda, C.; Chang, K.; Li, R. J.; Fakhry, C.; Xie, T. X.; Zhang, J.; Wang, J.; Zhang, N.; El-Naggar, A. K.; Jasser, S. A.; Weinstein, J. N.; Treviño, L.; Drummond, J. A.; Muzny, D. M.; Wu, Y.; Wood, L. D.; Hruban, R. H.; Westra, W. H.; Koch, W. M.; Califano, J. A.; Gibbs, R. A.; Sidransky, D.; Vogelstein, B.; Velculescu, V. E.; Papadopoulos, N.; Wheeler, D. A.; Kinzler, K. W.; Myers, J. N. *Science* **2011**, *333*, 1154.
- Agrawal, N.; Jiao, Y.; Bettegowda, C.; Hutfless, S. M.; Wang, Y.; David, S.; Cheng, Y.; Twaddell, W. S.; Latt, N. L.; Shin, E. J.; Wang, L. D.; Wang, L.; Yang, W.; Velculescu, V. E.; Vogelstein, B.; Papadopoulos, N.; Kinzler, K. W.; Meltzer, S. J. *Cancer Discov.* **2012**, *10*, 899.
- Amor-Mahjoub, M.; Suppini, J. P.; Gomez-Vrielyunck, N.; Ladjimi, M. *J. Chromatogr., B: Anal. Technol. Biomed. Life Sci.* **2006**, *844*, 328.
- Anslyn, E. V.; Dougherty, D. A. *Modern Physical Organic Chemistry*, Sausalito, CA: University Science Books, **2006**.
- Arvind, R.; Shimamoto, H.; Momose, F.; Amagasa, T.; Omura, K.; Tsuchida, N. *Int. J. Oncol.* **2005**, *27*, 1499.
- Bales, B. C.; Brown, P.; Dehestani, A.; Mayer, J. M. *J. Am. Chem. Soc.*, **2004**, *127*, 2832.
- Barton, D. H. R.; Doller, D. *Acc. Chem. Res.*, **1992**, *25*, 504.
- Basler, K.; Christen, B.; Hafen, E. *Cell* **1991**, *64*, 1069.
- Bayly, C. I.; Cieplak, P.; Cornell, W.; Kollman, P. A. *J. Phys. Chem.* **1993**, *97*, 10269.
- Becke, A. D., *J. Chem. Phys.* **1993**, *98*, 5648.

- Bermudez, O.; Pagès, G.; Gimond, C. *Am. J. Physiol. Cell Physiol.* **2010**, *299*, C189.
- Bianchi, M.; Bonchio, M.; Conte, V.; Coppa, F.; Di Furia, F.; Modena, G.; Moro, S.; Standen, S. *J. Mol. Catal.* **1993**, *83*, 107.
- Biggs, W. H.; Zipurski, S. L. *Proc. Natl. Acad. Sci. U.S.A.* **1992**, *89*, 6295.
- Bonchio, M.; Conte, V.; Di Furia, F.; Modena, G. *J. Org. Chem.* **1989**, *54*, 4368.
- Bonchio, M.; Conte, V.; Di Furia, F.; Modena, G.; Moro, S. *J. Org. Chem.* **1994**, *59*, 6262.
- Bonchio, M.; Conte, V.; Di Furia, F.; Modena, G.; Moro, S.; Edwards, J. O. *Inorg. Chem.* **1994**, *33*, 1631.
- Bott, C. M.; Thorneycroft, S. G.; Marshall, C. J. *FEBS Lett.* **1994**, *352*, 201.
- Breslow, R., In *Comprehensive Organic Synthesis*, Trost, B. M.; Fleming, I. Ed.; Pergamon Press, Oxford, United Kingdom, **1991**, *1997*, 1939–1952.
- Brodsky, B. H.; Du Bois, J. *J. Am. Chem. Soc.*, **2005**, *127*, 15391.
- Broeker, J. L.; Houk, K. N. *J. Org. Chem.* **1991**, *56*, 3651.
- Brückl, T.; Baxter, R. D.; Ishihara, Y.; Baran, P. S. *Acc. Chem. Res.* **2012**, *45*, 826.
- Bruder, J. T.; Heidecker, G.; Rapp, U. R. *Genes Dev.* **1992**, *6*, 545.
- Brunner, D.; Oellers, N.; Szabad, J.; Biggs, W. H.; Zipursky, S. L.; Hafen, E. *Cell* **1994**, *76*, 875.
- Burack, W. R.; Shaw, A. S. *J. Biol. Chem.* **2005**, *280*, 3832.
- Burkhard, K. A.; Chen, F.; Shapiro, P. *J. Biol. Chem.* **2011**, *286*, 2477.
- Butler, A.; Clague, M. J.; Meister, G. E. *Chem. Rev.* **1994**, *94*, 625.
- Butler, A.; Sandy, M. *Nature*, **2009**, *460*, 848.
- Camps, M.; Nichols, A.; Arkininstall, S. *FASEB J.* **2000**, *14*, 6.
- Camps, M.; Nichols, A.; Gillieron, C.; Antonsson, B.; Muda, M.; Chabert, C.; Boschert, U.; Arkininstall, S. *Science* **1998**, *280*, 1262.

- Canagarajah, B. J.; Khokhlatchev, A.; Cobb, M. H.; Goldsmith, E. *Cell* **1997**, *90*, 859.
- Carlson, S. M.; Chouinard, C. R.; Labadorf, A.; Lam, C. J.; Schmelzle, K.; Fraenkel, E.; White, F. M. *Sci. Signal.* **2011**, *4*, rs11.
- Casar, B.; Arozarena, I.; Sanz-Moreno, V.; Pinto, A.; Agudo-Ibanez, L.; Marais, R.; Lewis, R. E.; Berciano, M. T.; Crespo, P. *Mol. Cell. Biol.* **2009**, *29*, 1338.
- Casar, B.; Pinto, A.; Crespo, P. *Mol. Cell*, **2008**, *31*, 708.
- Case, D. A.; Darden, T. A.; Cheatham, III, T.E.; Simmerling, C.L.; Wang, J.; Duke, R. E.; Luo, R.; Walker, R.C.; Zhang, W.; Merz, K. M.; Roberts, B.; Hayik, S.; Roitberg, A.; Seabra, G.; Swails, J.; Goetz, A. W.; Kolossváry, I.; Wong, K. F.; Paesani, F.; Vanicek, J.; Wolf, R. M.; Liu, J.; Wu, X.; Brozell, S. R.; Steinbrecher, T.; Gohlke, H.; Cai, Q.; Ye, X.; Wang, J.; Hsieh, M.-J.; Cui, G.; Roe, D. R.; Mathews, D. H.; Seetin, M. G.; Salomon-Ferrer, R.; Sagui, C.; Babin, V.; Luchko, T.; Gusarov, S.; Kovalenko, A.; Kollman, P. A. **2012**, *AMBER 12*, University of California, San Francisco.
- Catalanotti, F.; Reyes, G.; Jesenberger, V.; Galabova-Kovacs, G.; De Matos Simoes, R.; Carugo, O.; Baccarini, M. *Nat. Struct. Mol. Biol.* **2009**, *16*, 294.
- Catling, A. D.; Schaeffer, H.-J.; Reuter, C. W. M.; Reddy, G. R.; Weber, M. J. *Mol. Cell Biol.* **1995**, *15*, 5214.
- Caunt, C. J.; Keyse, S. M. *FEBS J.* **2013**, *280*, 489.
- Cenci, S., Di Furia; Modena, F. G.; Curci, R.; Edwards, J. O. *J. Chem. Soc. Perkin Trans. 2*, **1978**, 979.
- Chen, K.; Baran, P.S., *Nature*, **2009**, *459*, 824.
- Chen, K.; Costas, M.; Kim, J.; Tipton, A. K.; Que, L., Jr. *J. Am. Chem. Soc.* **2002**, *124*, 3026.
- Chen, K.; Que, L. *Chem. Commun.* **1999**, 1375.
- Chen, K.; Que, L., Jr. *J. Am. Chem. Soc.* **2001**, *123*, 6327.
- Chen, M. S.; White, M. C. *Science*, **2007**, *318*, 783.
- Chen, M. S.; White, M. C. *Science*, **2010**, *327*, 566.

- Chen, R. H.; Sarnecki, C.; Blenis, J. *Mol. Cell Biol.* **1992**, *12*, 915.
- Chen, X.; Hao, X.-S.; Goodhue, C. E.; Yu, J.-Q. *J. Am. Chem. Soc.* **2006**, *128*, 6790.
- Chen, Z.; Gibson, T. B.; Robinson, F.; Silvestro, L.; Pearson, G.; Xu, B.; Wright, A.; Vanderbilt, C.; Cobb, M. H. *Chem. Rev.* **2001**, *101*, 2449.
- Chidambaram, N.; Chandrasekaran, S., *J. Org. Chem.*, **1987**, *52*, 5048.
- Chu, Y.; Solski, P. A.; Khosravi-Far, R.; Der, C. J.; Kelly, K. *J. Biol. Chem.* **1996**, *271*, 6497.
- Chuang, G. J.; Wang, W.; Lee, E.; Ritter, T. *J. Am. Chem. Soc.*, **2011**, *133*, 1760.
- Conte, V.; Di Furia, F.; Licini, G. *Appl. Catal., A* **1997**, *157*, 335.
- Cormier, K. W.; Lewis, M. *Polyhedron* **2009**, *28*, 3120.
- Covell, D. J.; White, M. C. *Angew, Chem. Int. Ed.* **2008**, *47*, 6448.
- Cowley, S.; Paterson, H.; Kemp, P.; Marshall, C. J. *Cell* **1994**, *77*, 1.
- Crabtree, R. H. J. *Chem. Soc., Dalton Trans.* **2001**, 2437.
- Curran, D. P.; Morgan, T. M.; Schwartz, C. E.; Snider, B. B.; Dombroski, M. A. *J. Am. Chem. Soc.* **1991**, *113*, 6607.
- da Silva, J. A. L.; da Silva, J. J. R. F.; Pombeiro, A. J. L. *Coord. Chem. Rev.* **2011**, *255*, 2232.
- Dang, A.; Frost, J. A.; Cobb, M. H. *J. Biol. Chem.* **1998**, *273*, 19909.
- Darden, T.; Perera, L.; Li, L.; Pedersen, L. *Structure* **1999**, *7*, R55.
- Davis, R. J. *J. Biol. Chem.* **1993**, *268*, 14553.
- DesMarteau, D. D.; Donadelli, A.; Montanari, V.; Petrov, V. A.; Resnati, G. *J. Am. Chem. Soc.* **1993**, *115*, 4897.
- Eames, J.; Watkinson, M. *Angew. Chem. Int. Ed.* **2001**, *40*, 3567.
- Eblen, S. T.; Slack-Davis, J. K.; Tarcsafalvi, A.; Parsons, J. T.; Weber, M. J.; Catling, A. D. *Mol. Cell Biol.* **2004**, *24*, 2308.

- Emmert, M. H.; Cook, A. K.; Xie, Y. J.; Sanford, M. S. *Angew Chem. Int. Ed.* **2011**, *50*, 9409.
- Emrick, M. A.; Hoofnagle, A. N.; Miller, A. S.; Eyck, L. F. T.; Ahn, N. G. *J. Biol. Chem.* **2001**, *276*, 46469.
- Emsley, P.; Lohkamp, B.; Scott, W. G.; Cowtan, K. *Acta Cryst. D.* **2010**, *66*, 486.
- Fantz, D. A.; Jacobs, D.; Glossip, D.; Kornfeld, K. *J. Biol. Chem.* **2001**, *276*, 27256.
- Farooq, A.; Zhou, M.M. *Cell. Signal.* **2004**, *16*, 769.
- Fekl, U.; Goldberg, K. I. *Adv. Inorg. Chem.* **2003**, *54*, 259.
- Ferrell, J. E. *TIBS* **1997**, *22*, 288.
- Ferrell, J. E.; Bhatt, R. R. *J. Biol. Chem.* **1997**, *272*, 19008.
- Fields, S.; Song, O. *Nature* **1989**, *340*, 245.
- Fortini, M. E.; Simon, M. A.; Rubin, G. M. *Nature* **1992**, *355*, 559.
- Fukuda, M.; Gotoh, I.; Gotoh, Y.; Nishida, E. *J. Biol. Chem.* **1996**, *271*, 20024.
- Fukuda, M.; Gotoh, Y.; Nishida, E. *EMBO J.* **1997**, *16*, 1901.
- Fukuyama, T.; Vranesic, B.; Negri, D. P.; Y. Kishi, Y. *Tetrahedron Lett.* **1978**, *19*, 2741.
- Gaussian 03, Revision E.01, M. J. Frisch; Trucks, G. W.; Schlegel, H. B.; Scuseria, G. E.; Robb, M. A.; Cheeseman, J. R.; Montgomery, Jr., J. A.; Vreven, T.; Kudin, K. N.; Burant, J. C.; Millam, J. M.; Iyengar, S. S.; Tomasi, J.; Barone, V.; Mennucci, B.; Cossi, M.; Scalmani, G.; Rega, N.; Petersson, G. A.; Nakatsuji, H.; Hada, M.; Ehara, M.; Toyota, K.; Fukuda, R.; Hasegawa, J.; Ishida, M.; Nakajima, T.; Honda, Y.; Kitao, O.; Nakai, H.; Klene, M.; Li, X.; Knox, J. E.; Hratchian, H. P.; Cross, J. B.; Bakken, V.; Adamo, C.; Jaramillo, J.; Gomperts, R.; Stratmann, R. E.; Yazyev, O.; Austin, A. J.; Cammi, R.; Pomelli, C.; Ochterski, J. W.; Ayala, P. Y.; Morokuma, K.; Voth, G. A.; Salvador, P.; Dannenberg, J. J.; Zakrzewski, V. G.; Dapprich, S.; Daniels, A. D.; Strain, M. C.; Farkas, O.; Malick, D. K.; Rabuck, A. D.; Raghavachari, K.; Foresman, J. B.; Ortiz, J. V.; Cui, Q.; Baboul, A. G.; Clifford, S.; Cioslowski, J.; Stefanov, B. B.; Liu, G.; Liashenko, A.; Piskorz, P.; Komaromi, I.; Martin, R. L.; Fox, D. J.; Keith, T.; Al-Laham, M. A.; Peng, C. Y.; Nanayakkara, A.; Challacombe, M.; Gill, P. M. W.; Johnson, B.; Chen, W.; Wong, M. W.; Gonzalez, C.; Pople, J. A. Gaussian, Inc., Wallingford CT, 2004.

Gaussian 09, Revision A.02, Frisch, M. J.; Trucks, G. W.; Schlegel, H. B.; Scuseria, G. E.; Robb, M. A.; Cheeseman, J. R.; Scalmani, G.; Barone, V.; Mennucci, B.; Petersson, G. A.; Nakatsuji, H.; Caricato, M.; Li, X.; Hratchian, H. P.; Izmaylov, A. F.; Bloino, J.; Zheng, G.; Sonnenberg, J. L.; Hada, M.; Ehara, M.; Toyota, K.; Fukuda, R.; Hasegawa, J.; Ishida, M.; Nakajima, T.; Honda, Y.; Kitao, O.; Nakai, H.; Vreven, T.; Montgomery, Jr., J. A.; Peralta, J. E.; Ogliaro, F.; Bearpark, M.; Heyd, J. J.; Brothers, E.; Kudin, K. N.; Staroverov, V. N.; Kobayashi, R.; Normand, J.; Raghavachari, K.; Rendell, A.; Burant, J. C.; Iyengar, S. S.; Tomasi, J.; Cossi, M.; Rega, N.; Millam, J. M.; Klene, M.; Knox, J. E.; Cross, J. B.; Bakken, V.; Adamo, C.; Jaramillo, J.; Gomperts, R.; Stratmann, R. E.; Yazyev, O.; Austin, A. J.; Cammi, R.; Pomelli, C.; Ochterski, J. W.; Martin, R. L.; Morokuma, K.; Zakrzewski, V. G.; Voth, G. A.; Salvador, P.; Dannenberg, J. J.; Dapprich, S.; Daniels, A. D.; Farkas, O.; Foresman, J. B.; Ortiz, J. V.; Cioslowski, J.; Fox, D. J. Gaussian, Inc., Wallingford CT, 2009.

Gavin, A. C.; Nebreda, A. R. *Curr. Biol.* **1999**, *9*, 281.

Gekhman, A. E.; Stolyarov, I. P.; Ershova, N. V.; Moiseeva, N. I.; Moiseev, I. I. *Doklady Chem.* **2001**, *378*, 150.

Goldsmith, E. J.; Akella, R.; Min, X.; Zhou, T.; Humphreys, J. M. *Chem. Rev.* **2007**, *107*, 5065.

Goldstein, S.; Meyerstein, D. *Acc. Chem. Res.* **1999**, *32*, 547.

Gómez, L., Garcia-Bosch, I.; Company, A.; Benet- Buchholz, J.; Polo, ; Sala, X.; Ribas X.; Costas, M. *Angew. Chem. Int. Ed.*, **2009**, *48*, 5720.

Gomperts, B. D.; Kramer, I. M.; Tatham, P. E. R. *Signal Transduction* **2009**, Elsevier, Burlington, MA, p. 328-331.

Groves, J. T.; Viski, P. *J. Org. Chem.*, **1990**, *55*, 3628.

Gutekunst, W. R.; Baran, P. S. *Chem. Soc. Rev.*, **2011**, *40*, 1976.

Hafen, E.; Basler, K.; Edstroem, J. E.; Rubin, G. M. *Science*, **1987**, *236*, 55.

Hamachi, K.; Irie, R.; Katsuki, T. *Tetrahedron Lett.*, **1996**, *37*, 4979.

Hanks, S. K.; Quinn, A. M.; Hunter, T. *Science* **1988**, *241*, 42.

Hanson, S. K.; Baker, R. T.; Gordon, J. C.; Scott, B. L.; Silks, L. A.; Thorn, D. L. *J. Am. Chem. Soc.* **2010**, *132*, 17804.

- Harris, W. A.; Stark, W. S.; Walker, J. A. *J. Physiol.* **1976**, *256*, 415.
- Hart, A. C.; Kramer, H.; Van Vactor, D. L.; Paidhungat, M.; Zipursky, S. L. *Genes Dev.* **1990**, *4*, 1835.
- Harvey, M. E.; Musaev, D. G.; Du Bois, J. *J. Am. Chem. Soc.*, **2011**, *133*, 17207.
- Hayashi, N.; Peacock, J. W.; Beraldi, E.; Zoubeidi, A.; Gleave, M. E.; Ong, C. J. *Cell Death Differ.* **2012**, *19*, 990.
- Haystead, T. A.; Dent, P.; Wu, J.; Haystead, C. M.; Sturgill, T. W. *FEBS Lett.* **1992**, *306*, 17.
- Hirao, T. *Chem. Rev.*, **1997**, *97*, 2707–2724.
- Holland, P. M.; Cooper, J. A. *Curr. Biol.* **1999**, *9*, R329.
- Hornak, V.; Abel, R.; Okur, A.; Strockbine, B.; Roitberg, A.; Simmerling, C. *Proteins* **2006**, *65*, 712.
- Huang, C.; Ghavtadze, N.; Chattopadhyay, B.; Gevorgyan, V. *J. Am. Chem. Soc.* **2011**, *133*, 17630.
- Hull, J. F.; Balcells, D.; Sauer, E. L. O.; Raynaud, C.; Brudvig, G. W.; Crabtree, R. H.; Eisenstein, O. *J. Am. Chem. Soc.* **2010**, *132*, 7605.
- Ishihara, Y.; Baran, P. S. *Synlett*, **2010**, 1733.
- Itoh, S.; Kondo, T.; Komatsu, M.; Ohshiro, Y.; Li, C.; Kanehisa, N.; Kai, Y.; Fukuzumi, S. *J. Am. Chem. Soc.* **1995**, *117*, 4714.
- Izaguirre, J. A.; Catarello, D. P.; Wozniak, J. M.; Skeel, R. D. *J. Chem. Phys.* **2001**, *114*, 2090.
- Jiang, N.; Ragauskas, A. J. *J. Org. Chem.* **2007**, *72*, 7030–33.
- Jullien-Flores, V.; Dorseuil, O.; Romero, F.; Letourneur, F.; Saragosti, S.; Berger, R.; Tavitian, A.; Gacon, G.; Camonis, J. H. *J. Biol. Chem.* **1995**, *270*, 22473.
- Kaoud, T. S.; Devkota, A. K.; Harris, R.; Rana, M. S.; Abramczyk, O.; Warthaka, M.; Lee, S.; Girvin, M. E.; Riggs, A. F.; Dalby, K. N. *Biochemistry* **2011**, *50*, 4568.
- Khokhlatchev, A. V.; Canagarajah, B.; Wilsbacher, J.; Robinson, M.; Atkinson, M.; Goldsmith, E.; Cobb, M. H. *Cell* **1998**, *93*, 605.

- Khokhlatchev, A.; Xu, S.; English, J.; Wu, P.; Shaefer, E.; Cobb, M. H. *J. Biol. Chem.* **1997**, *272*, 11057.
- Kim, C.; Chen, K.; Kim, J.; Que, Jr., L. *J. Am. Chem. Soc.* **1997**, *119*, 5964.
- Kim, J.; Ashenurst, J. A.; Movassaghi, M. *Science* **2009**, *324*, 238.
- Kim, J.; Harrison, R. G.; Kim, C.; Que, Jr., L. *J. Am. Chem. Soc.* **1996**, *118*, 4373.
- Kim, Y.; Rice, A. E.; Denu, J. M. *Biochemistry* **2003**, *42*, 15197.
- Kirihara, M.; Ochiai, Y.; Takahata, S. T. H.; Nemoto, H. *Chem. Commun.* **1999**, 1387.
- Knighton, D. R.; Zheng, J.; Ten Eyck, L. F.; Xuong, N.-H.; Taylor, S. S.; Sowadski, J. M. *Science* **1991**, *253*, 414.
- Kondoh, K.; Nishida, E. *Biochim. Biophys. Acta* **2007**, *1773*, 1227.
- Kong, J.; White, C. A.; Krylov, A. I.; Sherill, C. D.; Adamson, R. D.; Furlani, T. R.; Lee, M. S.; Lee, A. M.; Gwaltney, S. R.; Adams, T. R.; Ochsenfeld, C.; Gilbert, A. T. B.; Kedziora, G. S.; Rassolov, V. A.; Maurice, D. R.; Nair, N.; Shao, Y.; Besley, N. A.; Maslen, P. E.; Dombroski, J. P.; Daschel, H.; Zhang, W.; Korambath, P. P.; Baker, J.; Byrd, E. F. C.; Van, Voorhis, T.; Oumi, M.; Hirata, S.; Hsu, C.-P.; Ishikawa, N.; Florian, J.; Warshel, A.; Johnson, B. G.; Gill, P. M. W.; Head-Gordon, M.; Pople, J. A. *J. Computational Chem.* **2000**, *21*, 1532.
- Kong, Y.; Karplus, M. *Proteins* **2009**, *74*, 145.
- Kornev, A. P.; Haste, N. M.; Taylor, S. S.; Eyck, L. F. *Proc. Natl. Acad. Sci. U. S. A.* **2006**, *103*, 17783.
- Kramer, H.; Cagan, R. L.; Zipursky, S. L. *Nature* **1991**, *352*, 207.
- Leach, A. G.; Wang, R.; Wohlhieter, G. E.; Khan, S. I.; Jung, M. E.; Houk, K. N. *J. Am. Chem. Soc.* **2003**, *125*, 4271.
- Lee, C. T.; Yang, W. T.; Parr, R. G. *Phys. Rev. B.* **1988**, *37*, 785.
- Lee, J. S.; Cao, H.; Fuchs, P. L. *J. Org. Chem.* **2007**, *72*, 5820.
- Lee, S.; Bae, Y. S. *Mol. Cells* **2012**, *33*, 325.

- Lee, S.; Fuchs, P. L. *J. Am. Chem. Soc.* **2002**, *124*, 13978.
- Lee, S.-J.; Zhou, T.; Goldsmith, E. J. *Methods* **2006**, *40*, 224.
- Lee, T.; Hoofnagle, A. N.; Kabuyama, Y.; Stroud, J.; Min, X.; Goldsmith, E. J.; Chen, L.; Resing, K. A.; Ahn, N. G. *Mol. Cell* **2004**, *14*, 43.
- Leising, R. A.; Kim, J.; Perez, M. A.; Que, Jr., L. *J. Am. Chem. Soc.* **1993**, *115*, 9524.
- Lersch, M.; Tilset, M. *Chem. Rev.* **2005**, *105*, 2471.
- Levin-Salomon, V.; Kogan, K.; Ahn, N. G.; Livnah, O.; Engelberg, D. *J. Biol. Chem.* **2008**, *283*, 34500.
- Li, C.-J. *Acc. Chem. Res.* **2009**, *42*, 335.
- Lidke, D. S.; Huang, F.; Post, J. N.; Rieger, B.; Wilsbacher, J.; Thomas, J. L.; Pouysségur, J.; Jovin, T. M.; Lenormand, P. *J. Biol. Chem.* **2010**, *285*, 3092.
- Ligtenbarg, A. G. J.; Hage, R.; Feringa, B. L. *Coord. Chem. Rev.* **2003**, *237*, 89.
- Lin, L.; Wartmann, M.; Lin, A. Y.; Knopf, J. L.; Seth, A.; Davis, R. J. *Cell* **1993**, *72*, 269.
- Liu, S.; Sun, J. P.; Zhou, B.; Zhang, Z. Y. *Proc. Natl. Acad. Sci. U. S. A.* **2006**, *103*, 5326.
- Lu, J.; Tan, X.; Chen, C. *J. Am. Chem. Soc.* **2007**, *129*, 7768.
- Ma, Z.; Lu, J.; Wang, X.; Chen, C. *Chem. Commun.* **2011**, *47*, 427.
- MacFaul, P. A.; Ingold, K. U.; Wayner, D. D. M.; Que, Jr., L. *J. Am. Chem. Soc.* **1997**, *119*, 10594.
- MacFaul, P. A.; Wayner, D. D. M.; Ingold, K. U. *Acc. Chem. Res.* **1998**, *31*, 159.
- Maeda, Y.; Kakiuchi, N.; Matsumura, S.; Nishimura, T.; Kawamura, T.; Uemura, S. *J. Org. Chem.* **2002**, *67*, 6718.
- Mahalingam, M.; Arvind, R.; Ida, H.; Murugan, A. K.; Yamaguchi, M.; Tsuchida, N. *Oncol. Rep.* **2008**, *20*, 957.
- Makhlynets, O. V.; Rybak-Akimova, E. V. *Chem. Eur. J.* **2010**, *16*, 13995.

- Mansour, S. J.; Candia, J. M.; Matsuura, J. E.; Manning, M. C.; Ahn, N. G. *Biochemistry* **1996**, *35*, 15529.
- Mansour, S.J.; Matten, W.T.; Hermann, A.S.; Candia, J.M.; Rong, S.; Fukasawa, K.; Vande Woude, G.F.; Ahn, N.G. *Science* **1994**, *265*, 966.
- Matsumura, K. *J. Stomatol. Soc. Jpn* **1995**, *62*, 513.
- Matsumura, K.; Iritani, A.; Enomoto, S.; Torikata, C.; Matsuyama, S.; Kurita, A.; Kurahashi, H.; Tsuchida, N. *Genes Chromosomes Cancer* **2000**, *29*, 207.
- Matsuoka, S.; Ballif, B. A.; Smogorzewska, A.; McDonald, E. R.; Hurov, K. E.; Luo, J.; Bakalarski, C. E.; Zhao, Z.; Solimini, N.; Lerenthal, Y.; Shiloh, Y.; Gygi, S. P.; Elledge, S. J. *Science*, **2007**, *316*, 1160.
- McNeill, E.; Du Bois, J. *J. Am. Chem. Soc.* **2010**, *132*, 10202.
- Mello, R.; Fiorentino, M.; Fusco, C.; Curci, R. *J. Am. Chem. Soc.* **1989**, *111*, 6749.
- Michaudel, Q.; Thevenet, D.; Baran, P. S. *J. Am. Chem. Soc.* **2012**, *134*, 2547.
- Mihelich, E. D.; Daniels, K.; Eickhoff, D. J. *J. Am. Chem. Soc.* **1981**, *103*, 7690.
- Mimoun, H.; Chaumette, P.; Mignard, M.; Saussine, L. *New J. Chem.* **1983**, *7*, 467.
- Mimoun, H.; Mignard, M.; Brechot, P.; Saussine, L. *J. Am. Chem. Soc.* **1986**, *108*, 3711.
- Mimoun, H.; Saussine, L.; Daire, E.; Postel, M.; Fischer, J.; Weiss, R. *J. Am. Chem. Soc.* **1983**, *105*, 3101.
- Miyamoto, S.; Kollman, P. A. *J. Comp. Chem.* **1992**, *13*, 952.
- Moiseev, I. I.; Gekhman, A. E.; Shishkin, D. I. *New J. Chem.* **1989**, *13*, 683.
- Muda, M.; Theodosiou, A.; Gilleron, C.; Smith, A.; Chabert, C.; Camps, M.; Boschert, U.; Rodrigues, N.; Davies, K.; Ashworth, A.; Arkinstall, S. *J. Biol. Chem.* **1998**, *273*, 9323.
- Muzart, J. *Chem. Rev.* **1992**, *92*, 113.
- Muzart, J.; Pale, P.; Pete, J.-P. *Tetrahedron Lett.* **1982**, *23*, 3577.

- Neumann, C. S.; Fujimori, D. G.; Walsh, C. T. *Chem. Biol.* **2008**, *15*, 99.
- Newhouse, T.; Baran, P. S. *Angew. Chem. Int. Ed.* **2011**, *50*, 3362.
- Ni, Z.; Zhang, Q.; Xiong, T.; Zheng, Y.; Li, Y.; Zhang, H.; Zhang, J.; Liu, Q. *Angew. Chem. Int. Ed.* **2012**, *51*, 1244.
- Nicolaou, K. C.; Baran, P. S.; Zhong, Y.-L. *J. Am. Chem. Soc.* **2001**, *123*, 3183.
- Nizova, G. V.; Shul'pin, G. B. *Russ. Chem. Bull.* **1994**, *43*, 1146.
- Ochiai, M.; Miyamoto, K.; Kaneaki, T.; Hayashi, S.; Nakanishi, W. *Science* **2011**, *332*, 448.
- Otwinowski, Z.; Minor, W. *Methods Enzymol.* **1997**, *276*, 307.
- Paradine, S. M.; White, M. C. *J. Am. Chem. Soc.* **2012**, *134*, 2036.
- Pearson, A. J.; Han, G. R. *J. Org. Chem.* **1985**, *50*, 2791.
- Pearson, G.; Robinson, F.; Beers Gibson, T.; Xu, B.-E.; Karandikar, M.; Berman, K.; Cobb, M. H. *Endocr. Rev.* **2001**, *22*, 153.
- Philipova, R.; Whitaker, M. J. *J. Cell Sci.* **2005**, *118*, 5767.
- Polychronopoulos, S.; Verykokakis, M.; Yazicioglu, M. N.; Sakarellos-Daitsiotis, M.; Cobb, M. H.; Mavrothalassitis, G. *J. Biol. Chem.* **2006**, *281*, 25601.
- Punniyamurthy, T.; Rout, L. *Coord. Chem. Rev.*, **2008**, *252*, 134.
- Que, Jr., L.; Tolman, W. B. *Nature* **2008**, *455*, 333.
- Que, Jr., L.; Tolman, W. B. *Angew. Chem. Int. Ed.* **2002**, *41*, 1114.
- Radosevich, A. T.; Musich, C.; Toste, F. D. *J. Am. Chem. Soc.* **2005**, *127*, 1090.
- Ray, L. B.; Sturgill, T. W. *Proc. Natl. Acad. Sci. U. S. A.* **1988**, *85*, 3753.
- Reinke, R.; Zipursky, S. L. *Cell* **1988**, *55*, 321.
- Reis, P. M.; Silva, J. A. L.; Silva, J. J. R. F. d.; Pombeiro, A. J. L. *Chem. Commun.* **2000**, 1845.
- Rigas, J. D.; Hoff, R. H.; Rice, A. E.; Hengge, A. C.; Denu, J. M. *Biochemistry* **2001**, *40*, 4398.

- Robbins, D. J.; Cobb, M. H. *Mol. Biol. Cell* **1992**, *3*, 299.
- Robbins, D. J.; Zhen, E.; Owaki, H.; Vanderbilt, C.; Ebert, D.; Geppert, T. D.; Cobb, M. H. *J. Biol. Chem.* **1993**, *268*, 5097.
- Robinson, F. L.; Whitehurst, A. W.; Raman, M.; Cobb, M. H. *J. Biol. Chem.* **2002**, *277*, 14844.
- Robinson, M. J.; Stippec, S. A.; Goldsmith, E.; White, M. A.; Cobb, M. H. *Curr. Biol.* **1998**, *8*, 1141.
- Roskoski, R. *Biochem. Biophys. Res. Commun.* **2012**, *417*, 5.
- Roskoski, R. *Pharmacol. Res.* **2012**, *66*, 105.
- Rossomando, A. J.; Dent, P.; Sturgill, T. W.; Marshak, D. R. *Mol. Cell Biol.* **1994**, *14*, 1594.
- Roux, P. P.; Blenis, J. *Microbiol. Mol. Biol. Rev.* **2004**, *68*, 320.
- Sagui, C.; Pedersen, L. G.; Darden, T. A. *J. Chem. Phys.* **2004**, *120*, 73.
- Schönecker, B.; Zheldakova, T.; Liu, Y.; Kötteritzsch, M.; Günther, W.; Görls, H. *Angew. Chem. Int. Ed.* **2003**, *43*, 3240.
- Sharpless, K. B.; Verhoeven, T. R. *Aldrichimica Acta*, **1979**, *12*, 63.
- Sheridan, D. L.; Kong, Y.; Parker, S. A.; Dalby, K. N.; Turk, B. E. *J. Biol. Chem.* **2008**, *283*, 19511.
- Shilov, A. E.; Shul'pin, G. B. *Chem. Rev.* **1997**, *97*, 2879.
- Shul'pin, G. B.; Attanasio, D.; Suber, L. *J. Catal.* **1993**, *142*, 147.
- Shul'pin, G. B.; Kirillova, M. V.; Kozlov, Y. N.; Shul'pina, L. S.; Kudinov, A. R.; Pombeiro, A. J. L. *J. Catal.* **2011**, *277*, 164.
- Silva, T. F. S.; Luzyanin, K. V.; Kirillova, M. V.; da Silva, M. F. G.; Martins, L. M. D. R. S.; Pombeiro, A. J. L. *Adv. Synth. Catal.* **2010**, *352*, 171.
- Songyang, Z.; Lu, K. P.; Kwon, Y. T.; Tsai, L.-H.; Filhol, O.; Cochet, C.; Brickey, D. A.; Soderling, T. R.; Bartleson, C.; Graves, D. J.; DeMaggio, A. J.; Hoekstra, M. F.; Blenis, J.; Hunter, T.; Cantley, L. C. *Mol. Cell. Biol.* **1996**, *16*, 6486.

- Spellmeyer, D. C.; Houk, K. N. *J. Org. Chem.* **1987**, *52*, 959.
- Stahl, S. S.; Labinger, J. A.; Bercaw, J. E. *Angew. Chem. Int. Ed.* **1998**, *37*, 2180.
- Stavropoulos, P.; Çelenligil-Çetin, R.; Tapper, A. E. *Acc. Chem. Res.* **2001**, *34*, 745.
- Still, W. C.; Kahn, M.; Mitra, A. *J. Org. Chem.* **1978**, *43*, 2923.
- Stout, E. P.; Morinaka, B. I.; Wang, Y.-G.; Romo, D.; Molinski, T. F. *J. Nat. Prod.* **2012**, *75*, 527.
- Stout, E. P.; Wang, Y.-G.; Romo, D.; Molinski, T. F. *Angew. Chem., Int. Ed.* **2012**, *51*, 4877.
- Su, S.; Seiple, I. B.; Young, I. S.; Baran, P. S. *J. Am. Chem. Soc.*, **2008**, *130*, 16490.
- Talsi, E. P.; Chinakov, V. D.; Babenko, V. P.; Zamaraev, K. I. *J. Mol. Catal.* **1993**, *81*, 235.
- Talsi, E. P.; Shalyaev, K. V. *J. Mol. Catal.* **1994**, *92*, 245.
- Tan, X.; Chen, C. *Angew. Chem., Int. Ed.* **2006**, *45*, 4345.
- Tanoue, T.; Nishida, E. *Cell Signal.* **2003**, *15*, 455.
- Tanoue, T.; Adachi, M.; Moriguchi, T.; Nishida, E. *Nat. Cell Biol.* **2000**, *2*, 110.
- Tanoue, T.; Maeda, R.; Adachi, M.; Nishida, E. *EMBO J.* **2001**, *20*, 466.
- Tenaglia, A., Terranova, E., and Waegell, B., *Tetrahedron Lett.*, 1989, *30*, 5271.
- Tetard, D.; Verlhac, J.-B. *J. Mol. Catal. A: Chem.*, **1996**, *113*, 223.
- Tomlinson, S.; Ready, D. F. *Science* **1986**, *231*, 400.
- Turk, B. E. *Curr. Op. Chem. Biol.* **2008**, *12*, 4.
- Ueda, E. K.; Gout, P. W.; Morganti, L. *J. Chromatogr., A* **2003**, *988*, 1.
- Vaillancourt, F. H.; Yeh, E.; Vosburg, D. A.; Garneau-Tsodikova, S.; Walsh, C. T. *Chem. Rev.* **2006**, *106*, 3364.

- Van Aelst, L.; Barr, M.; Marcus, S.; Polverino, A.; Wigler, M. *Proc. Natl. Acad. Sci. U. S. A.* **1993**, *90*, 6213.
- Velusamy, S.; Punniyamurthy, T. *Org. Lett.* **2004**, *6*, 217.
- Viehe, H. G.; Janousek, Z.; Merenyi, R. *Acc. Chem. Res.* **1985**, *18*, 148.
- Vojtek, A. B.; Hollenberg, S. M.; and Cooper, J. A. *Cell* **1993**, *74*, 205.
- Wang, J.; Cieplak, P.; Kollman, P. A. *J. Comp. Chem.* **2000**, *21*, 1049.
- Wang, J.; Wang, W.; Kollman, P. A.; Case, D. A. *J. Mol. Graph. Model.* **2006**, *25*, 247.
- Wang, X.; Ma, Z.; Lu, J.; Tan, X.; Chen, C. *J. Am. Chem. Soc.* **2011**, *133*, 15350.
- Wang, X.; Wang, X.; Tan, X.; Lu, J.; Cormier, K. W.; Ma, Z.; Chen, C. *J. Am. Chem. Soc.* **2012**, *134*, 18834.
- Welle, F. M.; Beckhaus, H.-D.; Rüchardt, C. *J. Org. Chem.* **1997**, *62*, 552.
- Wendlandt, A. E.; Suess, A. M.; Stahl, S. S. *Angew. Chem. Int. Ed.* **2011**, *50*, 11062.
- Weng, S.-S.; Shen, M.-W.; Kao, J.-Q.; Munot, Y. S.; Chen, C.-T. *Proc. Natl. Acad. Sci. U.S.A.* **2006**, *103*, 3522.
- Whitehurst, A. W.; Wilsbacher, J. L.; You, Y.; Luby-Phelps, K.; Moore, M. S.; Cobb, M. H. *Proc. Natl. Acad. Sci. U. S. A.* **2002**, *99*, 7496.
- Wong, M. W.; Radom, L. *J. Phys. Chem.* **1995**, *99*, 8582.
- Wu, J.; Filutowicz, M. *Acta Biochim. Pol.* **1999**, *46*, 591.
- Xia, J.; Cormier, K. W.; Chen, C. *Chem. Sci.* **2012**, *3*, 2240.
- Xu, B.; Wilsbacher, J. L.; Collisson, T.; Cobb, M. H. *J. Biol. Chem.* **1999**, *274*, 34029.
- Yamazaki, S. *Org. Lett.* **1999**, *1*, 2129.
- Yang, D.; Wong, M.-K.; Wang, X.-C.; Tang, Y.-C. *J. Am. Chem. Soc.* **1998**, *120*, 6611.
- Yazicioglu, M. N.; Goad, D. L.; Ranganathan, A.; Whitehurst, A. W.; Goldsmith, E. J.; Cobb, M. H. *J. Biol. Chem.* **2007**, *282*, 28759.

- Yoon, S.; Seger, R. *Growth Factors* **2006**, *24*, 21.
- Yu, J.-Q.; Corey, E. J. *J. Am. Chem. Soc.* **2003**, *125*, 3232.
- Zalatan, D. N.; Du Bois, J. *Top. Curr. Chem.* **2010**, *292*, 347.
- Zhang, F.; Strand, A.; Robbins, D.; Cobb, M. H.; Goldsmith, E. *Nature* **1994**, *367*, 704.
- Zhang, W.; Basak, A.; Kosugi, Y.; Hoshino, Y.; Yamamoto, H. *Angew. Chem. Int. Ed.* **2005**, *44*, 4389.
- Zhang, Y.-H.; Yu, J.-Q. *J. Am. Chem. Soc.* **2009**, *131*, 14654.
- Zhang, Y.-Y.; Wu, J.-W.; Wang, Z.-X. *J. Biol. Chem.* **2011**, *286*, 16150.
- Zhao, Y.; Yim, W.-L.; Tan, C. K.; Yeung, Y.-Y. *Org. Lett.* **2011**, *13*, 4308.
- Zhao, Y.; Zhang, Z. Y. *J. Biol. Chem.* **2001**, *276*, 32382.
- Zheng, C. F.; Guan, K. L. *EMBO J.* **1994**, *13*, 1123.
- Zhou, B.; Zhang, J.; Liu, S.; Reddy, S.; Wang, F.; Zhang, Z. Y. *J. Biol. Chem.* **2006**, *281*, 38834.
- Zhou, T.; Sun, L.; Humphreys, J.; Goldsmith, E. J. *Structure* **2006**, *14*, 1011.
- Zhou, J.; Adams, J. A. *Biochemistry* **1997**, *36*, 15733.